NASA CR-159674
RI/RD79-217

NASA

FINAL REPORT

LIQUID OXYGEN/LIQUID HYDROGEN AUXILIARY POWER SYSTEM THRUSTER INVESTIGATION

by

E. E. Eberle and L. Kusak

Rockwell International
Rocketdyne Division

prepared for

NATIONAL AERONAUTICS AND SPACE ADMINISTRATION

December 1979

NASA-Lewis Research Center

Contract NAS3-20373

J. P. Wanhainen, Program Manager

1. Report No.	2. Government Accession No.	3. Recipient's Catalog No.
NASA CR-159674		

4. Title and Subtitle	5. Report Date
LIQUID OXYGEN/LIQUID HYDROGEN AUXILIARY PROPULSION SYSTEM THRUSTER INVESTIGATION Final Report	December 1979 6. Performing Organization Code
7. Author(s) E. E. EBERLE AND L. KUSAK	8. Performing Organization Report No. RI/RD79-217
9. Performing Organization Name and Address ROCKETDYNE DIVISION ROCKWELL INTERNATIONAL 6633 CANOGA AVE. CANOGA PARK, CA 91304	10. Work Unit No. 11. Contract or Grant No. NAS3-20373
12. Sponsoring Agency Name and Address NATIONAL AERONAUTICS AND SPACE ADMINISTRATION Lewis Research Center Cleveland, OH 44315	13. Type of Report and Period Covered FINAL October 1976-February 1979 14. Sponsoring Agency Code

15. Supplementary Notes

PROGRAM MANAGER, J. P. WANHAINEN, NASA-Lewis Research Center, Cleveland, OH 44315

16. Abstract

This program encompassed the design, fabrication, and demonstration of a 111 newton (25 lb) thrust, integrated auxiliary propulsion system (IAPS) thruster for use with LH_2/LO_2 propellants. Hydrogen was supplied at a temperature range of 22 to 33 K (40 to 60 R), and oxygen from 89 to 122 K (160 to 220 R). The thruster was designed to operate in both pulse mode and steady-state modes for vehicle attitude control, space maneuvering, and as an abort backup in the event of failure of the main propulsion system.

A dual-sleeve, tri-axial injection system was designed that utilizes a primary injector/combustor where 100% of the oxygen and 8% of the hydrogen is introduced; a secondary injector/combustor where 45% of the hydrogen is introduced to mix with the primary combustor gases; and a boundary layer injector that uses the remaining 45% of the hydrogen to cool the thrust throat/nozzle region.

Hot-fire evaluation of this thruster with a BLC injection distance of 2.79 cm (1.10 in.) indicated that a specific impulse value of 390 sec can be attained using a coated molybdenum thrust chamber.

Pulse mode tests indicated that a chamber pressure buildup to 90% thrust can be achieved in a time on the order of 48 msec. Some problems were encountered in achieving ignition of each pulse during pulse trains. This was interpreted to indicate that a higher delivered spark energy level (>100 mJ) would be required to maintain ignition reliability of the plasma torch ignition system under the extra "cold" conditions resulting during pulsing.

17. Key Words (Suggested by Author(s))	18. Distribution Statement
25-lb LH_2/LO_2 Thruster Plasma Ignition Attitude Control Abort Mode Thruster	

19. Security Classif. (of this report)	20. Security Classif. (of this page)	21. No. of Pages	22. Price*
UNCLASSIFIED	UNCLASSIFIED	186	

* For sale by the National Technical Information Service, Springfield, Virginia 22151

N80-15202 #

FOREWORD

The work herein was conducted at Rocketdyne, a division of Rockwell International, under Contract NAS3-20373, from October 1976 to February 1979. Mr. J. P. Wanhainen, NASA-Lewis Research Center, was NASA Program Manager. At Rocketdyne, Mr. H. G. Diem was Program Manager and Mr. E. E. Eberle was Project Engineer responsible for the technical direction of the program.

The important contributions to the conduct of the program and to the preparation of report material were made by the following personnel:

Engineering Development	Mr. L. Kusak
Engineering Test	Mr. T. T. Yokoi
Engineering Design	Mr. H. E. Marker
Aerothermodynamics	Mr. J. M. Shoji
Valve Support	Mr. R. G. Stephenson
Electrical Support	Mr. R. L. Goodwin
Materials and Processes	Mr. H. W. Carpenter

CONTENTS

ILLUSTRATIONS

TABLES

SUMMARY

The objective of this program was to provide the analysis, design, fabrication and test of a 111 N (25 pound) thrust, integrated auxiliary propulsion system (IAPS) thruster in which cryogenic propellants (LH_2/LO_2) are supplied at the valve inlets; specifically, hydrogen at a temperature from 22 K to 33 K (40 R to 60 R) and oxygen from 89 K to 122 K (160 R to 220 R). The thruster assembly included a propellant injection system, an igniter, two propellant valves, and a thrust chamber. The thruster was required to operate in both pulse and steady-state modes for vehicle attitude control, space maneuvering, and as an abort backup in the event of main propulsion system failure.

Propellant injection systems representing increasing levels of design complexity were evaluated for their performance capability, manifolding, and cooling requirements. A propellant injection system consisting of a dual-sleeve, triaxial injection/combustor design was selected because of its performance potential, development flexibility, and inherent compatibility with the combustor/thrust chamber walls. The dual-sleeve, triaxial injection system utilizes a primary injector/combustor where all of the oxygen and 8% of the hydrogen is introduced, a secondary injector/combustor where 45% of the hydrogen is injected through an annulus to mix and react with the oxygen-rich hot gas from the primary combustor, and a boundary layer coolant injector where the remaining 45% of the hydrogen is introduced through an annulus to cool the thrust chamber throat/nozzle region. The resulting stepdown in propellant mixture ratio from 50:1 (primary combustor) to 7.5:1 (secondary combustor) to 4:1 at the boundary layer coolant injector was determined from combustion model analyses to provide the maximum combustion performance capability with this injection/combustor system.

A spark-torch igniter, which was a direct outgrowth of the unit used on the Advanced Space Engine (ASE), was selected for the thruster. However, several design modifications were implemented to minimize trapped propellant volume and facilitate producibility. The spark plug consisted of a 0.254-cm (0.10-in.) diameter electrode with an 0.063-cm (0.025-in.) annular spark gap. An inductive discharge exciter was utilized because of its favorable discharge wave form and overall system simplicity.

A propellant valve trade study identified a direct acting solenoid, poppet-type valve unit as the most favorable valve/actuation concept. This valve configuration, which utilized a flat metal-to-metal seat closure, was employed. Actuation of the valves with a driver circuit was employed to impress a larger-than-normal voltage at valve opening and thus provide increased pulloff force to ensure rapid and repeatable opening.

Performance and thermal analyses indicated that minimum performance requirements could be attained with a thrust chamber wall temperature of approximately 2000 F. This temperature fell within the acceptable range for austenitic materials which maintain ductility at cryogenic temperatures, exhibit good oxidiation resistance, and are readily fabricable. Therefore, L-605 alloy was selected as one of the thrust chamber materials. For increased performance potential, a refractory metal chamber also was fabricated. A review of candidate thrust chamber

materials capable of operation at wall temperatures up to 1644 K (2500 F) in an oxygen/hydrogen environment was performed. Based on this study, unalloyed, low-carbon molybdenum was selected as the alternate high-temperature thrust chamber material.

The initial area of experimental investigation was the demonstration of reliable thruster ignition over a range of spark energy levels, propellant/hardware temperature, and starting valve sequence. While ignition was demonstrated at the 10 mJ level, 25 mJ was selected as a safe nominal value. All ignition characterization testing was conducted under simulated altitude conditions of 30,800 meters (101,000 feet).

Steady-state performance and heat transfer testing was conducted with the nominal mixture ratio stepdown values of 50:1, 7.5:1, 4:1 for the primary combustor, secondary combustor, and overall thruster, respectively. A range of boundary layer coolant (BLC) injection distances above the throat from 1.52 cm to 3.43 cm (0.60 in. to 1.36 in.) were evaluated. The results performance and chamber wall heat transfer trends indicated a limiting performance level of approximately 3% below the program minimum specific impulse requirement of 390 sec, while maintaining compatible thrust chamber throat temperatures.

Incomplete mixing of the secondary combustor hydrogen with the oxygen-rich primary combustor gas was identified as the most probable cause of the noted performance deficiency. An impingement injection concept to promote mixing of the secondary combustor hydrogen with the oxygen-rich hot gas from the primary combustor was therefore designed and fabricated. This was accomplished by injection of the secondary hydrogen radially into the oxygen-rich hot-gas stream through discrete orifices, rather than coaxially as with the baseline design. Hot-fire evaluation of the injection system with a BLC injection distance of 2.79 cm (1.10 in.) indicated that a specific impulse value of 390 sec can be attained with this injection system using the high temperature molybdenum thrust chamber.

Subsequent pulse mode characterization testing was conducted consisting of six initial 75-msec pulses, followed by a 30-sec burn, followed by a 60-sec thermal soak period, and then a final series of six pulses. These pulse mode tests indicated that rapid pressure buildup (48 msec to 90% thrust) can be achieved with a small cryogenic thruster. Facility bleeds and thermal management provisions within the thruster manifolding ensured the presence of good quality (liquid) propellants at the thruster injector, and thus the rapid thrust response. However, it appears that higher spark energy levels will be required. (>100 mJ) if reliable ignition is to be achieved under these "cold" propellant conditions. Random ignition failures were encountered at a spark energy level of 100 mJ, thus indicating a marginal condition for formation of a plasma within a truly liquid oxygen flow stream.

This program has demonstrated the practicality of a liquid hydrogen/liquid oxygen thruster down to a thrust level of 111 N (25 pounds) for use in advanced space applications. The problem areas encountered during this program were primary test stand related and were aggravated by measures to maintain very low propellant temperatures in the facility supply systems and the difficulty in measurement of small cryogenic propellant flowrates.

INTRODUCTION

System studies (Contract NAS3-18913) conducted to determine if a liquid oxygen/liquid hydrogen Auxiliary Propulsion System (APS) is advantageous for future high-energy cryogenic fueled vehicles have identified an integrated design that uses the main propulsion system tanks as the propellant source to be the best liquid/liquid concept as opposed to dedicated designs which use separate tanks. When compared with dedicated cryogenic and storable propellant systems, the integrated concept was found to have superior mission payload performance. More significantly, the inherent interchangeability of main and auxiliary propellants permits the Integrated Auxiliary Propulsion System (IAPS) to provide abort backup capability in the event of a main engine failure. These capabilities result in projected overall program cost savings that more than offset the higher development cost for a liquid oxygen/liquid hydrogen APS.

A critical technology area that required evaluation for the purpose of proving the viability of such a liquid oxygen/liquid hydrogen IAPS was the development of a small thruster capable of accepting propellants in the liquid state without the need for gasification as an intermediate step. Since no previous test experience existed in the thrust range of interest, i.e., 111 to 444 N (25 to 100 pounds), the subject program was initiated to provide the required technology base for a small cryogenic liquid propellant thruster. The thrust level selected for this feasibility demonstration program was at the lower end of the range of interest because the anticipated major problem area of propellant thermal management would be more acute at this lower level. Other design requirements and operating conditions selected for the thruster investigation program are contained in Table 1 .

The report presents the analyses, design, fabrication, and test activities associated with the development of a 111 N (25-pound) thrust, hydrogen-oxygen IAPS-type thruster in which cryogenic propellants were supplied at the propellant inlet valves; specifically, hydrogen at a temperature from 22 to 33 K (40 to 60 R) and oxygen from 89 to 122 K (160 to 220 R).

TABLE 1 . THRUST CHAMBER DESIGN SPECIFICATIONS AND OPERATION CONDITIONS

Parameter	Nominal Mode	Operating Range	Abort Mode
Thrust, newton (lb)	111 (25)	---	133 (30)
Chamber Pressure, N/ cm^2 (psi) abs	103 (150)	---	124 (180)
Overall Mixture Ratio	4	3 to 6	5.6
Nozzle Expansion Area Ratio	50	---	---
Hydrogen Inlet Temp., K (R)	28 (50)	20 to 30 (37 to 55)	28 (50)
Hydrogen Injector Manifold Temp. K (R)	71 (128)	71 to 126 (128 to 227)	---
Hydrogen Inlet Pressure, N/cm^2 (psi) abs	152 (220)	134 to 169 (195 to 245)	146 (212)
Oxygen Inlet Temp. K (R)	92 (165)	91 to 111 (163 to 200)	92 (165)
Oxygen Injector Manifold Temp., K (R)	141 (254)	127 to 159 (228 to 286)	---
Oxygen Inlet Pressure, N/cm^2 (psi) abs	152 (220)	134 to 169 (195 to 245)	146 (212)
Specific Impulse-Steady State, sec.	410 (goal)	---	410 (goal)
Specific Impulse-Steady State, sec. (minimum acceptable)	390	---	382
Specific Impulse-Pulsing, sec.	330 (goal)	---	---
Response to 90% Thrust, msec	75 (goal)	---	---
Response to 90% Thrust, msec (maximum time acceptable)	100	---	---
Minimum Impulse Bit, kg-sec (lb-sec)	.2268-.4536 (.5-1.0) (goal)		
Maximum Firing Duration, Design, Hr.	0.25	---	0.75
Design life, cycles	100,000	---	---
Design Operating Life, hours	80	---	---
Reliability goal	0.9993	---	---
Heat load to LOX system, Joule/min (Btu/hr)	2.64 (.15) (goal)		---
Heat load to LH_2 system, Joule/min (Btu/hr)	5.28 (.30) (goal)		---
Maximum Test Duration, sec.	300		300

DISCUSSION

The basic approach for the investigation was to use a baseline thruster configuration that was a direct outgrowth of earlier spark-torch igniter technology. This design concept (Fig. 1) featured a central spark igniter, an integral oxygen/hydrogen injector, and a combustor tube. All of the oxygen is injected from an annular gap surrounding the spark plug electrode. A small quantity of hydrogen is injected into the igniter combustor tube where it mixes with the oxygen immediately downstream of the electrode producing an oxidizing-rich hot-gas core (MR 50:1). The remainder of the hydrogen is injected at a downstream annulus and both reacts with oxygen-rich core gases and provides film cooling of the downstream thrust chamber wall.

This baseline configuration served as a point of departure for the establishment of improved design concepts to meet the thruster pulse-mode and steady-state operating requirements specified in Table 1 .

DESIGN ANALYSIS

This section addresses the critical technology associated with the design, fabrication, and test of a small cryogenic propellant thruster. Design analyses were conducted for all of the major subcomponents within the thruster assembly. These included the propellant injection system, ignition system, thrust chamber, and propellant valves. The results of these analyses served as guidelines for the subsequent hardware design, fabrication, and hot-fire test phases.

Propellant Injection System

The primary function of an injector is to introduce propellants within a combustor in a manner that will provide stable, high combustion efficiency without having any deleterious effects on the injector face or thrust chamber wall. These goals are generally attained by adhering to established design principles involving injection element geometry, feed system dynamics, and manifolding.

However, in addition to these basic injector principles, several special considerations were addressed in the design of an injector for the small cryogenic thruster. These additional considerations stemed from the minimum impulse bit goals and the introduction of cryogenic O_2/H_2 propellant to the thruster. These additional considerations stemed from the minimum impulse bit goals and the introduction of cryogenic O_2/H_2 propellant to the thruster. Minimum impulse bit size and high-performance goals necessitated efficient, low-volume propellant manifolding and feed systems, particularly on the liquid oxygen side. The propellants within these small feed system passages are consequently highly susceptible to freezing and/or boiling. The effects of propellants (liquid-oxygen) freezing within the injector are obvious; however, propellant boiling (two-phase flow) within the injector body also is detrimental because of flow instability caused by thermal choking. Thermal control of propellants within the injector body and feed system, therefore, received as much attention as the conventional injector design practices.

Propellant injection/combustor configurations representing increasing levels of design complexity were evaluated for their performance capability, manifolding,

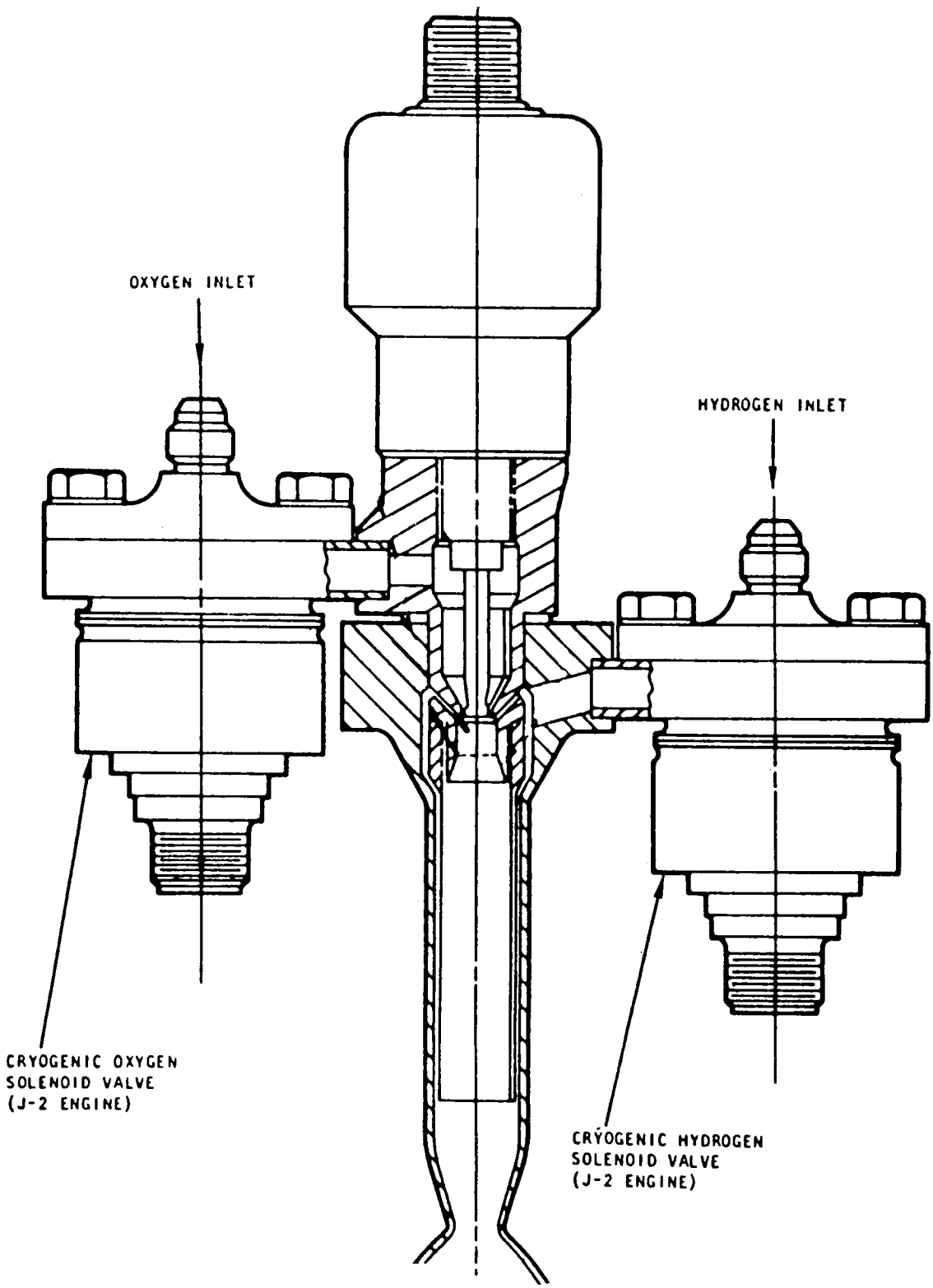

Figure 1. Baseline Thruster Concept

and cooling requirements. These injection/combustor configurations included a single-sleeve coaxial design, a dual-sleeve triaxial design, and a dual-sleeve hybrid injection design. Conceptual configuration layouts reflecting these injection/combustor designs were prepared to identify the most favorable arrangement for the thruster assembly components and to provide immediate design/ fabrication related feedback to complement the analyses effort, particularly in the areas of propellant injection systems, and pulse-mode operating characteristics. These preliminary design layouts for the single-sleeve, dual-sleeve triaxial and dualsleeve hybrid injection concepts are illustrated in Fig. 2 through 4 .

As stated earlier, the single-sleeve, coaxial design (Fig. 2) was a direct outgrowth of earlier spark-torch igniter technology, and features an oxygen-rich, hot-gas core surrounded by a hydrogen annulus that both reacts with the oxygen-rich, hot-gas core surrounded by a hydrogen annulus that both reacts with the oxygen-rich core gases and provides film cooling of the downstream thrust chamber wall. The primary advantage of the single-sleeve, coaxial configuration is its design simplicity; however, parametric performance and heat transfer analyses conducted indicated that the large sleeve recess depth required to meet the minimum program performance requirements resulted in excessive wall temperatures at the chamber throat.

The dual-sleeve, triaxial injection/combustor configuration (Fig. 3) incorporates design features that tend to correct the performance and chamber cooling problems associated with the single-sleeve injection concept, at the cost of greater design complexity. This is achieved by first injecting a portion of the hydrogen from a short inner sleeve where it mixes and reacts with the oxygen-rich core gases and then injecting the remainder of the hydrogen from a longer outer sleeve immediately upstream of the convergent nozzle section where it can effectively film cool the thrust chamber throat. Parametric performance and heat transfer analyses, conducted to define the most favorable combination or core mixture ratio and sleeve length, indicated that both satisfactory combustion performance and chamber cooling could be realized with this injection/ combustion configuration. A satisfactory performance and chamber cooling condition also is indicated with the dual-sleeve hybrid injection/combustor configuration (Fig. 4) in which a portion of the fuel is injected into the oxygen-rich core gases through individual impinging orifices, instead of through a concentric annulus as with the triaxial design. This configuration has the added potential for reducing the combustor length; however, because of the discrete location of the hydrogen injection orifices, the risk of a chamber wall compatibility problem is greater than with the dual-sleeve, triaxial injection concept.

Combustion Performance. Design analyses were performed relative to the characterization of key performance parameters for the candidate thruster propellant injection systems. Both the primary injection pattern involving the impingement of individual hydrogen jets on a single oxygen annulus (Fig. 5) and the secondary injection pattern involving an oxygen-rich hot-gas core (MR = 50) surrounded by a hydrogen annulus (Fig. 5) were evaluated from a mixing efficiency standpoint. For impinging injection streams, i.e., the primary injection pattern, optimum mixing is realized when the momentum of the hydrogen and oxygen streams are proportioned to result in mutual penetration within one another. If the

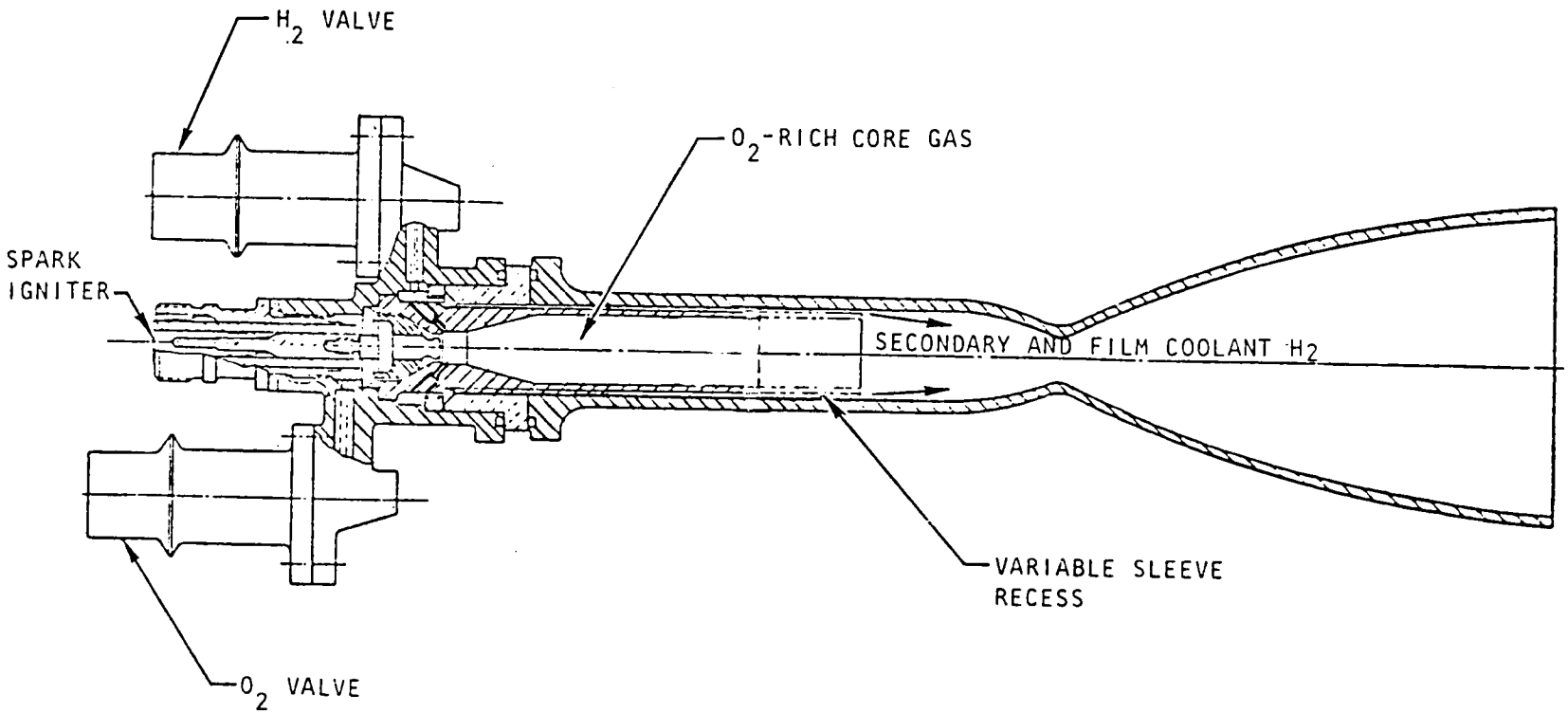

Figure 2 . Single-Sleeve Coaxial Injection System

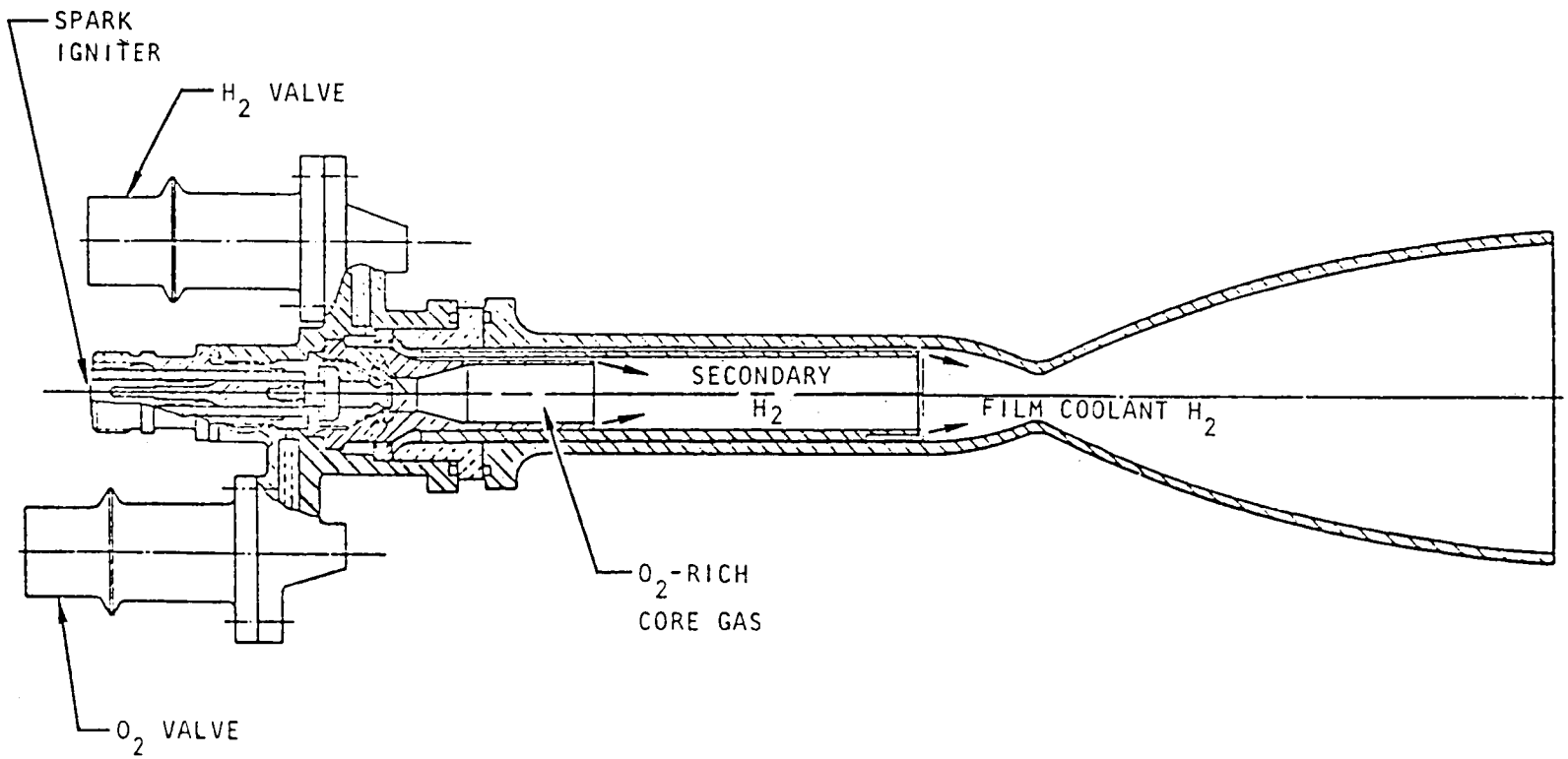

Figure 3 . Dual-Sleeve Triaxial Injection System

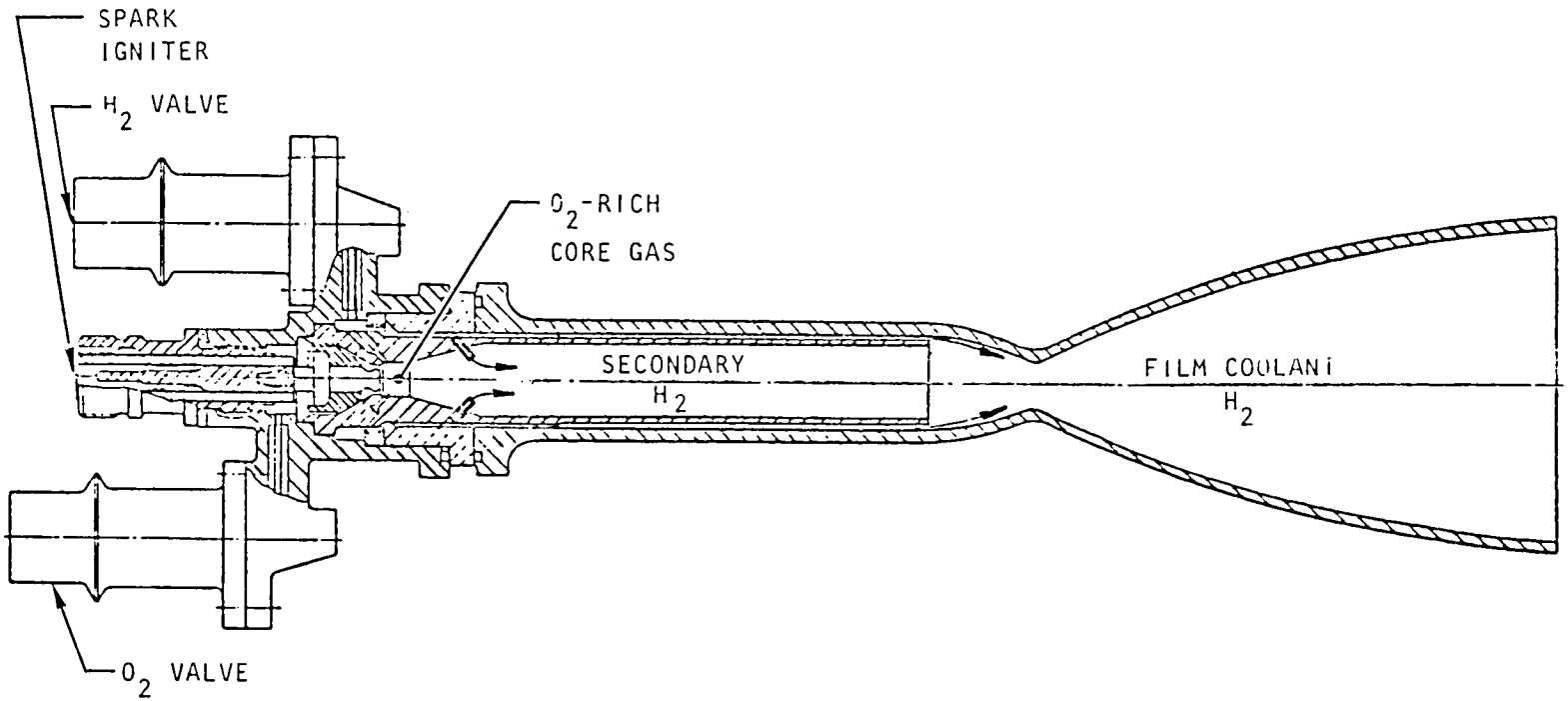

Figure 4 . Multi-Element Hybrid Injection System

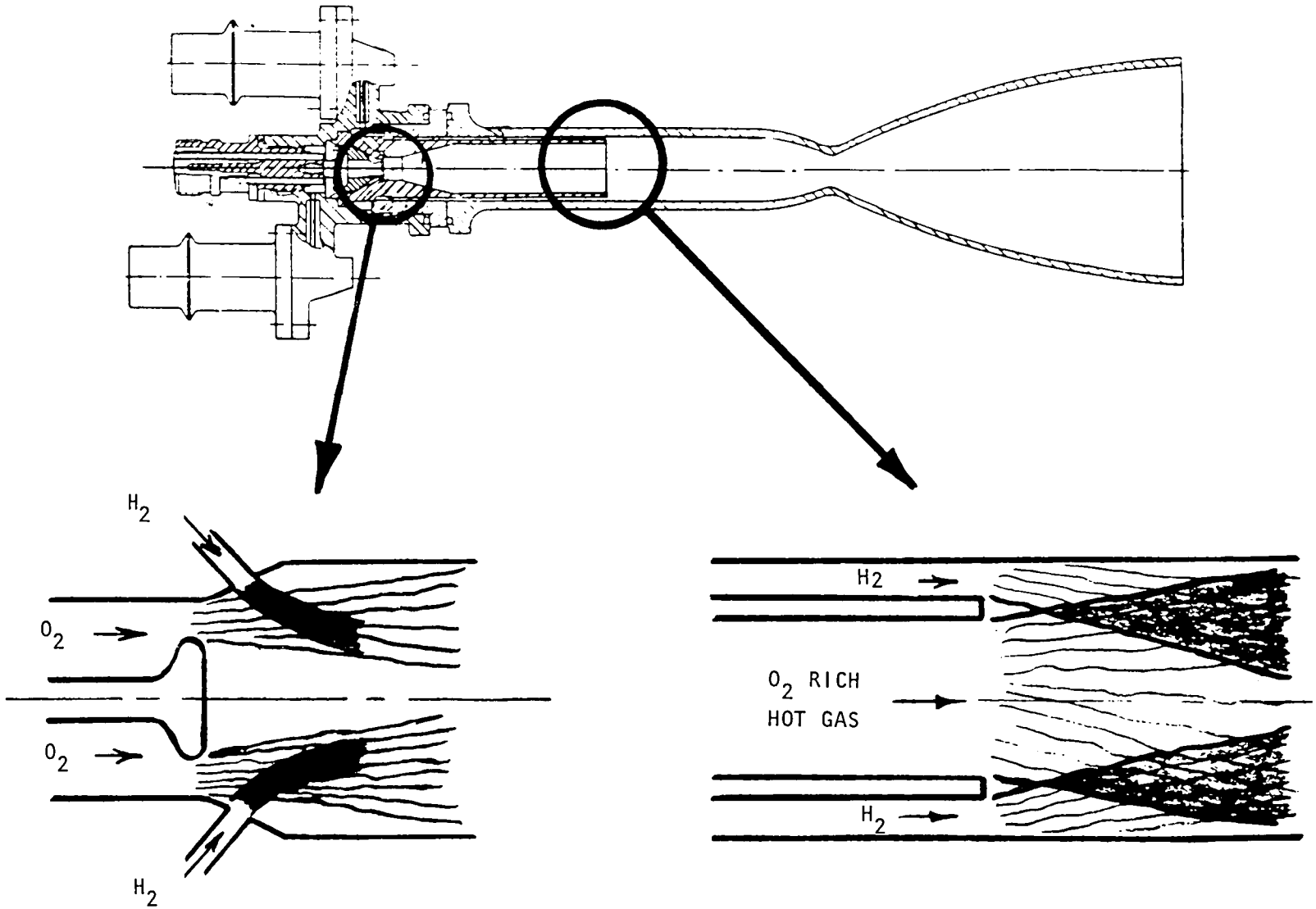

Figure 5 . Single-Sleeve Baseline Injection System

impinging hydrogen stream momentum is substantially greater than the axial oxygen stream, the hydrogen will penetrate through the oxygen shroud and enter the core region where further mixing can take place only by turbulent transport. If the impinging hydrogen stream momentum is insufficient to penetrate the axial oxygen stream, poor propellant mixing is again realized and the relatively slow turbulent transport becomes the primary mixing mechanism. The oxygen injection momentum was primarily dictated by spark plug gap geometry since this gap serves as the injection orifice for the liquid oxygen. Design analysis discussed in the Ignition System Analysis section resulted in the selection of a spark plug electrode geometry consisting of a 0.254-cm (0.100-in.) diameter electrode and a 0.063-cm (0.025-in.) spark gap. Because optimum mixing with impinging propellant streams is realized when the momentum of the fuel and oxidizer streams are proportioned to give mutual penetration within one another, the four impinging hydrogen orifices were therefore sized to best effect this condition. Under nominal operating conditions,a hydrogen orifice diameter of 0.063 cm (0.025 in.) appears to satisfy the desired penetration criteria. The penetration profile represented as Case II in Fig. 6 depicts the nominal operating point for the primary injection system. Also included in Fig. 6 , as Cases I and III, are penetration profiles for the propellant temperature operating range indicated in Table 1 . Based on these results, no significant change in behavior was indicated over the planned thruster operating range.

The candidate secondary injection systems consists of concentric tube designs and, consequently, performance characteristics are governed by shear-type mixing criteria. Unlike the primary impingement injection pattern, mixing is enhanced by large injection momentum difference between the propellants. Conventional concentric tube injection systems utilize a low-velocity core stream (oxidizer) and a high-velocity outer annular stream (fuel) to attain the desired shear-type mixing. However, because of the nearly equal injection gas densities at the thruster secondary injector, an extremely unfavorable geometric relationship (i.e., large-diameter core stream and small annulus gap) existed when shear mixing was attempted by means of a low-velocity core and a high-velocity surrounding annulus. Consequently, the alternative of utilizing a high-velocity core stream and a low-velocity surrounding annular stream was employed. Figure 7 illustrates the geometric relationship between an earlier IR&D, sleeve injection system that had a hot-fire shear ΔV of approximately 30.5 m/sec (100 ft/sec) and an alternate high-shear, single-sleeve injection system with a ΔV of approximately 213 m/sec (700 ft/sec). The more favorable geometric relationship between the oxygen and hydrogen streams for improved mixing is apparent with the "alternate design" configuration.

To characterize the performance behavior of the secondary injection system, a gas-gas combustion model was formulated based on criteria established in Ref. 1. This model describes the turbulent diffusion of a flame in a duct and empirically accounts (earlier IR&D thruster test results) for the effect of turbulent and viscous-shear mixing. The model is capable of providing composition, temperature, and velocity profiles of the combustion products anywhere inside the combustion chamber and was baselined to the hot fire combustion performance results from an earlier IR&D thruster program.

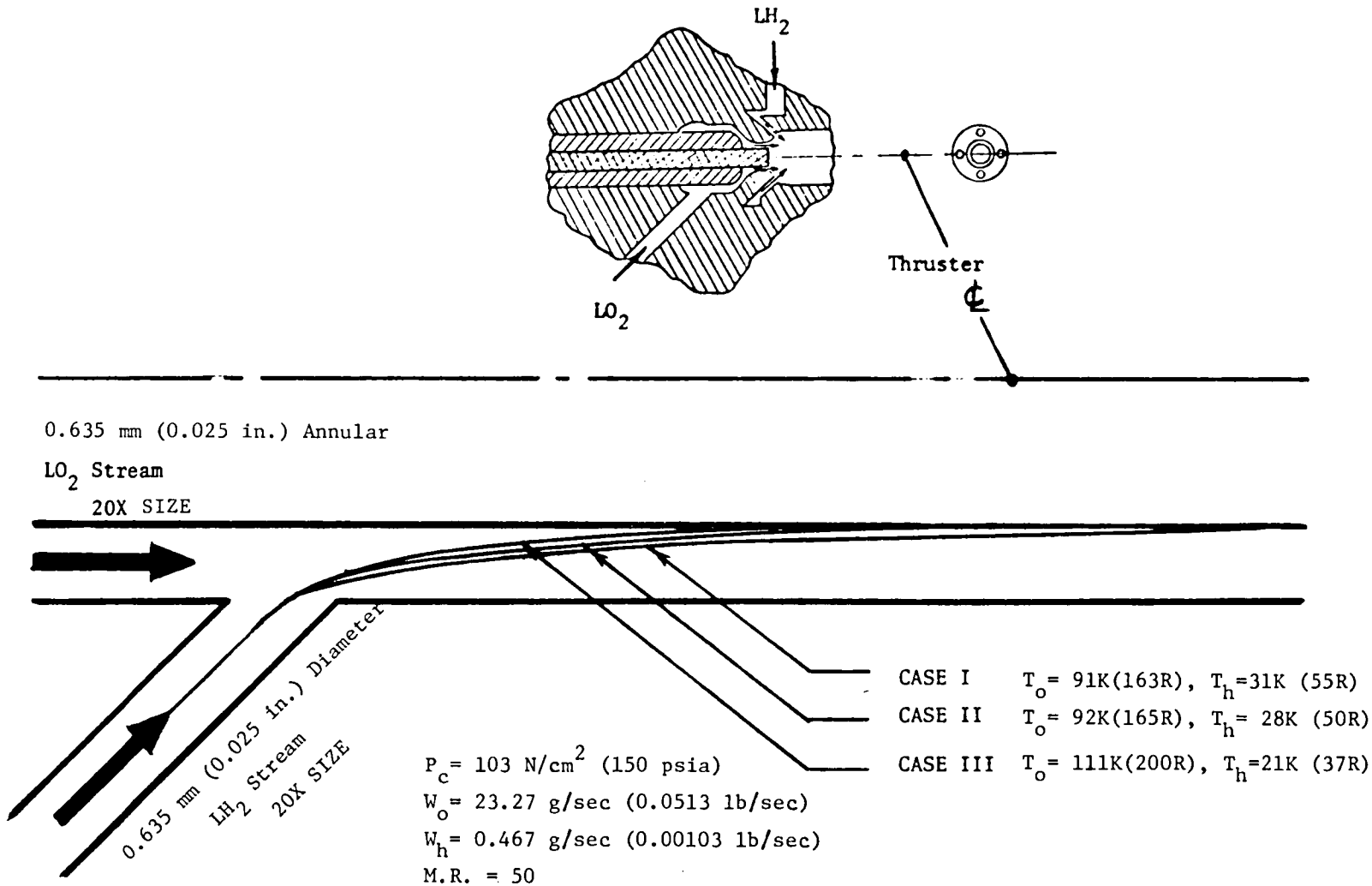

Figure 6. Primary Injection System Propellant Stream Impingement Characteristics

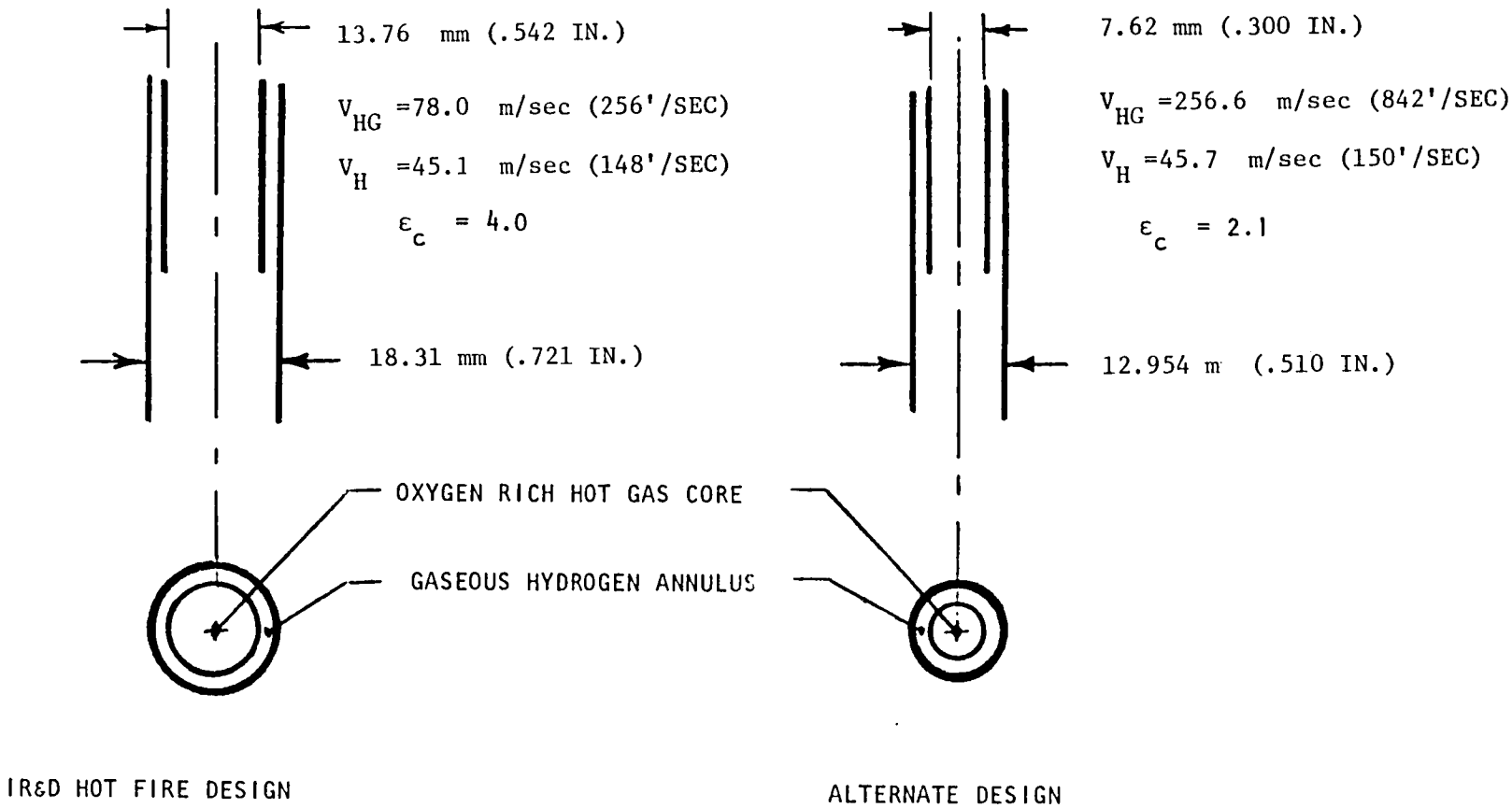

Figure 7 . Single-Sleeve Injection Geometry Comparison

As illustrated in Fig. 8 (heavy lines), the combustion model results appear to indicate less of a performance sensitivity with core mixture ratio than was originally inferred from the IR&D hot-fire test data.

Inputing the propellant injection/geometry parameters for the single-sleeve IR&D and alternate high shear injection configurations illustrated in Fig. 7 into the combustion model, resulted in the predicted combustion performance values shown in Fig. 9 . These data indicated that even with the improved mixing characteristics of the high shear design, the combustion efficiency of the single-sleeve injection system still fell short of the required minimum value of 91%, particularly since this injection configuration is limited by thrust chamber wall heat transfer considerations to sleeve recess depths of approximately 3.8 cm (1.5 inch). Thrust chamber wall cooling considerations for all of the candidate injection/combustor concepts are discussed in the Chamber Cooling section.

Parametric combustion performance analyses were also performed for the dual-sleeve, triaxial injection configuration (Fig. 3). Because this configuration involved the injection of hydrogen at two separate axial locations along the length of the thrust chamber, the combustion performance trends at each location were established. The combustion performance trends with core mixture ratio and combustor length at the first hydrogen injection location are illustrated in Fig. 10 . The injected hydrogen at this location mixes and reacts with the oxygen-rich hot gas (MR = 50) from the plasma-torch igniter. The combustor efficiency values represented in Fig. 10 are based on the theoretical performance for the respective core mixture ratio over the range of 15 to 5. The physical significance of the noted trend is that, as the core mixture ratio is decreased, a larger quantity of hydrogen must mix and react with the oxygen-rich hot gas and, therefore, a greater combustor length is necessary for a given combustion efficiency. With a combustor length of 6.35 cm (2.5 in.), combustion efficiency values ranged from 100% for a core mixture ratio of 15 to 96% for a core mixture ratio of 5.

Similar parametric combustion performance analyses were performed at the second hydrogen injection location. The injected hydrogen at this location mixes and reacts with the hot gas from the core chamber and also serves as boundary layer coolant (BLC) for the chamber throat and nozzle. The combustion performance trends with core mixture ratio and combustor length at the second hydrogen injection location are illustrated in Fig. 11 . The combustion efficiency values represented in Fig. 11 are based on the theoretical performance for the overall thruster mixture or 4.0, and show an increasing efficiency trend with a decrease in core mixture ratio over the range of 20 to 5. The physcial significance of this trend is that, as the core mixture ratio is decreased, a smaller quantity of hydrogen must mix and react with the core hot gas and, therefore, a shorter combustor length is possible for a given combustion efficiency. With a combustor length of 2.54 cm (1.0 in.), combustion efficiency values ranged from 95.5% for a core mixture ratio of 5 to a value of 86% for a core mixture ratio of 20.

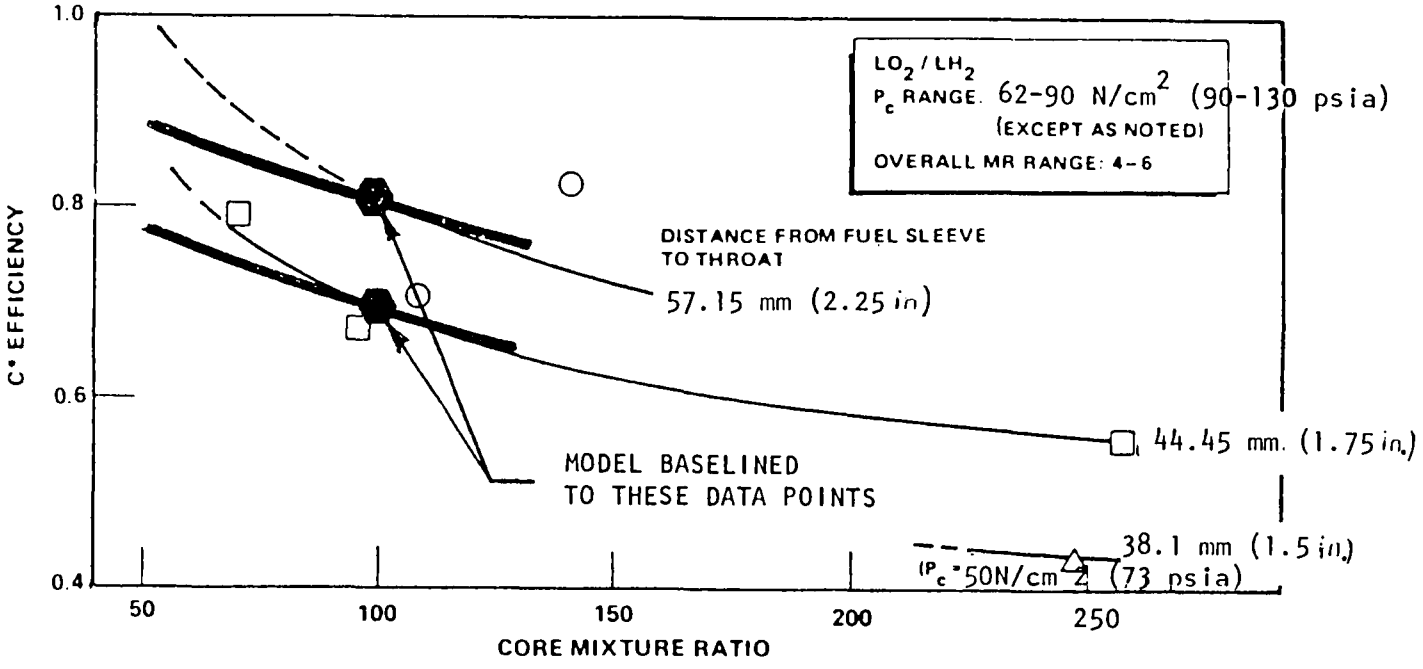

Figure 8 . Combustion Model Correlated With IR&D Single-Sleeve Thrust Chamber Hot-Fire Performance Trends (25-pound thrust)

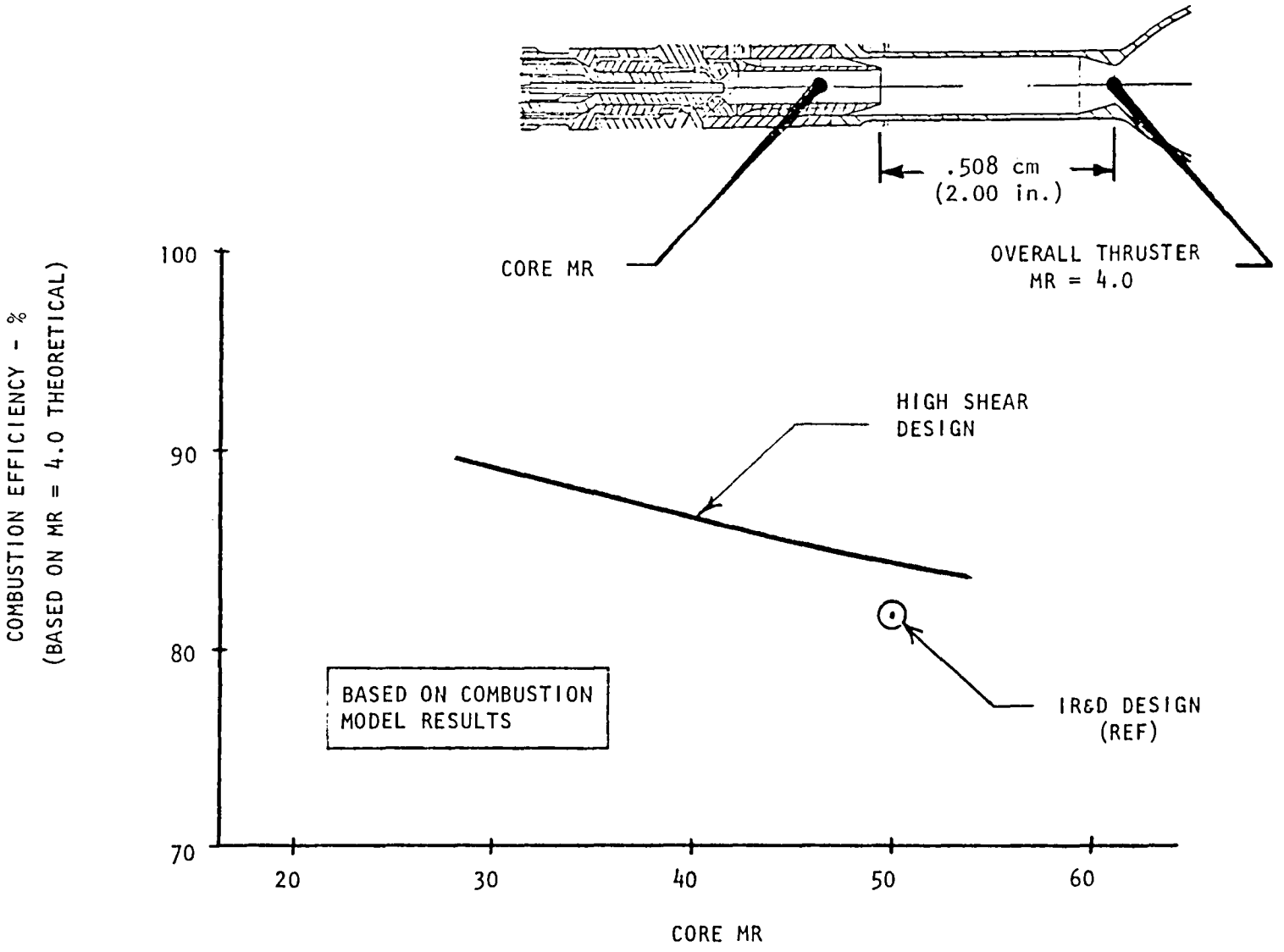

Figure 9 . Single-Sleeve Performance Trends With Core Oxidant-Fuel Mixture Ratio

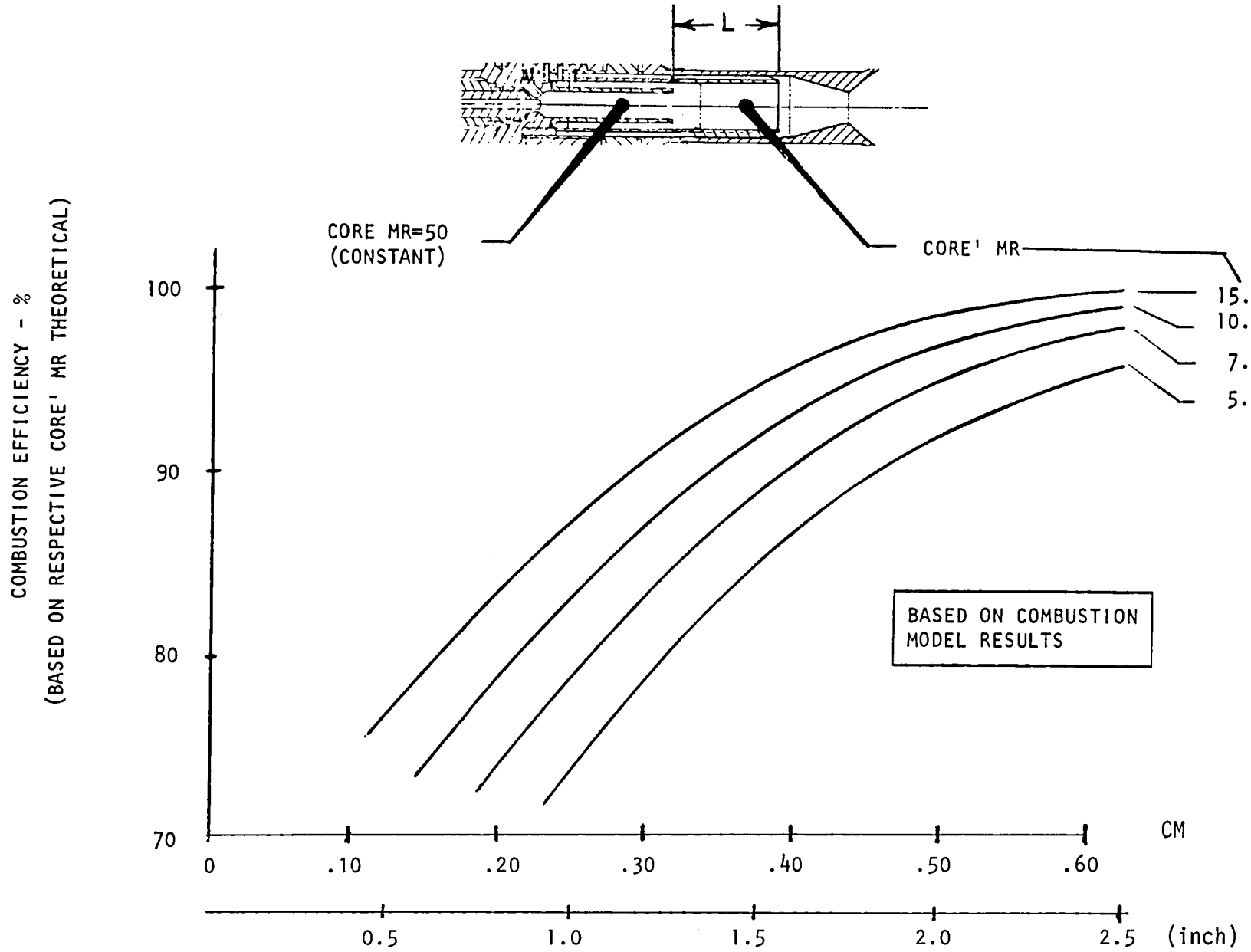

Figure 10. Dual-Sleeve Performance Trends With Secondary Combustor Length Variation (L) for Several Core' Mixture Ratios

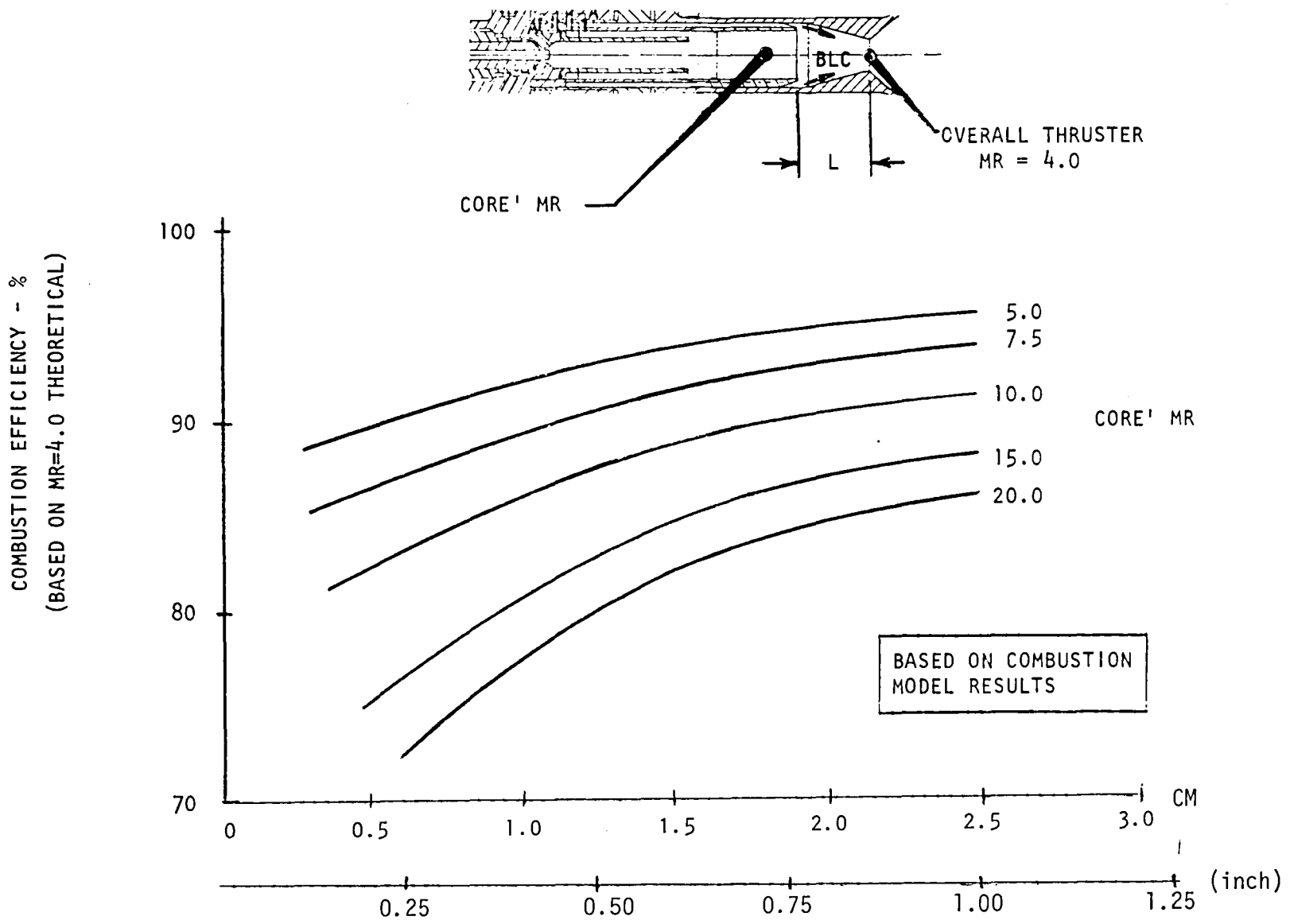

Figure 11. Dual-Sleeve Performance Trends With Boundary Layer Coolant Injection Location

A comparison of the combustion efficiency characteristics of both the first injection point (Fig. 10) and the second injection point (Fig. 11), shows a countering trend with core mixture ratio. Therefore, a composite combustion efficiency plot of the results from both the first and second injection points was generated and is depicted in Fig. 12. This composite performance plot indicates that the combustion performance efficiency with the dual-sleeve, triaxial injection system is maximized at a core mixture ratio of approximately 7.5. The predicted combustion efficiency utilizing an igniter mixture ratio of 50, a core mixture ratio of 7.5, and a throat or overall thruster mixture of 4 is greater than 92%, which exceeded the value necessary to meet the program minimum requirement.

Based on the combustion performance analyses discussed above, the relative performance capability of the three candidate injection/combustor concepts was determined and is presented in Fig. 13. For this comparative assessment, a maximum chamber throat temperature of 1644 K (2960 R) was established. As noted earlier, the large sleeve recess depth required to meet the program minimum performance requirement results in excessive wall temperatures at the chamber throat with the single-sleeve injection concept.

A maximum sleeve recess depth of 3.81 cm (1.5 in.) is indicated for a throat temperature of 1644 K (2960 R). Corresponding combustion performance values for this recess depth are 82 and 85% for a core mixture ratio of 50:1 and 30:1, respectively. This large performance deficiency relative to program minimum requirements, together with a lack of design flexibility for improving its performance capability during development testing, made the single-sleeve injection concept a high risk and, therefore, was not considered a viable configuration for this program.

A review of the performance and chamber wall cooling capabilities of the dual-sleeve (triaxial) design showed that the predicted performance level was within the range of program minimum performance requirements. Furthermore, design flexibility with this concept enabled propellant flows within the thruster to be varied for optimization of performance and cooling characteristics during development testing. The predicted effect of such flow variations on combustion efficiency within the secondary combustor is illustrated in Fig. 14.

The predicted combustion performance level of the dual-sleeve (hybrid) design also was within the range of program minimum requirements. A slightly higher capability is indicated with this hybrid dual-sleeve injection concept over that of the triaxial dual-sleeve concept because impingement of the secondary hydrogen with the primary core hot gases would result in improved mixing characteristics within the secondary combustor. However, because of the discrete location of the hydrogen injection orifices, the risk of chamber wall compatibility problems is greater than with the dual-sleeve, triaxial injection concept.

Based on the above combustion performance and chamber wall cooling considerations, the dual-sleeve, triaxial injection/combustor concept (Fig. 3) offered the best opportunity for meeting the overall program objectives and, therefore, was selected at the baseline injection'combustor configuration.

Propellant Thermal Control. Thermal control of the propellants within a cryogenic thruster is a key design consideration if pulse-mode minimum impulse bit

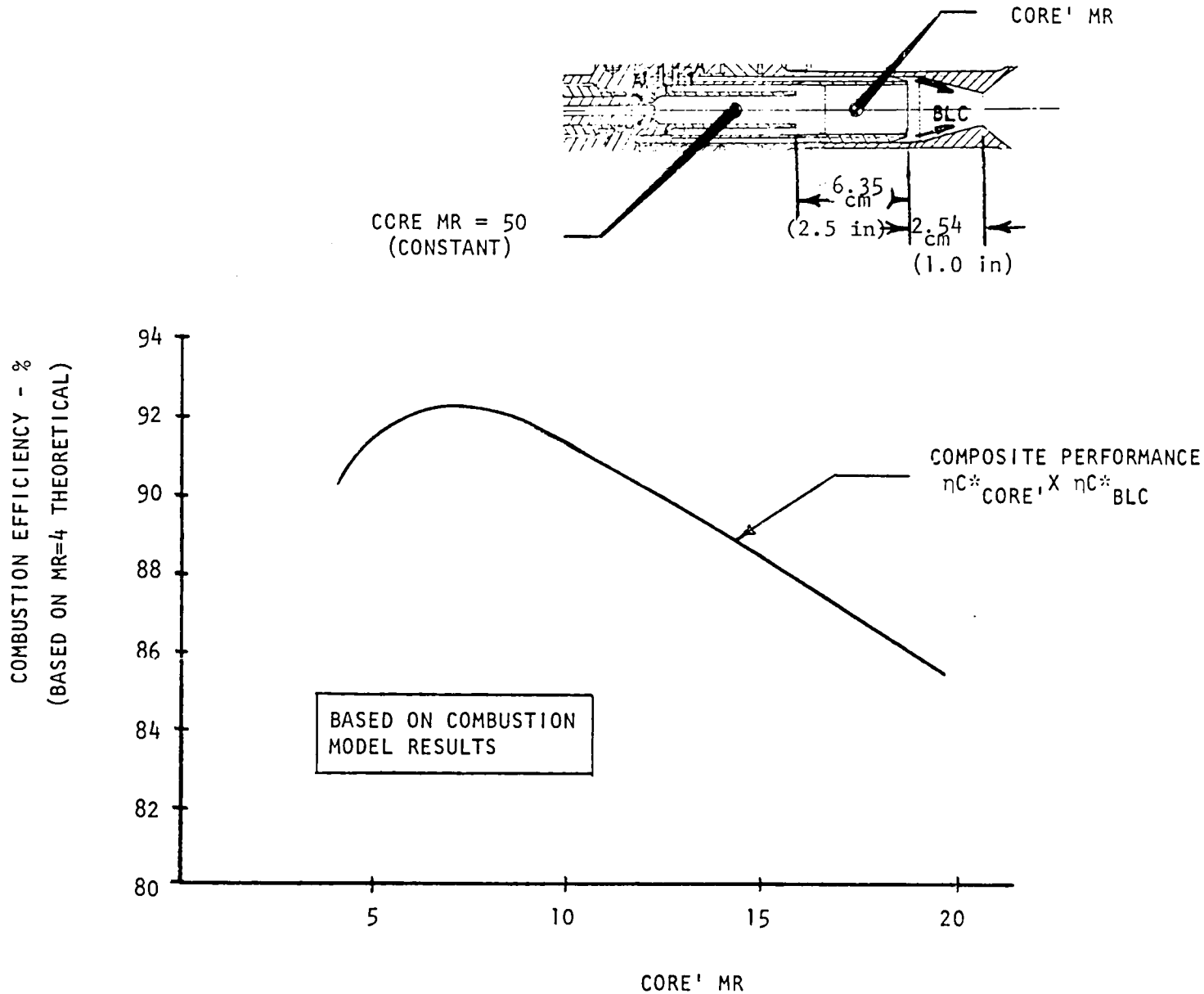

Figure 12. Dual-Sleeve Composite Performance Trends With Core' Oxidant-Fuel Mixture Ratio Variation

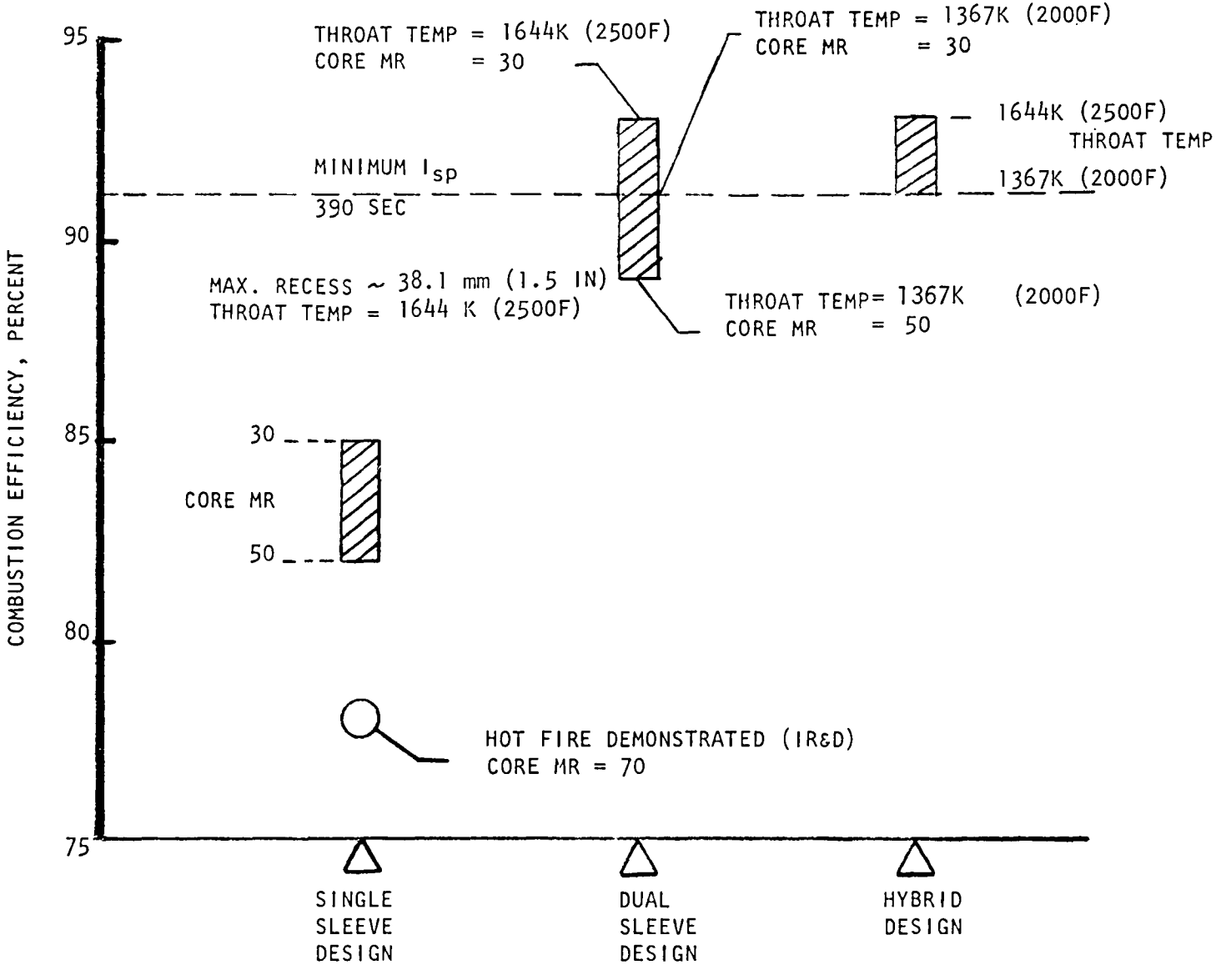

Figure 13. Relative Performance Capability of Candidate Injection Concepts

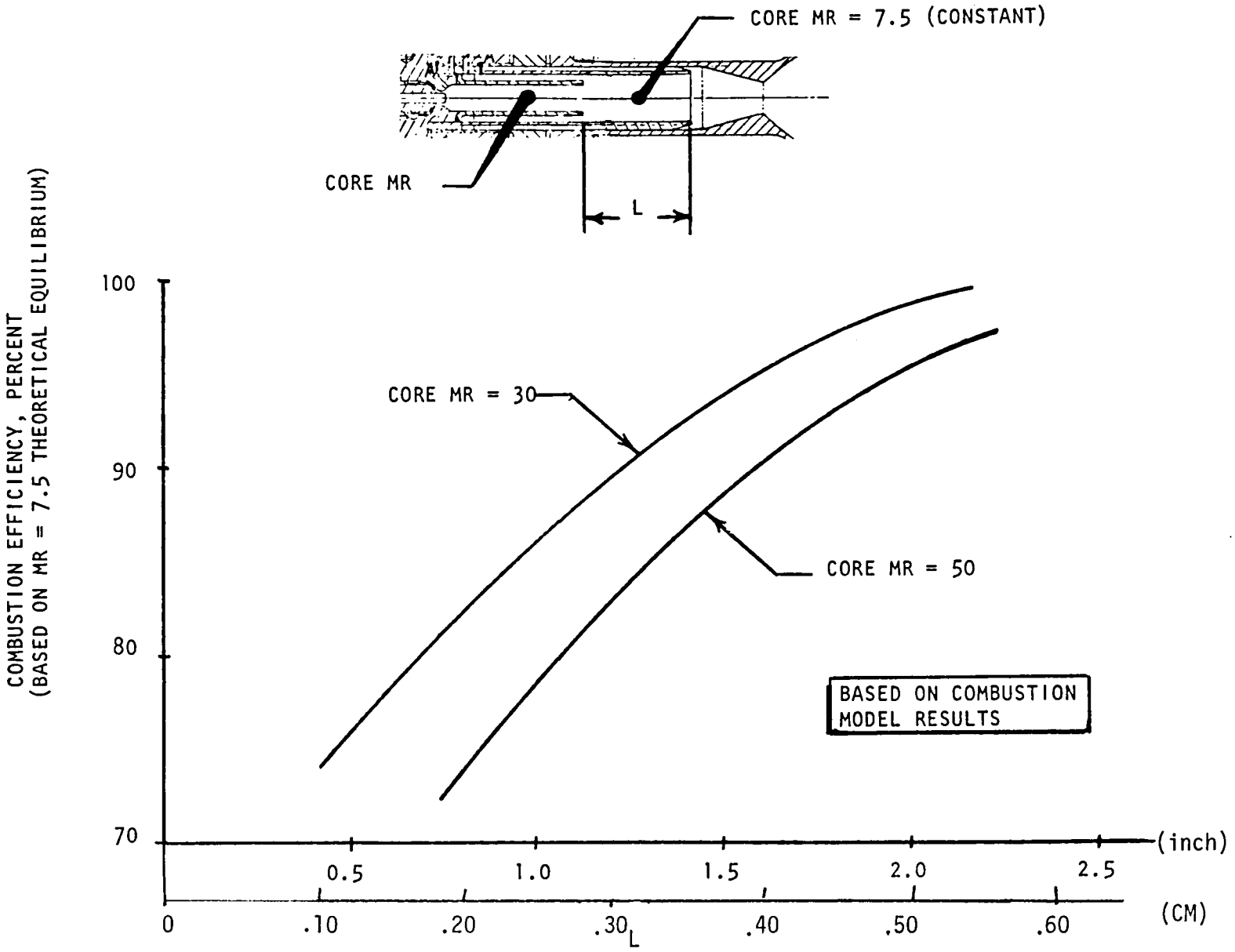

Figure 14. Dual-Sleeve Performance Trends With Secondary Combustor Length (L) Variation for Two Core Mixture Ratios

goals are to be realized. Therefore, parametric analysis were conducted for several candidate propellant manifolding thermal insulation systems.

Five thermal liner/insulator configurations for the propellant inlet manifold were evaluated and are shown in Fig. 15. For the configuration with the thin metallic liners, a two-dimensional thermal model was constructed and the thermal standoffs were assumed to be in intimate contact with 10% of the body area. For the other configurations, a one-dimensional model was used. The results of these analyses for the hydrogen manifold are presented in Fig. 16 through 20.

The magnitude of the heat flux is a direct measure of the heat input to the propellant. The heat fluxes at 5 msec (Fig.16) are high for all liner/insulator configurations. Only the thin-steel liner configuration resulted in a heat flux being a factor of 2 lower than the other configurations. After 5 msec, the wall material cools down and the heat flux correspondingly decays. Comparing the all-plastic and all-steel configurations, the hydrogen-side surface of the plastic responded more rapidly (low diffusivity), although a major portion (90% of the thickness) of the plastic remained essentially at the initial temperature.

At 100 msec (Fig. 16), the 0.013-cm (0.005-inch) steel liner with thermal standoffs in a plastic body resulted in a lower heat flux than the same liner in a steel body. This trend is due to the low thermal conductivity of the plastic retarding the conduction of the residual heat.

The heat flux distributions (shown in Fig. 16) were translated into hydrogen enthalpy increases for an assumed manifolding surface area of 1.29 cm^2 (0.2 $in.^2$), Fig. 17. The enthalpy increase profiles are similar to the heat flux profiles since the two parameters are directly proportional. Also, assuming a hydrogen outlet pressure of 138 N/cm^2a (200 psia), the ratio of the outlet-to-inlet hydrogen density was computed, as shown on the right side of Fig. 17. The initially high heat flux resulted in approximately a 75% density change for all configurations except the 0.013-cm (0.005-in.) steel liner configurations, where the density change is 40%. A large initial density change will tend to reduce the propellant flowrate and retard the thermal response. After 100 msec, all configurations resulted in a density change of 10% or less.

Parametric data of allowable propellant manifold surface area for a given propellant enthalpy increase or density ratio were developed for the heat fluxes corresponding to the 5-msec time slice (Fig. 18). These data show that to maintain a hydrogen density change of 20%, a surface area less than 0.690 cm^2 (0.107 $in.^2$) must be used for the assumed conditions.

Variations in heat input to the hydrogen with changes in propellant mass velocity and initial manifold temperature also were evaluated. As shown in Fig. 19, a 50% reduction in hydrogen mass velocity resulted in a 23% reduction in the peak enthalpy gain and a change in peak density change of 40 to 30% for the 0.013-cm (0.005-in.) steel liner configuration. For an all plastic configuration, a 50% reduction in mass velocity resulted in a 43% change in the peak enthalpy change which translated into a change in peak density change of 74 to 48%. After approximately 10 msec, the influence of the different mass velocities is negligible.

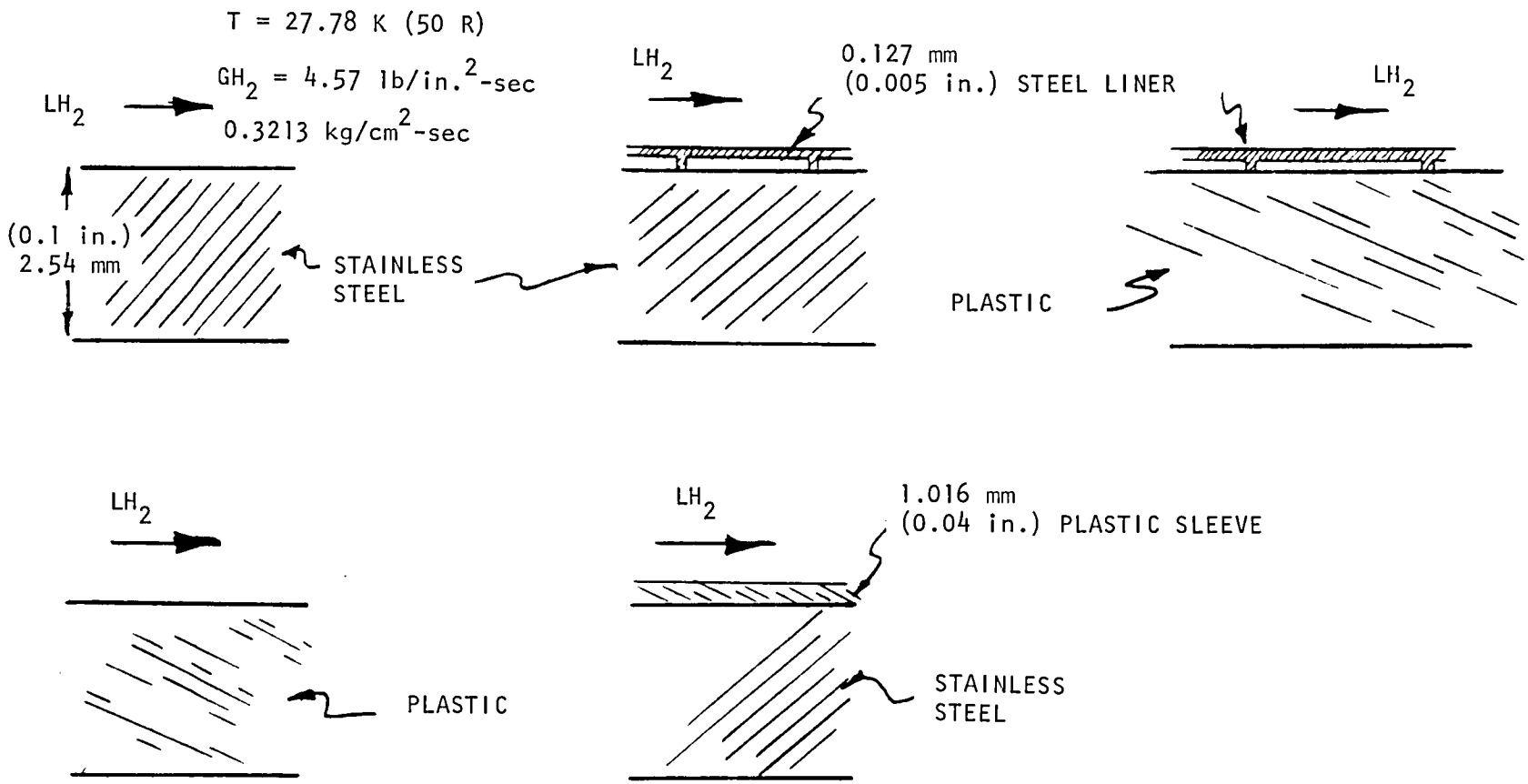

Figure 15 . Typical Thermal Liner/Insulation Concepts

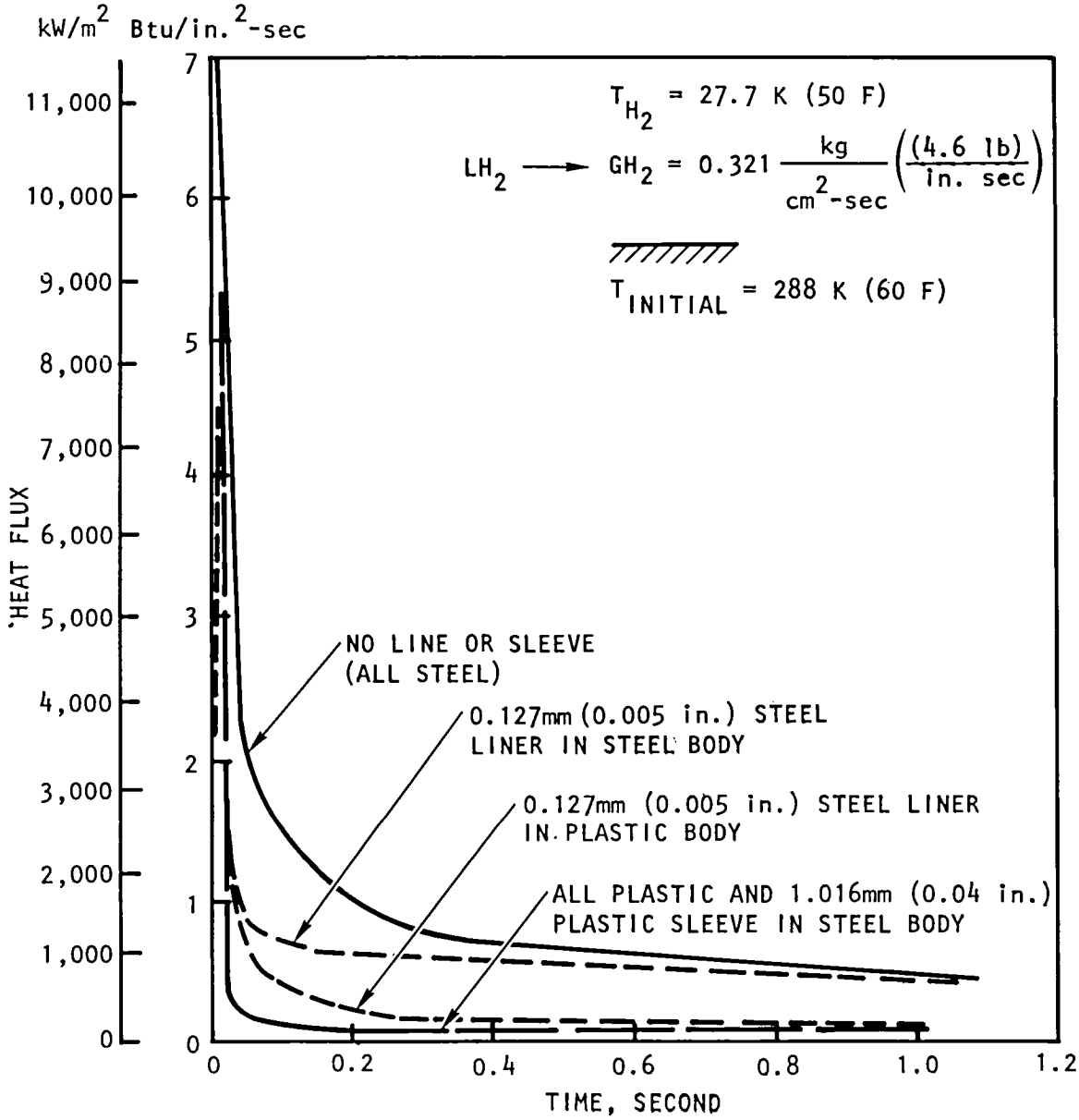

Figure 16 . Heat Flux Variation (0 to 1.0 second) of Five Thermal Liner/Insulator Configurations

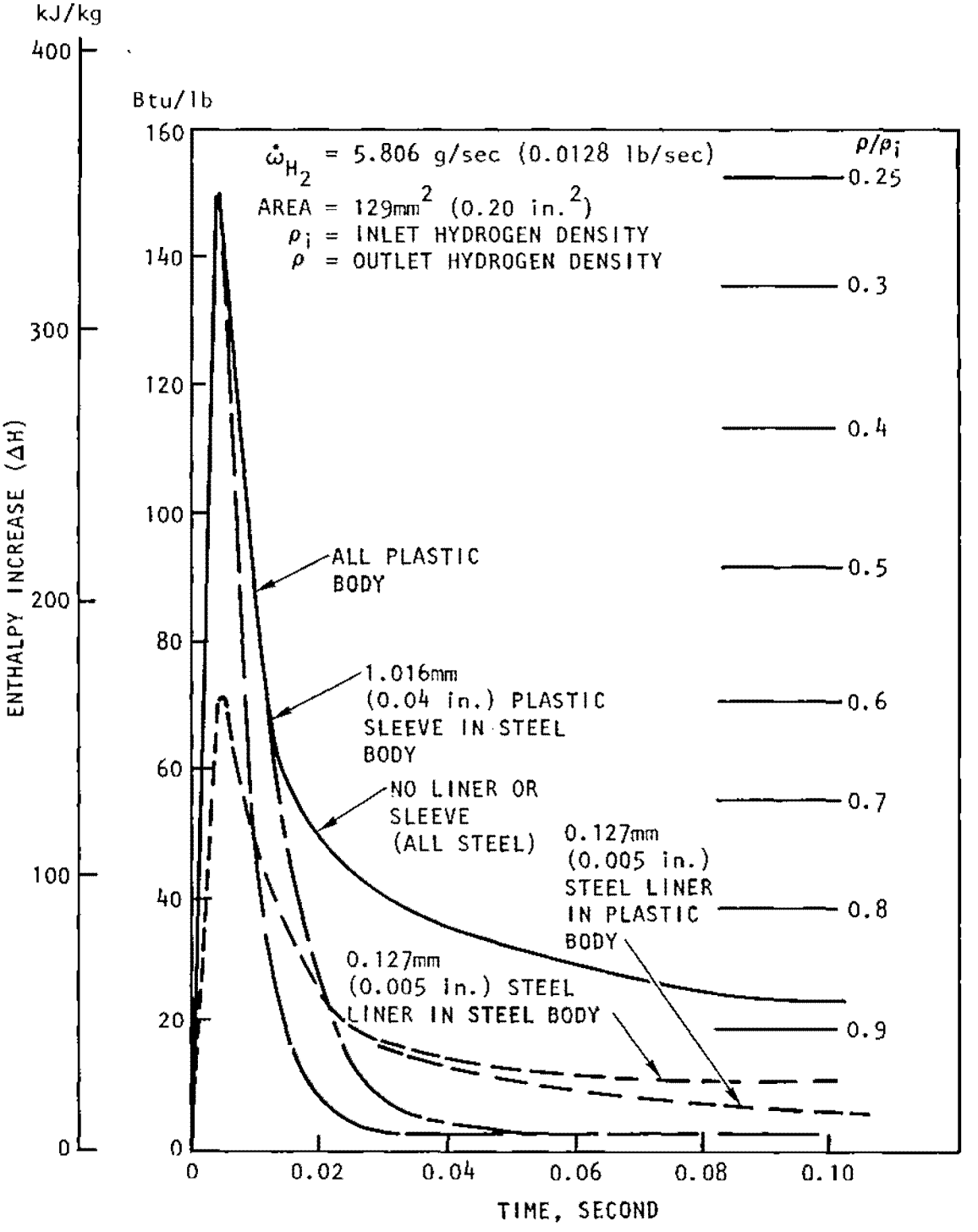

Figure 17. Hydrogen Enthalpy and Density Variation in the Propellant Manifold With Various Thermal Liner Configurations

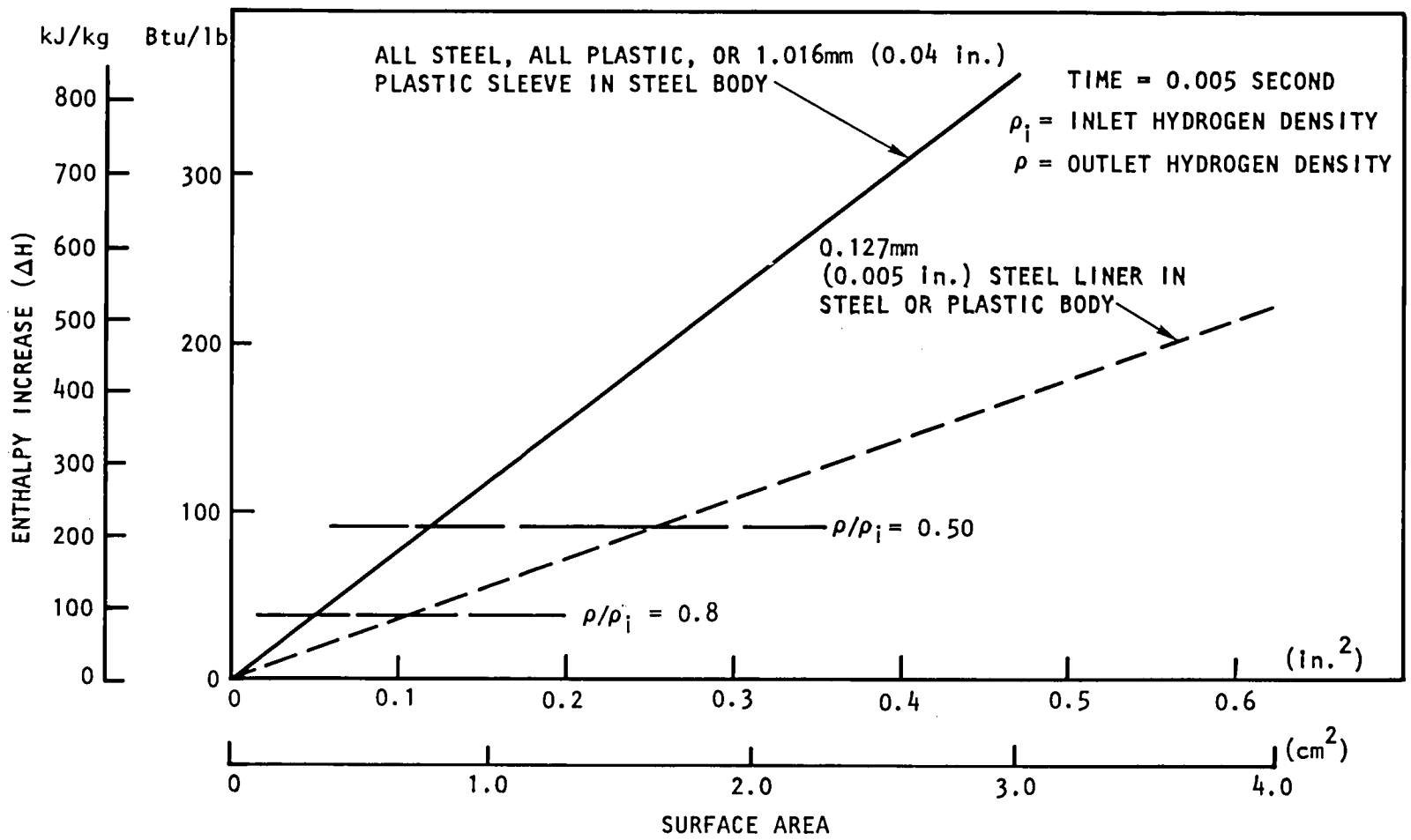

Figure 18. Propellant Enthalpy Increase With Hydrogen Manifold Surface Area for Two Thermal Liner/Insulator Configurations

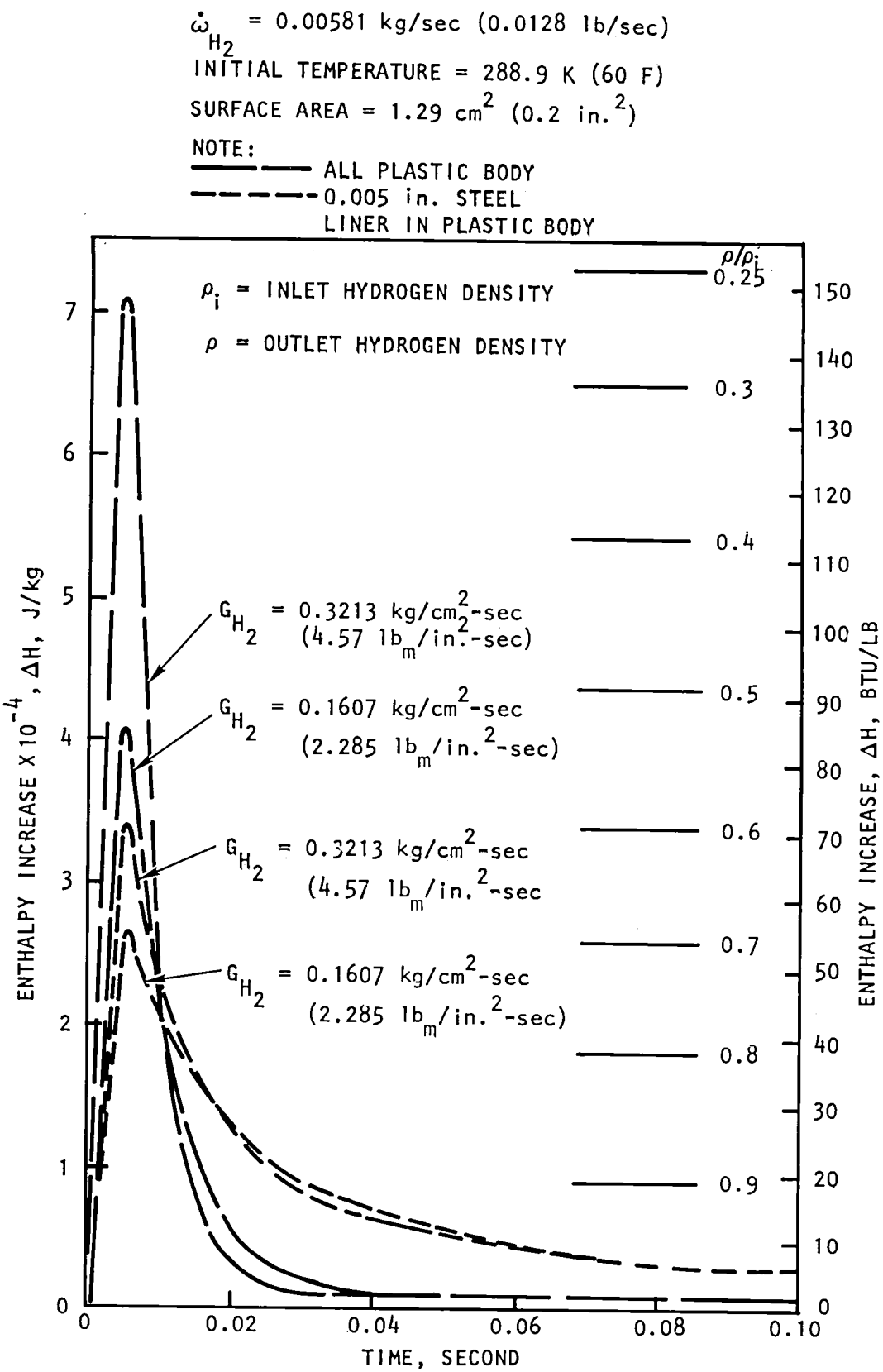

Figure 19. Hydrogen Enthalpy and Density Variation With Flowrate

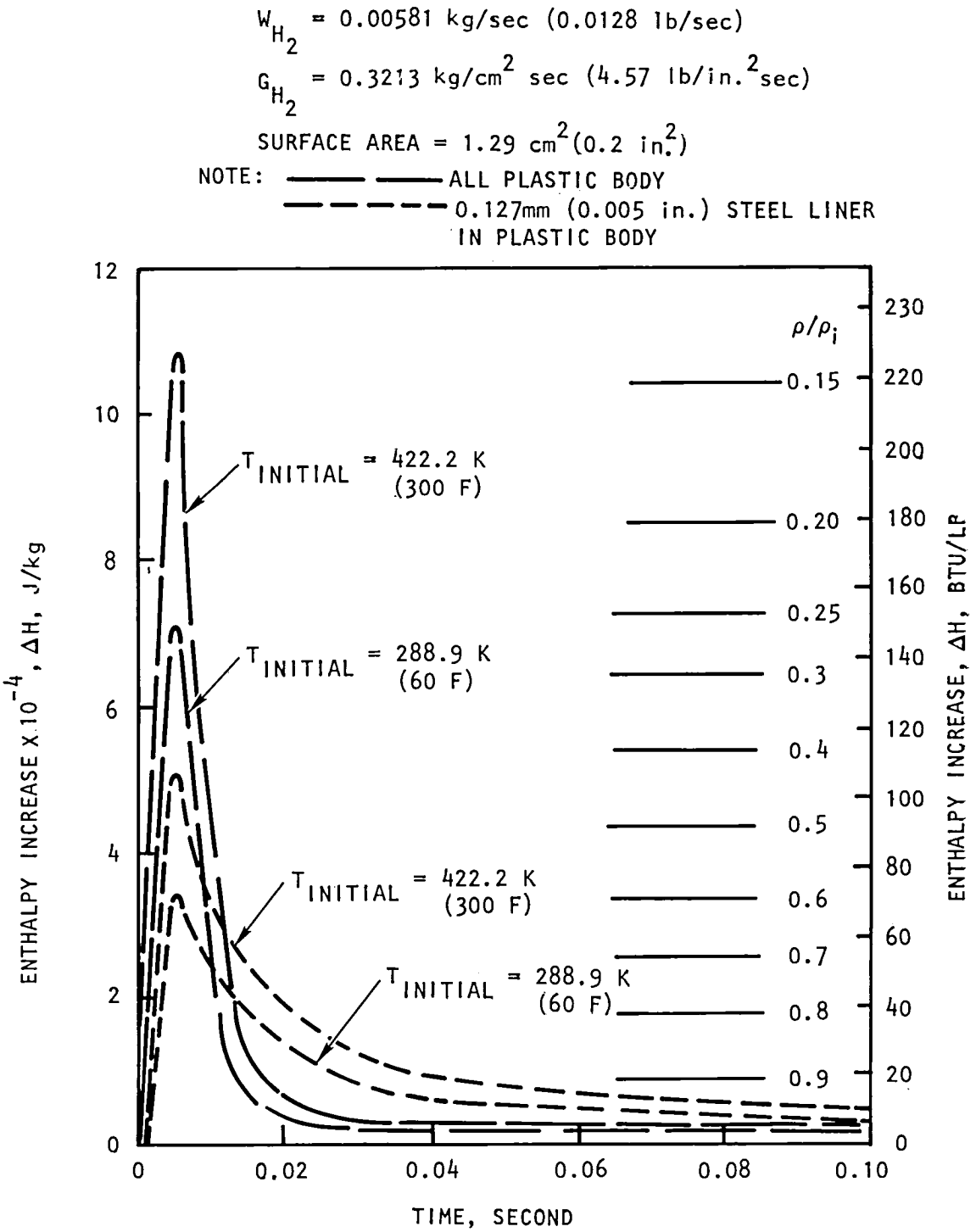

Figure 20. Hydrogen Enthalpy and Density Variation in the Propellant Manifold With Initial Hardware Temperature

The influence of the initial hardware temperature is presented in Fig. 20. For the thin metallic liner configuration, an increase in initial hardware temperature from 289 to 422 K (520 to 760 R) resulted in a 50% increase in peak enthalpy gain and a change in peak density change from 40 to 56%. The all-plastic configuration resulted in a 50% increase in peak enthalpy gain and a change in peak density change from 75 to 85%.

A similar propellant thermal analysis was performed on the oxidizer side. The enthalpy gain and resulting density change are shown in Fig. 21. With all-steel or plastic body, the analysis indicated two-phase oxidizer flow during the first 7 to 8 milliseconds, and with the 0.013-cm (0.005-in.) steel liner, an all-liquid condition with only a 3.5% density change.

These parametric thermal analyses indicate that a propellant manifold thermal insulation system that utilizes a thin-walled 0.013-cm (0.005-in.) metallic liner is relatively insensitive to variations in propellant mass velocity and initial hardware temperature, and has superior insulative characteristics, which results in minimum heat input to the propellant during the critical initial flow period. Therefore, this system was selected as being most favorable for small cryogenic thruster application. In addition, as illustrated in Fig. 22, critical propellant/coolant flows are metered at a location within the hardware which results in a common pressure/thermal environment, thus further desensitizing the thruster to any thermally induced flow unbalance caused by variable mission duty cycles.

Combustion Stability

The dual-sleeve injection/combustor configuration was evaluated for the purpose of identifying any potentially hazardous combustion instability modes. Feed system-coupled stability problems occur when one or more of the propellant feed systems couple with the combustion process. For a system to be unstable, the closed-loop gain must be greater than 1 and have positive feedback. The closed-loop gain is the product of the gains of combustion chamber pressure to feed system flowrate and feed system flowrate to combustion chamber pressure. The phase shift is generated by system responses and the combustion burning rate. Therefore, when analyzing a system, the feed system gain, the combustion process gain, and the combustion burning rate all need to be evaluated to determine if all three may occur at a specific frequency to generate an instability.

The dual-sleeve thruster configuration has three locations where propellant is injected. All of the oxidizer is injected at the inlet end where it is burned with a small amount of fuel at a mixture ratio of 50. About half way down the combustor, additional fuel is injected, reducing the mixture ratio to 7.5. Near the throat, additional fuel is injected as boundary layer coolant for the throat and nozzle regions. Each of these injection regions was assessed relative to their potential for feed system-coupled stability problems.

Primary Injector. At this location, all of the oxidizer and sufficient fuel is injected to react with only 16% of the oxidizer (MR = 50). This results in a gain from the oxidizer reaction which is substantially lower than for a combustion process having a mixture ratio near stoichiometric, and has a stabilizing influence relative to feed system-combustion process coupling.

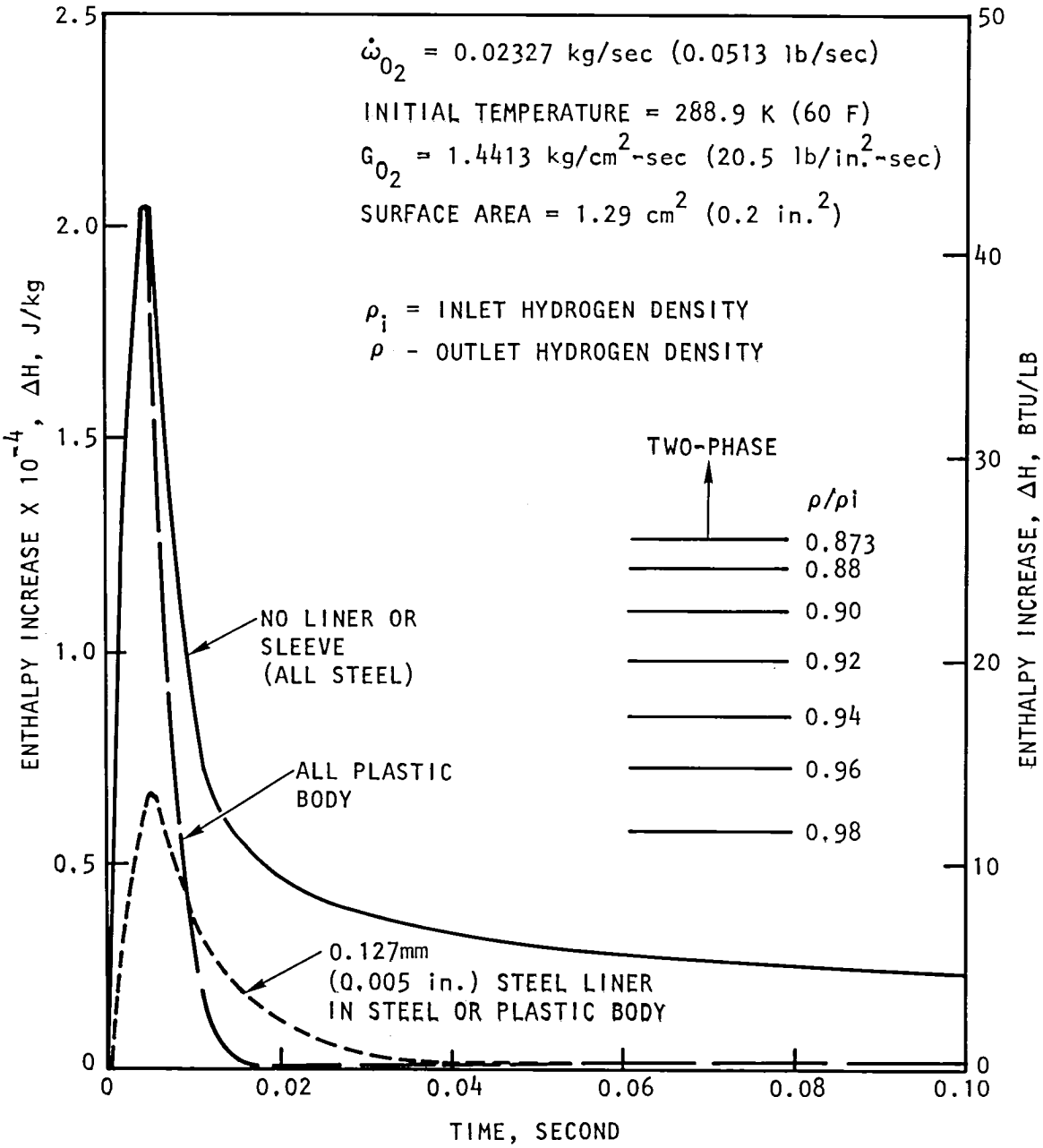

Figure 21. Oxygen Enthalpy and Density Variation in The Propellant Manifold With Test Duration

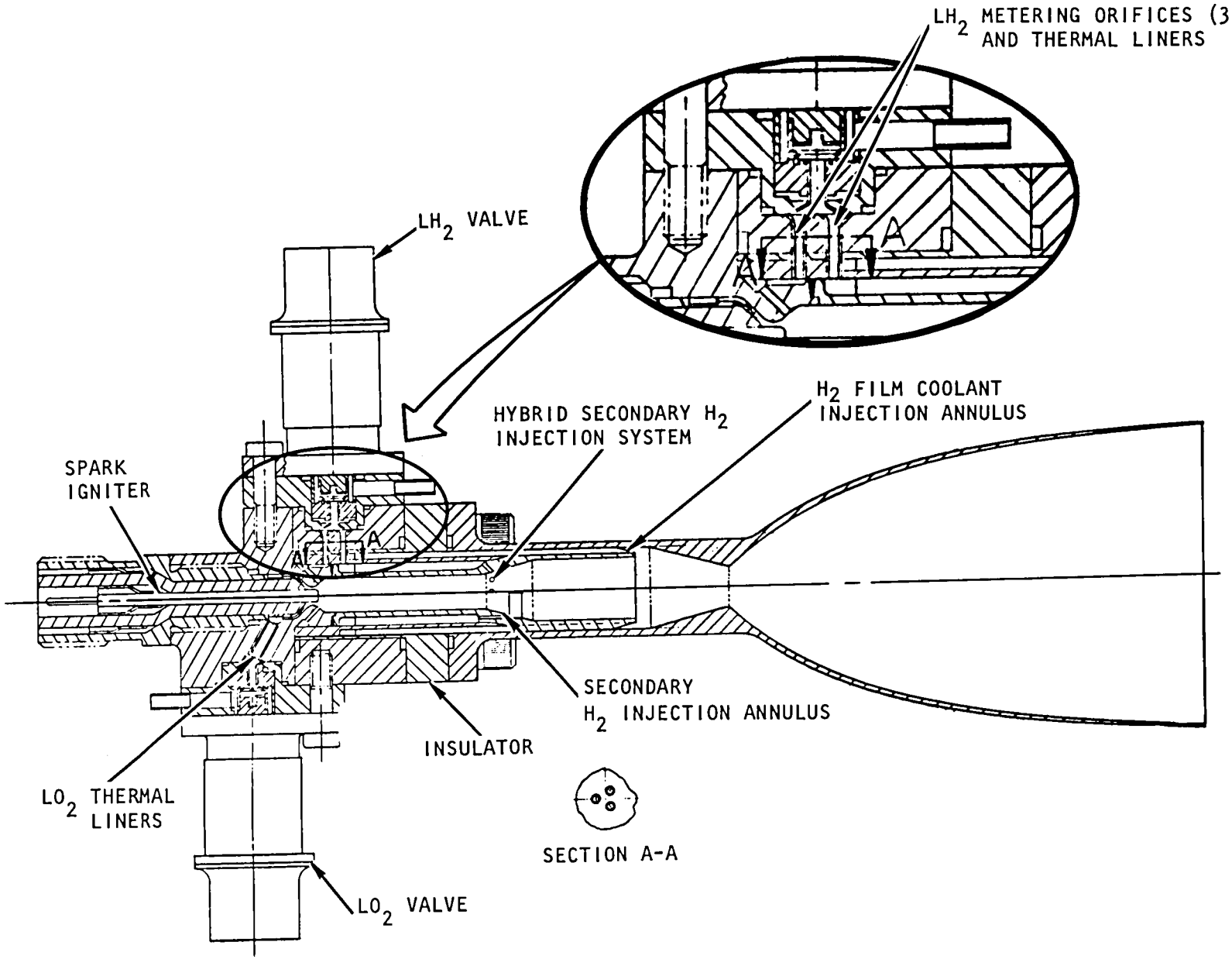

Figure 22. Dual-Sleeve/Hybrid Thruster Configuration

At the nominal mainstage operating conditions, the primary injector presusre drops are approximately 25% of chamber pressure; this value has been shown to provide adequate margin against feed system coupling in previous combustors. In addition, the system response characteristics between the valves and the chamber are very fast due to the small injector volumes and liquid propellants (over 10,000 Hz "break" frequencies). Consequently, the injector flowrate cannot oscillate without the valve flowrate oscillating for frequencies below 10,000 Hz. The valve pressure drop, therefore, adds damping to the system in the same manner as injector pressure drop, and can be considered equally effective. This results in a total effective system pressure drop of 47% of chamber pressure for frequencies up to 10,000 Hz.

To determine the frequency range in which coupling could occur, an estimate of the oxidizer injection time delay was made. Using an impingement distance of 0.23 cm (0.09 in) and injection velocity of 3.66 m/sec (12 ft/sec), the time to impingement is 6.25×10^{-4} seconds. Since burning cannot occur until impingement occurs, a typical range of potential time delays is from one to three times the time to impingement. In addition, to provide the positive feedback necessary for a feed system-coupled instability, the injection time delay needs to contribute approximately 180 degrees of phase shift. Therefore, the highest frequency at which the oxidizer side could couple is 800 Hz $[1/(2 \times 6.25 \times 10^{-4})]$ and the lowest frequency is approximately 270 Hz. Over this frequency range, the injector valve pressure drop provides effective damping. On the fuel side, the range of frequency over which coupling could occurs is 800 to 2400 Hz. Because these frequencies are well below the injector break frequency of 10,000 Hz, the injection/valve pressure drop also will provide effective damping on the fuel side. Therefore, there is a high margin against any feed system-coupled instability with the primary injector for liquid/liquid propellant injection.

Under two-phase propellant flow conditions, a lower system response would exist because the acoustic velocity can decrease by an order of magnitude, thus reducing the injector "break" frequency below 1000 Hz. This could remove the valve pressure drop as an effective damping source to the system. However, the density of propellants under two-phase flow conditions would be decreased and result in an increased injector pressure drop for improved system damping. This effect, together with the fact that only a small portion of the oxidizer is actually reacting in the primary combustor, virtually ensures that coupling at the primary injector will not occur even under two-phase propellants flow conditions.

Similarly, acoustic instability modes are unlikely with the primary injector because the resonant frequencies of the tangential and radial modes are sufficiently high to preclude the burning rate from sustaining unstable operation. The first longitudinal mode has the lowest resonant frequency of approximately 7500 Hz. HOwerver, the main injector mixture ratio of 50:1 results in only a small portion of the primary injector flowrate actually reacting and, consequently, an equivalent reduction in the amount of energy release available to support any unstable operation.

Secondary Injector. At this location, enough fuel is injected (2.633 g/sec; 0.0058 lb/sec) to reduce the overall mixture ratio from 50:1 to 7.5:1. Because

the thrust chamber first longitudinal mode has a pressure node near the secondary fuel injector, significant coupling cannot occur with this longitudinal mode. Potential coupling could occur with the thrust chamber second longitudinal mode (frequency about 15,000 Hz). However, for coupling to occur at this frequency, a combustion time delay of 3.3×10^{-5} seconds is required. Because this time delay represents only the first 0.05 cm (0.02 in.) of the secondary chamber, only a small quantity of fuel will react with the oxidizer-rich hot gas at this rate. Therefore, coupling with the thrust chamber second longitudinal mode should not occur because of the inability of the secondary injector combustion process to support such a high frequency.

Boundary Layer Coolant Injector. The remaining fuel (2.724 g/sec; 0.0060 lb/sec) is injected a short distance upstream of the thrust chamber throat for boundary layer cooling of the throat/nozzle regions and to reduce the overall mixture ratio from 7.5:1 to 4.0:1. Because the hot gas from the secondary combustion chamber is at a mixture ratio below stoichiometric, no additional reaction with the fuel boundary layer coolant occurs. Therefore, combustion process responses which are necessary to support a feed system instability do not exist at the boundary layer coolant injector.

Based on the above assessment, a considerable feed system and acoustic stability margin was projected for the baseline dual-sleeve injection/combustion configuration.

Ignition System

A study to establish design guidelines for a spark ignition system which is applicable to small cryogenic O_2/H_2 propellant thrusters was conducted. The spark plug/gap geometry is a key design issue because it has a direct influence on the hydraulic behavior of the primary injection system, spark plug energy level, and electrode life. The Advanced Space Engine (ASE), oxygen-rich, spark-torch igniter configuration, which demonstrated satisfactory ignition during an earlier company sponsored 111 N (25 pound) thruster program was utilized as a design baseline for this study. Several design deficiencies were identified relative to the adaptation of the baseline ASE igniter configuration for a small cryogenic thruster. Figure 23 illustrates both the baseline ASE igniter and a candidate igniter configuration for the current IAPS thruster development program. A major design deficiency which was corrected with the candidate igniter configuration involved a large trapped propellant volume and electrode geometry. The candidate configuration results in a reduction in oxidizer trapped volume from 1.392 cm^3 to 0.213 cm^3 (0.085 $in.^3$ to 0.013 $in.^3$) over that of the ASE baseline configuration. In addition, the electrode diameter was reduced from 0.51 cm to 0.25 cm (0.20 in. to 0.10 in.).

An ignition system having the following design features was selected:

Spark Type - Inductive
Spark Energy - 10 MJ (nominal)
Spark Rate - 100 Hz (nominal)
Electrode Material - Nickel 200
Electrode Spacing - 0.062 cm (0.025 in.)

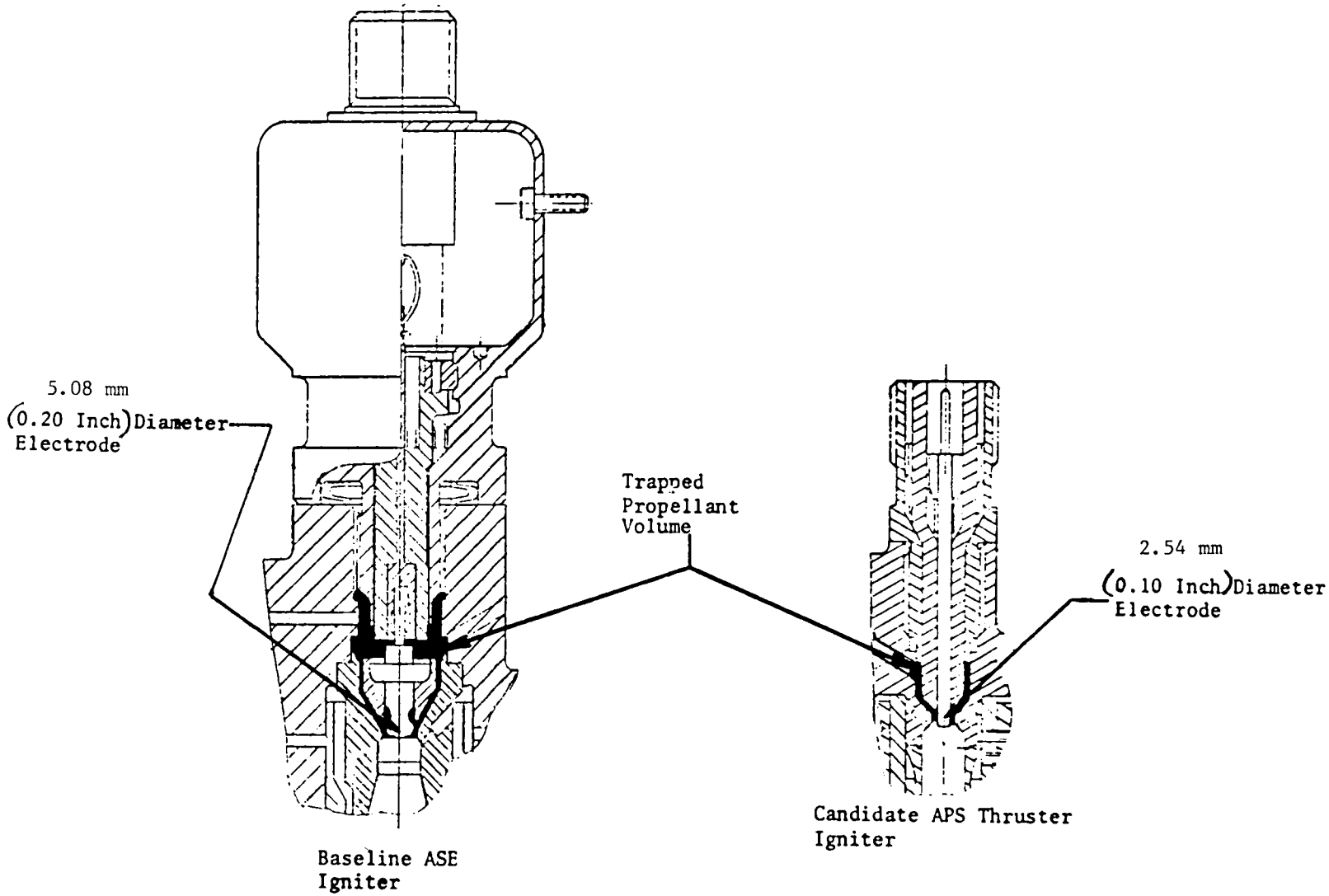

Figure 23. Spark Igniter Configurations

Rationale for selection of these design features is presented below:

Spark Type. Two types of spark exciters are in common use, capacitive discharge and inductive discharge. The electrical systems for these two spark types are illustrated by the block diagram in Fig. 24. The capacitive system requires four to five power-conditioning functions, whereas the inductive system requires only two. Thus, from a circuit complexity standpoint, the inductive type is more attractive. Second, the high-voltage transformation/energy storage function can usually be performed with a single transformer in the inductive system, whereas several discrete components are required for the same function in the capacitive system. This both reduces component count, and narrows the areas where intermediate or high voltages must be handled.

When the above circuit advantages of the inductive system are combined with the potential for reduced spark energy levels, the capability for compact exciter packaging can be realized. In practice, the inductive exciter conditioning electronics and high-voltage transformer can readily be packaged with the spark plug as an integral unit.

An additional advantage of an inductive spark type over a capacitive spark type is illustrated in Fig. 25, and lies in its inherent spark wave form. The sustained nature of the inductive spark wave form provides for a greater period for ignition than with the arc-type nature of the capacitive spark wave form. This inductive spark characteristic is a decided advantage for pulse-mode thruster application.

Spark Energy. A limited data base existed relative to the definition of the minimum spark energy level for oxygen plasma generation. Ignition tests on the SSME program have demonstrated O_2/H_2 ignition at energy levels as low as 0.5 to 10 mJ. From these tests, it was decided to operate the SSME integral exciter at 10 mJ. Test on the ASE program and on an IR&D small thruster development program have demonstrated oxygen plasma ignition at 100 mJ. During an earlier extended temperature range ACPS thruster investigation (Contract NAS3-16775), successful ignition with a plasma-torch igniter was reported at an energy level down to 10 mJ.

To provide further information in this area, and to evaluate other ignition system parameters, an in-house test program was conducted. A series of ambient temperature and cryogenic temperature tests with variable energy settings were performed in a GN_2/LN_2 environment over the operating conditions typical of a small crogenic thruster. These data substantiated the 10 mJ base for the "optimum" spark energy. Final verification of the minimum igniter spark energy level was established under actual hot-fire conditions during the experimental phase of this program.

Spark Rate. The minimum repeatable impulse goals of a thruster dictate that ignition delay must be minimized. For pulse widths of 50 ms, this implies that the minimum time between sparks should be less than 5 ms to avoid significant ignition delay. This, in turn, implies that, for the typical inductive current and voltage wave form of Fig. 25, the spark frequency should be in the range of 100 to 200 Hz.

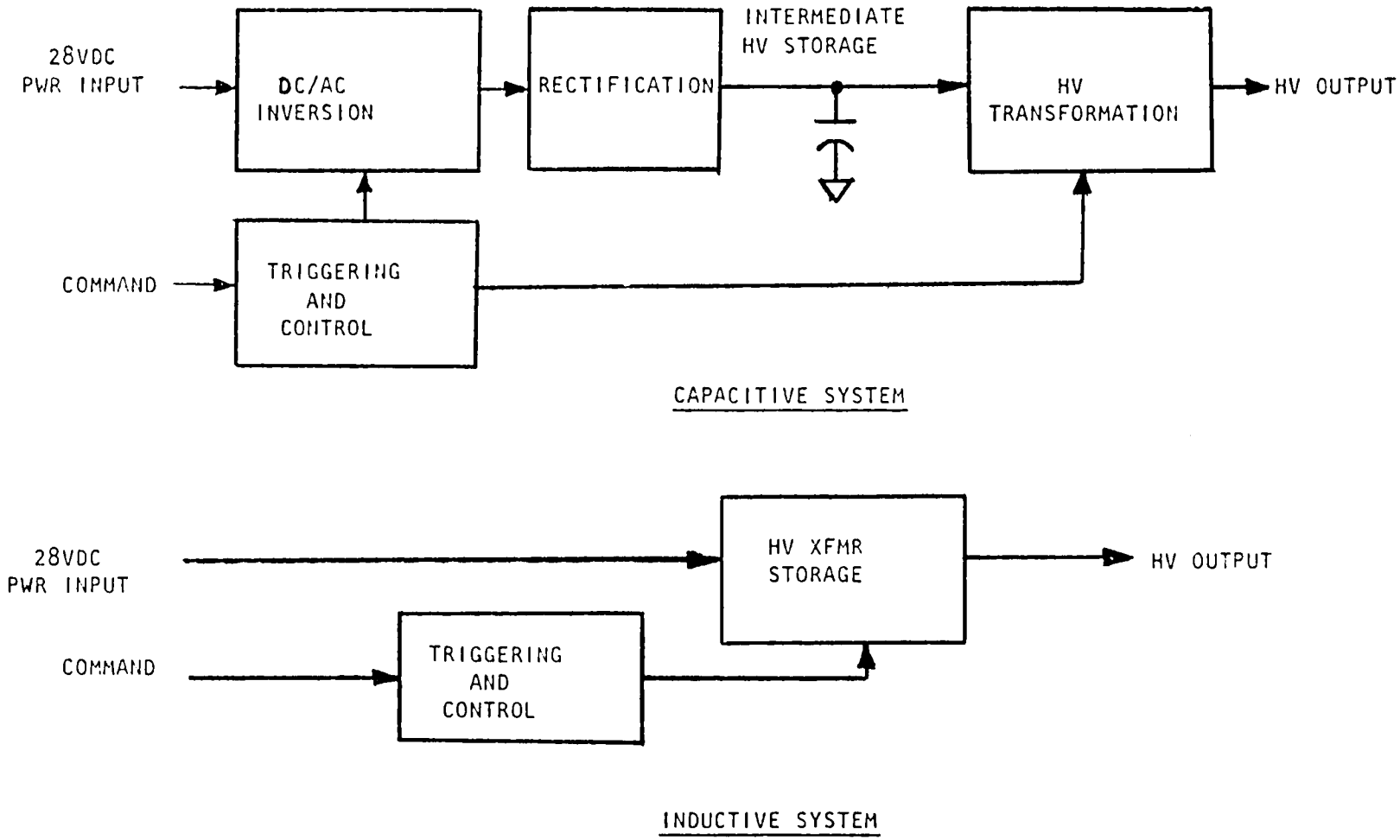

Figure 24. Typical Spark Exciter Systems

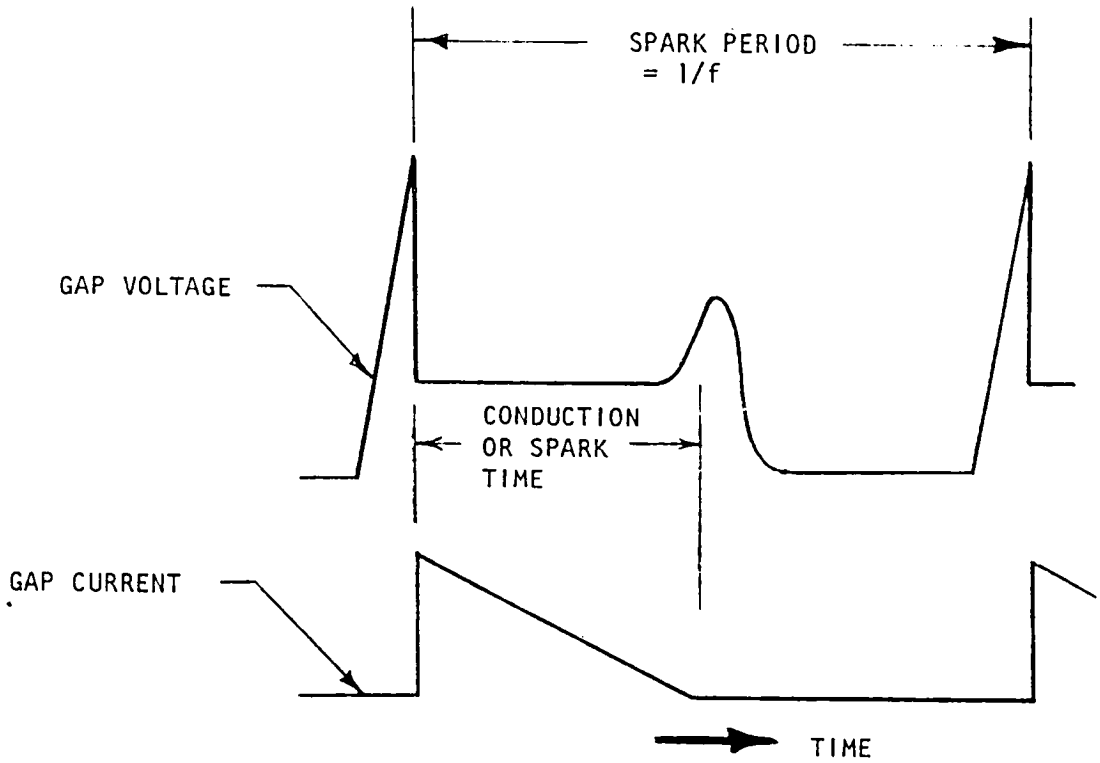

TYPICAL INDUCTIVE WAVEFORM

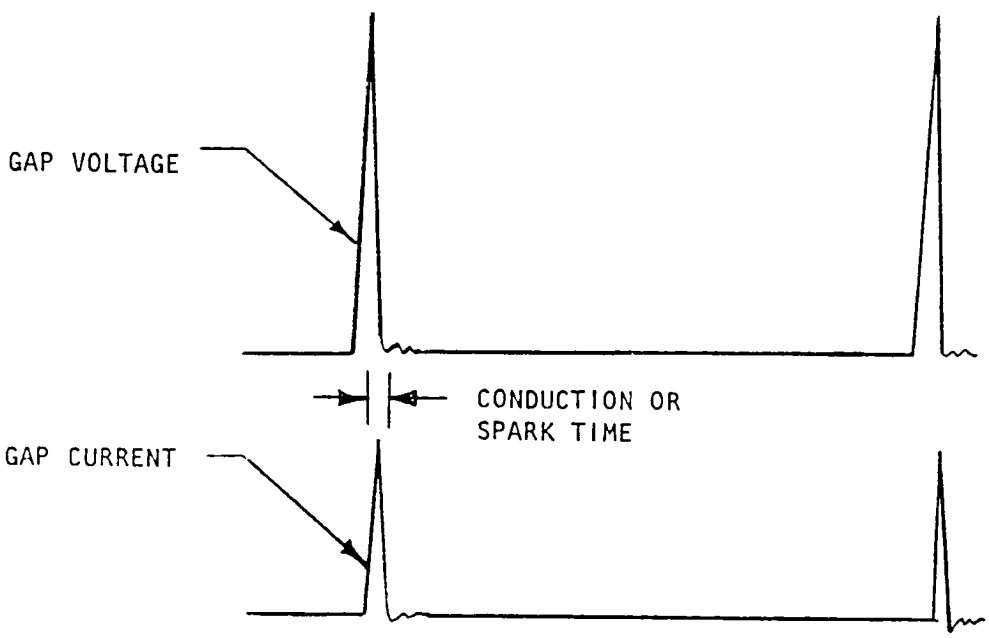

TYPICAL CAPACITIVE WAVEFORM

Figure 25. Spark Waveform Comparison for Equal Spark Rates and Total Energy per Spark

Electrode Material. With inductive-type spark discharge systems having a spark current in the range of 1 to 100 mA, electrode materials have only a slight influence on the gap current and voltage characteristics. Because most common electrode metals exhibit an electrode drop on the order of 20 to 50 V, this potential variation is not significant in comparison to a typical gap sustaining voltage of 500 V. Thus, electrode materials can be selected on the basis of material compatibility, cost, life, or mechanical properties rahter than for their electrical characteristics. Because both the gap current and projections of electrode temperatures are low, Nickel 200, 304 CRES, and Inco 625 all were candidate materials for this application. However, because of the substantial experience with Nickel 200 electrode material, this was selected as the baseline material for the thruster assembly.

Electrode Spacing. Some general guidelines were established to assist in the selection of gap spacing. A small gap is desirable in that the voltage required to break the gap down varies directly with the spacing. Thus, the problems of generating and handling high voltages is lessened. Unfortunately, excessively small gaps introduce machining tolerance difficulties and are subject to contamination and fouling. Considering that radial tolerance control of 0.005 cm (0.002 in.) is readily attainable, a nominal minimum gap aof 0.063 cm (0.025 in.) appeared reasonable. This will result in a tolerable variation in gap dimension of [8%. At a nominal pressure of 2 atm, 140 V per 0.0025 cm (0.001 in.) is required for gap breakdown. Thus a gap of 0.062 cm (0.025 in.) would require 3.5 kV to break down. Assuming that voltages over approximately 10 kV begin to introduce conditioning difficulties, it appears that the nominal gap spacing of 0.062 cm (0.025 in.) is favorable for end-item thruster application.

In addition to the establishment of the above ignition system hardware design guidelines, an analysis was conducted to determine the acceptable propellant inlet temperature range to ensure both satisfactory ignition and preclude hardware overheating. A conservative upper mixture ratio (o/f) limit for satisfactory cryogenic propellant ignition was selected to be approximately 100, based on a review of the literature and earlier IR&D thruster results. The lower mixture ratio limit, which is dictated by hardware heat load considerations, was selected at 30. Igniter mixture ratio behavior with propellant inlet temperature variation is illustrated in Fig. 26. Both the oxygen and hydrogen propellant flowrates to the igniter decrease as the temperature of the propellants increase. An increase in oxygen temperature, therefore, decreases the igniter mixture ratio and, in the limit, would result in hardware overheating. As illustrated in Fig. 26, a significant shift in igniter mixture occurs as the oxygen temperature approaches the two-phase regime. A design goal, therefore, was to limit the heat input to the oxygen propellant to approximately 46.5 J/g (20 Btu/lb) to avoid the two-phase flow regime. However, a heat input of twice this value still resulted in an igniter mixture ratio of 30 with a liquid oxygen quality of 75%. While this provides a degree of margin, operation in the two-phase regime is somewhat unpredictable and should be avoided.

A shift in igniter mixture also occurs due to hydrogen temperature variations; however, as illustrated in Fig. 26 , an increase in hydrogen temperature increases the igniter mixture and, in the limit, would result in a nonignitable

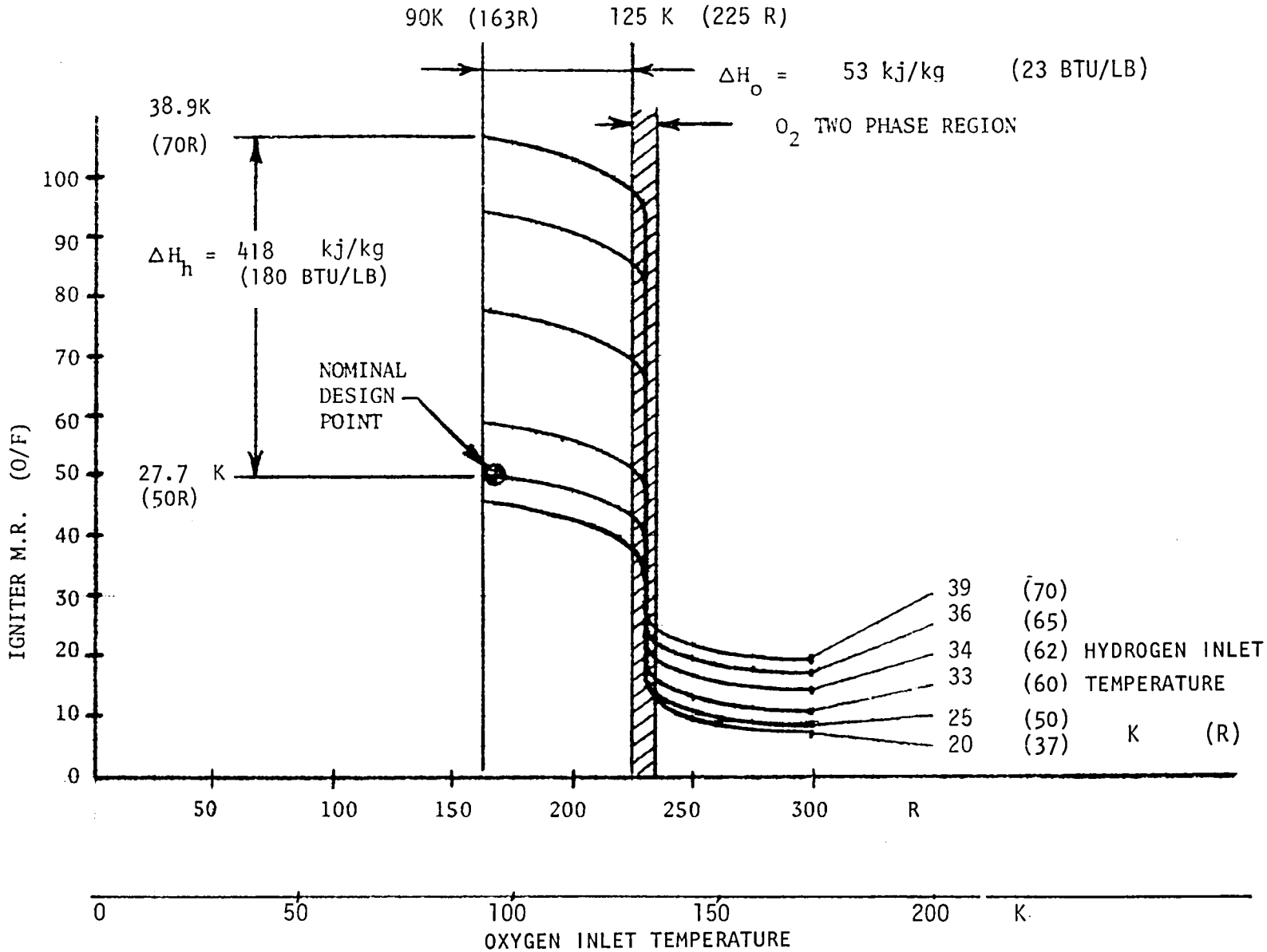

Figure 26. Igniter Mixture Ratio Behavior With Propellant Temperature Variation

condition. A design goal, therefore, was to limit the heat input to the hydrogen propellant to less than 419 J/g (180 Btu/lb) during all anticipated mission duty cycles mixes. Thermal control insulation systems within the thruster propellant manifolds were therefore selected to preclude start transient propellant temperature rises that exceed these limits to ensure satisfactory propellant ignition and minimize the risk of hardware overheating.

Chamber/Injector Cooling

The three basic cooling techniques employed for each of the candidate thruster injection systems are illustrated in Fig. 27. The major portion of the cylindrical portion of the fuel with one (single-sleeve design) or two (dual-sleeve and hybrid design) sleeves. The remaining portion of the combustion chamber and nozzle is cooled using a combination of film and radiation cooling.

The gas-side heat transfer coefficient for the cylindrical portion of the combustion chamber was calculated using the Bartz relationship and applying a 20% safety factor. The coefficient 8.978×10^{-6} kcal/cm^2-sec-K (0.001277 Btu/in.^{2} -sec-R) was assumed constant along the length of the combustor. For all candidate thruster configurations, the full core mixture ratio combustion gas temperature was used and, for the second sleeve of the dual-sleeve design, the film-cooling influence of the injected fuel was neglected to provide conservative heat transfer results.

The gas-side heat transfer coefficient distribution (Fig. 28) for the remaining portion of the combustion chamber and the nozzle was determined using the Rocketdyne boundary layer computer program that utilizes an integral solution of the momentum and energy equations.

Single-Sleeve Injection Design. A detailed thermal analysis of the convectively cooled inner sleeve for the single-sleeve injection design (Fig. 2) was performed. A slotted nickel sleeve with a 0.076-cm (0.03-in.) wall thickness was evaluated. For the 50-to-1 core mixture ratio, gas-side wall temperature distributions were obtained for coolant slot depths varying from 0.10 to 0.25 cm (0.04 to 0.10 in.) with a 0.10-cm (0.04-in.) slot width and sleeve lengths up to 7.6 cm (3.0 in.), Fig. 29. The sharp transition in the axial wall temperature distribution is the result of suddenly changing from the liquid to the gaseous hydrogen coolant correlation at a fixed value of coolant temperature. In reality, this transition will occur over a range of temperature and the wall temperature variation would be more gradual. Sleeve coolant pressure drops with variation in sleeve length and coolant slot depths are presented in Fig. 30. These data indicate that wall temperatures of less than 700 K (800 F) are readily obtainable with coolant pressure drops below 3.45 N/cm^2 (5 psi). The influence of core mixture ratio on sleeve cooling for the single-sleeve design is discussed in the dual-sleeve cooling analysis.

Film cooling thermal analyses were performed for the chamber wall region immediately downstream from the exit of the inner core sleeve. Wall temperature distributions for various film coolant injection locations were obtained, assuming a 0.25-cm (0.10-in.) coolant slot height, a core mixture ratio of 50 to 1, an overall mixture ratio of 4 to 1, a 2.2 to 1 chamber contraction ratio, and a 85% film-coolant efficiency. In these analyses, the gas-side conditions

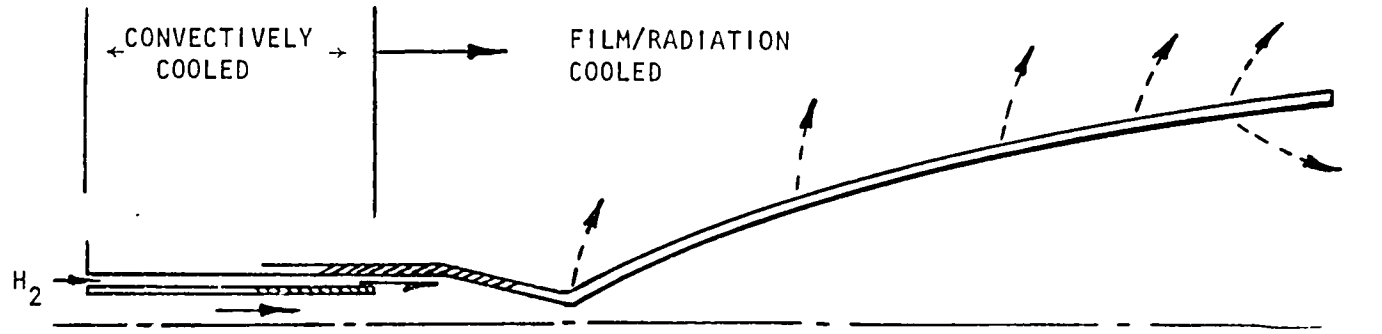

SINGLE SLEEVE DESIGN

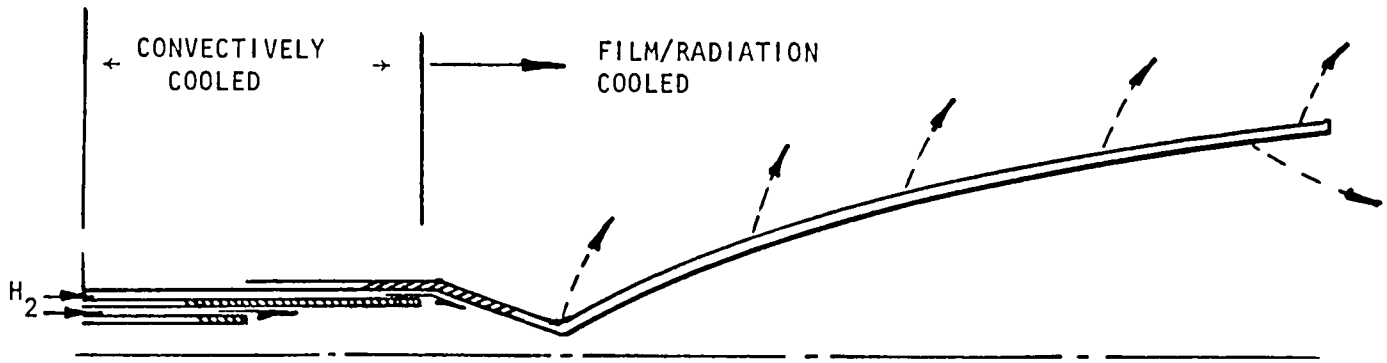

DUAL SLEEVE AND HYBRID DESIGNS

Figure 27. Thrust Chamber Cooling Approach

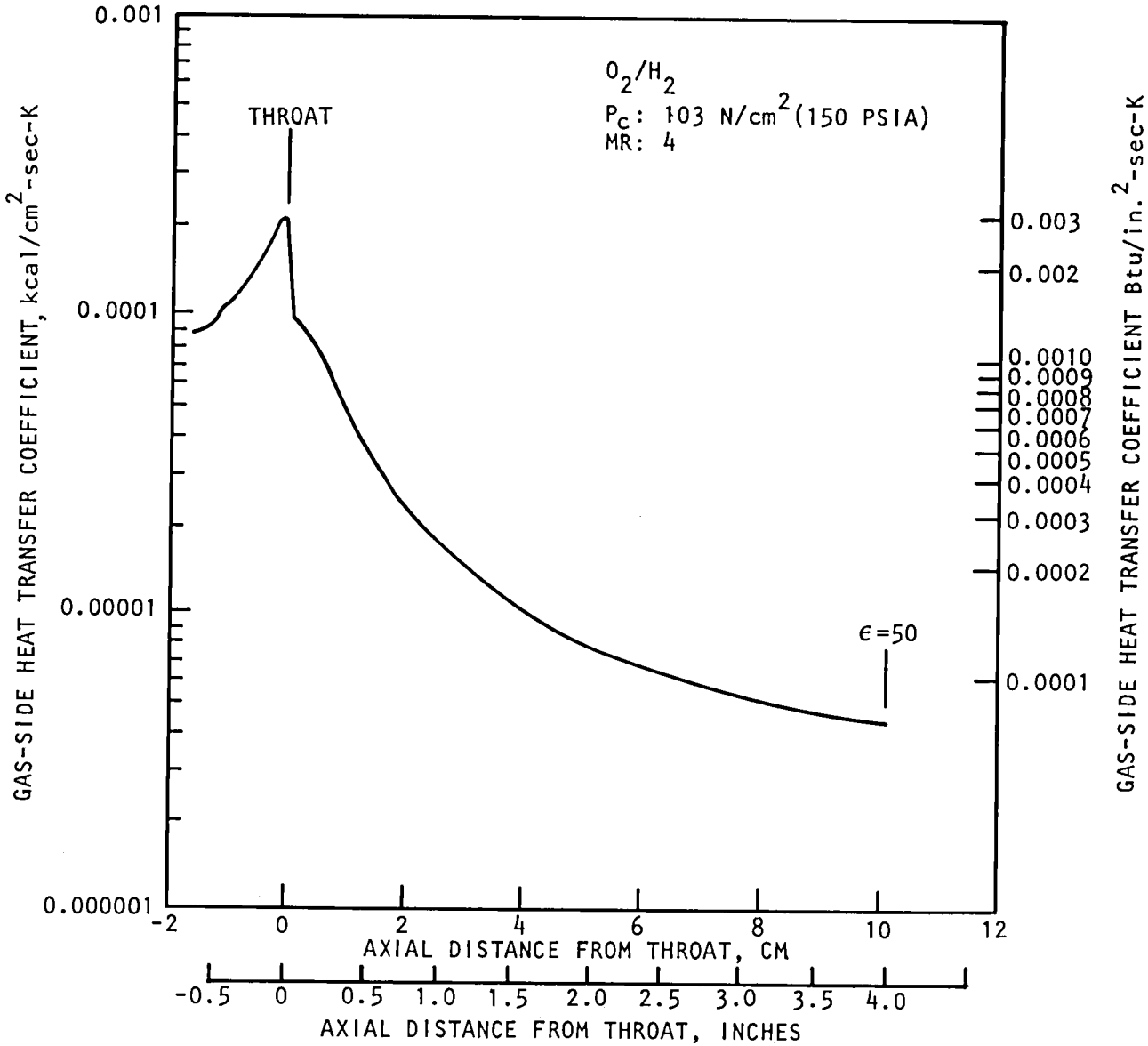

Figure 28. Typical Gas-Side Heat Coefficient Distribution

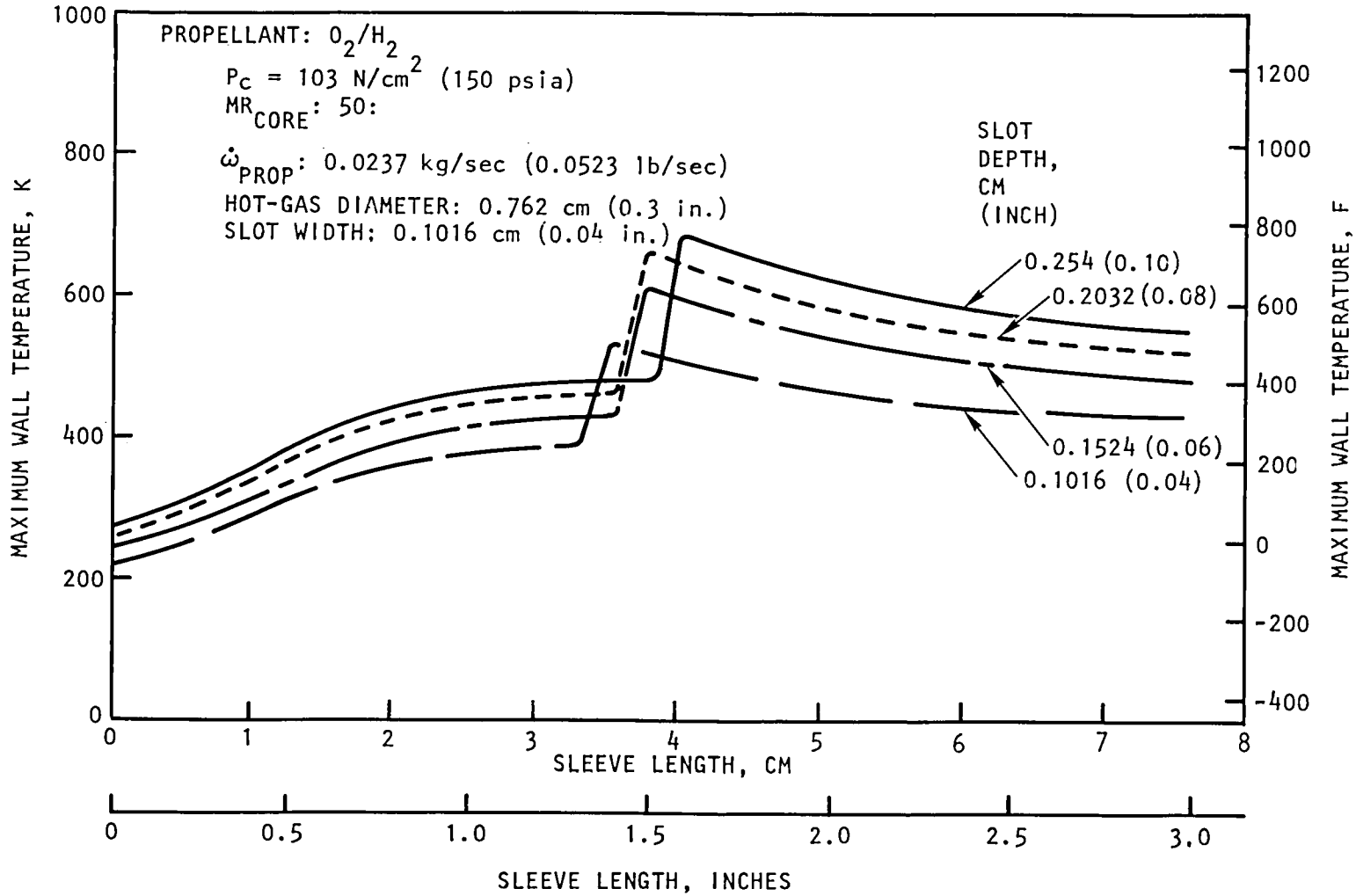

Figure 29. Primary Sleeve Wall Temperature Distribution (MR_{core} = 50-to-1)

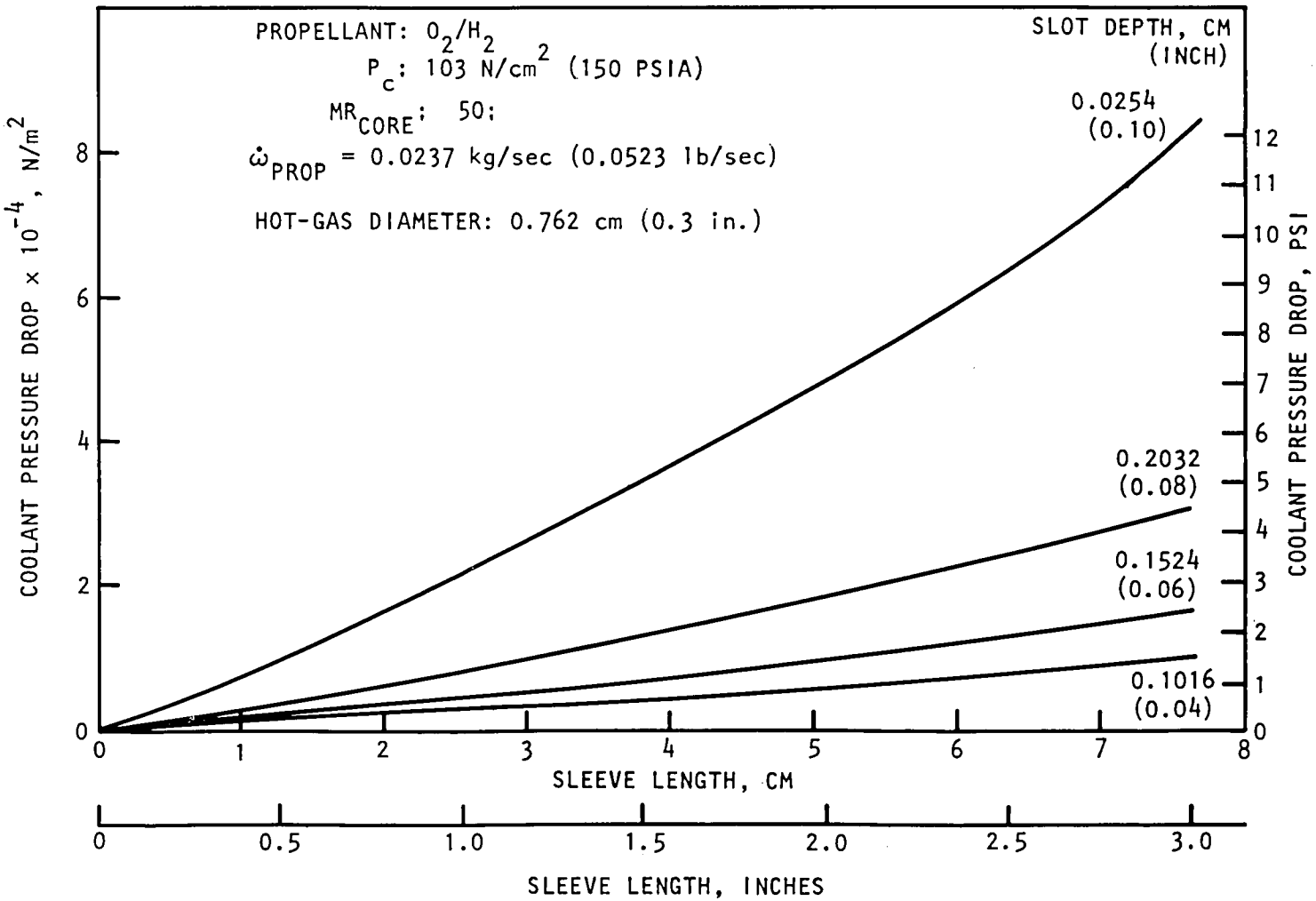

Figure 30. Primary Sleeve Coolant Pressure Drop Variation With Sleeve Length and Slot Depth (MR_{core} = 50:1)

were determined assuming a completely mixed combustion gas (mixture ratio of 4 to 1). With these assumptions, the predicted results (Fig. 31) indicated that the film coolant must be injected 3.8 cm (1.5 in.) or less from the chamber throat for L605 as the chamber material. If the chamber material is capable of withstanding temperatures approaching 1644 K (2500 F), the film-coolant injection location may be further upstream.

Dual-Sleeve Injection Designs. A similar chamber wall thermal analysis was conducted for the dual-sleeve injection designs (Fig. 3). As mentioned previously, the conservative assumption was made that completed mixing occurred instantaneously between the film coolant from the first fuel sleeve and the 50 to 1 mixture ratio core gas. Also, theheat transfer coefficient calculated was assumed constant along the length of the sleeve. Therefore, the thermal results apply equally well for both the annular and hybrid secondary injection systems.

Variables that were evaluated relative to the secondary combustor sleeve included the wall material, coolant slot configuration (number, width, and dpeth), and mixture ratio. The mixture ratio of the combustor gas contained within the second sleeve influences both the combustion gas temperature and sleeve coolant flow. The variation in coolant flow for both sleeves with core mixture ratio of the second sleeve is presented in Fig. 32. As the secondary combustor core mixture ratio is decreased, the available coolant flow for the second sleeve decreases and that for the first sleeve increases. Low secondary combustor core mixture ratios are desirable for high combustion performance, but are undesirable from a cooling standpoint because of the resulting increase in hot-gas temperature and reduction in available coolant flow. The coolant flow curve for the second sleeve in Fig. 32 also represents the influence of core mixture ratio on coolant flow for the single-sleeve design.

Thermal analysis results relative to the convectively cooled first and second sleeve for the dual-sleeve injection design are presented in Fig. 33 through 36. Nickel secondary sleeve configurations employing a coolant slot width of 0.102 cm (0.04 in.), and coolant slot depths of 0.102 and 0.203 cm (0.04 and 0.08 in.) were evaluated over a range of hot-gas mixture ratio from 10 to 25. As shown in Fig. 33, these thermal results indicate that the mixture ratio within the secondary combustor sleeve should be greater than 10 to 1 for a nickel sleeve. Further analysis indicated that smaller slot dimensions of 0.076 by 0.051 cm (0.03 by 0.020 in.) resulted in a 422 K (300 F) lower wall temperature with the nickel sleeve at a second combuster sleeve mixture ratio of 10 to 1 (Fig. 34).

The variation in maximum wall temperature for the first sleeve with second sleeve core mixture ratio and slot geometry are presented in Fig. 35 . As shown earlier in Fig. 32 , the first sleeve coolant flow decreases with an increase in mixture ratio. As such, the maximum wall temperature increases.

Combining the first and second sleeve thermal results (Fig. 36), a second sleeve core mixture ratio of 12 to 1 results in approximately the same maximum wall temperature, 867 K (1100 F), for both fuel sleeves. The increase in second combustor sleeve core mixture ratio is the result of decreased coolant flow and increased combustion gas temperature. As shown in Fig. 37 , coolant pressure drops of less than 6.9 N/cm^2 (10 psi) can be achieved for both sleeves.

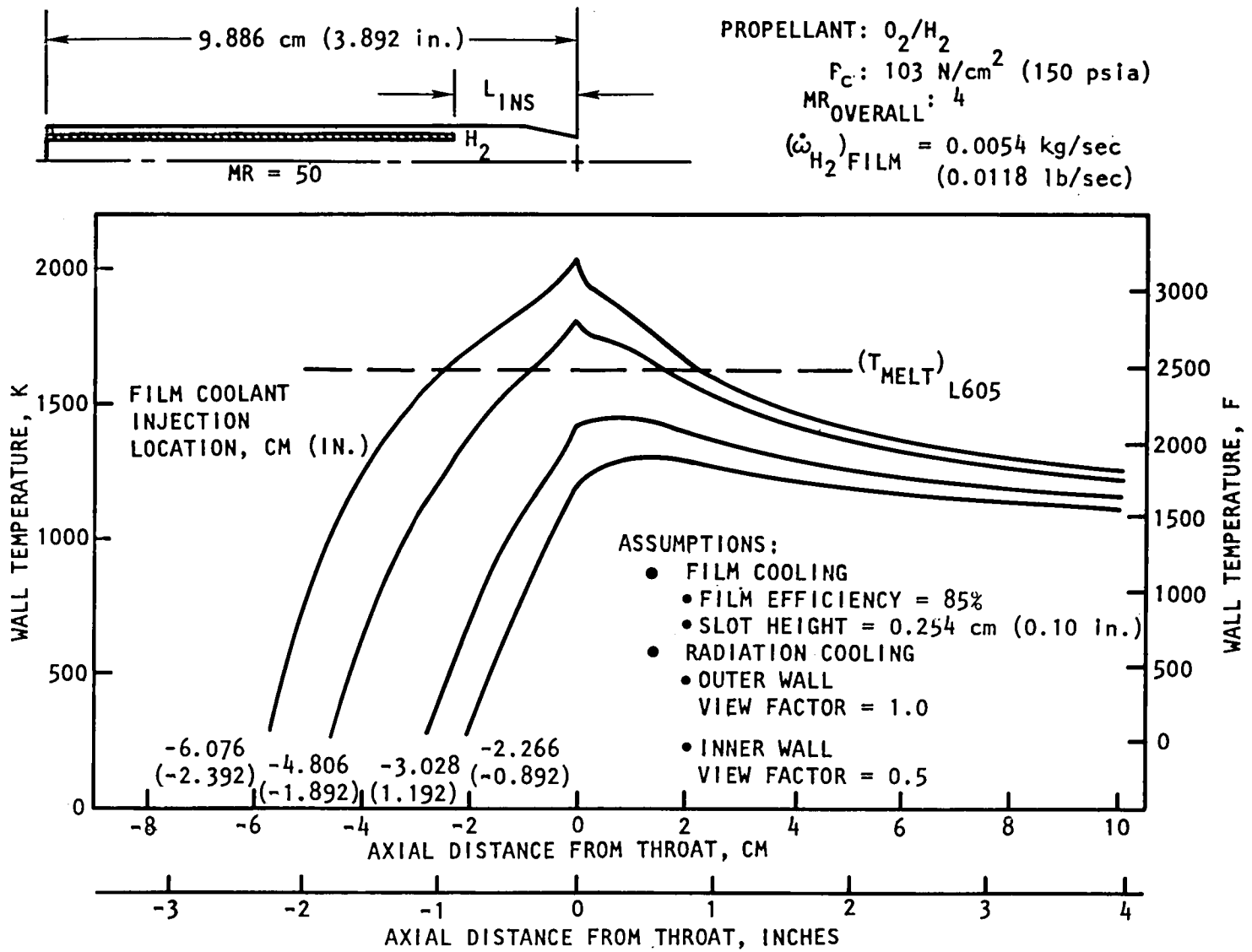

Figure 31. Chamber Wall Temperature Variation With Film Coolant Injection Location (Single Fuel Sleeve Design)

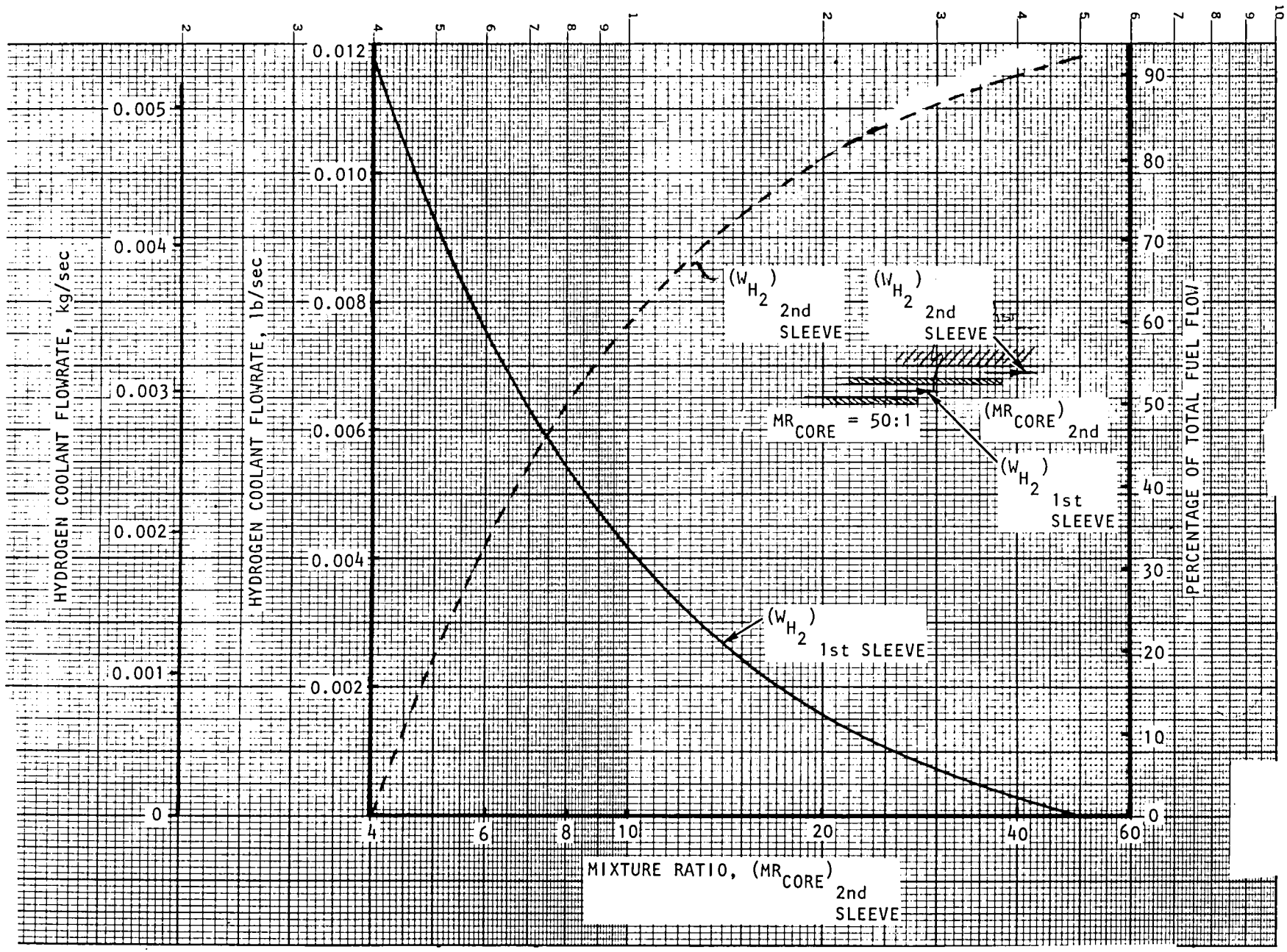

Figure 32. First and Second Coolant Flow Variation With Second Sleeve Core Mixture Ratio

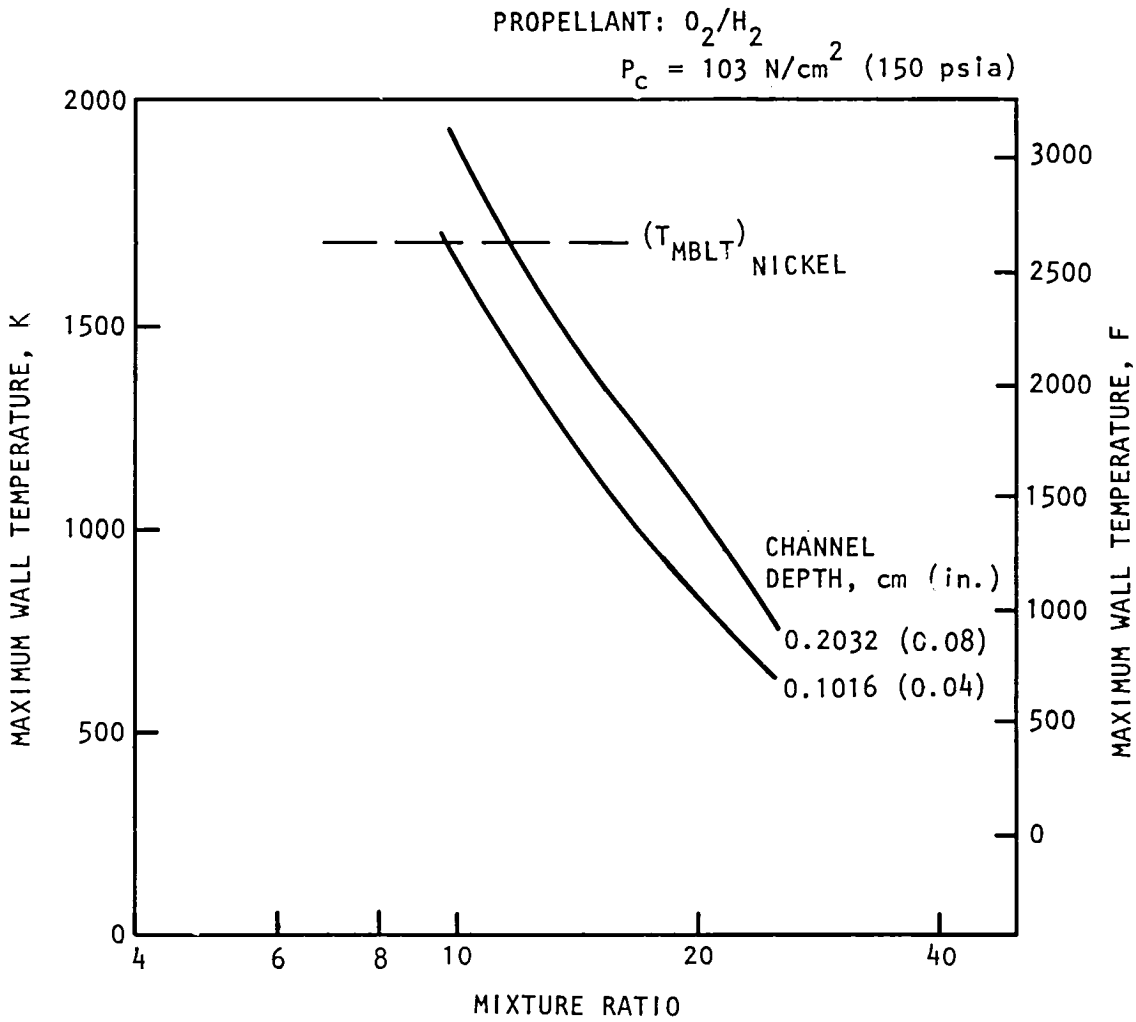

Figure 33. Maximum Wall Temperature Variation With Mixture Ratio (Secondary Fuel Sleeve)

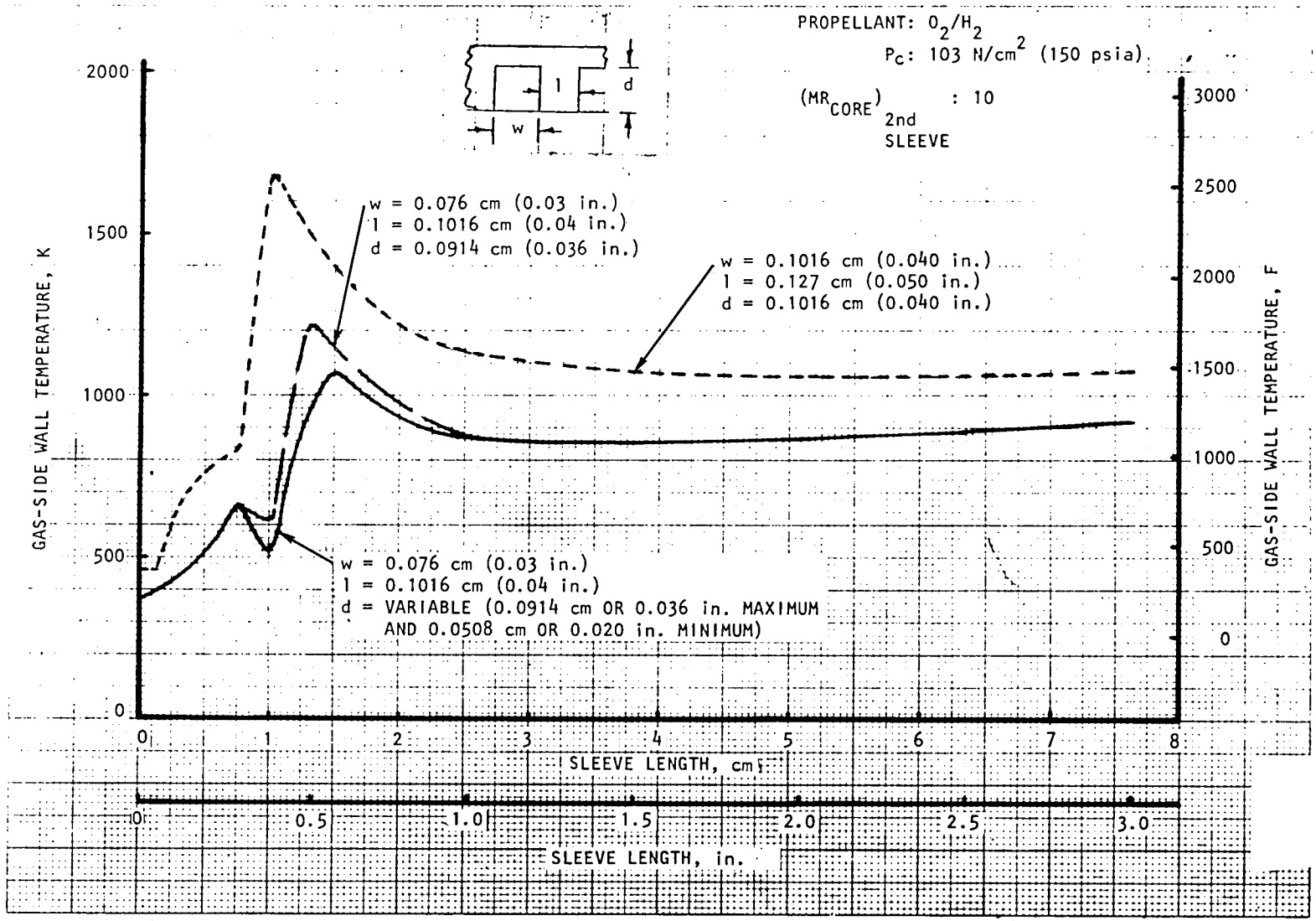

Figure 34. Influence of Coolant Slot Geometry and Second Sleeve Core Mixture Ratio of the Maximum Wall Temperature (First Sleeve)

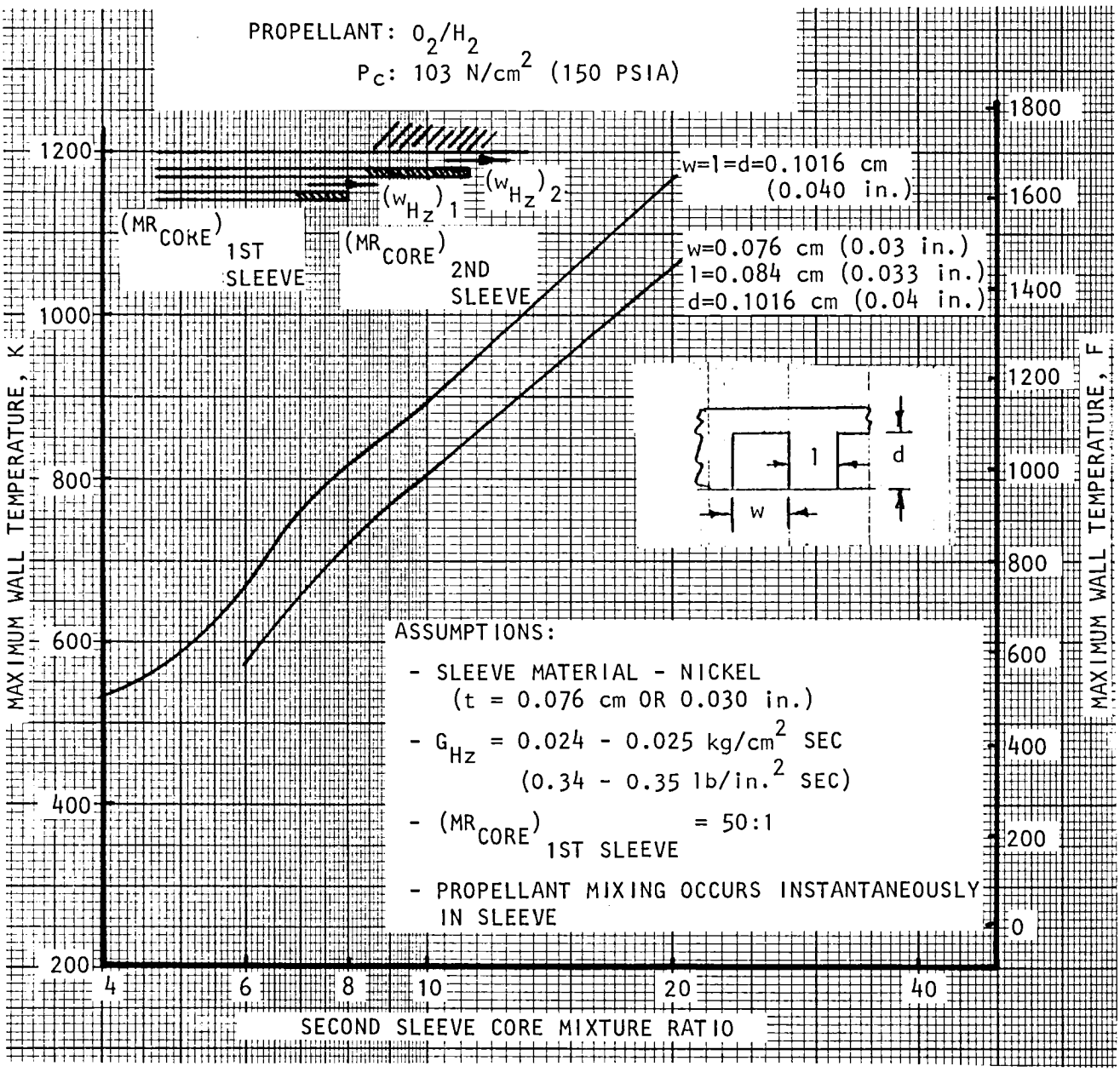

Figure 35. Influence of Coolant Slot Geometry and Second Sleeve Core Mixture Ratio on the Maximum Wall Temperature (First Sleeve)

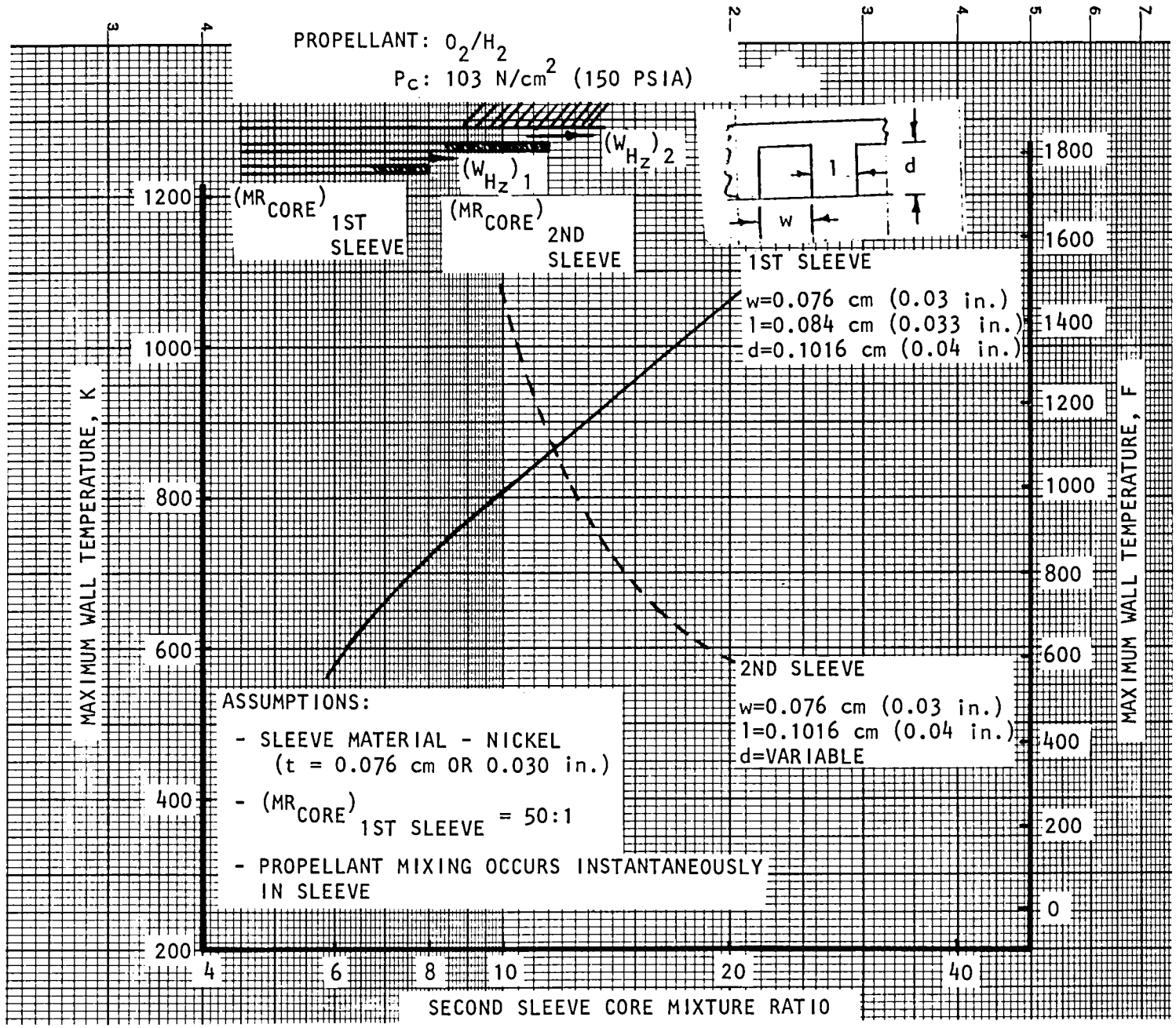

Figure 36. Maximum Wall Temperature Variations for First and Second Sleeves (dual sleeve and hybrid designs)

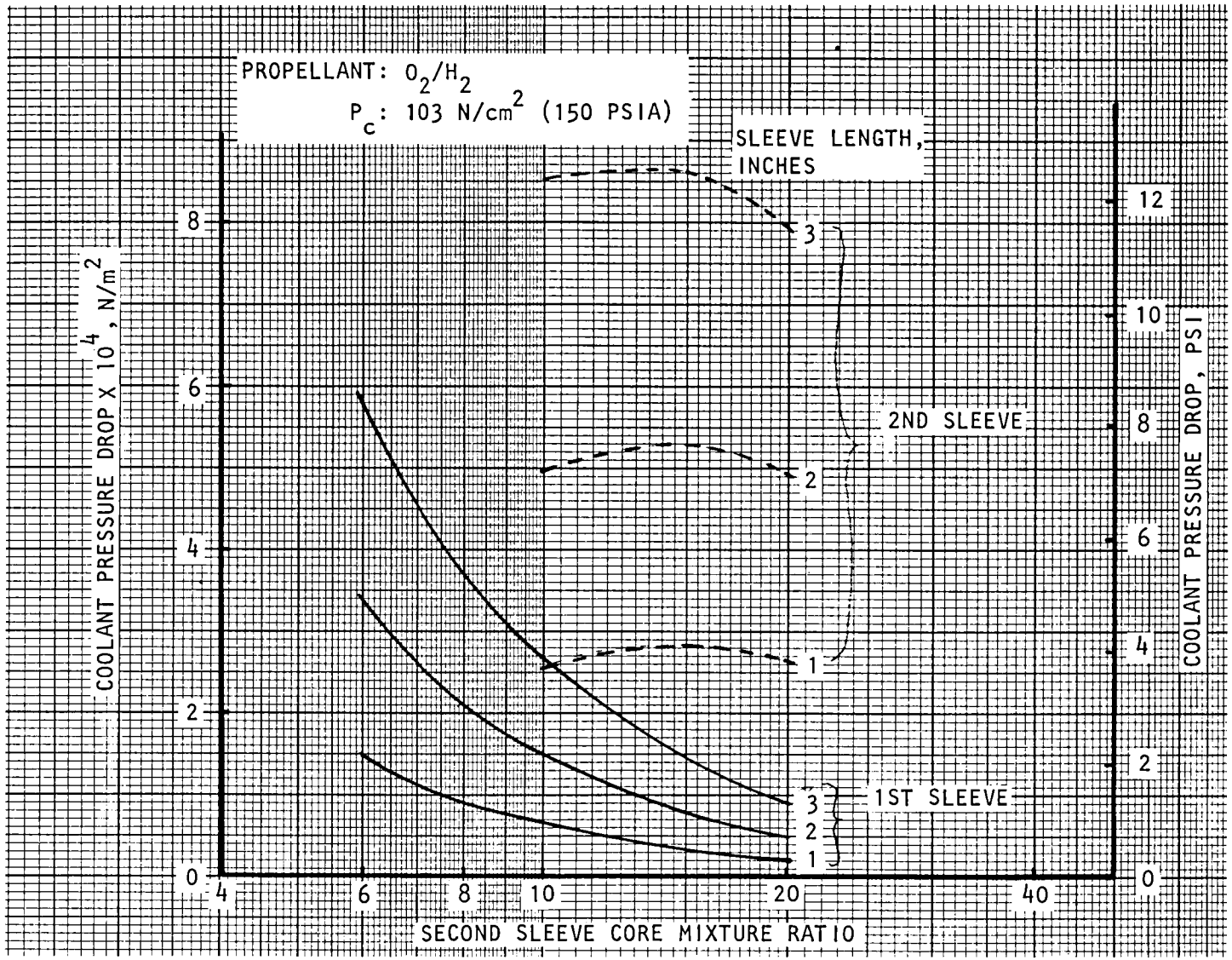

Figure 37. Coolant Pressure Drop Variations for First and Second Sleeves (dual sleeve and hybrid designs)

As mentioned previously, a low second sleeve core mixture ratio is desirable from a performance standpoint. Therefore, further analysis to achieve a second sleeve design capable of operation at a second sleeve core mixture ratio of 7.5 to 1 was performed. The influence of smaller land widths, smaller slots, and a copper sleeve were analyzed. As shown in Fig. 38 , for a 0.076-cm (0.03-in.) slot width and a minimum slot depth of 0.051 cm (0.02 in.), the smaller land widths resulted in only slightly lower wall temperatures. Decreasing the slot width, land width, and minimum slot depth further resulted in a second sleeve design having a 1058 K (1445 F) maximum wall temperature. This was achieved with a nickel sleeve utilizing a 0.051-cm (0.02-in.) slot and land width and a minimum slot depth of 0.051 cm (0.02 in.), (Fig. 39). Changing the sleeve material to copper resulted in a 56 to 111 K (100 to 200 F) lower wall temperature (Fig. 40), but the allowable operational temperature of copper is 222 to 333 K (400 to 600 F) lower than that of nickel and, consequently, nickel provides a better cooling margin.

Assuming a 0.091-cm (0.036-in.) film coolant slot height, an overall thruster mixture ratio of 4 to 1, a 3.6 to 1 contraction ratio, an 85% film-coolant efficiency, and a 5.08-cm (2-in.) second sleeve length, curves of maximum wall temperature versus second sleeve core mixture ratio were obtained for various axial film-coolant injection locations (Fig. 41). As for the single-sleeve design, the gas-side conditons were determined assuming a completely mixed combustion gas (mixture ratio of 4 to 1) which would result in conservative wall temperature predictions. For a 1644 K (2500 F) maximum wall temperature, a film-coolant injection location less than 2.54 cm (1.0 in.) upstream of the throat, resulted. The injection location decreased to less than 1.27 cm (0.5 in.) for a 1367 K (2000 F) maximum wall temperature.

Thermal analysis for abort mode operation (124 N/cm^2, 180 psia) chamber pressure and 5.6 to 1 overall mixture ratio) with the dual-sleeve configuration was performed. For this operating mode, a 71.7 primary sleeve core mixture ratio and a 10.4 secondary sleeve core mixture ratio resulted, assuming the nominal operating condition hydrogen flow split. This condition results in an increase in the maximum gas-side wall temperature of the convectively cooled secondary sleeve from 1058 K to 1083 K (1445 to 1489 F), because of the resulting 10.5% decrease in coolant flow. Assuming the combustion gas temperature for a 100% combustion efficiency, the film-cooled throat region of the thrust chamber resulted in a maximum wall temperature change from 1458 K to 1748 K (2164 to 2687 F) for a 1.90-cm (0.75-in.) film-coolant injection distance, because of the 16% increase in heat flux and a 10.5% reduction in film-coolant flow.

Detail analyses were conducted to evaluate the three-dimensional axial heat conduction effect at the secondary combustor sleeve exit. The coolant channel configuration at the secondary combustor sleeve exit is dictated by the requirements for cooling the sleeve and the desirability of having a developed annular stream flow for film-cooling the thrust chamber throat. The three candidate sleeve exit configurations evaluated are shown in Fig. 42 . Configuration No. 1 was designed to provide a gradual transition from discrete channel flow to complete annular film-cooling flow. Configuration No. 2 permits some distance (approximately 4 diameters) for the coolant to form the desired annular injection stream, while still attempting to maintain a high sleeve coolant velocity

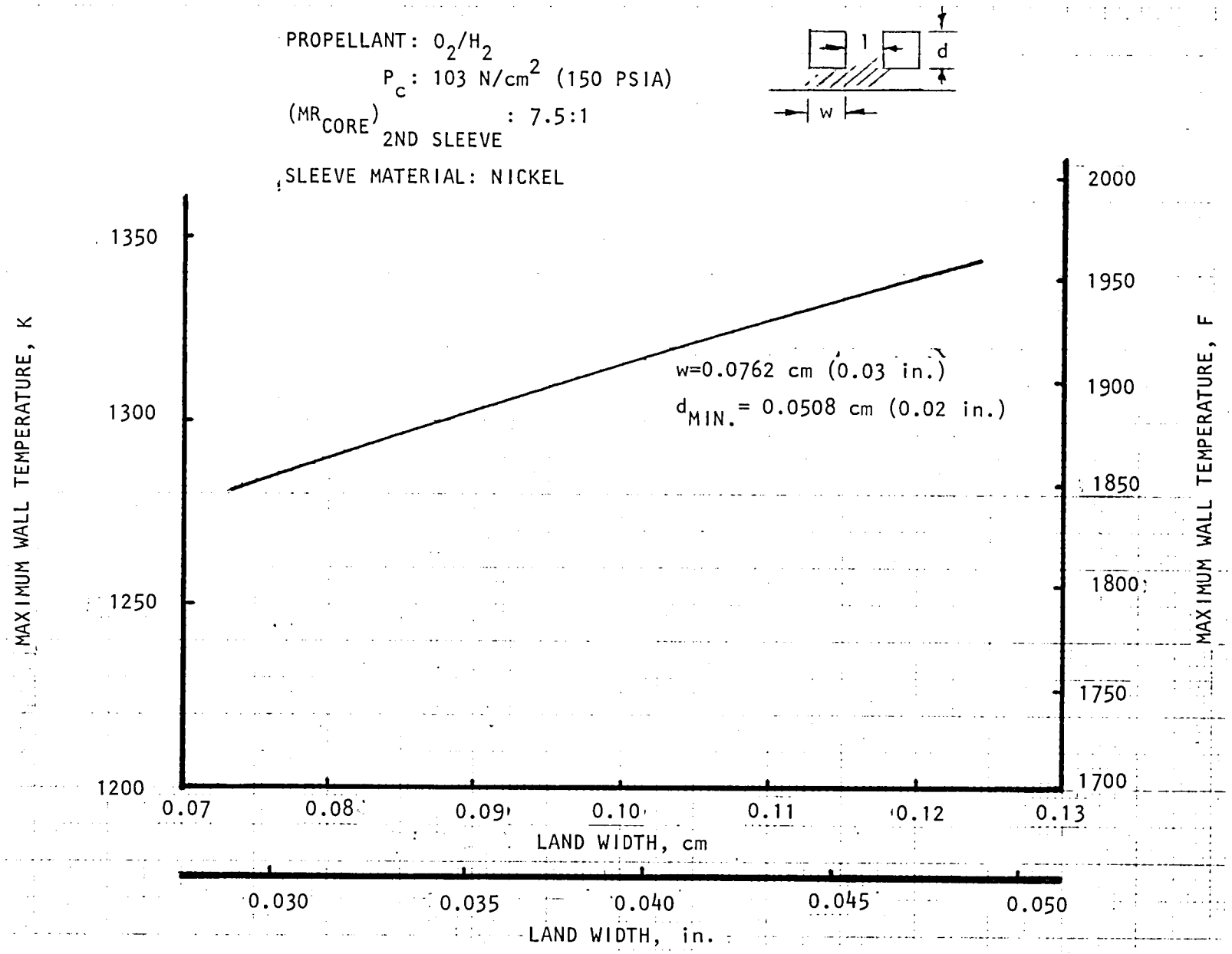

Figure 38. Second Sleeve Maximum Wall Temperature Variation With Land Width for Second Sleeve Core Mixture Ratio of 7.5 [0.762 mm (0.03 inch) Slot Width and 0.508 mm (0.02 inch) Minimum Slot Depth]

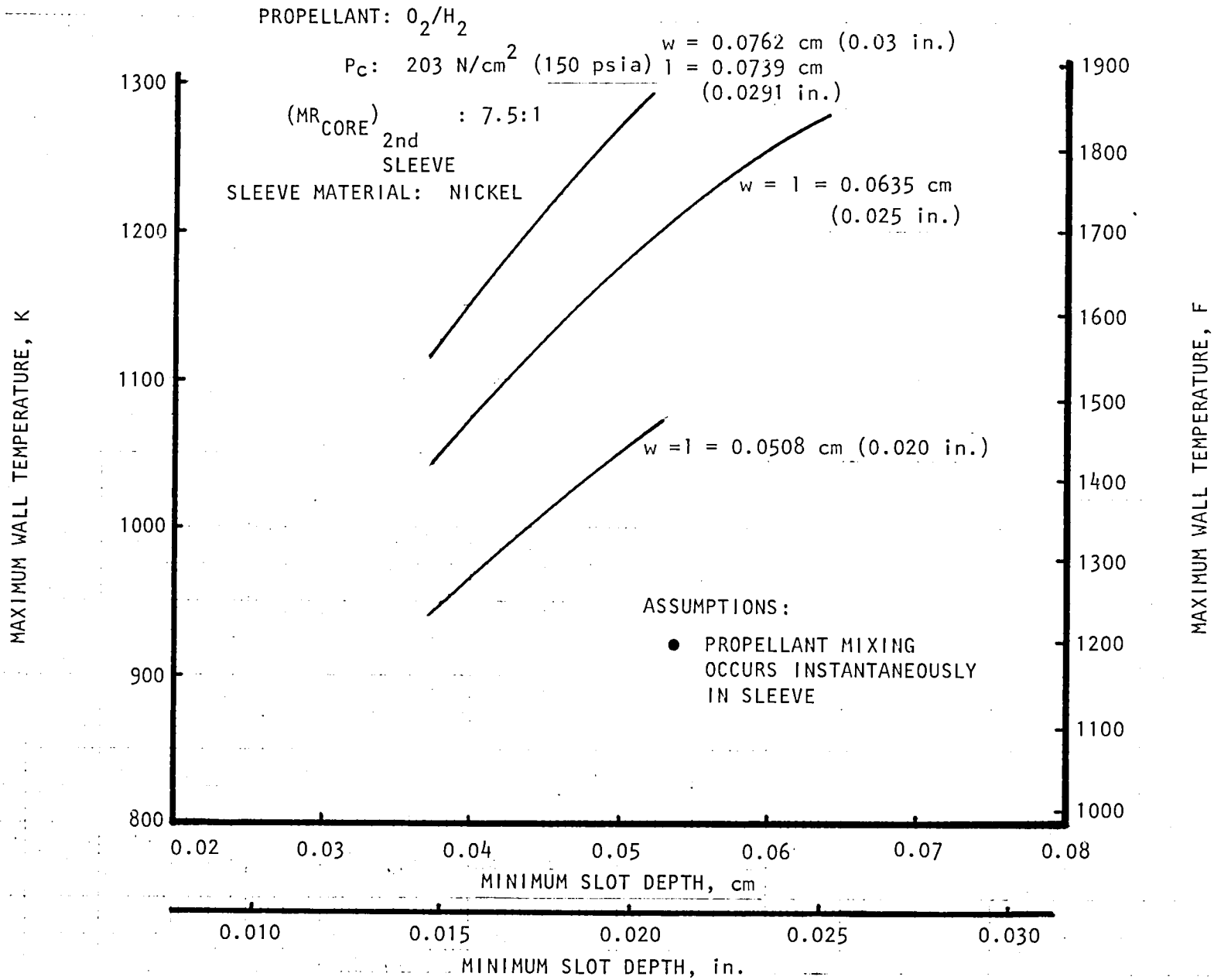

Figure 39. Influence of Slot Geometry for Nickel Second Sleeve at Second Sleeve Core Mixture Ratio of 7.5

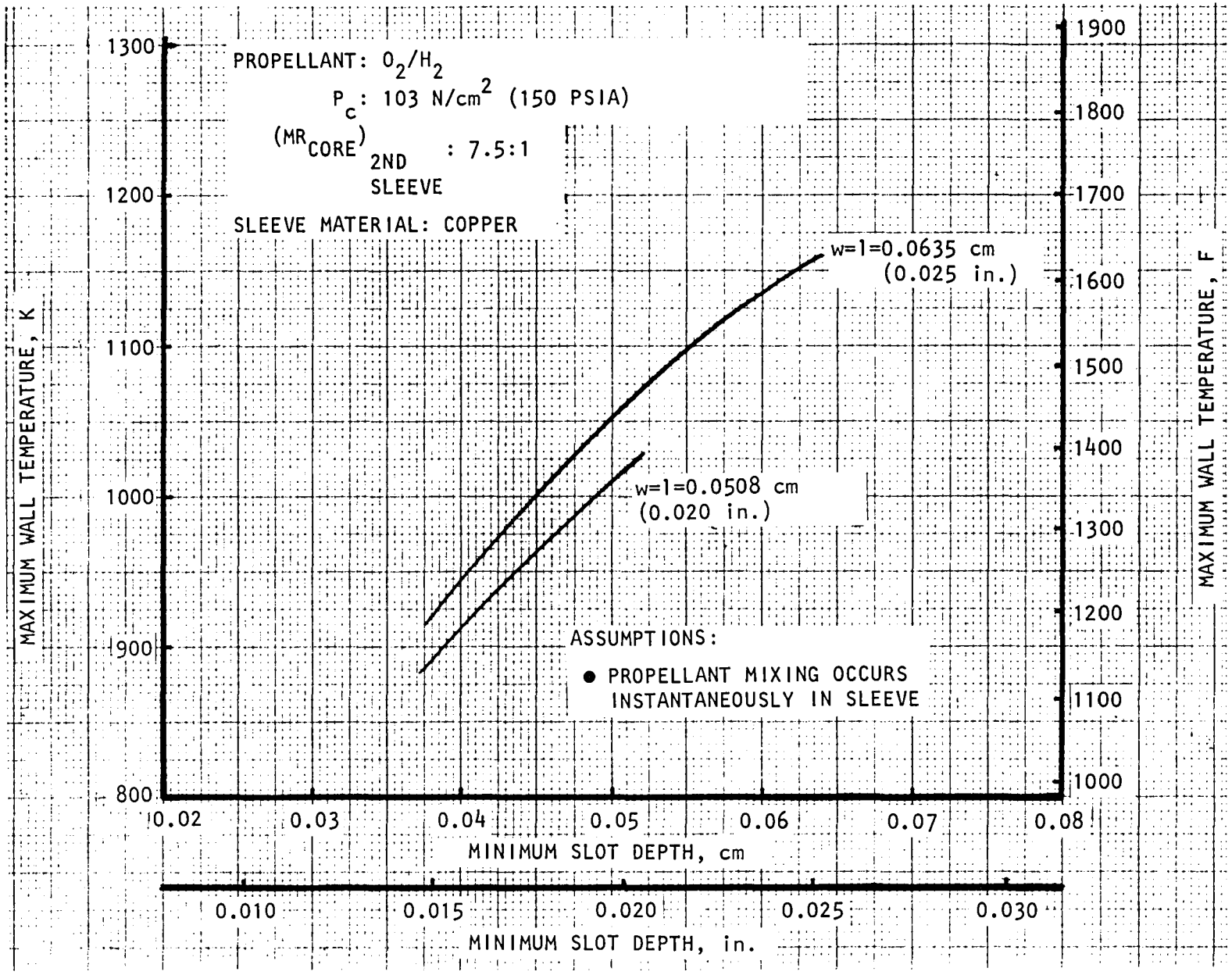

Figure 40. Influence of Slot Geometry for Copper Second Sleeve at Second Sleeve Core Mixture Ratio of 7.5

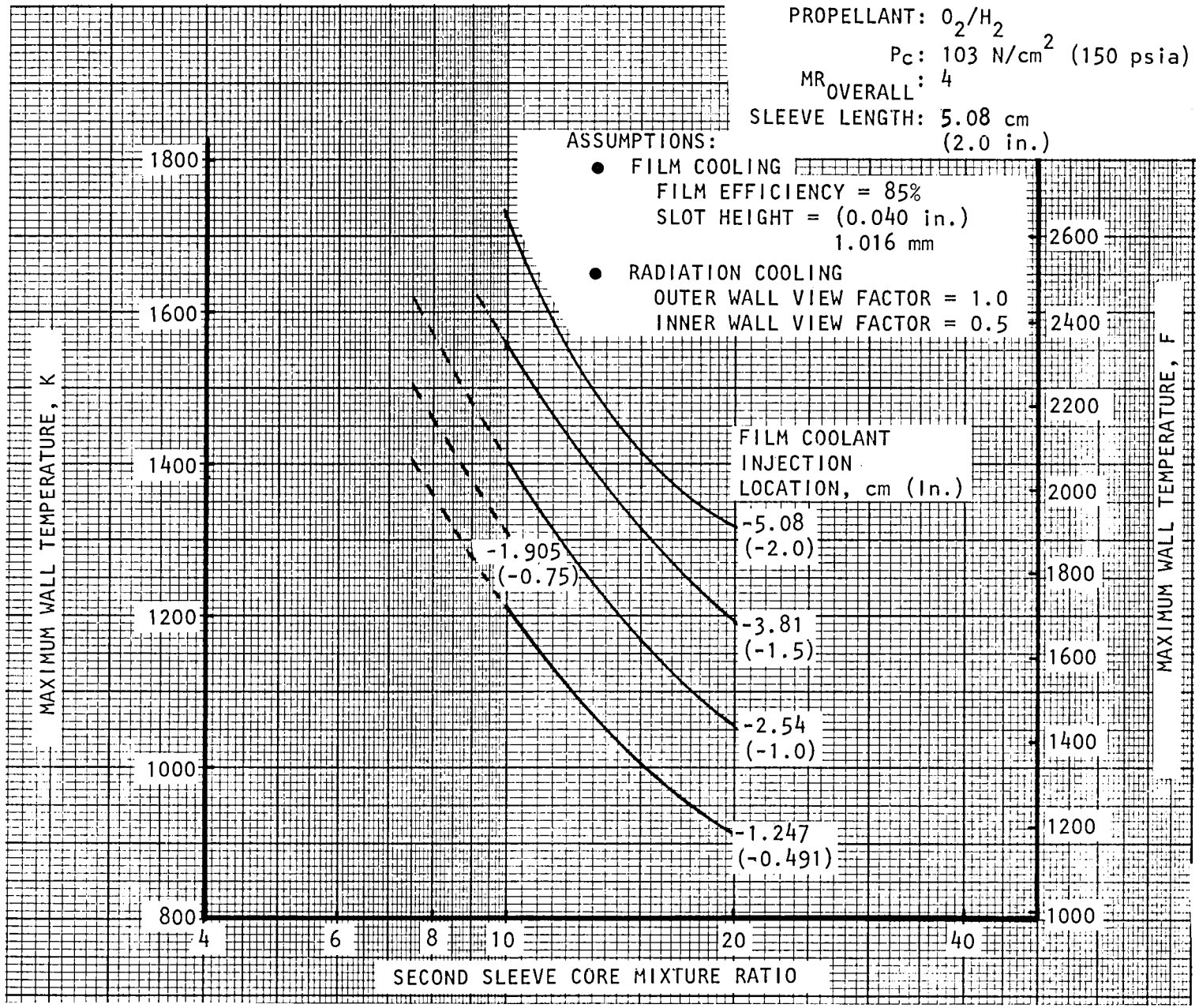

Figure 41. Variation of Maximum Wall Temperature of Film/Radiation Cooled Portion of Chamber With Second Sleeve Core Mixture Ratio and Film Coolant Injection Location

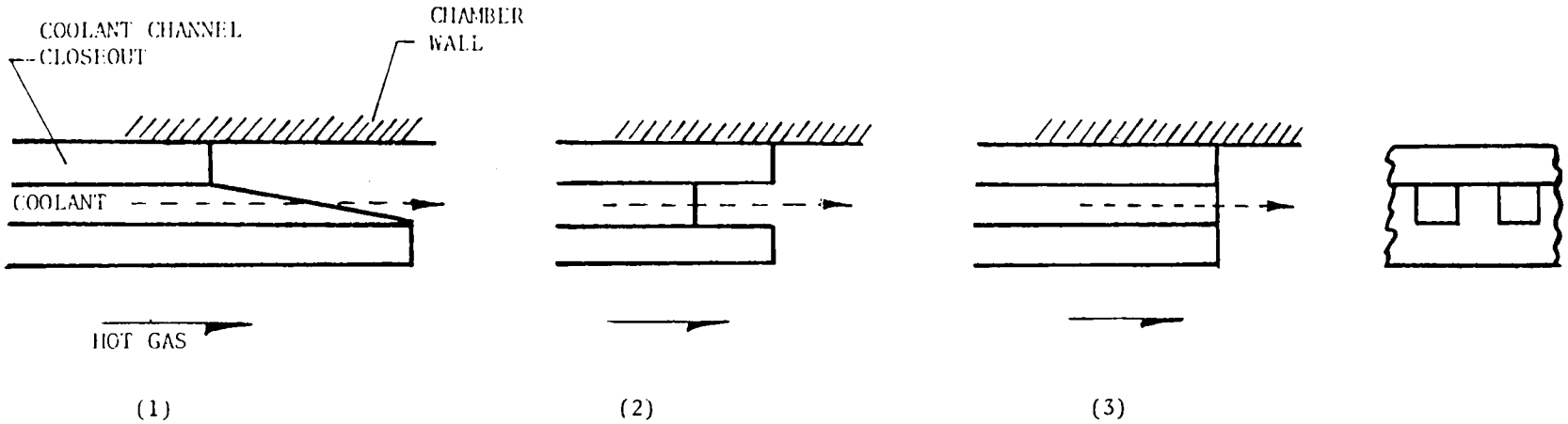

Figure 42. Candidate Second Sleeve Exit Configurations

for cooling. Convective cooling of the secondary combustor sleeve is the primary consideration of Configuration No. 3. Three-dimensional models of the first two configurations were developed and analyzed for a nominal secondary combustor core mixture ratio of 7.5.

As shown in Fig. 43 and 44, the first and second configurations resulted in maximum combustor sleeve wall temperatures exceeding 1367 K (2000 F), which is excessive for a nickel sleeve. The top left corners of Fig. 43 and 44 reflect the sleeve exit which is exposed to the hot-gas stream. The temperature profile for Configuration No. 3 is presented in Fig. 45 and results in a maximum wall temperature at the sleeve exit of 987 K (1316 F).

These analyses indicate that elimination of the coolant lands for the purpose of developing an annular injection stream had a significant effect on maximum sleeve wall temperatures. This is largely due to the loss of two-dimensional heat conduction and the reduction in coolant mass velocity. Therefore, exit Configuration No. 1 will be utilized only when the secondary combustor sleeve is terminated within the convergent portion of the thrust chamber, i.e., throat to secondary sleeve recess depths of 1.40 to 1.9 cm (0.55 to 0.75 in.). Termination of the secondary sleeve within the cylindrical portion of the thrust chamber will require the use of exit configuration No. 3. The small channel land widths of the selected secondary combustor sleeve design 0.051 cm (0.020 in.) and the fact that the coolant at the sleeve exit is in a gaseous state will enhance the formation of an annular film-coolant stream within a relatively short distance from the point of injection. Assuming a 7-degree flow expansion angle, the 48 discrete streams (48 coolant channels) should coalesce into an annulus in approximately 0.20 cm (0.08 in.).

The variation in the maximum wall temperature with film-coolant injection location is presented in Fig. 46 for both the abort mode and nominal operating conditions, assuming a secondary combustor sleeve core mixture ratio of 7.5 to 1 at nominal operating conditions. When the reduction in combustion gas temperature associated with a 90% combustion efficiency is applied, the maximum chamber throat wall temperature is reduced from 1748 to 1546 K (2687 to 2323 F).

The parametric thermal analysis discussed above defined design criteria for the candidate thruster configurations and provided design guidelines relative to the key thrust chamber cooling parameters, i.e., second sleeve core mixture ratio, slot geometry for the convectively cooled sleeves, and film-coolant injection location. Detailed design and analysis of the convectively cooled sleeve and the film/radiation-cooled portion of the portion of the selected thruster configuration are discussed in the Hardware Design and Fabrication section.

Injector Cooling. The cooling of the primary injector face by the fuel and oxidizer flowing within the injector was analyzed for a core mixture ratio of 50 to 1 utilizing the calculated gas-side heat transfer coefficient for the first sleeve. A two-dimensional model with 0.063 cm (0.025 in.) fuel injection orifices and a 0.063-cm (0.025-in.) annulus gap for the oxidizer was evaluated. At the combustion gas temperature for a core mixture ratio of 50 to 1, the influence of varying the gas-side heat transfer coefficient from the full reference value down to 25% of the full value was determined (Fig. 47).

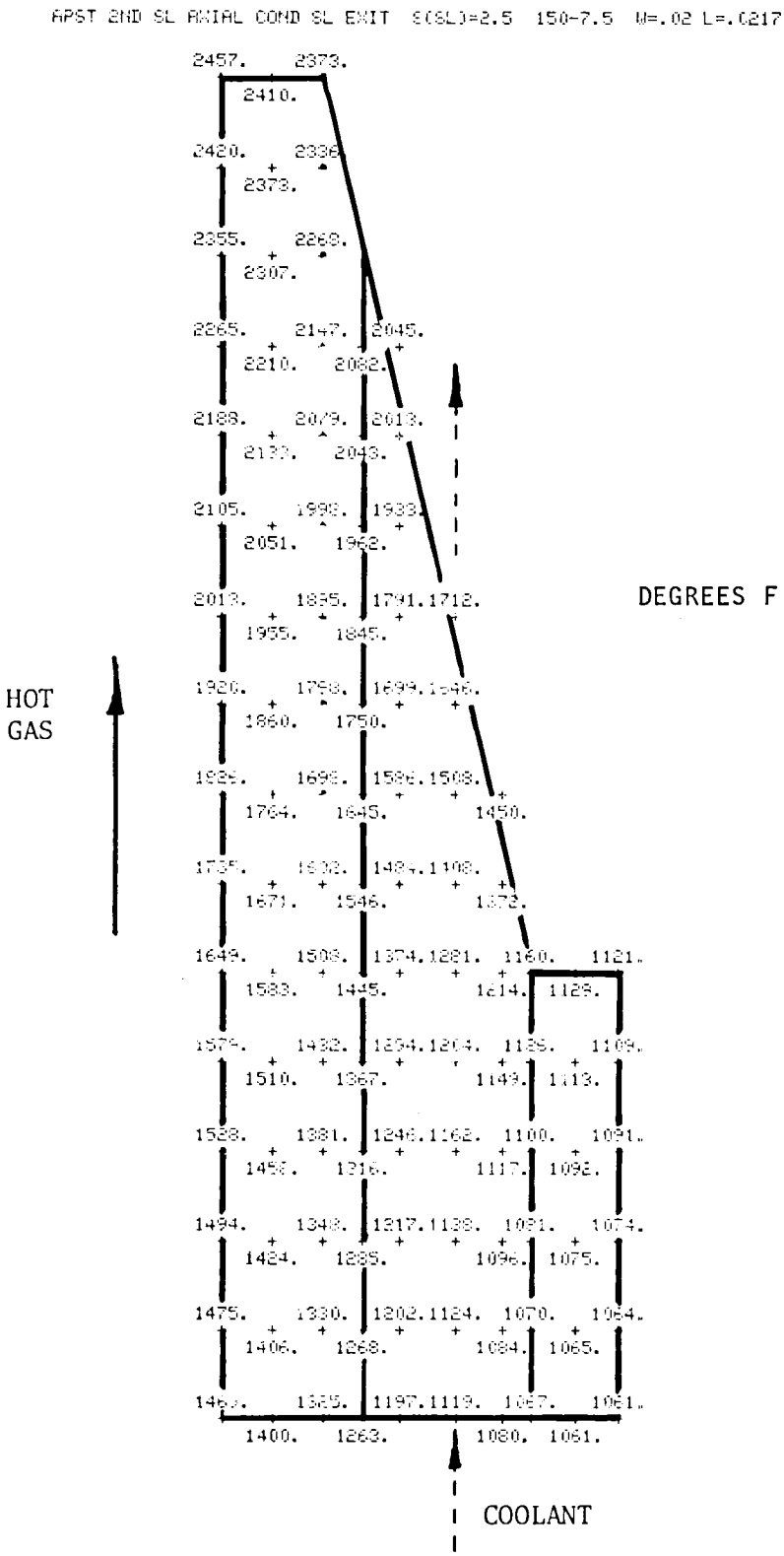

Figure 43 . Configuration No. 1 Thermal Results

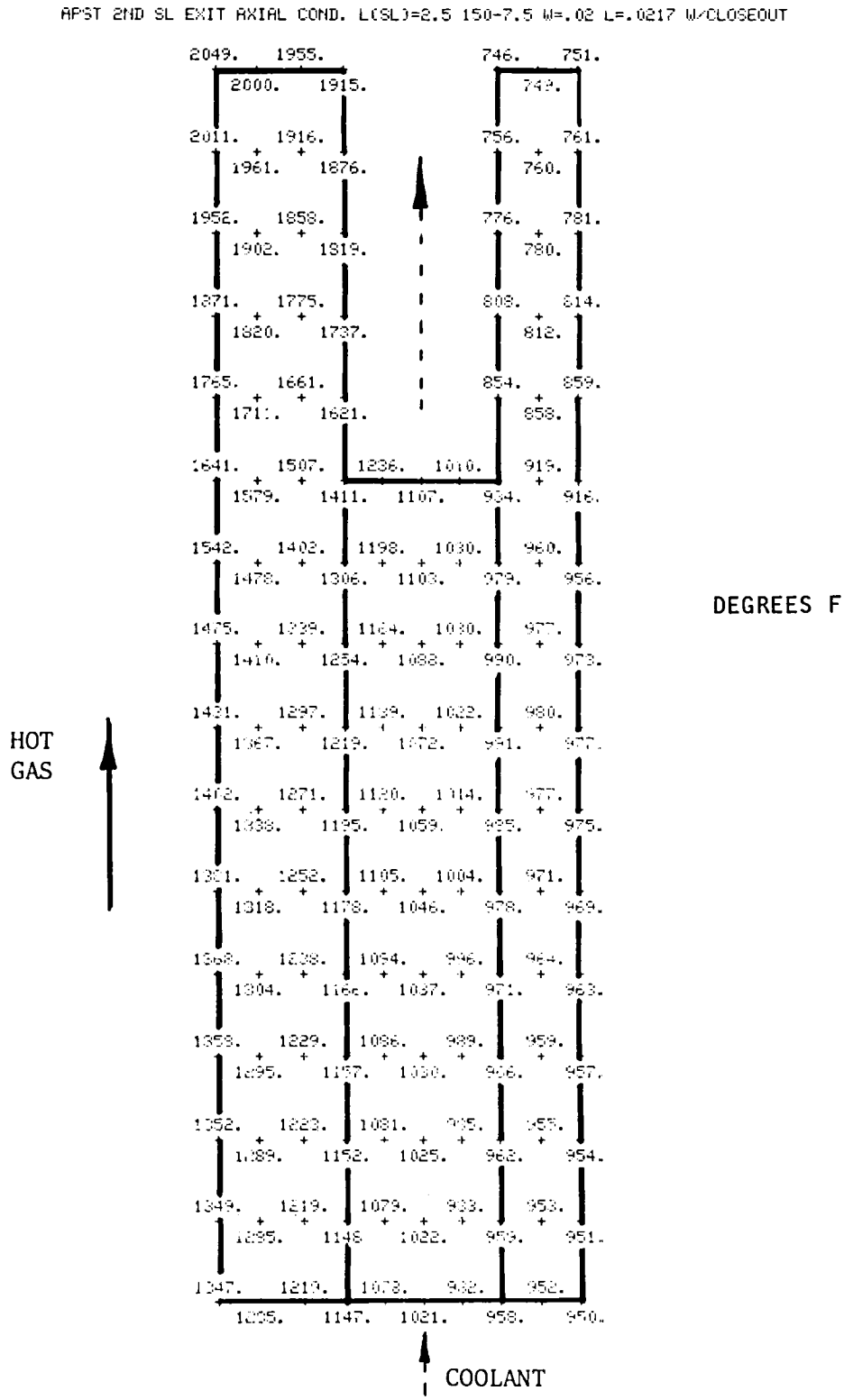

Figure 44. Configuration No. 2 Thermal Results

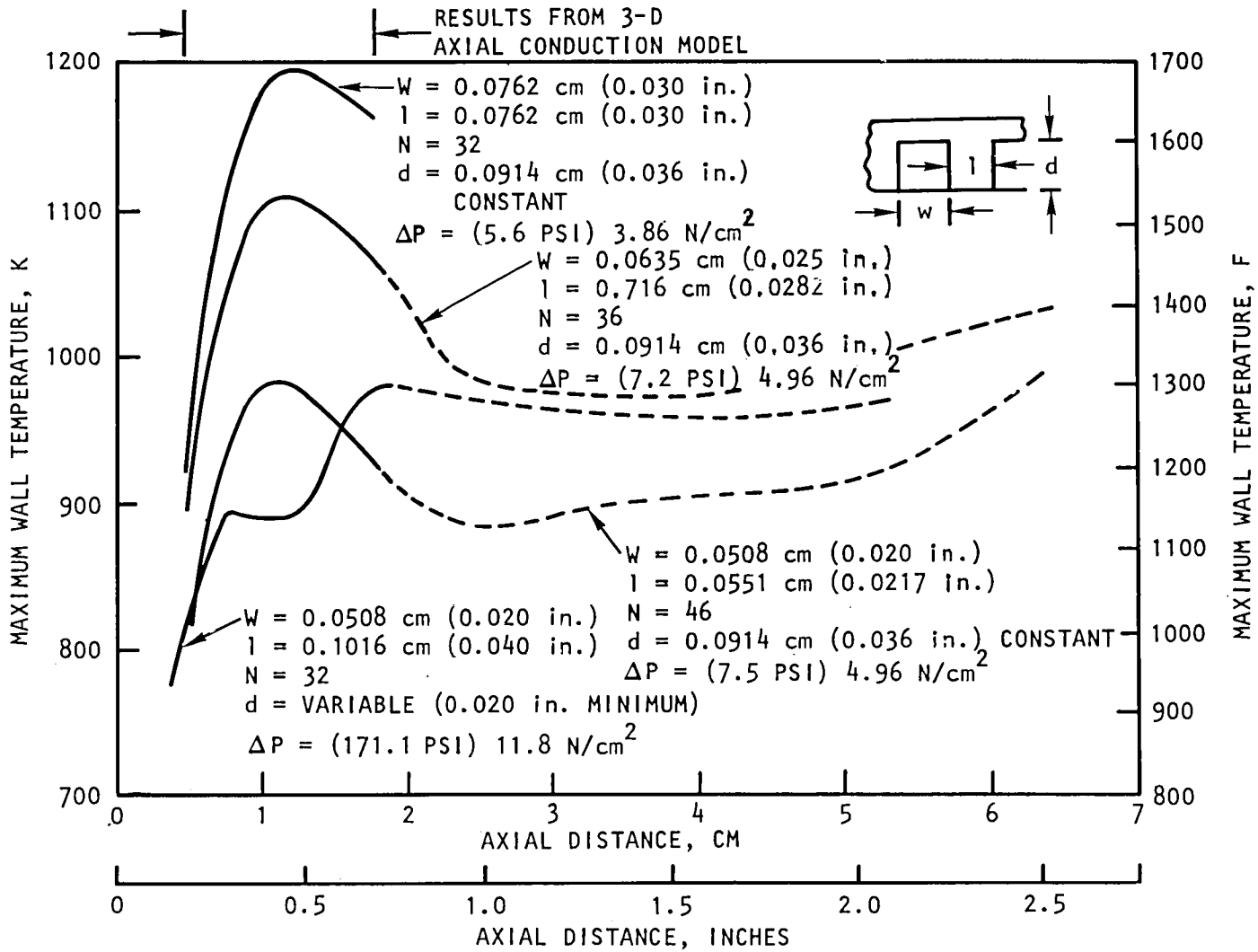

Figure 45. Wall Temperature Distributions for Various Secondary Sleeve Coolant Channel Designs

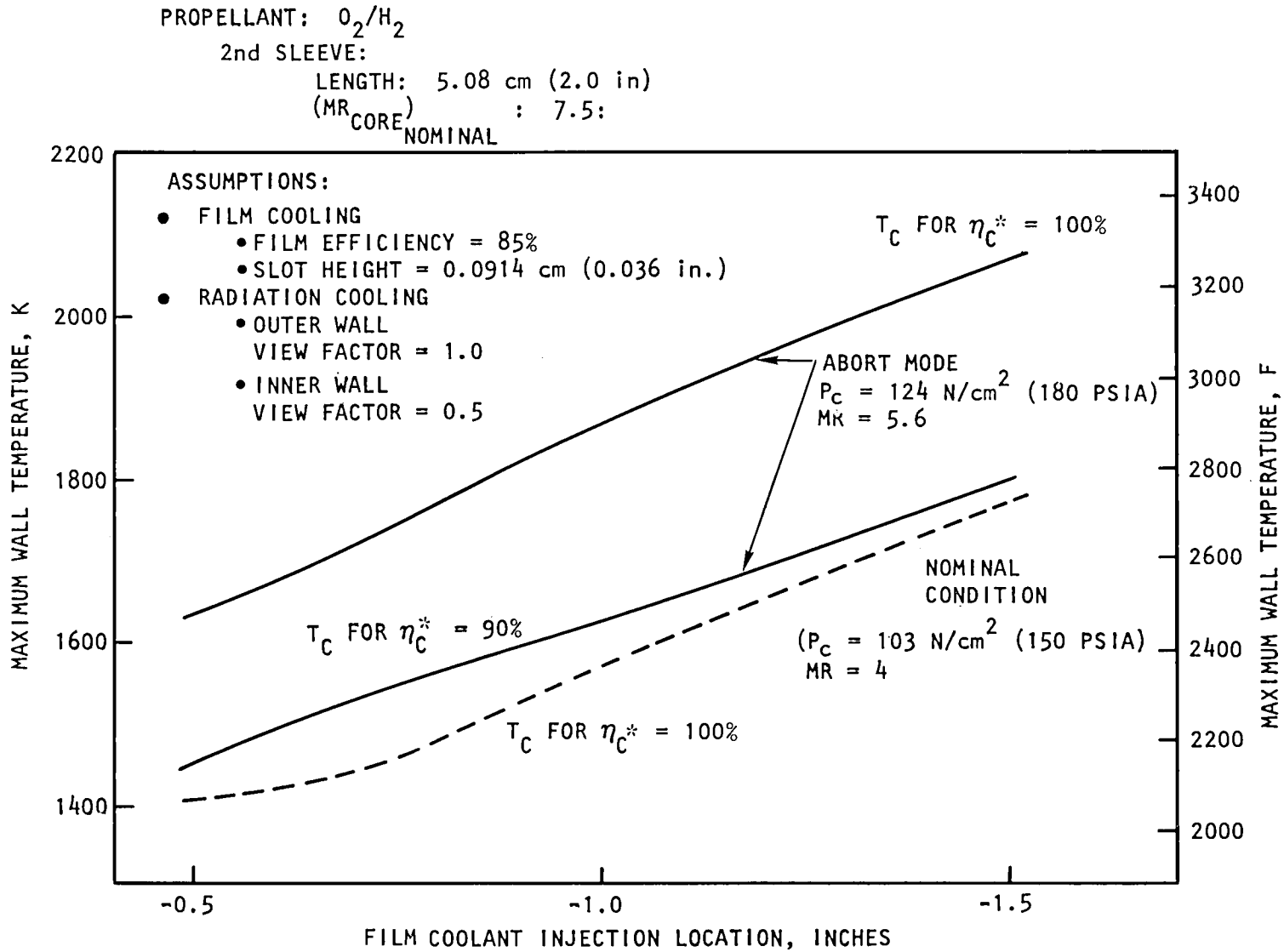

Figure 46. Film-Cooled Chamber Maximum Wall Temperature Variation With Film Coolant Injection Location [$(MR_{Core})_{second\ sleeve\ nominal}$ = 7.5; 50.8 cm (2.0 inch) second sleeve]

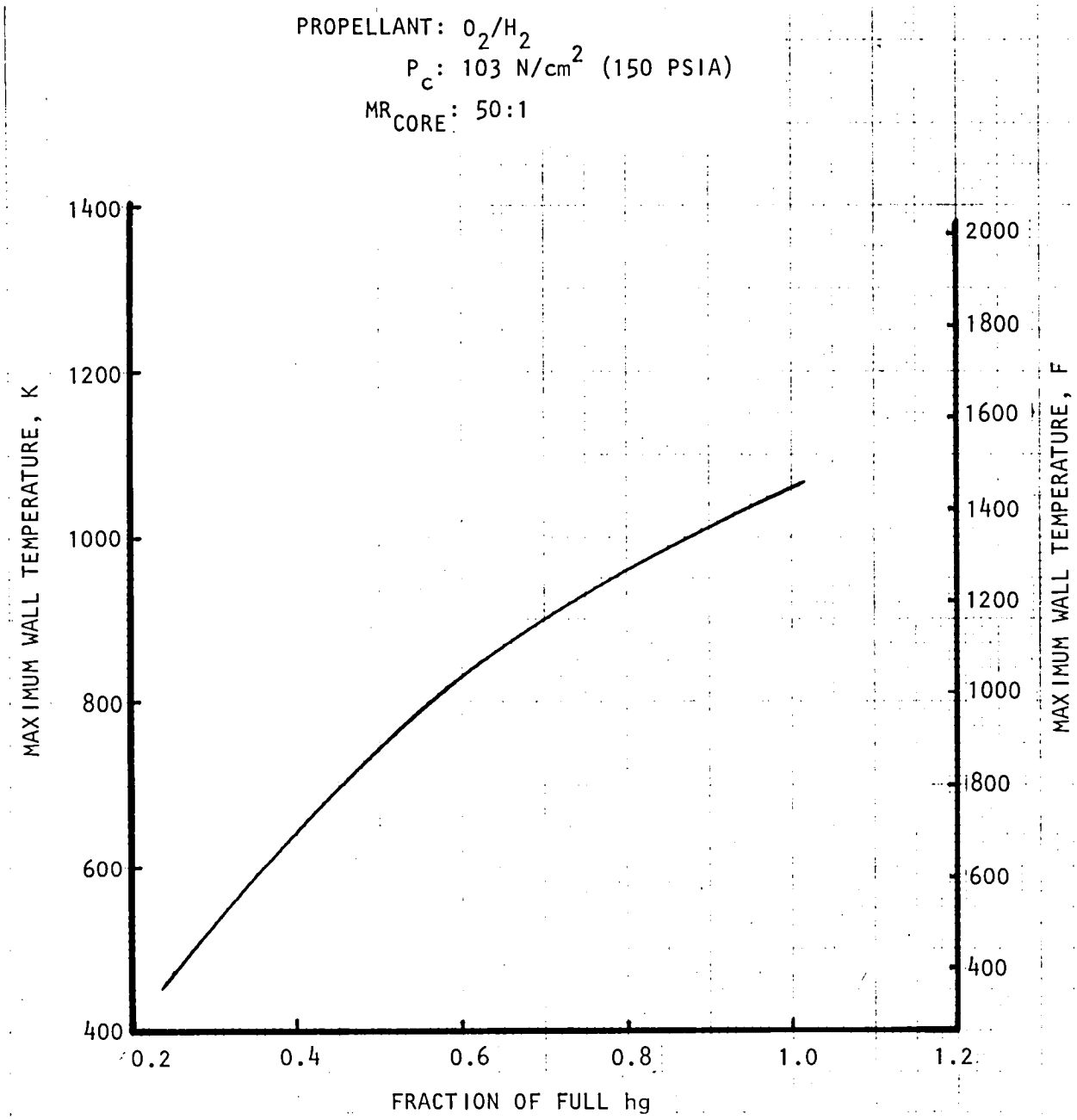

Figure 47. Injector Region Maximum Wall Temperature Variation With Heat Transfer Coefficient (MR_{Core} = 50:1)

Typically, the injector end heat transfer coefficient is approximately 50% of the chamber value (full reference value); at this value, a maximum wall temperature of 746 K (883 F) was obtained as shown in Fig. 48. This maximum temperature occurs on the gas-side surface furthest removed from the fuel injector passage. This temperature is acceptable for the injector body and, in actuality, this temperature would be lower since the convective cooling within the fuel sleeve will influence this region.

Structural/Life Assessment. Stress/strain analyses were conducted to identify any serious chamber fatigue or creep rupture problem areas associated with the candidate propellant injection/cooling configuration, which might preclude attainment of the high cyclic life and duration goals. These analysis indicated that the injector and thrust chamber (L-605) are structurally adequate at the operating chamber pressure of 124 N/cm^2 (180 psia) and a temperature of 1367 K (2000 F). The minimum safety factors at these conditions are 8.6 on yield and 14.0 on ultimate and occur at the chamber throat. These analyses also showed that a minimum safety factor of 4.0 existed on creep rupture for the required 80 hours of operation.

Propellant Valves

A propellant valve design trade study was performed to define the most favorable valve/actuation concept for the thruster feasibility demonstration program. In addition, attention was directed toward identifying any design concepts that may not be desirable for support of the existing thruster development program, but may be more suitable for planned end-item usage.

Salient design requirements which were utilized for this trade study are included in Table 2 . Valve/actuation concepts which were evaluated relative to these design requirements were:

1. Rotary Valves, (ball, butterfly, and plug types)
2. Bellow-Disk Valves
3. Pinch Valves
4. Flexible-Tube Valves
5. Poppet Valves
6. Pneumatic Actuation
7. Electrical Actuation

Both single and bipropellant valves were addressed. In general, any of the single valve concepts can be incorporated into a bipropellant configuration. Some are more readily adaptable than others for reasons of size, complexity, propellant isolation, etc. Usually, a common actuator is a feature of a bipropellant valve. With mechanical linkage of both propellant valving elements to a common actuator, the effects of variations in propellant conditions on response matching in opening and closing the two propellant elements are minimized. Mechanical coupling of the elements minimizes the potential for out-of-tolerance oxidizer/fuel mixture ratios. Axial clearance in the valving element linkage can be minimized for essentially coincident opening and closing

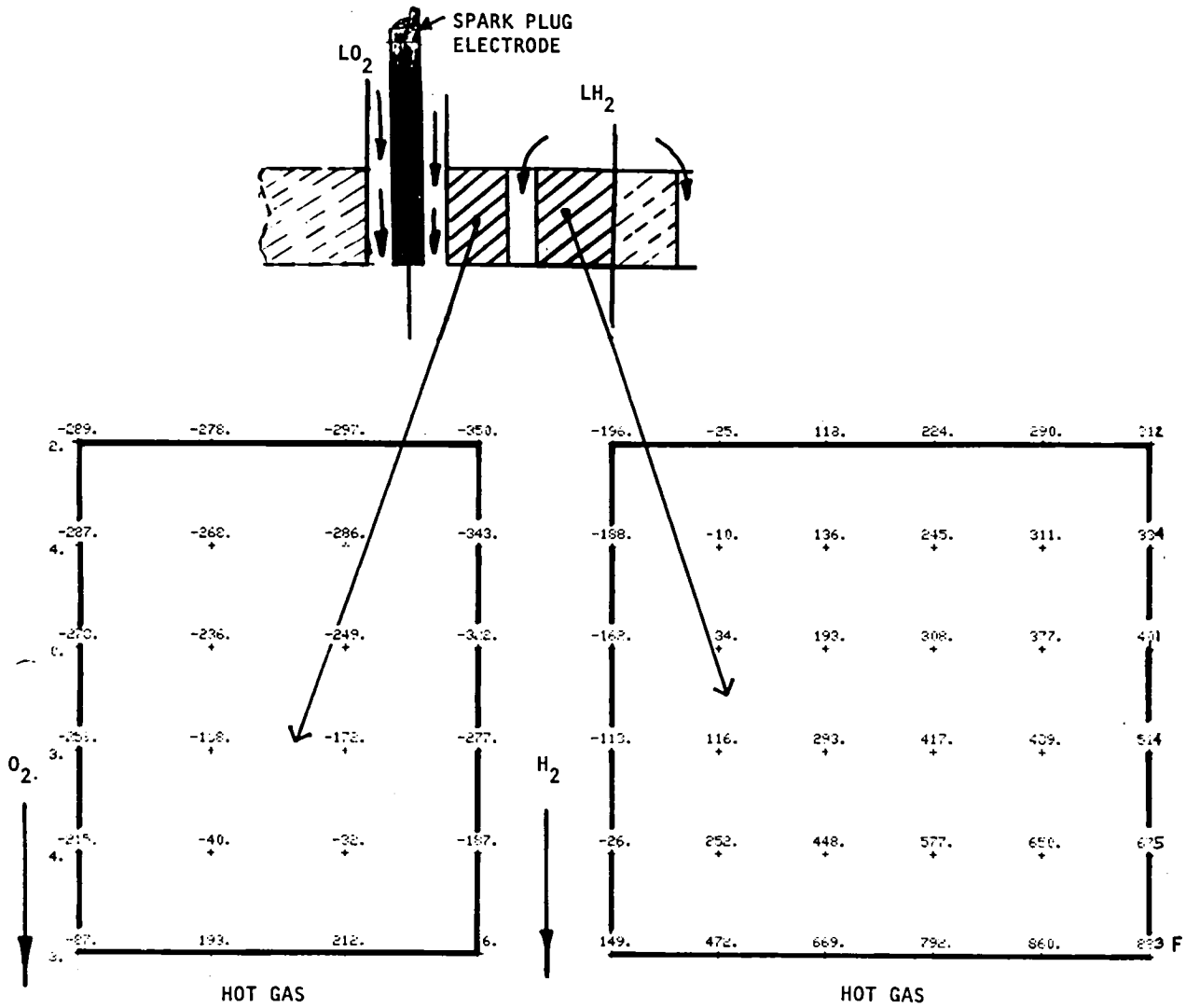

Figure 48. Injector Region Temperature Distribution (0.5 hg and MR_{core} = 50:1)

TABLE 2. SALIENT PROPELLANT VALVE TRADE STUDY DESIGN REQUIREMENT

1.	Propellants	Hydrogen Oxygen
2.	Operating Temperature Range	20 - 422K (37 to 760R)
3.	Propellant Temperature Range	
	Hydrogen	20 - 31K (37 to 55R)
	Oxygen	90 - 111K (163 to 200R)
4.	Propellant pressures at Valve Inlet	
	Hydrogen	134 - 193 N/cm_2^2 (195 to 280 psia)
	Oxygen	134 - 193 N/cm^2 (195 to 280 psia)
5.	Pressure Drop (Maximums):	
	Hydrogen	17.0 N/cm_2^2 (25 psid)
	Oxygen	17.0 N/cm^2 (25 psid)
6.	Actuation Requirements	
	a. Pneumatic	To be determine
	b. Electrical	To be determined
	c. Hydraulic	Not available
7.	Opening and Closing Response (Goal)	Total time (delay + Travel) from signal to end of motion = 10 milliseconds maximum. Travel (motion) = 5 μsec max
8.	Internal Leakage (Goal)	100 sccm/hr with Gaseous Helium at operating pressure and temperature per items 3 and 4
9.	External Leakage	1 X 10^{-6} sccm/sec with Gaseous Helium at operating pressures and temperature per items 3 and 4
10.	Operating Life (Goal)	1,000,000 Cycles
11.	Failure Criteria - The valve shall fail safe closed upon loss of actuation power.	

of both propellant elements. Also, the axial clearance can be designed to permit partial opening of the fuel element prior to cracking of the oxidizer element from its seat. A fuel-lead opening will be accompanied by a fuel-lag closing. These conclusions are valid for actual mechanical linkage of the valving elements. A disadvantage of this approach is the need for seals to prevent propellant mixing within the bipropellant valve.

While end-item operational and failure mode considerations appeared to favor the use of a bipropellant concept, the single valve approach provides more flexibility for a development demonstration program in which parametric relationships involving start-shutdown sequencing will be evaluated. The basic valve design concepts were therefore assessed relative to both their merits as single valves and on their potential for incorporation into bipropellant valve assemblies.

Rotary Valves. A typical concept for a rotary valve would employ a linear motion actuator, a rotary shaft seal, and a stationary valve closure seal. The valving element could be of the ball, butterfly, or plug type. Linear actuator motion is converted to rotary motion either by rack and pinion gearing or by an articulated linkage arrangement. Opening and closing of the valve is controlled by the linear actuator in response to its power mode.

Conventional rotary valves require sliding or scrubbing relative motion, especially in valves with fast response and high velocities, and impose limitations on cycle-life endurance capabilities.

The required 20 to 422 K (37 to 760 R) operating temperature range restricted the use of elastomer or plastic seals. The program design leakage goals impose closure seal leakage limits beyond the demonstrated capabilities of metal-to-metal valve seals with relative rotary motion.

Use of a linear-displacement metal bellows seal to prevent shaft external leakage is a design alternate to the use of rotary shaft face seals or lip seals. The bellows seal complied with program design requirements for essentially zero external leakage. The use of a flexing seal, however, compromised reliable attainment of the design goal of 1,000,000 open-close valve cycles.

A variation of the rotary valve design concept is one in which a flat plate, or blade, is rotated to block or to open the valve flow path. Compressible circumferential seals at the upstream and downstream port interface with the blade cavity to effect a closure seal. Blade valves require the shortest axial distance between the inlet and outlet blade and stationary seals. The cryogenic temperature operating range limited the selection of pliable materials for tight sealing. Flexible metal seals, compatible with the temperature range, have the inherent disadvantage of scrubbing contact at high velocities accompanying fast valve response.

The two basic power modes available for valve actuation are pneumatic or electrical. A pneumatic actuator requires the use of a pilot solenoid to initiate valve action opening or closing. The delay required for a pilot valve plus pneumatic charging, travel, and venting times would make meeting the desired

response time impractical. The speeds required would require large pilot valves, and the actuator would undoubtedly incur impact and rebound problems at each end of the stroke.

The primary disadvantages of electric-motor valve actuators, for direct actuation of valves with significant force levels and fast response, are space vehicle limitations on electric power demands, high weight-to-power ratios, and low torque-to-inertia ratios. Capability for acceleration to the motor running speed required for full valve stroke within 0.010 second results in a large motor inertia, as reflected at the gear train output shaft, and would introduce impact and rebound problems similar to those encountered with high-speed pneumatic actuators. In addition, no convenient method of fail-safe closing is available.

A final item that precludes the rotary valve from being a viable concept involves valve sizing. The equivalent orifice diameter for this application was 0.193 cm (0.076 in.). This size lies below the practical manufacturing limit for ball, butterfly, and plug-type rotary valve components.

Miscellaneous Valves. There are several miscellaneous valve concepts ranging from bellows-disk valves, diaphragm seals, pinch valves, flexible-tube valves, etc., to the linear displacement equivalent of the angular displacement blade valve discussed earlier.

These valves were all rejected upon close examination by some of the problems that beset rotary valves. The environmental temperature range of 20 to 422 K (37 to 760 R) precluded the use of conventional flexing material for effecting valve actuation. Bellows-diaphragms of metal have not exhibited the life-cycle capability required for this application. Thus, none of these concepts were serious contenders for the intended application.

Poppet Valves. When evaluating poppet valves, the primary difference lies in the actuation method. A poppet valve may be pneumatically actuated using an electrical pilot valve for event initiation or use direct electric actuation, such as a solenoid valve.

There are many applications where the flow capacity of the valve and/or ultra-low ΔP performance requires the use of a relatively large flow diameter. The attendant result is a large seating diameter and, correspondingly, a large seating area. The inlet propellant prressure thereby produces a large unbalanced force that must be overcome to initiate and accomplish valve opening. This is the typical application for a pneumatically (or, in some cases, hydraulically) actuated valve using an electrical pilot involving only small forces to initiate action. Because flow requirements for this application indicate a valve equivalent orifice diameter of only 0.193 cm (0.076 in.), the use of such a pilot-operated poppet valve is not warranted. The maximum initiation force for poppet movement was calculated to be less than 8.9 N (2.0 pounds). Therefore, the simplest, most direct approach to valve actuation is to utilize a direct solenoid-actuated poppet valve. This design concept also offered the advantage of eliminating critical dynamic seals other than the main poppet-seat closure seal, which contributes to extended cycle-life endurance capability.

Basic approaches to poppet-seat closures are to use either soft- or hard-seating elements. In a poppet valve, the use of a soft-seating element could result in stroke variations as a result of material cold-flow and/or multiple impacts. This would be especially critical for small thruster valves where the total valve stroke is only a few millimeters. Soft valve seating would, therefore, be detrimental to minimum impulse repeatibility and potentially to steady-state performance.

Hard valve seating, conversely, ensures repeatable stroke and outlet diameter dimensions for the total life of the component. Experience at Rocketdyne has resulted in a method for overcoming scuffing normally associated with hard poppet-seat interfaces. This involves the use of a flat-faced, metal-to-metal poppet and seat with two concentric seat lands. Contact between the poppet and the inner land provides the closure seal. When the poppet is seated on the inner land, there are a few thousandths of a millimeter clearance between the poppet and the outer land. When the valve is open and is stroking to the closed position, angularity between the plane of the poppet sealing surface and the plane of the inner seat land sealing surface results in impact at the seat outer land. The potential for sealing surface impact deformation or abrasion is thereby minimized. This poppet and seat concept places the design emphasis on poppet guiding to minimize scuffing of the poppet against the seat as seating occurs. In addition, the poppet is carried within a lifter which allows the poppet to be fully independent of the armature mass to reduce impact and to eliminate poppet rebounding.

Based on the results of this trade study, a direct solenoid-actuated, poppet-type valve with metal-to-metal seating was selected. Since fast response and repeatability are important, an existing valve was ideally suited for this application. A sectional view of the valve is presented in the Hardware Design and Fabrication section. The valve utilizes a metal-to-metal seat design and a solenoid coil construction which lends itself to thermal isolation techniques. This feature is important since the flowrates are small, and excess heat input to the incoming propellants is undesirable for pulse mode operation. Actuation of the valve with a driver circuit will be utilized to impress a larger-than-normal voltage at valve opening, and thus provide the increased pulloff force to ensure rapid and repeatable opening. As soon as the valve motion is underway, the voltage will be dropped to the hold-open valve. This will then allow rapid and repeatable closing since the lowered voltage will result in a lower flux field for collapse time within the coil.

HARDWARE DESIGN AND FABRICATION

Based on the previously described analyses, a propellant injection system consisting of a dual-sleeve, triaxial injection/combustor design was selected because of its performance potential, development flexibility, and inherent compatibility with the combustor/thrust chamber walls (Fig. 49). The dual-sleeve, triaxial injection system utilizes a primary injector/combustor where all of the oxygen and 8% of the hydrogen is introduced, a secondary injector/combustor where 45% of the hydrogen is injected through an annulus to mix and react with the oxygen-rich hot gas from the primary combustor, and a boundary layer coolant injector where the remaining 47% of the hydrogen is introduced through an annulus to cool the thrust chamber throat/nozzle region. The resulting stepdown in propellant mixture ratio from 50:1 (primary combustor) to 7.5:1 (secondary combustor) to 4:1 at the boundary layer coolant injector was determined from previously described analyses to provide the maximum combustion performance capability with this injection/combustor system.

Ignition system design criteria developed during the Design Analysis portion of the program defined an igniter spark plug configuration for the thruster assembly. The selected spark plug geometry is illustrated in Fig.49 and consists of a 0.25-cm (0.10-in.) diameter electrode with a 0.063-cm (0.025-in.) annular spark gap. An inductive discharge exciter with a spark energy of 10 mJ was selected for the baseline ignition system.

A previously described propellant valve trade study identified a direct-acting solenoid, poppet-type valve unit as the most favorable valve/actuation concept for a small thruster assembly. Integration of such a valve configuration within the thruster assembly on both the oxygen and hydrogen propellant sides is illustrated in Fig. 49.

Performance and thermal analyses also indicated that program minimum performance requirements could be attained with a thrust chamber wall temperature of approximately 1367 K (2000 F). This temperature falls within the acceptable range for austenitic materials that maintain ductility at cryogenic temperatures, exhibit good oxidation resistance, and are readily fabricable. Because of these favorable physical characteristics, and the potential for meeting program performance requirements with a maximum thrust chamber wall temperature of 1367 K (2000 F), L-605 alloy was selected as one of the thrust chamber materials. A refractory metal is necessary if chamber wall temperatures in excess of 1367 K (2000 F) are to be tolerated for the sake of increased performance potential. Therefore, a review of candidate thrust chamber materials capable of operation at wall temperatures up to 1644 K (2500 F) in an oxygen/hydrogen environment was performed. Based on this study, unalloyed, low-carbon molybdenum was selected as the alternate high-temperature thrust chamber chamber material.

This section describes the detail design and fabrication of the major subcomponents within the thruster assembly. These include the injector/combustor system, ignition system, propellant valve, and thrust chamber.

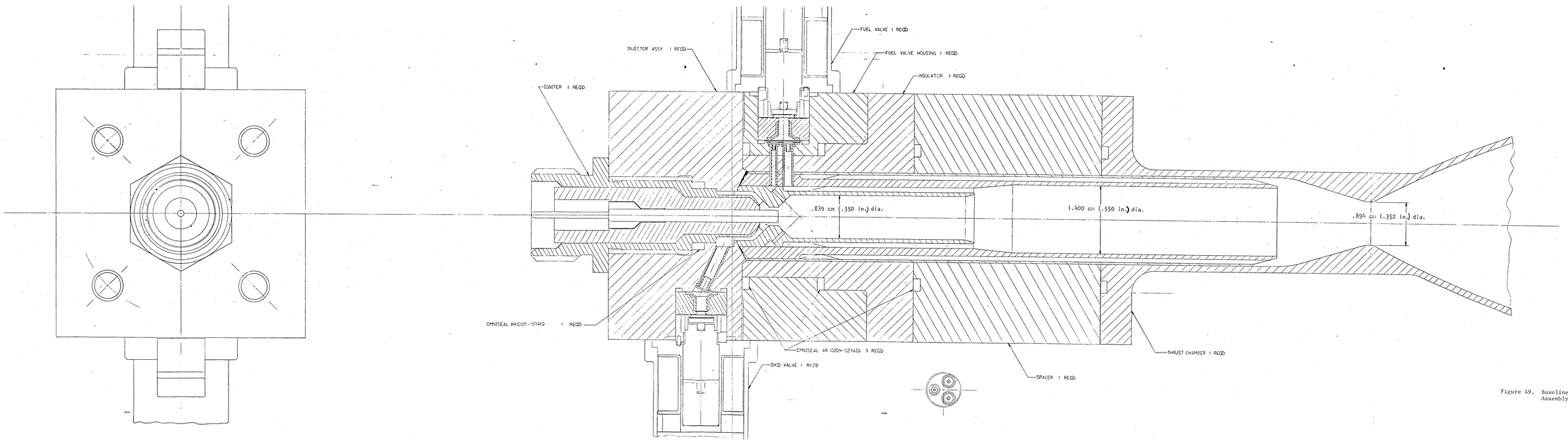

Figure 49. Baseline Thruster Assembly Design Layout

Injector/Combustor System

A detail drawing of the dual-sleeve, triaxial injection system is included as Fig. 50. The injection system was designed to permit parallel fabrication of two separate parts to minimize manufacturing flow time. One part, the forward housing, is fabricated from 304L stainless-steel material and includes mounting cavities for both the oxygen valve and spark plug igniter. The other part consists of an aft sleeve assembly that is fabricated from nickel material and incorporates both the sleeve/combustor coolant passages and the separate hydrogen injection elements spaced along the length of the combustion chamber.

Sequential fabrication of the aft sleeve assembly was initiated by machining eighteen 0.101 x 0.101 cm (0.040 by 040 in.) coolant slots within the primary combustor (MR = 50) sleeve (Fig. 51). Previous thermal analysis has indicated that this coolant channel configuration would result in a maximum primary sleeve wall temperature of approximately 478 K (400 F) and a pressure drop of less than 3.5 N/cm^2 (5 psi). The low combustor head-end wall temperature and low pressure drop are favorable both from a heat soakback and propellant flow control standpoint.

Following machining of the four primary injector hydrogen orifices at the forward end of the sleeve, an internal mandrel was installed and the coolant channels were filled with "rigidax" preparatory to nickel electrodeposition closeout of the channels (Fig. 52). Sufficient nickel was deposited to both closeout the primary combustor coolant channels and form the secondary combustor sleeve on the aluminum mandrel. Sixteen channels approximately 0.254 cm (0.100 in.) wide and 0.091 cm (0.036 in.) deep were then machined into the forward end of the sleeve assembly to transfer hydrogen to the forty eight 0.051 cm (0.020 in.) wide and 0.091 cm (0.036 in.) deep secondary combustor coolant channels which were machined into the aft end of the sleeve assembly (Fig. 53). Two-dimensional heat transfer analyses indicated that because of hydrogen coolant property variations and a change from liquid to gaseous cooling correlations at approximately 83 K (150 R), a sharp peak in secondary sleeve wall temperature occurred approximately 0.76 cm (0.3 in.) downstream from the secondary injection point (Fig.54). Because this large temperature gradient can result in axial heat conduction along the sleeve length, which would tend to reduce the peak value, a three-dimensional thermal model was constructed having 780 nodes and capable of handling the axial variation of coolant bulk temperature and coolant-side film coefficient. A typical comparison of two-dimensional and three-dimensional maximum wall temperatures is illustrated in Fig. 54 . The actual maximum wall temperature of 982 K (1308 F) was 314 K (566 F) lower than the two-dimensional value. Because of this substantial reduction in temperature, the possibility of utilizing larger channel sizes and land widths was investigated. However, as shown in Fig. 45 , to maintain a coolant pressure drop of less than 5.5 N/cm_2 (8 psi) for flow control, the larger channel sizes resulted in higher wall temperatures, even with the axial conduction influence. Therefore, a 0.051 cm (0.020 in.) by 0.091 cm (0.036 in.) channel size was selected for the secondary combustor sleeve. For improved indexing during machining, the number of coolant channels was increased from 46 to 48, which resulted in a land width of 0.051 cm (0.020 in.).

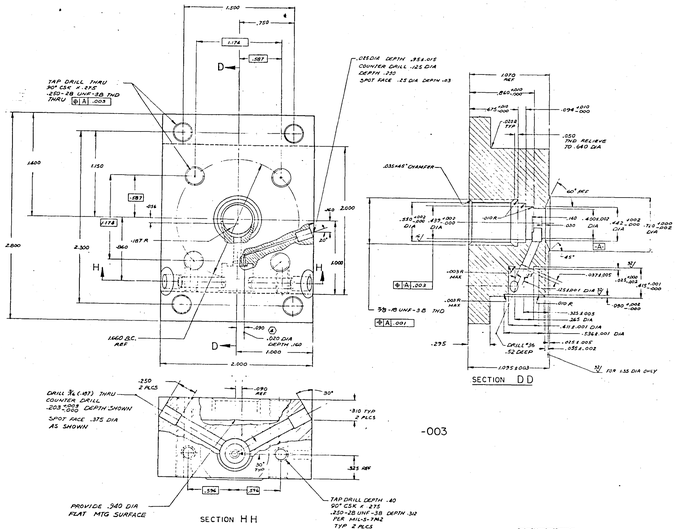

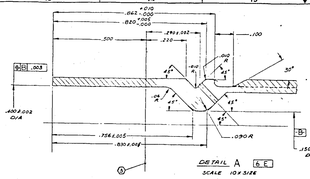

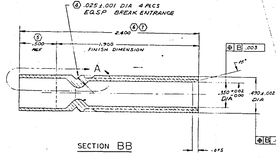

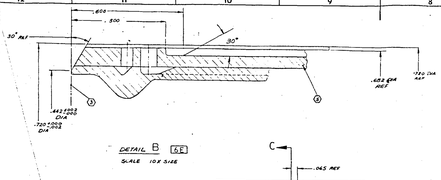

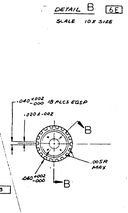

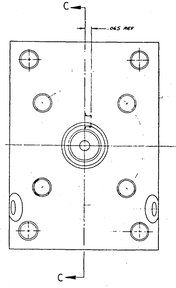

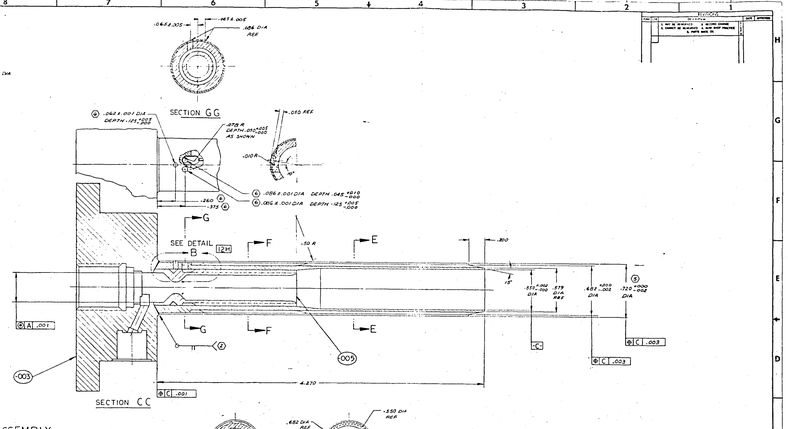

Figure 50. Auxiliary Propulsion System Thruster Injector Assembly

(7) PLANNING NOTE: LENGTH NEED FOR FABRICATION
(8) EDM HOLES TO MATCH HOLES IN 99R0105732. BOLT 99S010572 TO THIS PART PRIOR TO FINAL EDM OPERATION CONSULT ENGINEERING FOR PROPER ORIENTATION
(9) ELECTRO DEPOSIT NICKEL PER ENGINEERING INSTRUCTION
(10) MAY BE PERFORMED BY ELECTRO-DISCHARGE MACHINING
(11) MACHINING DATUM PLANE PRIOR TO ED HOLD AND AFTER ELECTRO DEPOSITE OF NICKEL
(12) E.B.W. PER MS 10740-042 & MACHINE PER RA0103-016

-005	NICKEL 200		
-003	304 L CRES		
NO	MATERIAL	SIZE	SPECIFICATION

-001
-10

1XZ42-3/1/77-C1C

Figure 51. Primary Combustor Sleeves

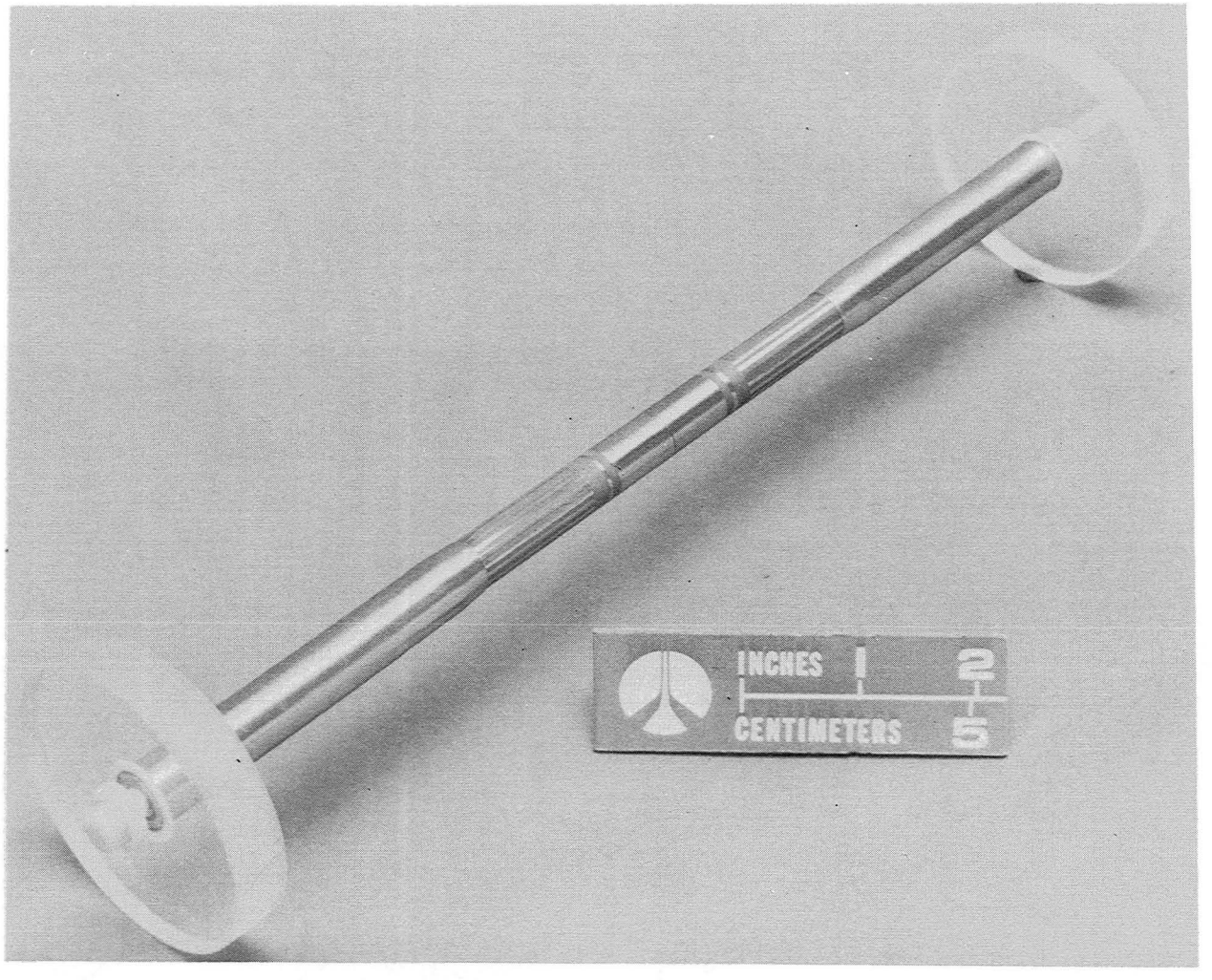

1ST42-3/11/77-C1*

Figure 52. Primary Combustor Sleeves With Channels Rigidaxed and Installed on Electroform Mandrel

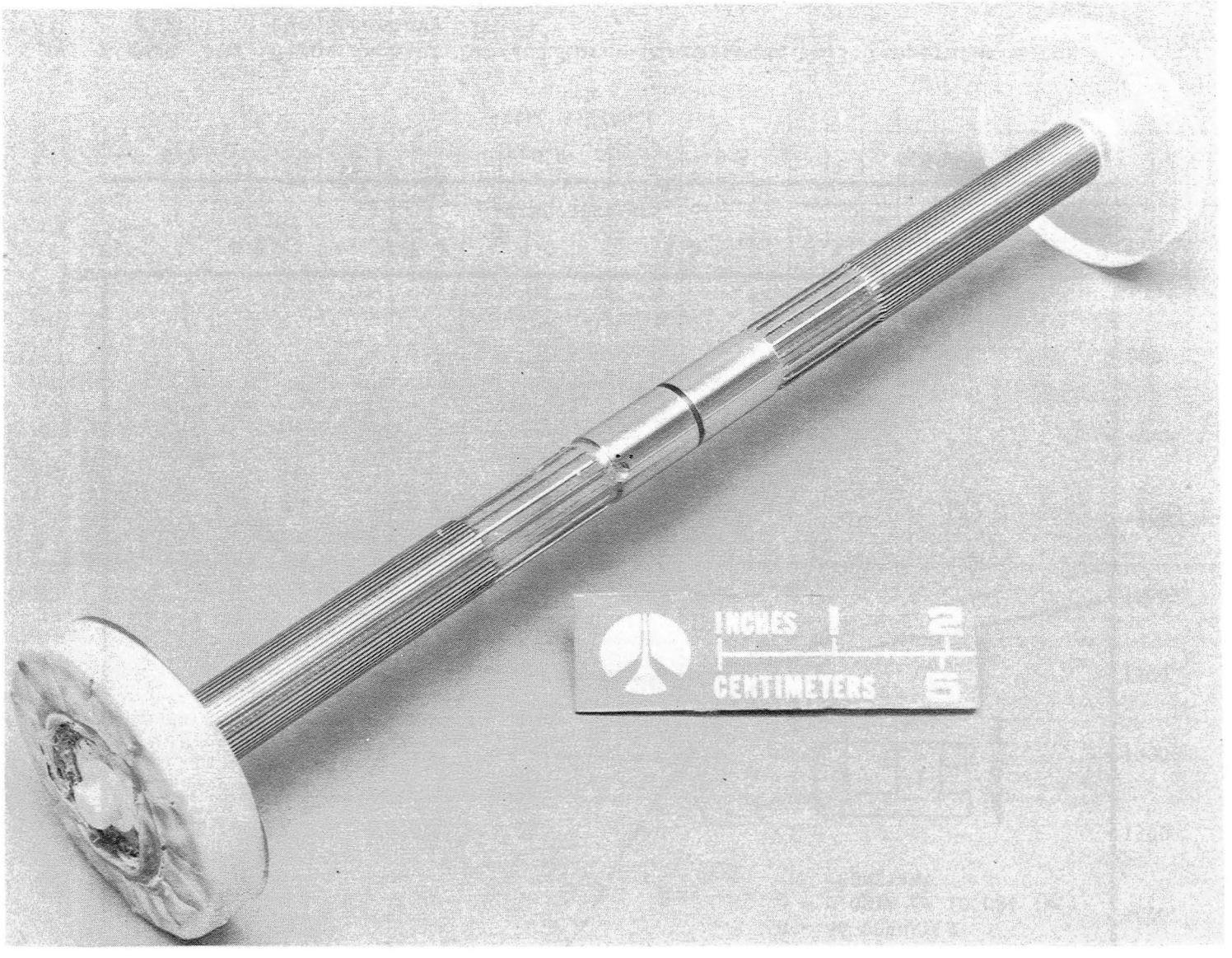

1ST42-4/1/77-C1*

Figure 53. Secondary Combustor Sleeve on Electroform Tooling

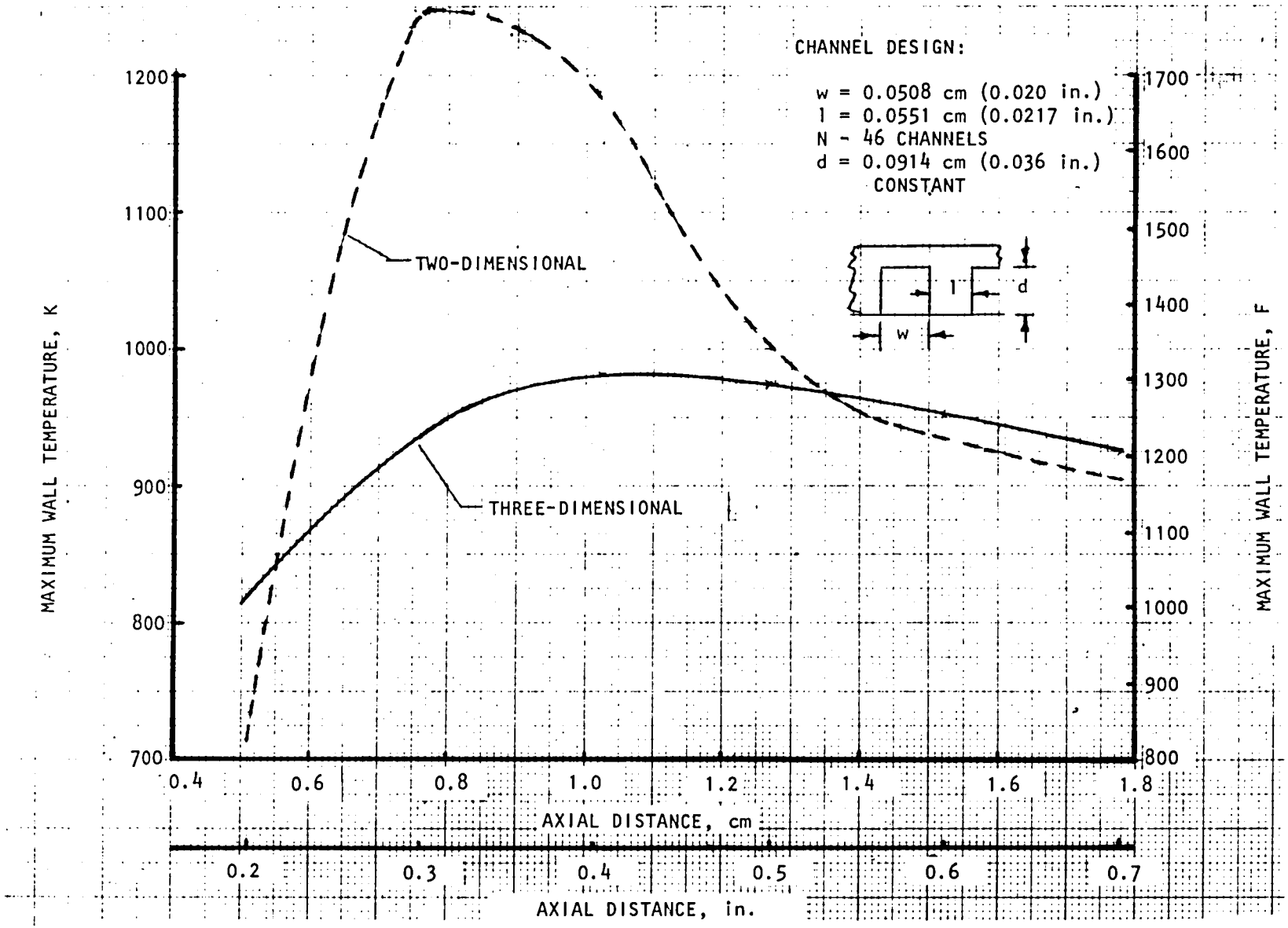

Figure 54. Comparison of Two-and Three-Dimensional Wall Temperatures for the Secondary Sleeve

To minimize coolant system parasitic pressure losses, the number of coolant channels in the forward section of the secondary sleeve was selected to be 16. This results in a 1.7 times increase in flow area over that of the aft coolant channels. The approach of utilizing an even multiple reduction in the number of channels allows visual and mechanical inspection to ensure obstruction-free coolant channels.

Following a final electrodeposition process to close out the secondary sleeve coolant channels (Fig. 55), the aft sleeve was final machined and electron-beam welded to the forward housing to complete the injection system assembly. The completed injector/combustor system assembly is shown in Fig. 56. An internal view showing the three hydrogen injection locations within the injector/combustor system assembly is shown in Fig. 57. At the first location, approximately 8% of the hydrogen is injected through four primary combustor orifices where it reacts with all of the oxygen which is injected through a central annular spark gap (MR = 50). At the second location, which is located 3.8 cm (1.5 in.) downstream of the primary injection orifices, approximately 45% of the hydrogen is injected through 18 orifices where it reacts with the oxygen-rich hot gas from the primary combustor. And finally, at the third location, which is located 5.8 cm (2.3 in.) downstream from the secondary injection orifices, the remaining 47% of the hydrogen is introduced through 48 orifices to both react with the secondary combustor hot gases and cool the thrust chamber throat/nozzle region. Two injector/combustor system assemblies were fabricated.

Ignition System

The fabrication drawing of the selected spark-torch igniter is illustrated in Fig. 58. This igniter design is a direct outgrowth of the unit used on the Advanced Space Engine (ASE). However, several design modifications which were discussed earlier, were implemented to minimize trapped propellant volume and facilitate producibility. The spark-torch igniter consists of a nickel electrode, an alumina ceramic insulator, and an outer 321 CRES housing. The electrode and outer housing are sealed to the insulator with nickel brazed seals. An external electrical connector was designed for attachment with an existing cable to an inductive exciter unit. The igniter is capable of sustaining a maximum voltage of 10 kV. A Teflon insert was placed over the forward end of the ceramic prior to installation to protect the insulator from thermal/mechanical shock and improve oxygen flow distribution at the electrode injection annulus.

Eight igniter spark plugs (Fig. 59) were procured from Simmonds Precision Industries, Inc.

Propellant Valves

An earlier trade study (Design Analysis section) resulted in the selection of a solenoid-actuated poppet valve with a flat metal-to-metal seat closure. The selected valve concept matched the size, operational capability, and detailed design features of a qualified three-way solenoid valve from the Saturn program (NA5-27273). Therefore, design analysis was directed toward defining the necessary rework to meet current program design/operational requirements. The reworked propellant valve design is illustrated in Fig. 60 .

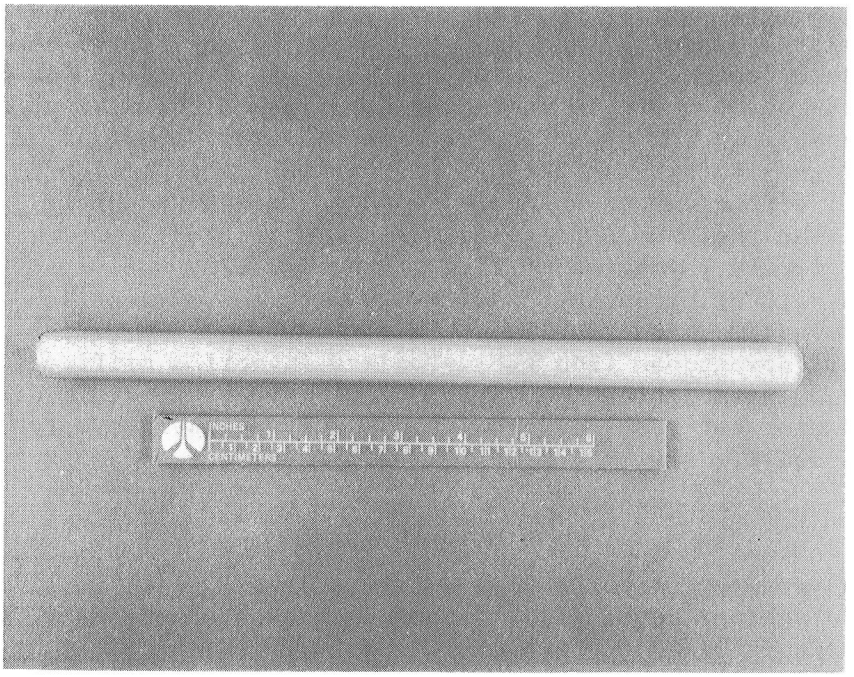

Figure 55. Combustor Sleeve Assembly After Final Coolant Channel Closeout

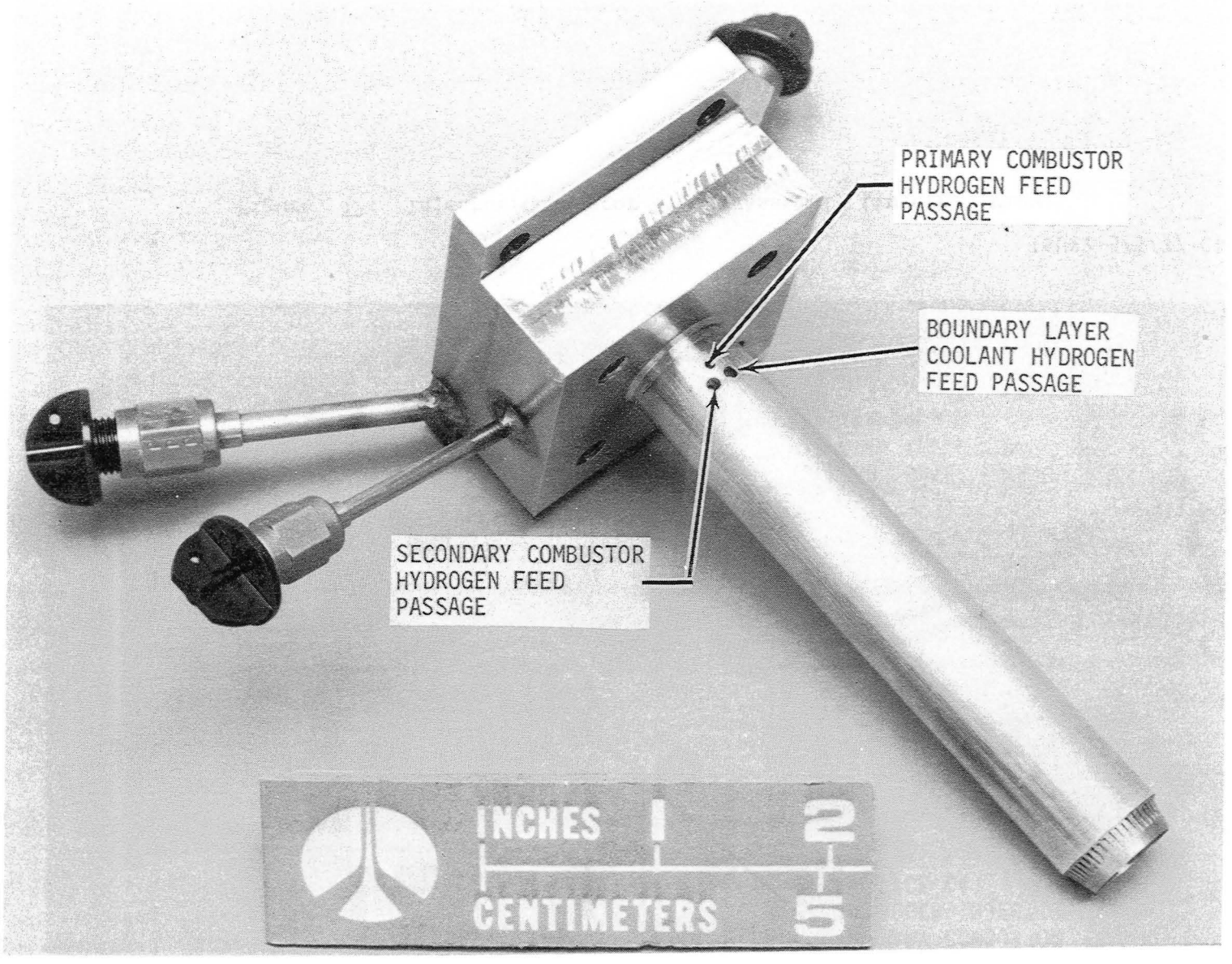

1SU22-5/5/77-C1E*

Figure 56. Injector/Combustor System Assembly (External View)

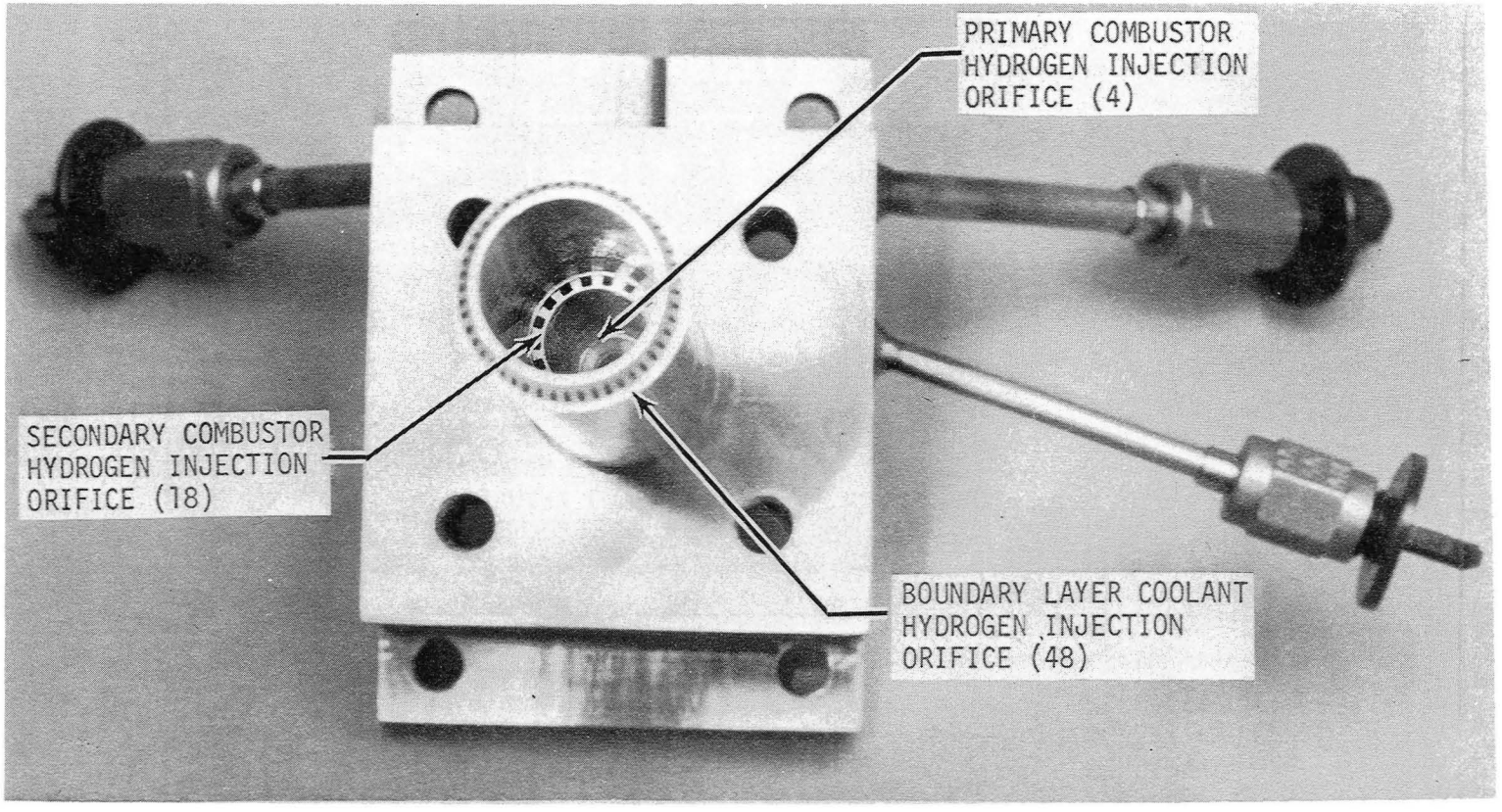

1SU22-5/5/77-C1B*

Figure 57. Injector/Combustor System Assembly (internal view)

DO NOT SCALE — WORK TO DIMENSIONS GIVEN

ITEM	PART NO.	NAME	MATERIAL
1.		ELECTRODE	NICKEL 200
2.		INSULATOR	ALUMINA 85-95%
3		WASHER	NICKEL 200
4.		SEAL, INNER	NICKEL 200
5		SHELL, IGNITER	STAINLESS STEEL AISI 321
6.		BUSHING, SEAL	NICKEL 200

REVISIONS							
ZONE	CHANGE NO	STA CHG	STA REV	DESCRIPTION	DATE	D'MAN	APPD

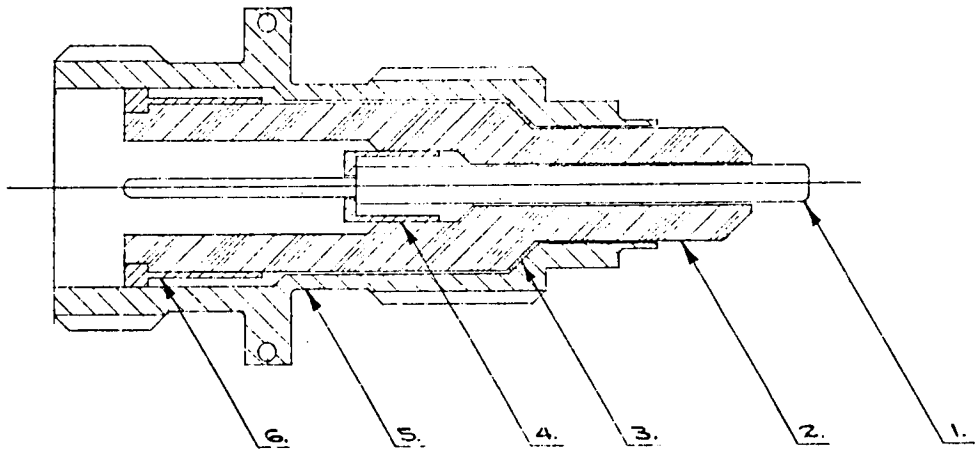

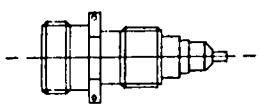

FULL SIZE

TOLERANCES UNLESS OTHERWISE SPECIFIED	DRAWING INTERPRETATION PER ESD SPEC 105555	DRAWN N.D. LAWRENCE 2-15-77
FRACTIONS ± 1/32 DECIMALS ± .010 ANGLES ± 2°		CHECKED
MATERIAL SPEC	STD PROCEDURE ☐ YES ☐ NO	ENG D'MAN
		STDS
PROCESS SPEC	NEXT ASSEMBLY	ENG APPD
		PROD APPD
ENGINEERING APP	PREPARED UNDER CONTRACT	
	FURNISHED UNDER CONTRACT	

Simmonds Precision
ENGINE SYSTEMS DIVISION NORWICH, NEW YORK 13815

SPARK PLUG, PROPOSED
(PN-49876)
(ROCKETDYNE PN-AP77-002)

CODE IDENT NO	SIZE	PART NO
83311	C	126961

SCALE 4:1 WT REF SHEET

Figure 58. Proposed Spark Plug

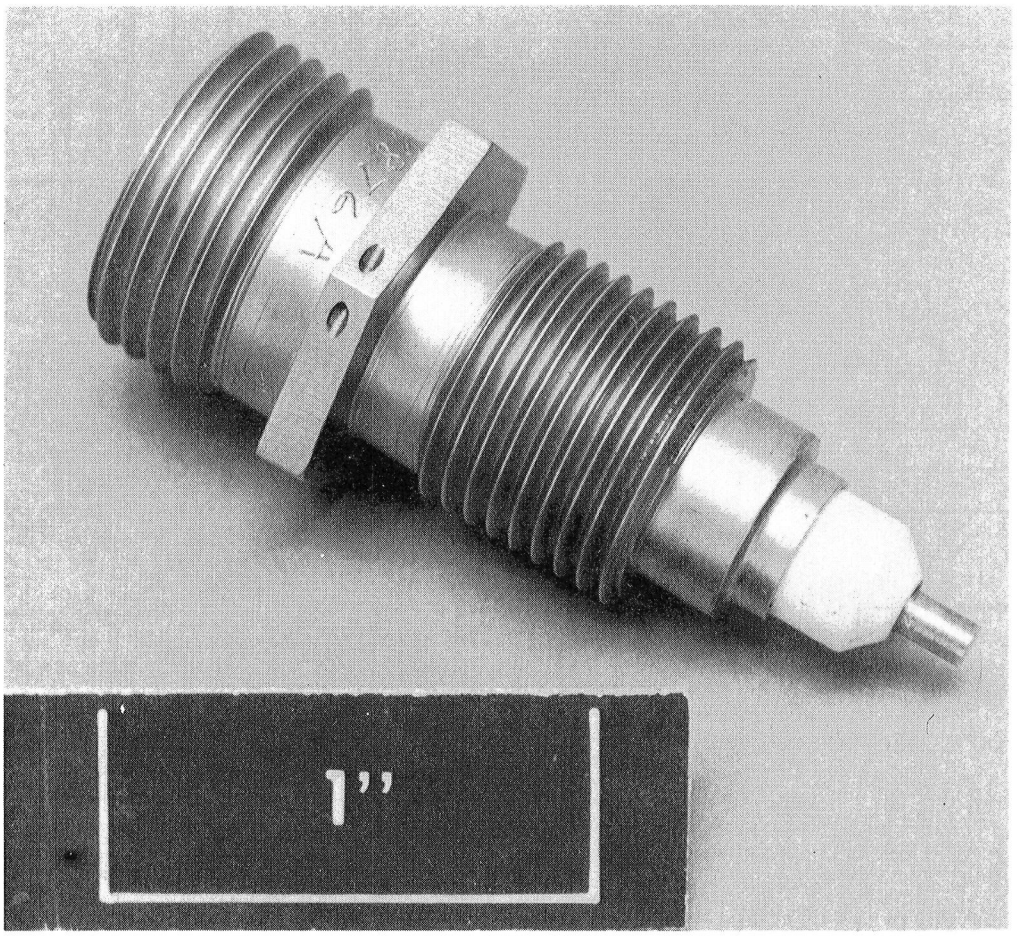

ISU-5/5/77-C1G*

Figure 59. Igniter Spark Plug

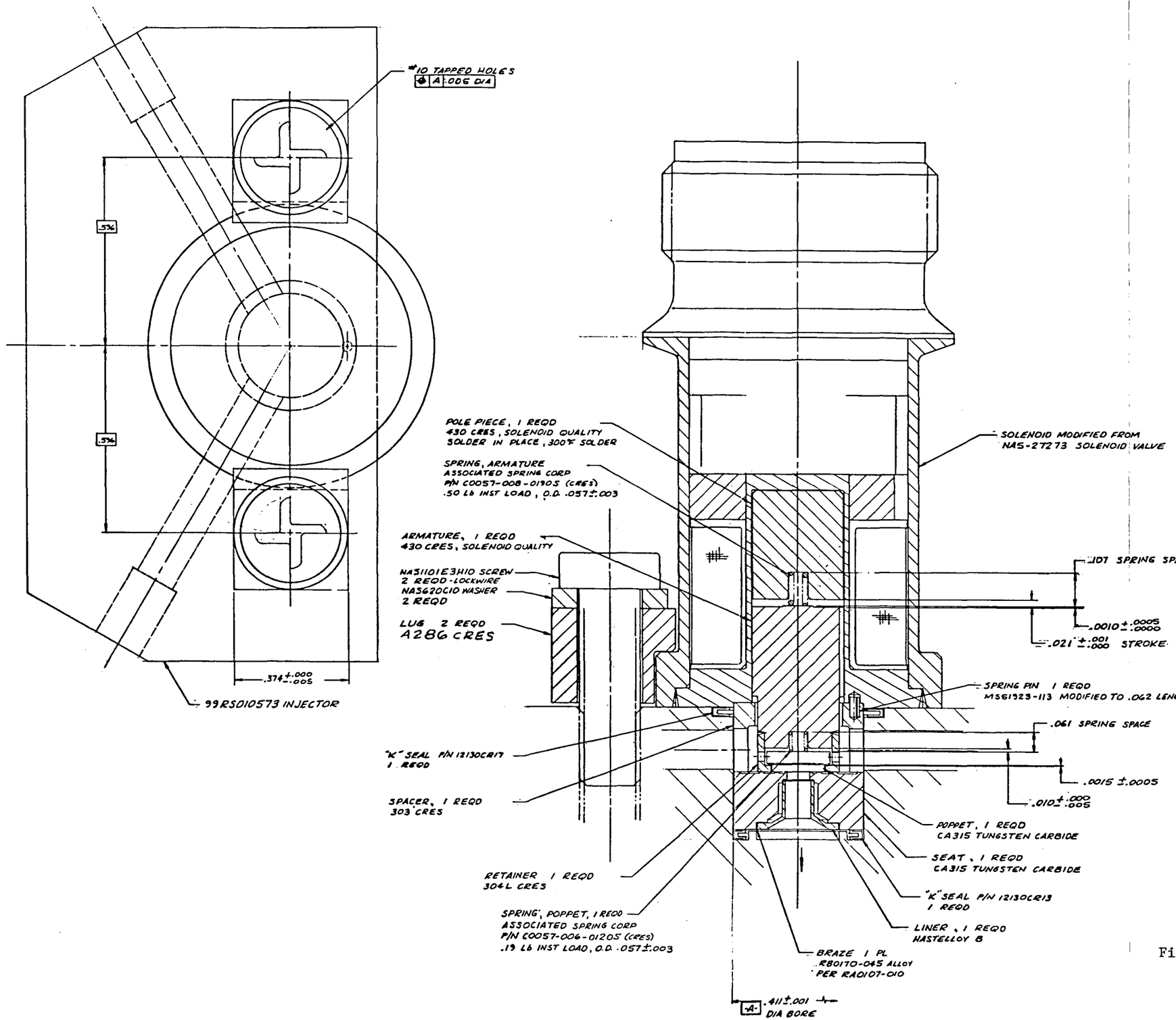

Figure 60. 11.3 kg (25 lb) Thrust LH_2/LO_2 Engine Propellant Valve

The existing NA5-27273 solenoid valve utilized a push-type action which was not favorable for this application because, to minimize propellant trapped volume, the coil-valve unit must be integrated with the thruster assembly. The solenoid was therefore converted to a pull-type action by soldering a pole piece into the bore and fabricating a new armature unit. The armature unit includes a poppet, compression spring, and a retainer. The retainer provides a positive stop for the armature and thus absorbs the impact force resulting from the armature mass and velocity during closure. An axial clearance between the retainer and poppet permits self-alignment of the poppet for compliance with the seat. The poppet spring provides a small bias force for seating at low supply pressures. The armature spring has approximately twice the force of the poppet spring to ensure positive contact between the armature retainer and the seat. The pole piece and armature are fabricated from solenoid quality 430 stainless steel, both for its high electrical resistivity, which enhances rapid response by minimizing eddy currents during low-temperature operation, and for its saturation flux density. A thin, dense chrome plate was applied to the armature for wear resistance.

The poppet and seat are a flat seal design and were fabricated from fine grain tungsten carbide, which provides wear resistance and a favorable surface texture. The seat has an inner and an outer land. The outer land, which is slightly below the plane of the inner land, acts as an alignment bumper for the poppet, while the inner land provides the seal. The seat member includes a thermal liner to minimize transient heat input to the propellant.

A valve seat diameter of 0.208 cm (0.082 in.) and a minimum valve stroke of 0.048 cm (0.019 in.) are required to meet the valve pressure drop allocation of 13.8 N/cm^2 (20 psi). At the maximum propellant inlet pressure, the combination of armature spring and propellant pressure unbalance forces is approximately 8.9 N (2 pounds). This value was determined from a series of force-stroke-current tests to be well within the valve actuation capability for the selected coil-armature arrangement.

Details for three propellant valve assemblies (one spare) were fabricated and are illustrated in Fig. 61. The valves were assembled and subjected to a series of dimensional and functional checks including:

1. Stroke Measurement
2. Proof-Testing and External Leakage
3. Internal Leakage
4. Cyclic Actuation
5. Response Time
6. Pull-in/Dropout Current
7. Flow Resistance

Based on the results of these bench tests, it was concluded that the valve assemblies were functionally suitable for thruster installation. A valve opening and closing response time of less than 5 and 3 msec, respectively, at an inlet pressure of 275 N/cm^2 (400 psig) was demonstrated during these bench checkout tests.

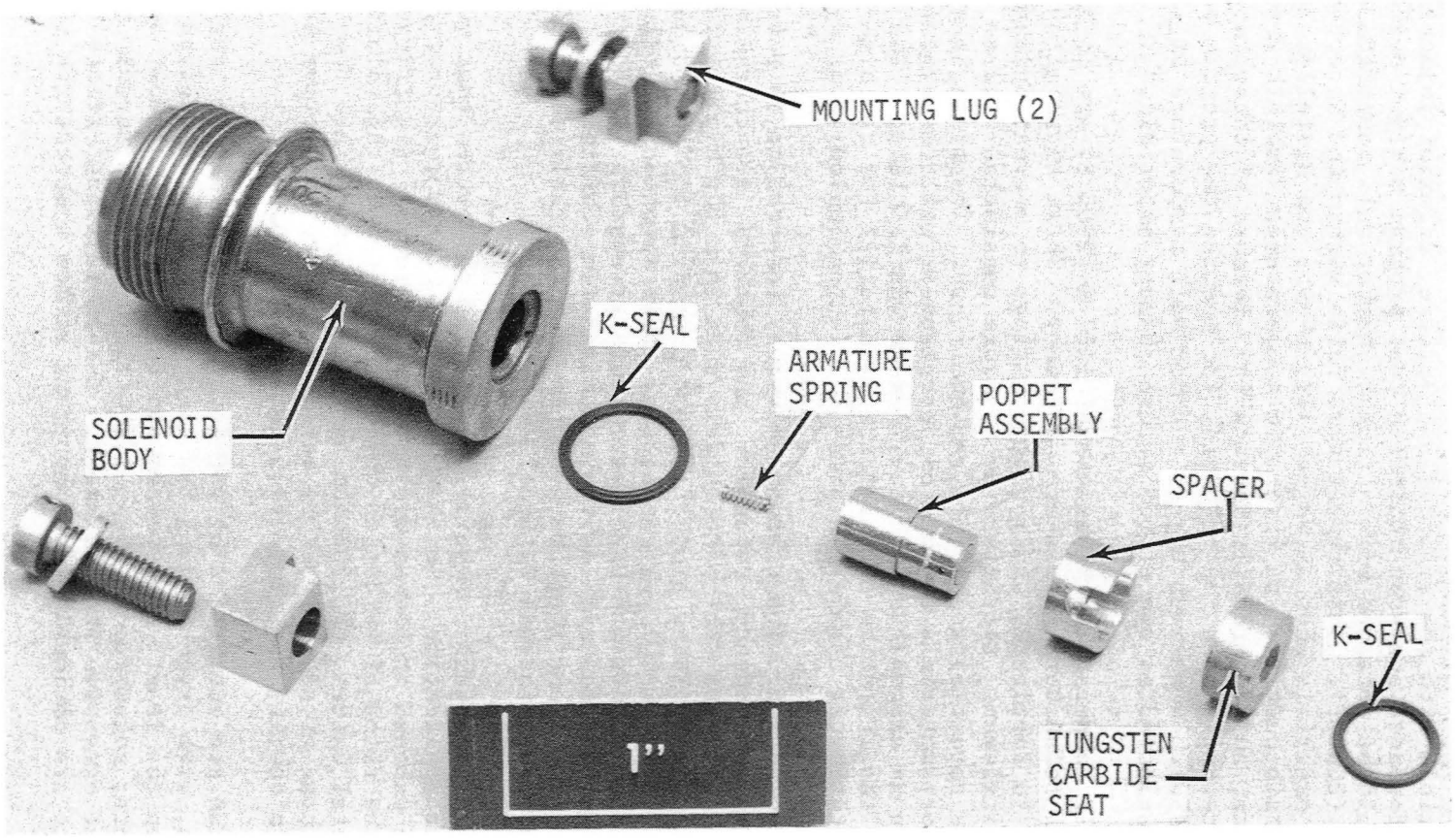

1SU22-5/5/77-C1D*

Figure 61. Propellant Valve Details

Thrust Chamber

Detailed design analysis was conducted relative to a thrust chamber configuration which was compatible with the selected dual-sleeve, triaxial injection system. Earlier performance analyses indicated that program minimum performance requirements could be attained with a thrust chamber wall temperature of approximately 1367 K (2000 F). This temperature falls within the acceptable range for austenitic materials such as Haynes 188, L-605, and Hastelloy X. These materials maintain ductility at cryogenic temperatures, exhibit good oxidization resistance, and are readily fabricable. Because of these favorable physical characteristics and the potential for meeting the program performance requirements with a maximum thrust chamber wall temperature of 1367 K (2000 F), L-605 was selected as one of the thrust chamber materials.

If thrust chamber wall temperatures in excess of 1367 K (2000 F) are to be tolerated, the use of refractory metals are necessary. While these alloys are expensive, difficult to fabricate, and require coatings to prevent oxidation and/or hydrogen embrittlement, refractory metals were considered because of the increased performance potential resulting from their use. Therefore, a study of candidate refractory materials capable of operation at wall temperatures up to 1644 K (2500 F) in an oxygen/hydrogen environment was initiated. The rationale leading to the selection of a refractory material for the high-temperature capability thrust chamber is presented in the following paragraphs.

Refractory Material Selection. The elements commonly referred to as refractory metals, i.e., tungsten, molybdenum, columbium, and tantalum, are characterized by several physical properties that particularly suit them for high-temperature thrust chamber application. These properties are presented in Table 3 along with similar properties for L-605 for comparison. Most importantly, refractory metals have high melting points and high temperature strengths. In addition, the high thermal conductivities and low thermal expansion coefficients, particularly for molybdenum and tungsten, tend to decrease their susceptibility to thermal shock and thermal fatigue.

However, refractory metals exhibit several deleterious properties that must be addressed in their application. As shown in Fig. 62 , the refractory metals oxidize rapidly when exposed to air at elevated temperatures. Significant differrences exist in the rates of oxidation which are related to the volatility of the respective metal oxides. Molybdenum and tungsten oxides are the most volatile. However, none of the refractory metal oxides are protective and, consequently, require coating for protection from oxidation.

Refractory metals also are embrittled by the interstitial elements: carbon, nitrogen, and oxygen, with oxygen having the greatest effect for a given concentration and carbon the least. Molybdenum and tungsten are the most sensitive to these elements; columbium and tantalum will accept considerably more contamination without excessive embrittlement. The embrittling effects of the interstitial elements are obviously more important at low temperatures than high temperatures.

TABLE 3. PROPERTIES OF REFRACTORY METALS (UNALLOYED)

Metal	Melting Point K	Melting Point (F)	Thermal Conductivity $W/m/m^2/K$ (Btu/ft/ft^2/hr/F)	Coefficient of Thermal Expansion μ m/m/F (μ-in./in./F)	Ultimate Tensile Strength @ 1644 K (2500 F) N/cm^2	(ksi)
W	3684	(6170)	167.2 (96.6)	4.5 (2.5)	31000	(45)
Mo	2883	(4730)	146.2 (84.5)	4.9 (2.7)	5511	(8)
Cb	2519	(4474)	54.5 (31.5)	6.8 (3.8)	4133	(6)
Ta	3269	(5425)	54.5 (31.5)	6.5 (3.6)	6889	(10)
L-605	1603	(2425)	22.7 (13.1)	16.9 (9.4)	0	

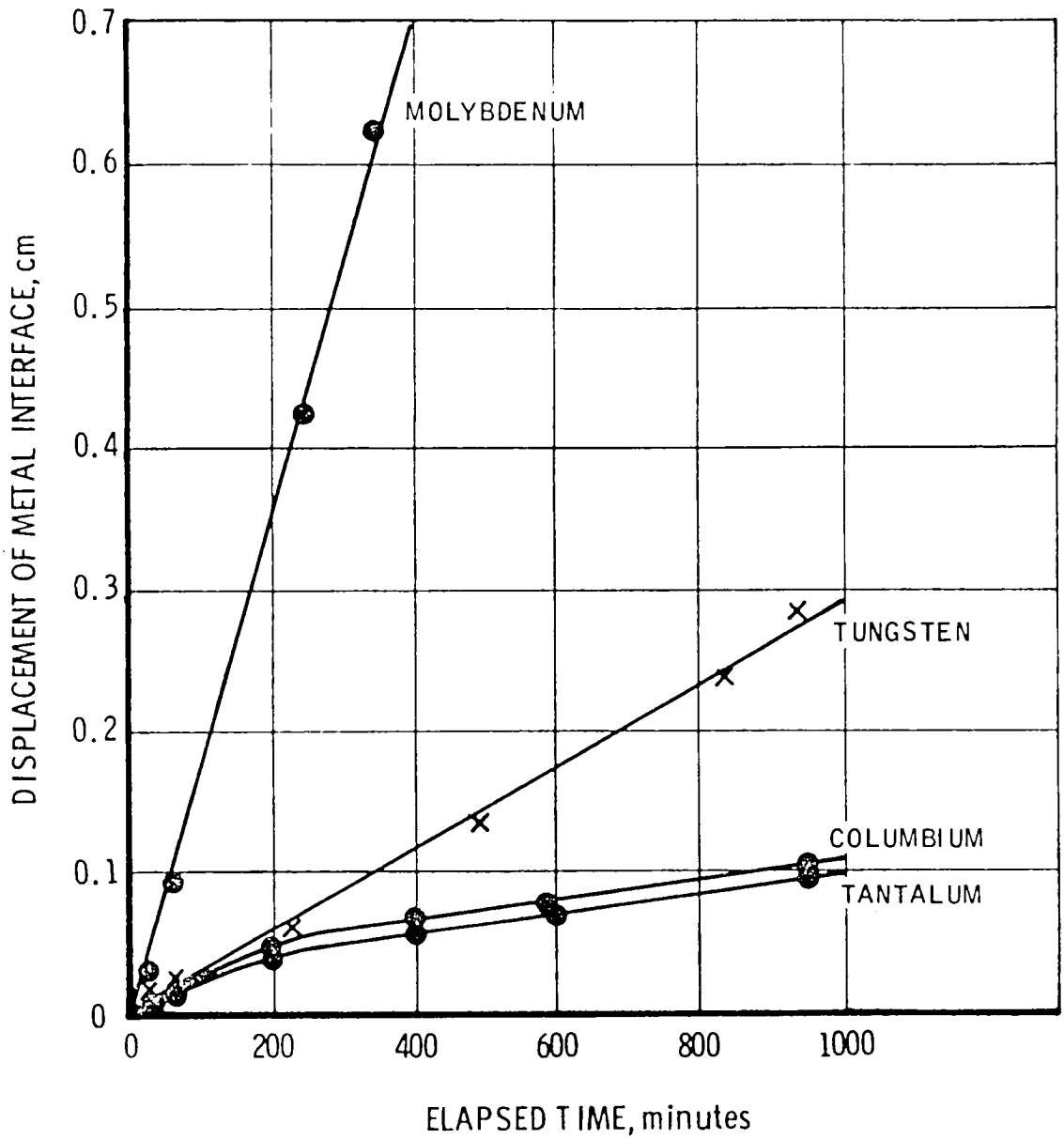

Figure 62 . Oxidation of Mo, Ta, and Cb in Flowing Air at 1367 K (2460 R)

Hydrogen has little effect on the mechanical properties of molybdenum and tungsten (Ref. 2). In these metals, hydrogen is difficult to introduce, is soluble in only a small degree, evolves relatively easily, and hydrides are not formed. Thus, molybdenum and tungsten can be used in hydrogen environments without detrimental effects. In contrast to molybdenum and tungsten, columbium and tantalum are greatly affected by hydrogen, even catastrophically under certain conditions at lower temperatures. The solubility of hydrogen in these metals decreases as the temperature increases. The tantalum-hydrogen system is very similar. At lower temperatures, columbium is embrittled by the formation of a stable hydride (β) and, under certain conditions, this embrittlement can be catastrophic, leading to fragmentation of the columbium. Although the formation of the hydride results in the greatest embrittlement of columbium, significant embrittlement of columbium by hydrogen still occurs at temperatures above which the hydride is stable. Above the hydride region, the greatest embrittlement occurs at moderately elevated temperatures at which hydrogen solubility and hydrogen absorption rates are high. The above discussion of hydrogen embrittlement pertains to columbium alloys, tantalum and its alloys, as well as pure columbium. Since the thrust chamber material will be exposed to hydrogen at temperatures from 367 K (200 F) and up, columbium and tantalum and their alloys were eliminated from consideration for this application because of the potential for severe hydrogen embrittlement.

Refractory metals all have an atomic arrangement designated as body-centered cubic (BCC). Metals having such a structure undergo a transition in behavior from ductile to brittle with decreasing temperature. In most BCC metals, this transition occurs at cryogenic temperatures and is not troublesome. Transition temperatures among the refractory metals vary greatly, as shown in Fig. 63, and these transition temperatures are influenced by many variables. The transition temperature is higher for recrystallized material than for cold-worked (and stress-relieved) material, and it is increased by increased interstitial element content, increased strain rate, and usually by alloying. It is preferable that the ductile-brittle transition temperature is below room temperature for ease in fabrication and below the service temperature to minimize the potential for fracturing.

Since the thrust chamber material will be subject to temperatures as low as 200 K (360 R), tungsten and tungsten alloys were eliminated from consideration for the application because of high ductile-brittle transition temperatures.

Molybdenum was therefore selected as the high-temperature material for the backup thrust chamber. Pure molybdenum was selected over molybdenum alloys because of its lower ductile-brittle transition temperature and because it has adequate strength at 1655 K (2500 F). Figure 63 shows that the ductile-brittle transition temperature is below room temperature for recrystallized molybdenum. The ductile-brittle transition temperature is lower for stress-relieved, cold-worked molybdenum, and it is further decreased by maintaining low interstitial element contents. Table 4 shows the interstitial content of vacuum arc-cast, low-carbon unalloyed molbdenum and unalloyed powder metallurgy

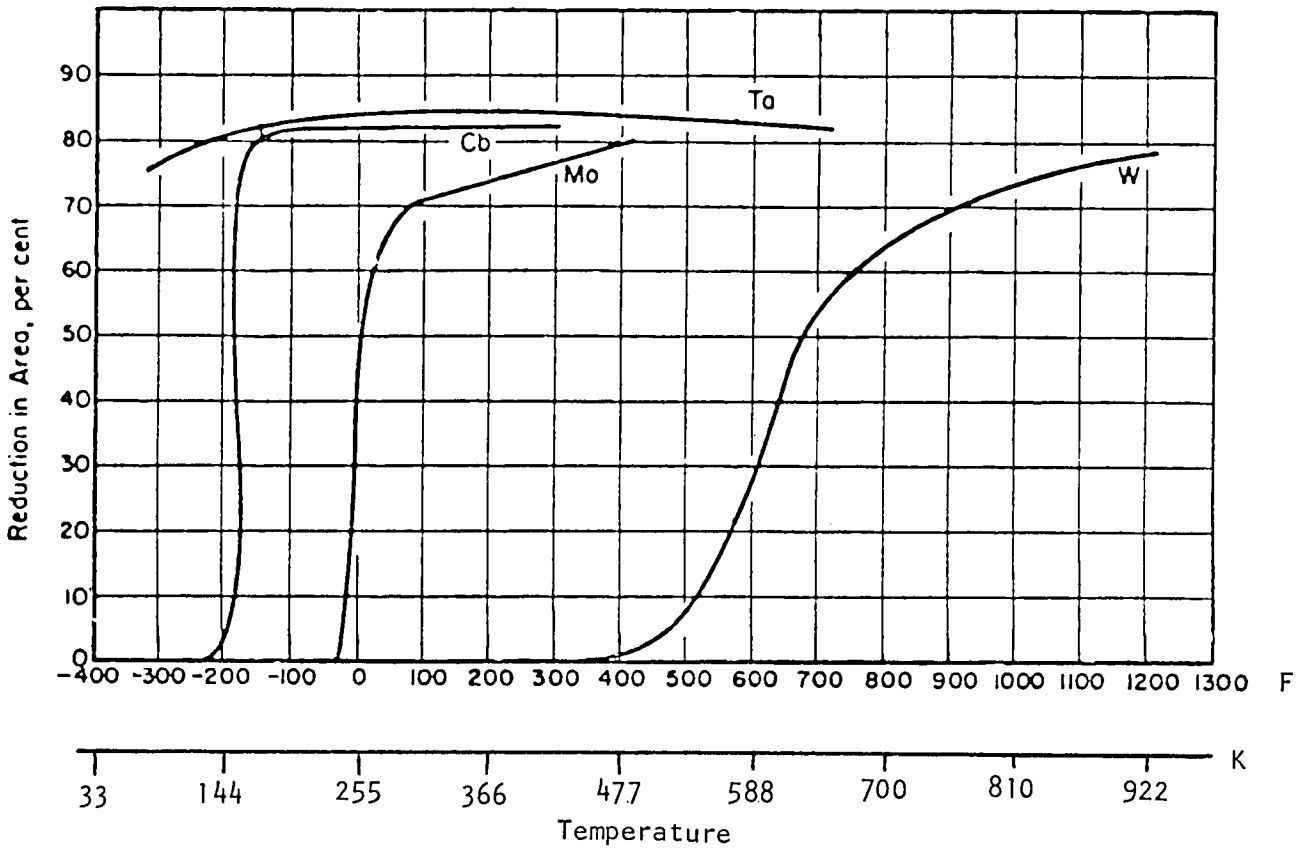

Figure 63. Tensile Transition Ranges for Recrystallized Refractory Metals

TABLE 4. INTERSTITIAL ELEMENT VENDOR-GUARANTEED ANALYSIS FOR MOLYBDENUM

Element	Vacuum Arc-Cast, Low Carbon, Unalloyed Molybdenum weight %	Unalloyed Powder Metallurgy Molybdenum weight %
Oxygen	0.0015 Max.	0.005 Max.
Nitrogen	0.002 Max.	0.001 Max.
Carbon	0.005 Max.	0.003 Max.
Hydrogen	0.0005 Max.	0.002 Max.
Molybdenum	99.97 Min.	99.30 Min.

molybdenum (vendor-guaranteed analyses). Of the interstitial elements, oxygen has by far the greatest effect in increasing the ductile-brittle transition temperature followed by nitrogen, then carbon, and finally hydrogen, with a negligible effect. Thus, the vacuum arc-cast, low-carbon unalloyed molybdenum was selected because of its lower oxygen content and higher overall purity over that of power metallurgy molybdenum.

Cooling Considerations

A detailed evaluation of the film-cooled convergent, throat, and nozzle section was conducted for the 4.18 contraction area ratio chamber and the nominal 7.5 secondary combustor core mixture ratio. Assuming an 85% film-cooling efficiency, the wall temperature distributions for various film-coolant injection locations are presented in Fig. 64 for 100 and 90% combustion performance efficiencies. At an axial injection location of 1.90 cm (0.75 in.), the maximum wall temperatures are 1485 K (2214 F) and 1312 K (1902 F) for the two respective combustion efficiencies.

From Fig. 64, it was apparent that a significant axial temperature gradient 811 K (1000 F) exists from the throat to a location 2.54 cm (1 in.) upstream of the throat. This temperature gradient would result in substantial axial heat conduction, which would decrease the peak wall temperature values. Futhermore, this axial heat conduction can be enhanced by increasing the thickness of the convergent and throat sections of the thrust chamber, as shown in Fig. 65. A three-dimensional thermal model was therefore constructed for the film-cooled convergent and throat section, and these results indicate that a reduction in maximum wall temperature of approximately 298 K (75 F) can be realized.

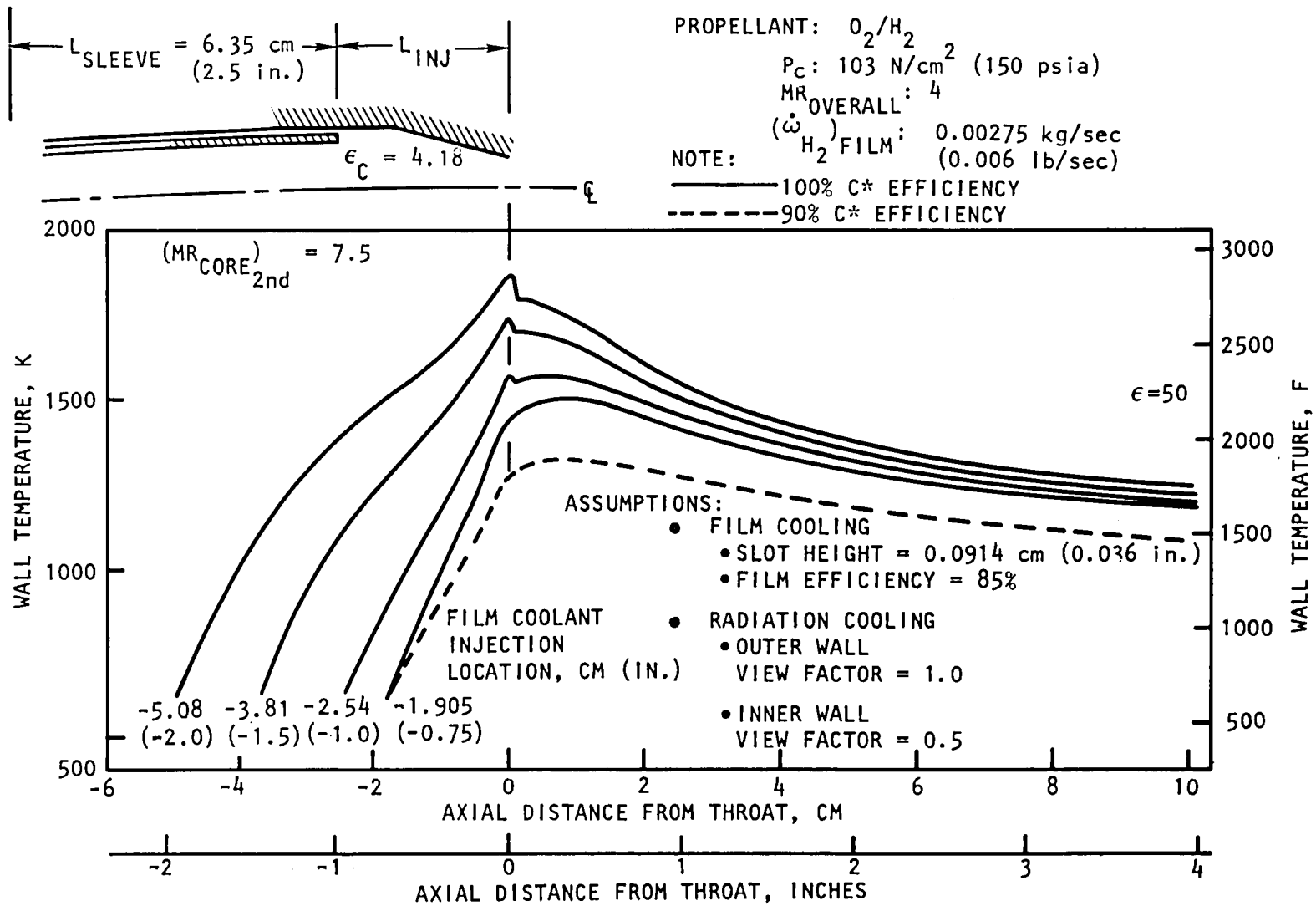

Figure 64. Film-Cooled Chamber Wall Temperature Distribution

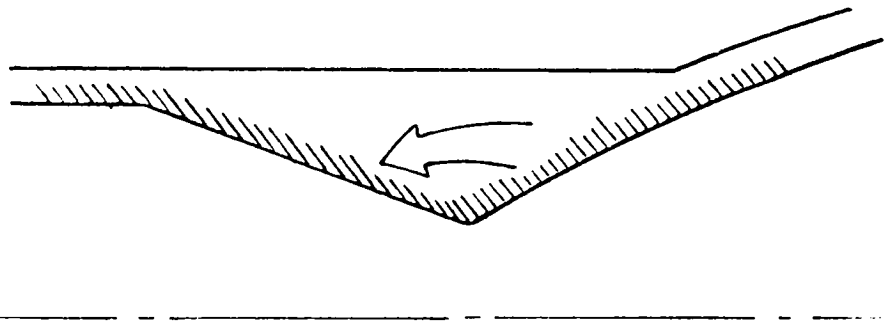

Figure 65. Axial Heat Conduction Influence of Film-Cooled Chamber Throat Section

Nozzle Contour Design

Attainment of the high specific impulse performance requirement necessitates an efficient thrust chamber expansion nozzle. For the specified expansion area ratio of 50:1, a highly efficient parabolic bell nozzle contour of 100% length (based on a 15-degree half-angle cone) has been selected. Table 5 presents the overall nominal operating conditions and pertinent design parameters of the selected nozzle. The optimum parabolic contour was defined using a bell nozzle contour computer program that used a starting transonic line flow computer program. The nozzle geometric efficiency was determined to be 0.9945. The resulting nozzle contour and the design wall pressure profile for the nominal operating conditions is presented in Fig. 66 and 67, respectively. The nozzle exit pressure is 0.02 N/cm^2 (0.29 psia).

TABLE 5. NOZZLE DESIGN PARAMETERS

Chamber Pressure, N/cm^2 (psia)	103 (150
Mixture Ratio	4.0
Nozzle Area Ratio	50
Throat Diameter, cm (in.)	0.984 (0.352)
Exit Diameter, cm (in.)	6.322 (2.489)
Throat Upstream Radius, cm (in.)	0.670 (0.264)
Throat Downstream Radius, cm (in.)	0.178 (0.070)
Throat-Nozzle Half-Angle, degrees	29
Nozzle Exit Half-Angle, degrees	5
Nozzle Length, cm (in.)	10.152 (3.997)
Nozzle Percent Length, %	100

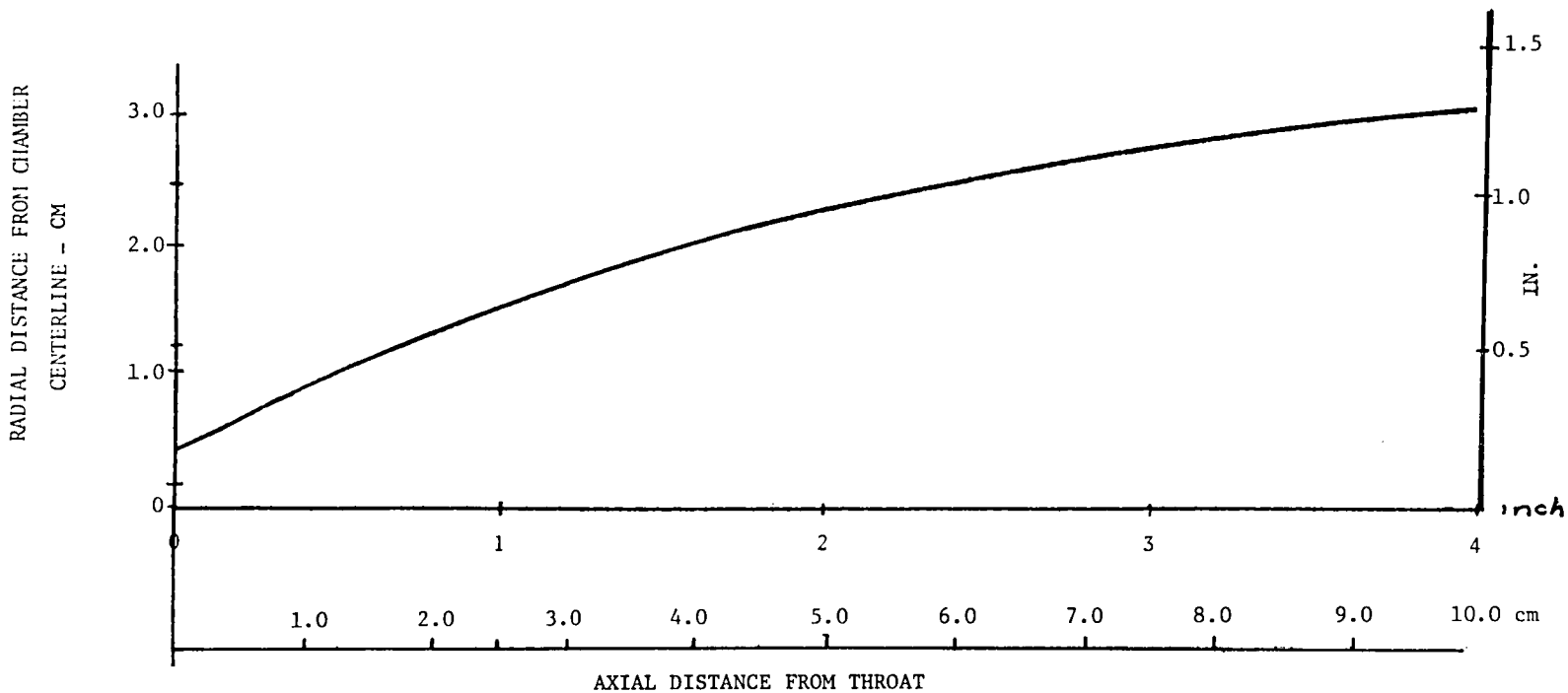

Figure 66. Expansion Nozzle Wall Contour

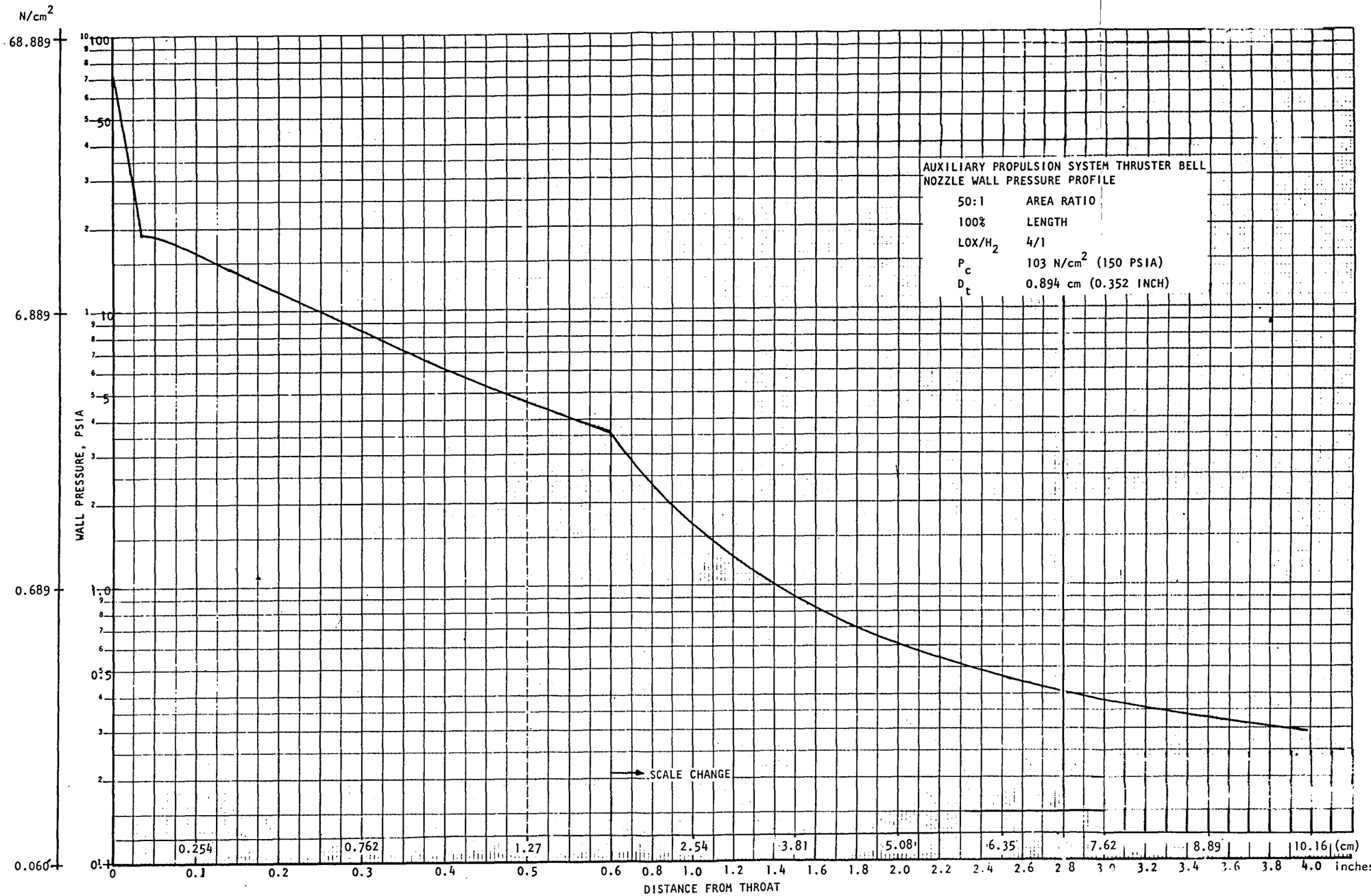

Figure 67. Nozzle Wall Pressure Profile

A photograph of the L-605 thrust chamber is shown in Fig. 68 , and the detail fabrication drawing and photograph of the high-temperature molybdenum thrust chamber is shown in Fig. 69 and 70 , respectively.

Thruster Assembly

After completion of the major hardware components, final assembly per Fig. 71 was accomplished. Figure 72 illustrates the several components within the thruster assembly and Fig. 73 shows the assembled thruster. Major components included within Fig. 72 in a right to left order are: the thrust chamber, a development spacer for combustor length variation, the Kel-F insulator to impede heat flow from the thrust chamber to the valve area, the fuel valve/housing assembly, the propellant injection/combustor system assembly, and the igniter spark plug.

Following assembly of the thruster hardware, the propellant valves were subjected to a final leak check with gaseous helium at a pressure of 275N/cm^2 (400 psia), and zero leakage was detected during a 3-minute hold period which followed 50 valve actuation cycles.

Water flow calibration of the injector/combustor propellant injection system was subsequently performed to verify that the desired three-way hydrogen flow split existed within the thruster assembly, i.e., primary combustor hydrogen circuit, secondary combustor hydrogen circuit, and boundary layer coolant hydrogen circuit. Flow distribution of these circuits is controlled by means of metering orifices which are located immediately downstream of the thruster propellant valve. By changing these orifices, the mixture ratio distribution within the thruster can be altered to enhance cooling or combustion performance. The original set, which was installed within the thruster assembly, was designed to give a mixture ratio distribution of 50:1 in the primary combustor and 12:1 in the secondary combustor, when operating at an overall thruster mixture ratio of 4:1. While combustion model results indicate that the optimum mixture ratio distribution for combustion performance was 30:1 (primary combustor) and 7.5.1 (secondary combustor), a 50:1 and 12:1 mixture ratio distribution within the primary and secondary combustor, respectively, represented a reasonable compromise between cooling and performance considerations and, was therefore, selected for the initial thruster configuration.

The desired mixture ratio distribution was achieved with the following metering orifice sizes:

Primary Combustor Hydrogen - 0.035 cm (0.014 in.)
Secondary Combustor Hydrogen - 0.056 cm (0.022 in.)
Boundary Layer Coolant Hydrogen - 0.084 cm (0.033 in.)
Primary Combustor Oxygen - 0.102 cm (0.040 in.)

The lines in Fig. 74 represent the desired hydraulic behavior of the various flow circuits within the thruster, and the symbols represent the data from water-flow calibration. These cold-flow results indicated that the desired mixture ratio distribution within the initial thruster assembly was achieved with the calculated metering orifice sizes.

Following vacuum drying, the thruster assembly was shipped to the Rockwell B-1 Division for hot-fire evaluation.

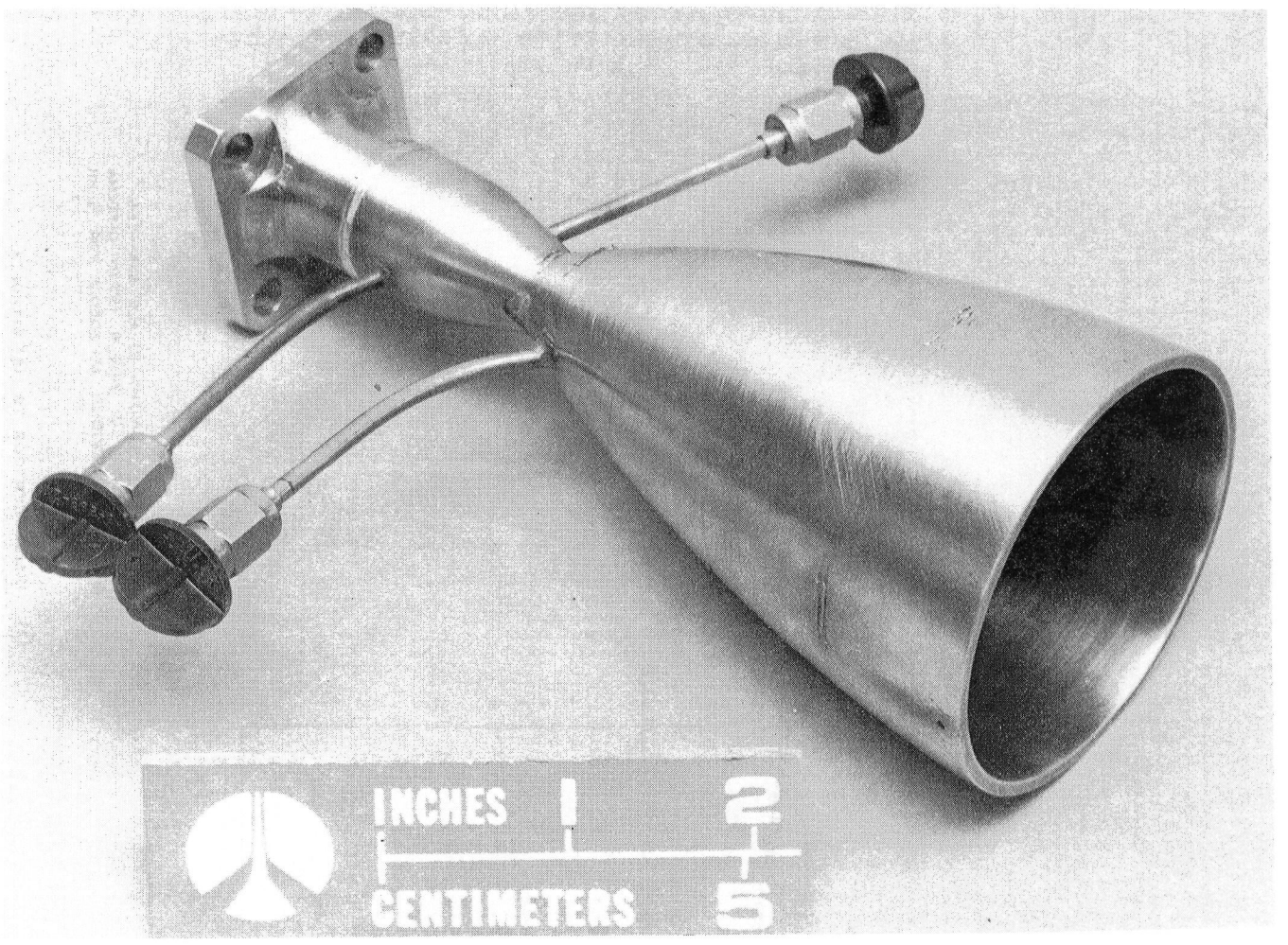

1SU22-5/5/77-C1F*

Figure 68. L605 Workhorse Thrust Chamber

PT	X (2)	R (2)
1	.000	.176
2	.022	.179
3	.034	.185
4	.078	.209
5	.110	.226
6	.165	.255
7	.275	.311
8	.462	.401
9	.707	.509
10	1.079	.653
11	1.580	.815
12	2.269	.989
13	3.215	1.156
14	3.997	1.245

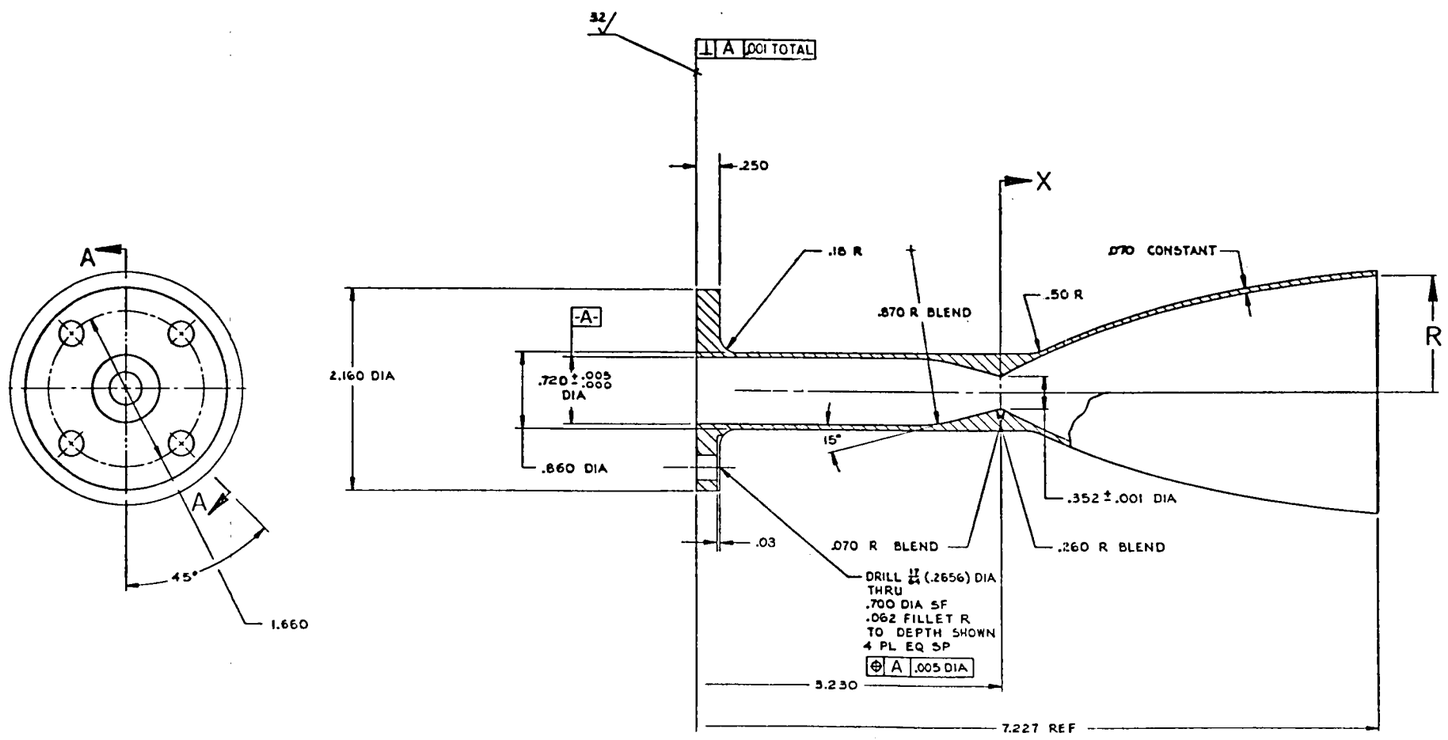

SECTION A-A

3. ADD DURAK-B COATING TO ALL SURFACES BY CHROMIZING CO. 2100 W. 139TH, GARDENA CA., 90249. PREOXIDIZE AT 2000°F FOR ½ HR.

(2) INSIDE CONTOUR TO LIE WITHIN A TOLERANCE BAND .004 WIDE EQUIDISTANT OF INDICATED BASIC STATION DIMENSIONS "X" & "R."

1. MACHINE PER RA0103-016.

NOTE: UNLESS OTHERWISE SPECIFIED

Figure 69. High-Temperature Molybdenum Thrust Chamber

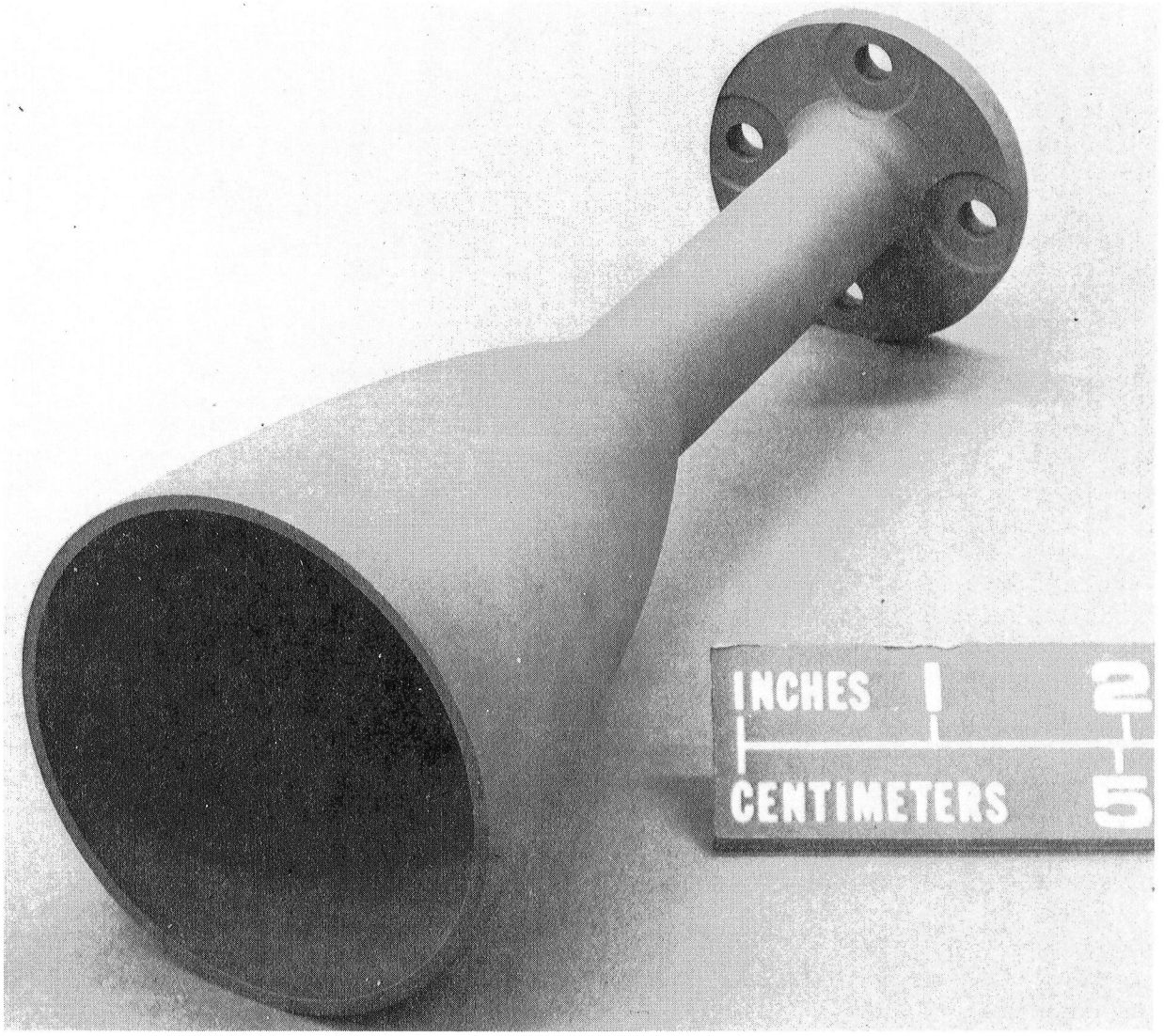

Figure 70. Thrust Chamber Assembly (Molybdenum)

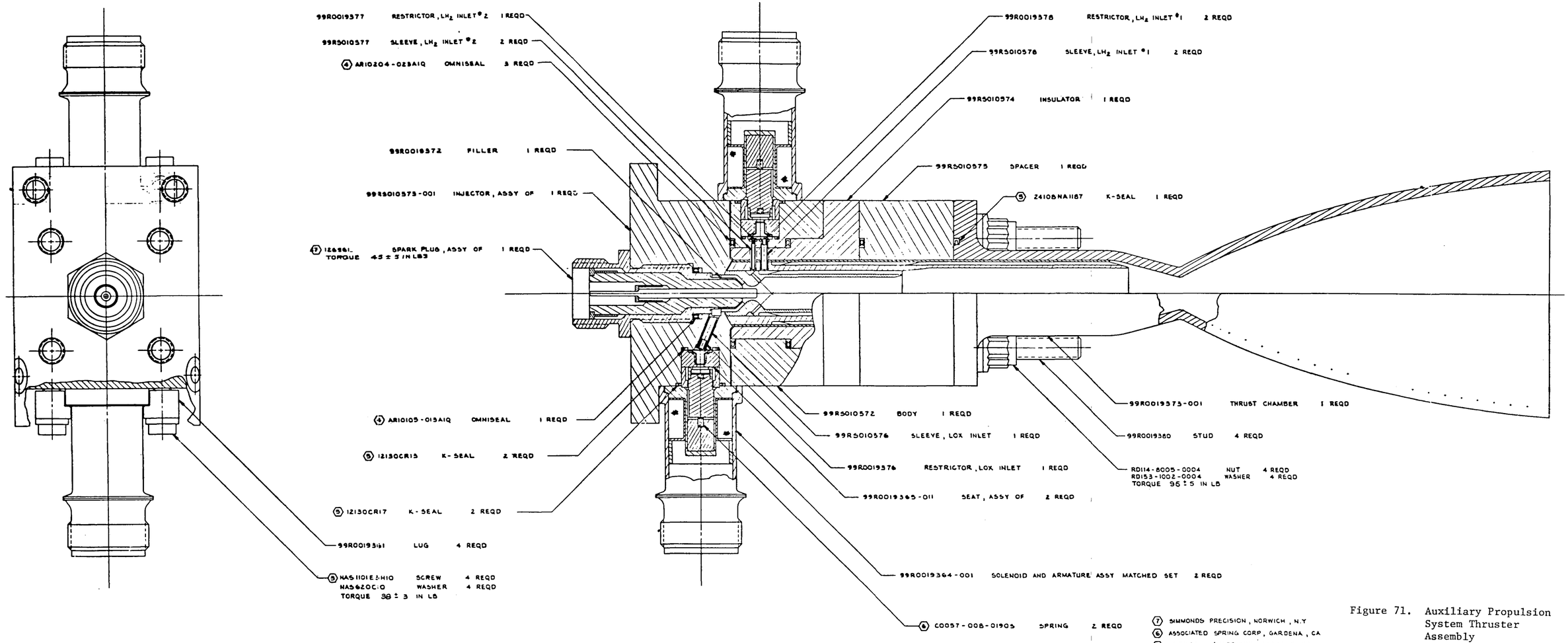

Figure 71. Auxiliary Propulsion System Thruster Assembly

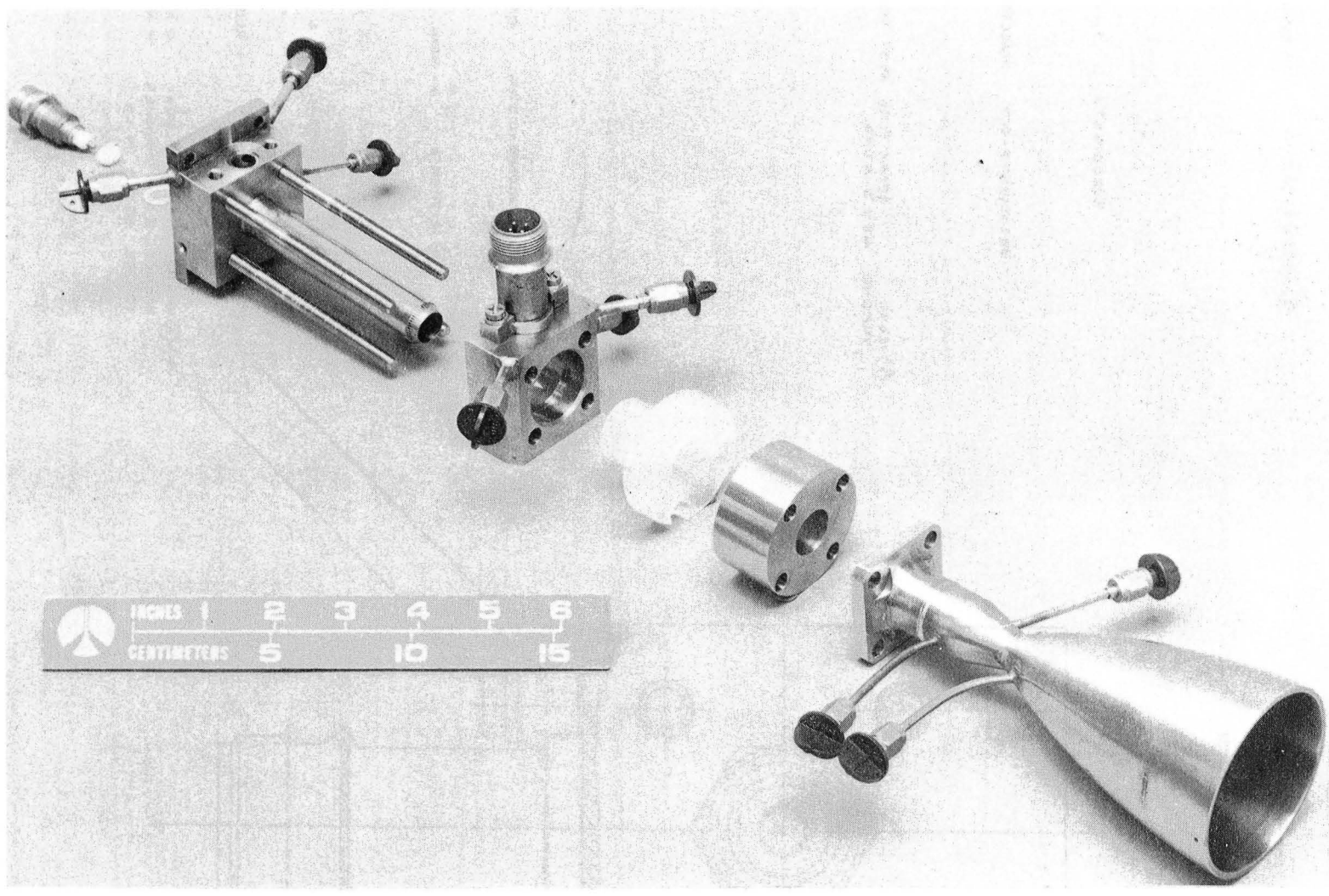

1SU22-5/5/77-C1-1*

Figure 72. Thruster Components

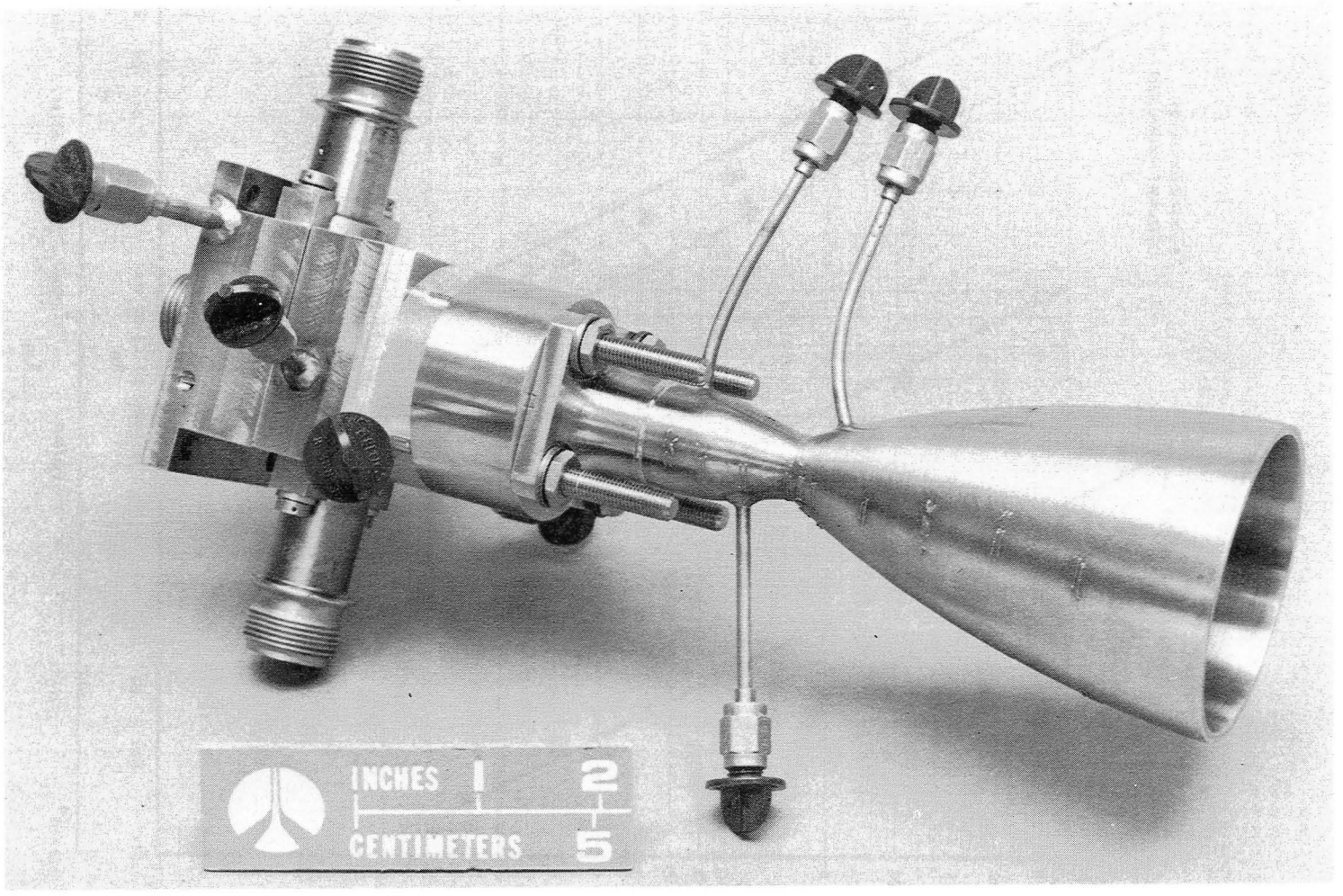

1SU22-5/5/77-C1H*

Figure 73 . Thruster Assembly

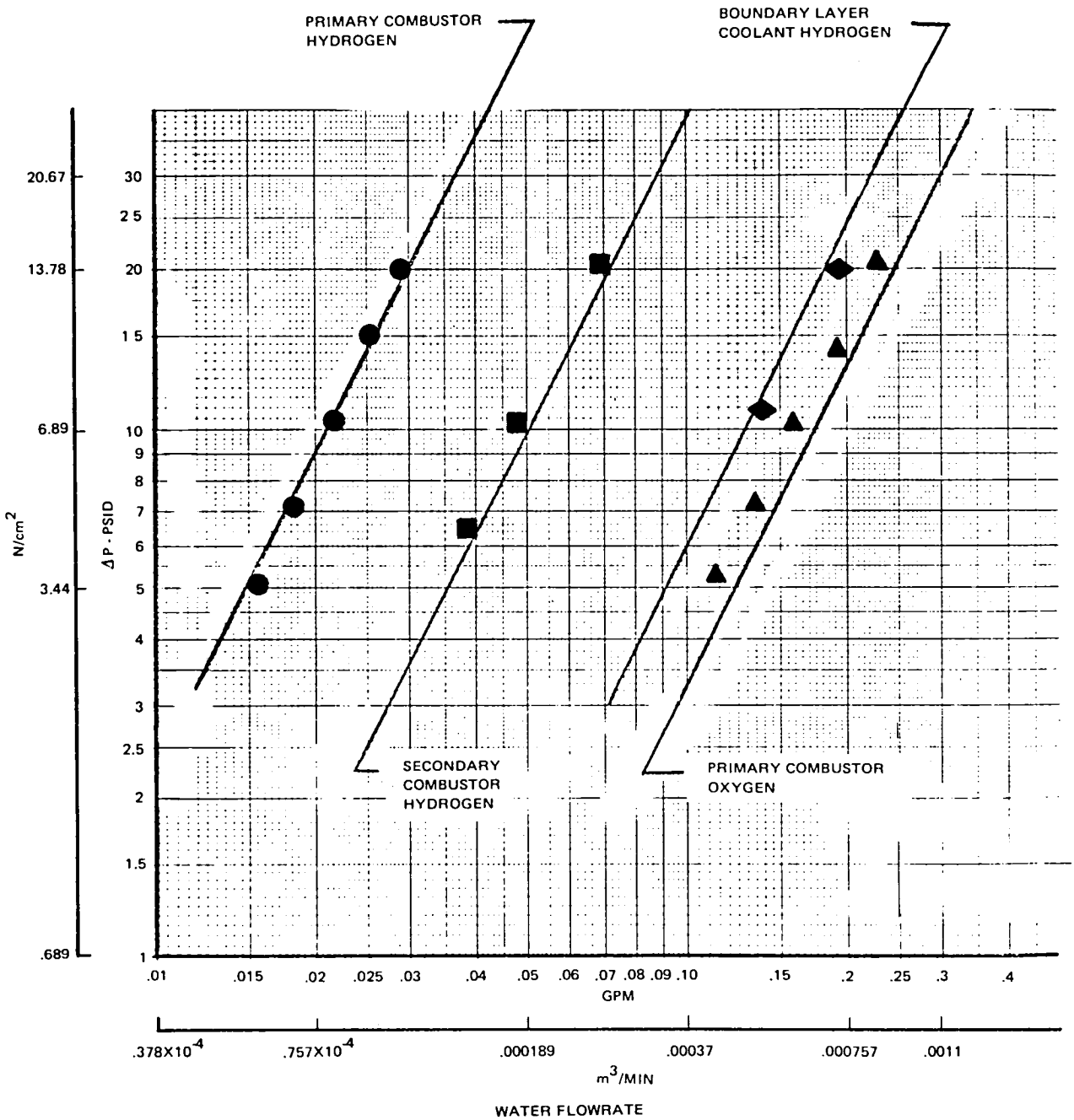

Figure 74. Thruster Hydrogen Circuit Flow Characteristics

HOT-FIRE TESTING

All hot-fire test activities were conducted in cell 107 of the Thermodynamics Laboratory, Los Angeles Division, Rockwell International Corporation, El Segundo, California. An overall view of the test facility is shown in Fig. 75. The major details of the propellant supply systems are shown in Fig. 76. The various test facility systems are discussed in detail below.

The initial tests of the hot-firing program were conducted on 23 June 1977, and continued through March 1979.

TEST FACILITY AND OPERATING PROCEDURES

Liquid Hydrogen Supply System

The liquid hydrogen tank shown in Fig. 76 is a 0.246 m^3 (65 gallon), 6.21 x 10^4 N/m^2 (900 psig), triwall, stainless-steel vessel. In use, a vacuum was maintained in the inner jacket, and the outer jacket was kept filled with liquid nitrogen. All tank connections were made through a top flange. The liquid hydrogen was drawn up from the bottom of the tank by means of a "dip-leg" tube. Helium gas was used to pressurize the tank and to purge LH_2 systems.

Tanking of liquid hydrogen was done using a 7.57 m^3 (200 gallon) capacity portable dewar. This dewar was pressurized to a level of 5.86 x 10^5 N/m^2 (85 psig) for propellant transfer operations.

The LH_2 propellant supply lines leading from the tank to the thruster were of a triwall construction. The inner line was stainless-steel tubing with an 0.64 cm (0.25 in.) outside diameter and an 0.089 cm (0.035 in.) wall thickness. A liquid hydrogen refrigerant flow was maintained through the inner jacket, and a vacuum was maintained in the outer jacket. The propellant line jacketing was terminated shortly before reaching the thruster. The final run of unjacketed line was approximately 46 cm (18 in.) long, as shown in Fig. 77. A "hair pin" loop was used in the line from the venturi mounting block to the thruster mount to minimize line stiffness changes and to minimize thrust cell side-loading effects due to line temperature changes. For later tests, which evaluated thruster pulsing performance, these line sections were modified to extend the jacketed lines to within about 5 cm (2 in.) of the thruster. This improved the ability to maintain the liquid hydrogen quality in these line sections during the OFF portion of each pulse cycle.

The LH_2 refrigerant flowrate and flow configuration was adjusted to result in hydrogen temperatures equal to or below 27.8 K being delivered to the LH_2 venturi meter. The refrigerant flowrates were adjusted by varying the sizes of fixed orifices in various subsystems, and by breaking up the overall flow system into a number of parallel flow circuits (rather than flowing all sections in a series hookup). A bypass of flow system also was provided that tapped off the LH_2 propellant supply system just downstream of the venturi meter. The bypass control valve was automatically sequenced off just prior to the actuation of the engine mounted main fuel valve.

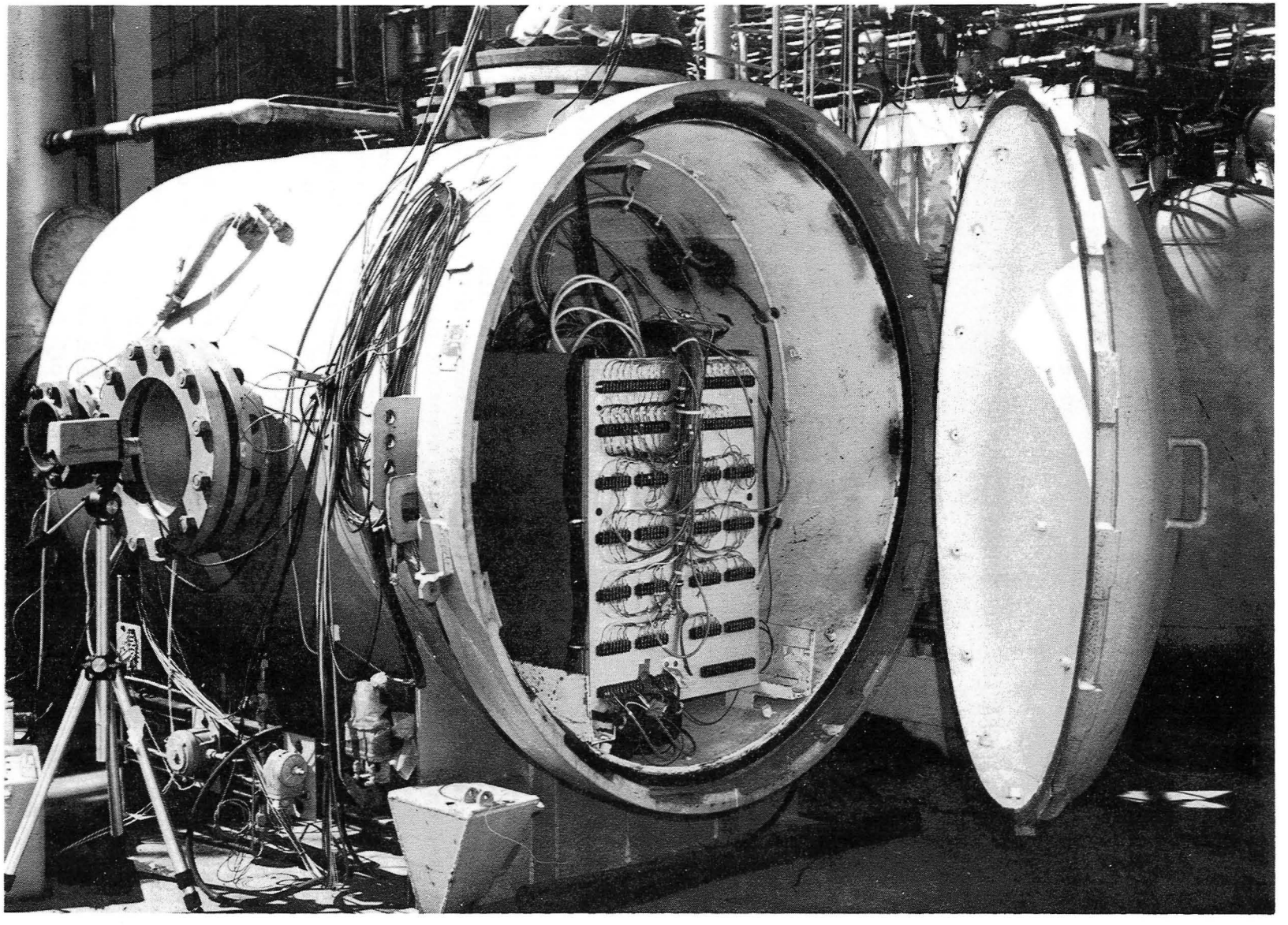

Figure 75. Overall View of 25-pound Thruster Test Facility

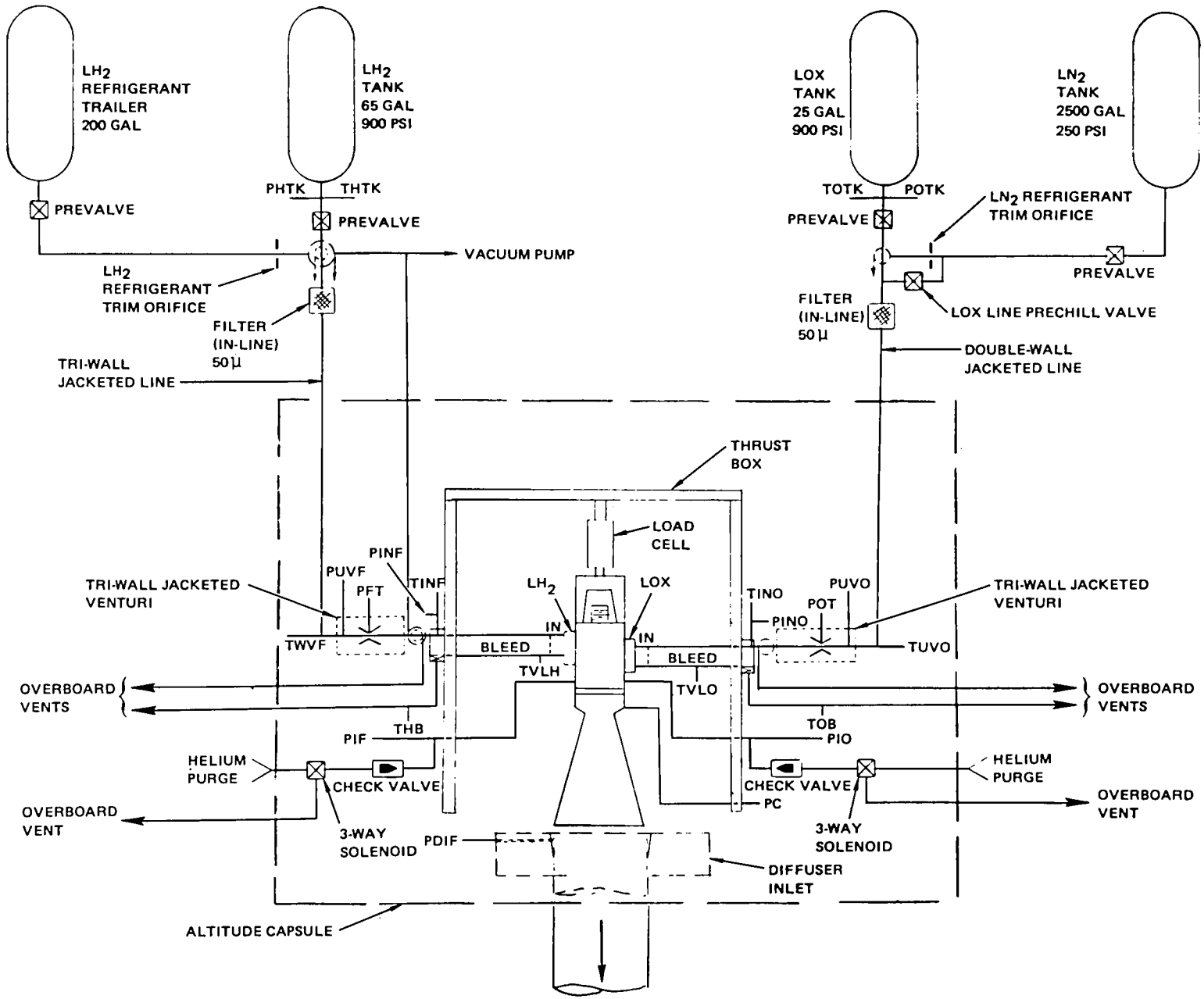

Figure 76. LOX/LH_2 25-Pound Thrust Propulsion System Propellant Supply Schematic

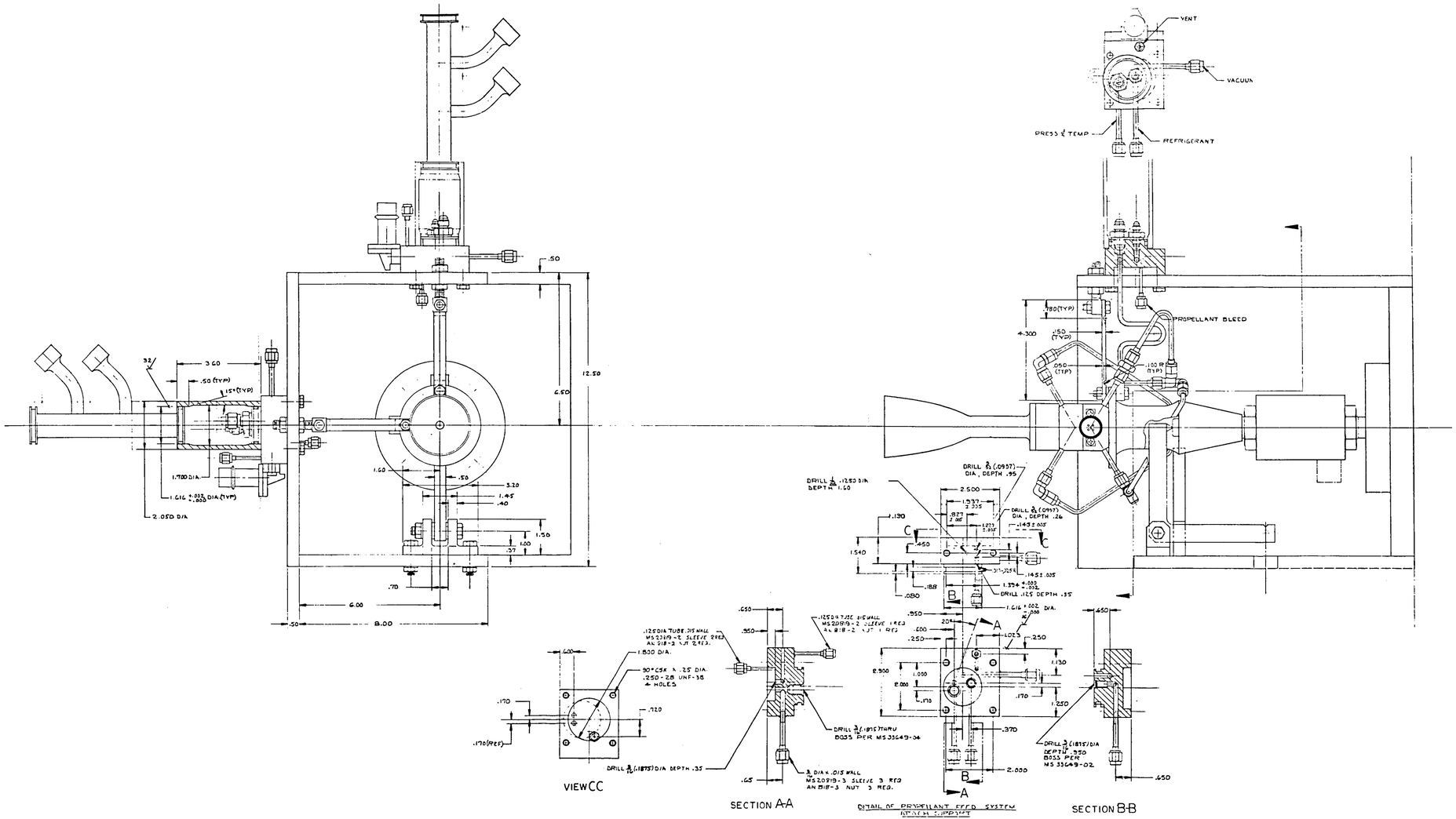

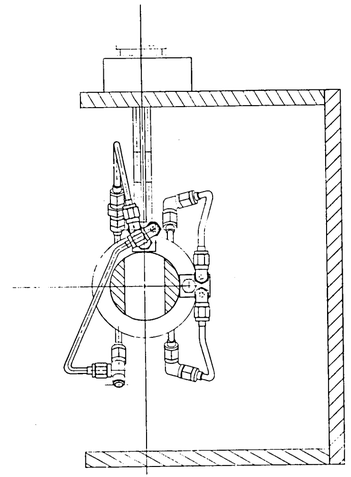

Figure 77. IAPS Mounting Provisions

A 50-micron (nominal rating) stainless-steel filter was used in the LH_2 system. This filter precluded the possibility of allowing the passage of particles that might be of sufficient size to affect the proper operation of the various thruster components.

Liquid Oxygen Supply System

As shown in Fig. 76, the liquid oxygen supply system used a stainless-steel, 9.46×10^2 m^3 (25 gallon) capacity tank with a maximum working pressure rating of 6.21×10^4 N/m^2 (900 psig). This tank has an external jacket that was kept full of liquid nitrogen. A 9.46 m^3 (2500 gallon) storage capacity liquid nitrogen vessel, with a maximum working pressure rating of 1.72×10^4 N/m^2 (250 psig), was used as the refrigerant flow supply tank. As shown in Fig. , it was possible, by selective actuation of isolation valves, to flow LN_2 through both the LO_2 supply system and the line jackets for preliminary system chilldown.

The LO_2 propellant supply lines from the tank to the thruster were furnished with a single jacket. The inner line was stainless-steel tubing with an 0.64 cm (0.25 in.) outside diameter and a 0.089 cm (0.035 in.) wall thickness. A liquid nitrogen refrigerant flow was maintained through the jacket passages. As in the case of the LH_2 system, a final run of approximately 46 cm (18 in.) line leading to the htruster was unjacketed. This section was provided with foam insulation and, during chilldown and test, was in a vacuum environment. The unjacketed run length was used to maximize thrust measurement accuracy. As in the case of the LH_2 system, the system was reworked to provide jacketing to within approximately 13 cm of the thruster for pulse mode operations.

The LN_2 refrigerant flowrate was controlled by varying the supply pressure and by varying the sizes of fixed system orifices to allow delivery of liquid oxygen to the LO_2 venturi meter at temperatures as low as 91.7 K (165 R).

A bypass flow system was provided which tapped off the LO_2 propellant supply system immediately downstream of the venturi meter. The bypass control valve maintained a continuous flow through that portion of the system until just prior to actuation of the engine-mounted, main oxidizer valve. The programmed closing of the bypass system valve and opening of the oxidizer main valve were controlled by a sequencer.

Gaseous helium was used for the oxidizer tank pressurization system and for all line purges.

Environmental System

All firings were conducted in an evacuated capsule to allow for full expansion of the thruster exhaust gases and to minimize propellant supply system heat leaks. To accommodate the 50:1 expansion area ratio of the thruster nozzle, the pressure environment was targeted to be 1.034×10^3 N/m^2 (0.15 psia) or less. This corresponded to a pressure altitude of approximately 30,800 m (101, 000 ft).

The altitude capsule is shown in Fig. 78. This was a 1.52 m (5 ft) ID vessel, 2.44 m (8 ft) long. A number of view ports existed, which permitted visual examinations of the hardware and also of continuous monitoring of firings by means of a television camera. Additional ports were provided for propellant supply system entries, instrumentation, and control system wires.

The altitude capsule vacuum pressure level was maintained by means of a bank of five Kinney Model KD 850 vacuum pumps. The altitude capsule was connected to the existing 0.76 m (30 in.) diameter duct permanently installed on the roof of the test cell building (see Fig. 75). The connecting duct was a 0.30 m (12 in.) diameter pipe, approximately 9.14 m (25 ft) long, equipped with flexible bellows to allow free thermal expansion.

The rated capacity of the vacuum system was 101.9 m^3/min (3600 cfm) at the required suction pressure level. Since the volumetric flowrate of the thruster at an assumed temperature of 367 K (660 R) was calculated to be approximately 510 m^3/min (18,000 cfm), an auxiliary system was required to allow this flow level to be accommodated. A self-powered diffuser (shown in Fig. 78) was therefore provided to allow suitable recompression of the thruster exhaust gases to accommodate the vacuum pump volumetric flowrate limitations.

This diffuser had an approximate 6.35 cm (2.5 in.) internal diameter, an exit diameter of 12.1 cm (4.75 in.), and an overall length of 1.14 m (45 in.). A water-cooled jacket was provided to limit the temperature rise of the mild steel diffuser. An assortment of spacers was available to interpose between the diffuser mounting flange and the altitude capsule. This allowed the accommodation of various thruster body lengths resulting from addition or removal of thruster body spacers. Smaller adjustments, as would result in a typical thruster nozzle to diffuser gap of 0.48 cm (0.19 in.), were obtained by loosening the attachment bolts and moving the thrust structure.

A 4.58 cm (2 in.) valve was used to allow atmospheric air to enter the capsule when it was necessary to remove the vacuum. Since the connecting series of large piping does not have remotely actuated vacuum valves, this also pressurized those parts of the system.

Thruster Installation Details

Details of the thruster installation may be seen in Fig. 77 and 78. The thrust-absorbing structure was a buildup box section made of 1.27 cm (0.5 in.) thick steel plates welded together. A large cavity existed in the structure, open at the top, which was filled with lead shot to create a seismic mass with strong internal damping.

Two steel flexures, located 90 degrees apart, were used to permit axial motion of the thruster, while supporting the weight of the hardware and absorbing side loads. The thruster was bolted to a thrust mount that threaded into the body of the load cell. The mount was partially relieved (see Fig. 77) to provide access to the igniter plug and to accommodate the thrust calibration fixture. This calibration fixture was a ball-bearing mounted, right-angled lever system which permitted hanging weights on the horizontal arm.

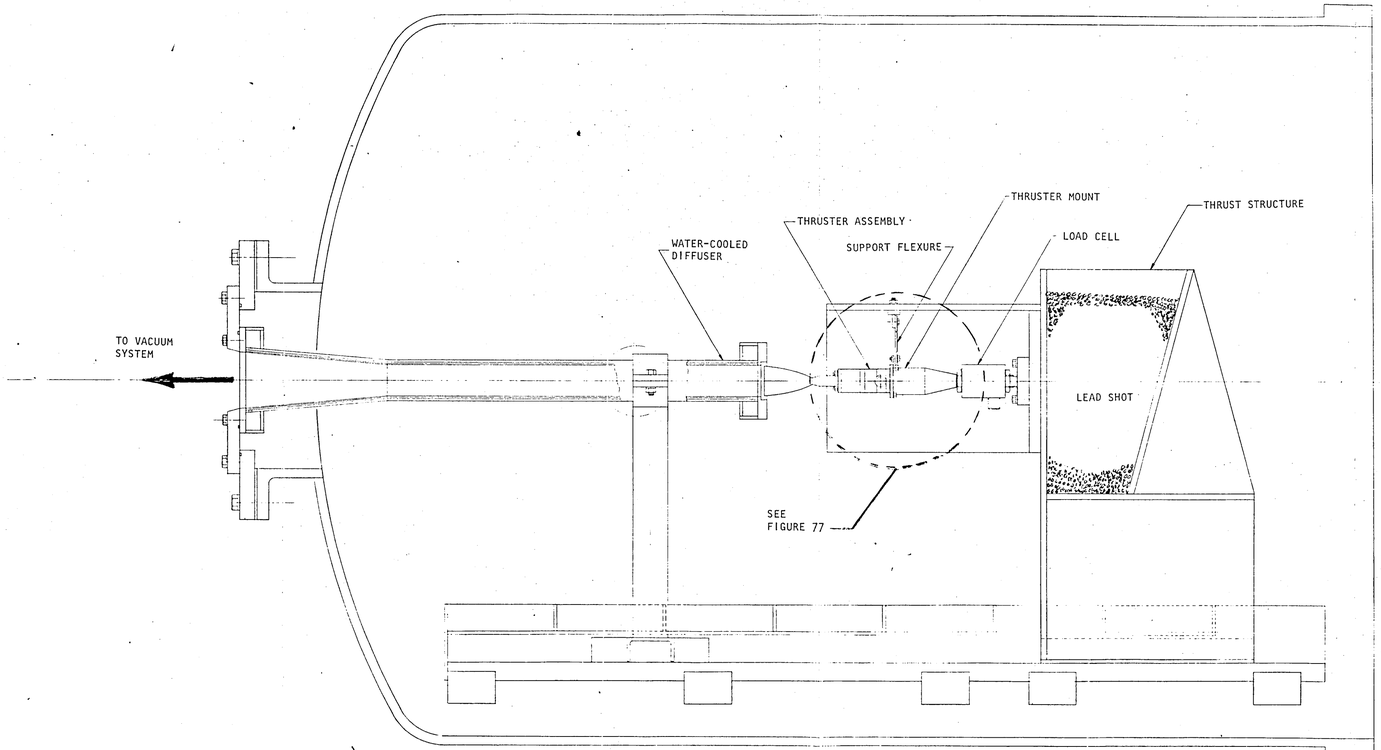

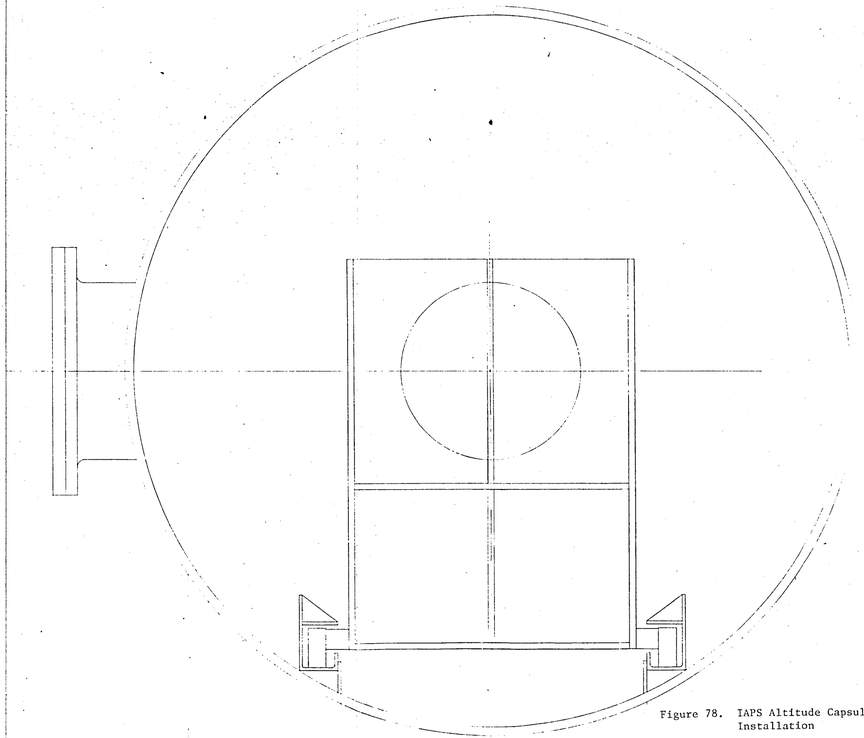

Figure 78. IAPS Altitude Capsule Installation

To provide an igniter cable pressurization capability, the hollowed out portion of the thrust mount was covered by means of two saddle pieces. The upper cover plate was made from aluminum and the lower cover piece was made from commercial PVC piping. Both pieces were sealed to the thrust mount with a two-component silicone rubber casting compound (RTV 511), and held in place by means of hose clamps. A polyethylene tube encased the igniter cable and penetrated the altitude capsule wall. This polyethylene tube was sealed around the igniter cable by means of a close-fitting rubber stopper at the outside end of the tube. A regulated supply of GN_2, maintained at an approximate 1.08×10^6 N/m^2 (15.7 psia) pressure level, was connected to the polyethylene tube to increase resistance to high-voltage breakdown of the igniter cable assembly.

Instrumentation and Controls

Instrumentation. The instrumentation complement for this experimental program is shown in Table 6. The pressure transducers used were mainly Taber, bonded strain gage-type instruments of the ranges shown in Table 6. For the venturi pressure measurements, Taber transducers were used interchangeably with Entran EPS-1032 type transducers. These Entran transducers were miniaturized, high-response, semiconductor instruments used primarily to obtain high-response measurements.

Two different load cells were used to make thrust measurements. The initial installation is shown in Fig. 79. This used a Kulite-Bytrex semiconductor load cell with a 2.224×10^4 N (5000 lb) load capacity. This load cell was selected to provide a high stiffness and, thus, to result in, a high response. The load cell was calibrated over the range of 0 to 2.224×10^2 N (50 lb).

A second load cell was employed during the latter portion of the test program. This substitution was made to investigate the possibility that some loss of thrust measurement accuracy was resulting because only 0.5% of the rated capacity of the load cell was being used. The second load cell may be seen in Fig. 80. This was a Baldwin-Lima-Hamilton bonded strain-type transducer with a 444.8 N (100 lb) rating. This load cell was calibrated over the range of 0 to 1.334×10^2 N (30 lb).

Temperature measurements made used either thermocouples or temperature bulbs, as shown in Table 6. Rosemont temperature bulbs were used to measure the inlet temperatures of the propellant as delivered to the venturi meters. The cryogenic range temperature measurements were made with copper/constantan thermocouples.

Elevated temperatures, such as exhibited by the thruster surfaces during firing, were monitored with chromel/alumel thermocouples welded directly to the monitored surface.

The locations of most of the Table 6 listed temperature measurements are shown in Fig. 81.

TABLE 6. INSTRUMENTATION LIST

SYSTEM	PARAMETER	ID	PID	RANGE		REDLINE	ASTRODATA	BRUSH	OSC	VISUAL	LOCATION	COMMENTS
LOX	LOX Tank Pr.	PØTK		0-500 psig	0-3.45x10^6 N/m^2		X		X	X	LOX TANK	
	LOX Tank Temp.	TØTK		-320 to -180F	78-156K		X				LOX TANK	Thermocouple, Cu/Cn
	LOX Venturi Upstream Pr.	PUVØ		0 - 250 psig	0-1.72x10^6 N/m^2		X	X			Venturi	Entran EPS-1032-250
	LOX Venturi Upstream Temp.	TUVØ		-320 to 0°F	78-256 K		X	X			Fac. line	Rosemont bulb
	LOX Venturi Throat Pr.	PØT		0 - 250 psig	0-1.72x10^6 N/m^2		X	X			Venturi	Entran EPS-1032-250
	LOX inlet Pr.	PINØ		0 - 250 psig	0-1.72x10^6 N/m^2		X		X		Fac. line	
	LOX inlet temp.	TINØ		-320 to 0°F	78-256K		X				Fac. line	Thermocouple, Cu/Cn
	LOX Inj. Pr.	PIØ		0 - 250 psig.	0-1.72x10^6 N/m^2		X		X		Thruster	
	LOX Bleed Temp.	TØB		-320 to 0°F	78-256K		X			X	Fac. line	Thermocouple, Cu/Cn
	MLV LOX Cavity Temp	TVLØ		-320 to 0°F	78-256K		X				Thruster	Thermocouple, Cu/Cn
Hydrogen	LH_2 Tank Pr.	PHTK		0-500 psig	0-3.45x10^6 N/m^2		X		X	X	LH_2 Tank	
	LH_2 Tank Temp	THTK		-424 to -324F	20-76K		X				LH_2 Tank	Thermocouple, Cu/Cn
	LH_2 Venturi Upstream Pr.	PUVF		0 - 250 psig	0-1.72x10^6 N/m^2		X	X			Venturi	Entran EPS-1032-250
	LH_2 Venturi Upstream Temp.	TUVF		-424 to -324F	20-76K		X	X			Fac. line	Rosemont bulb
	LH_2 Venturi Throat Pr.	PFT		0 - 250 psig	0-1.72x10^6 N/m2		X	X			Venturi	Entran EPS-1032-250
	LH_2 Inlet Pr.	PINF		0 - 250 psig	0-1.72x10^6 N/m^2		X		X		Fac. line	
	LH_2 Inlet Temp.	TINF		-424 to -324F	20-76K	X	X				Fac. line	Thermocouple, Cu/Cn
	LH_2 Inj. Pr.	PIF		0 - 250 psig	0-1.72x10^6 N/m^2		X		X		Thruster	
	LH_2 Bleed Temp.	THB		-424 to -324F	20-76K		X			X	Fac. line	Thermocouple, Cu/Cn
	MFV LH_2 Cavity Temp.	TVLH		-424 to -324F	20-76K		X				Thruster	Thermocouple, Cu/Cn

TABLE 6. (CONTINUED)

SYSTEM	PARAMETER	ID	PID	RANGE		REDLINE	ASTRODATA	BRUSH	OSC	VISUAL	LOCATION	COMMENTS
Thrust Chamber	Temp #1	TC1		0 - 2000F	256-1367K	X	X	X			TC throat 0°	Thermocouple,Cr/Al
	Temp #2	TC2		0 - 2000F		X	X	X			TC1 + 90°	
	Temp #3	TC3		0 - 2000F		X	X	X			TC1 + 180°	
	Temp #4	TC4		0 - 2000F		X	X	X			TC1 + 270°	
	Temp #5	TC5		0 - 2000F			X				0°, ϵ = 3	
	Temp #6	TC6		0 - 2000F			X				90°, ϵ = 3	
	Temp #7	TC7		0 - 2000F			X				0°, ϵ = 5.75	
	Temp #8	TC8		0 - 2000F			X				90°, ϵ = 5.75	
	Temp #9	TC9		0 - 2000F			X				0°, ϵ = 50	
	Temp #10	TC10		0 - 2000F			X				0°, ϵ = 50	
	Temp #11	TC11		0 - 2000F			X				0°, ϵ = 12.72	
	Temp #12	TC12		0 - 2000F			X				90°, ϵ = 12.72	
	Temp #13	TC13		0 - 2000F			X				0°, ϵ = 29.1	
	Temp #14	TC14		0 - 2000F			X				90°, ϵ = 29.1	
	Temp #15	TC15		0 - 2000F			X				0°, ϵ = 41.1	
	Temp #16	TC16		0 - 2000F			X				90°, ϵ = 41.1	
	Temp #17	TC17		0 - 2000F			X				0°, X = -.72	
	Temp #18	TC18		0 - 2000F			X				90°, X = -.72	
	Temp #19	TC19		0 - 2000F			X				0°, X = -.35	
	Temp #20	TC20		0 - 2000F	256-1367K		X				90°, X = -.35	

TABLE 6. (CONCLUDED)

SYSTEM	PARAMETER	ID	PID	RANGE		REDLINE	ASTRODATA	BRUSH	OSC	VISUAL	LOCATION	COMMENTS
General	Chamber Pr.	PC		0 to 200 psig	$0\text{-}1.379\times10^{6}$ N/m^2	X	X	X	X	X	Thruster	
	Thrust	F		0 to 50 lb	0-222 n		X	X	X	X	Load cell	By Trex A-60927 JP5000-10,000.
	Capsule Pr	PCAP		0 to 15 psia	$0\text{-}1.034\times10^{5}$ N/m^2	X	X	X		X	Capsule	
	Diffuser Inlet Pr	PDIF		0 to 20 psia	$0\text{-}1.379\times10^{5}$ N/m^2		X				Diffuser	
	Vacuum System Suction Pr.	PVAC		0 to 20 psia	$0\text{-}1.379\times10^{5}$ N/m^2		X				FAC	
	Main LOX Valve Control signal	MLV		PIP	PIP				X		FAC	On-off
	Main Fuel Valve Control signal	MFV		PIP	PIP				X		FAC	On-off
	Start Signal	START		PIP	PIP				X	X	FAC	On-off
	Spark Monitor	SPARK		PIP	PIP				X		FAC	On-off
	LOX Bleed Valve Control signal	OX BLD		PIP	PIP				X		FAC	On-off
	LH_2 Bleed Valve Control signal	H2BLD		PIP	PIP				X		FAC	On-off
	LOX Manifold Skin Temp.	TLM		-320 to +100F	78-311 K		X				Thruster LOX Manifold	Thermocouple,Cu/Cn
	LH_2 Manifold Skin Temp	THM		-424 to +100F	20-311 K		X				Thruster LH_2 Manifold	Thermocouple,Cu/Cn
	Exhaust Duct Skin Temp.	TEXH		0 to 2000F	256-1367 K	X	X	X		X	Exh. Duct	Thermocouple,Cr/A
	Vacuum Pump Inlet Temp	TVAC		0 to 600F	256-589 K	X	X	X		X	Exh. Duct	Thermocouple,Cr/A

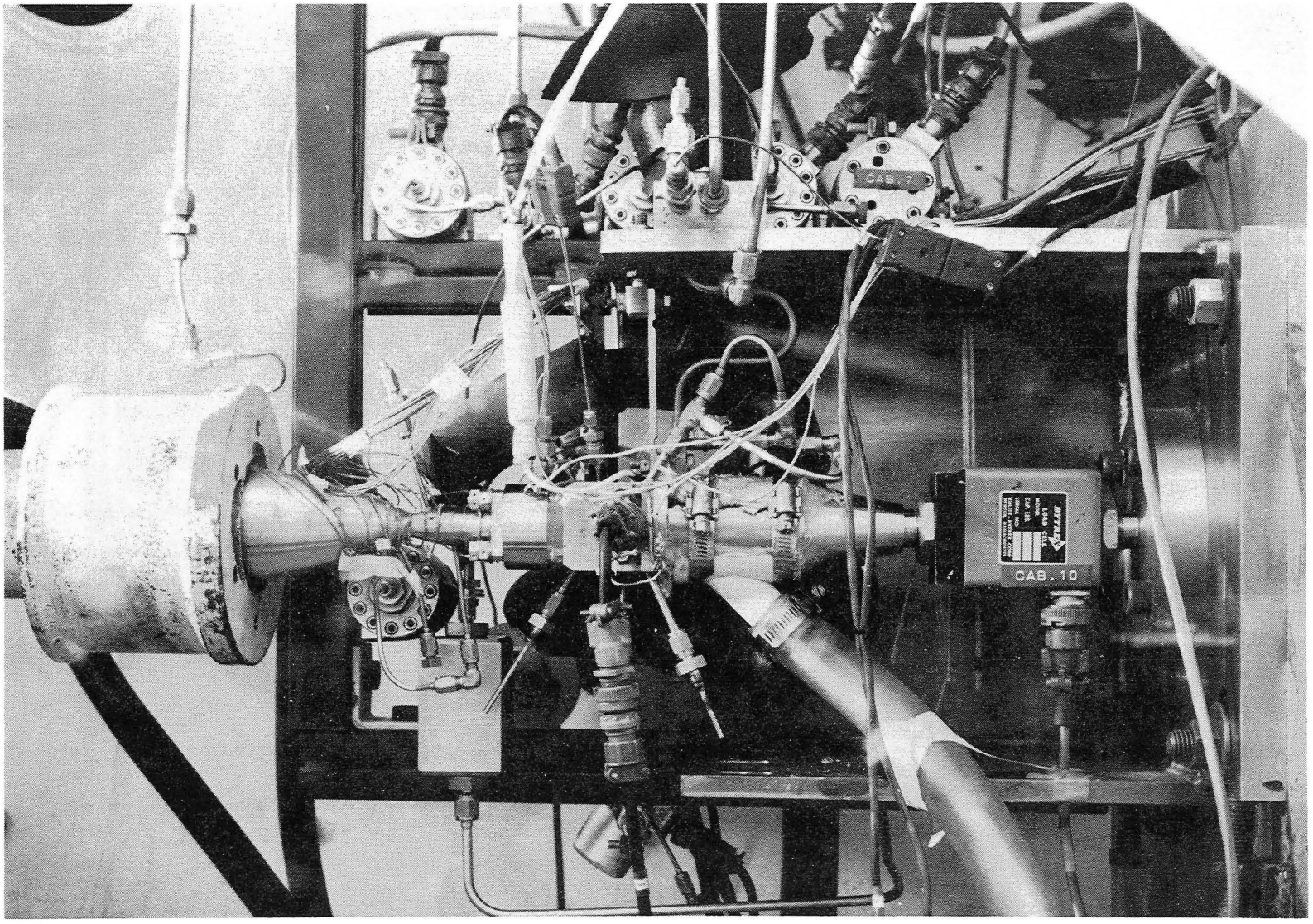

Figure 79 . Thruster Installation With Provisions for Pressurization of High-Voltage Spark Plug Cable

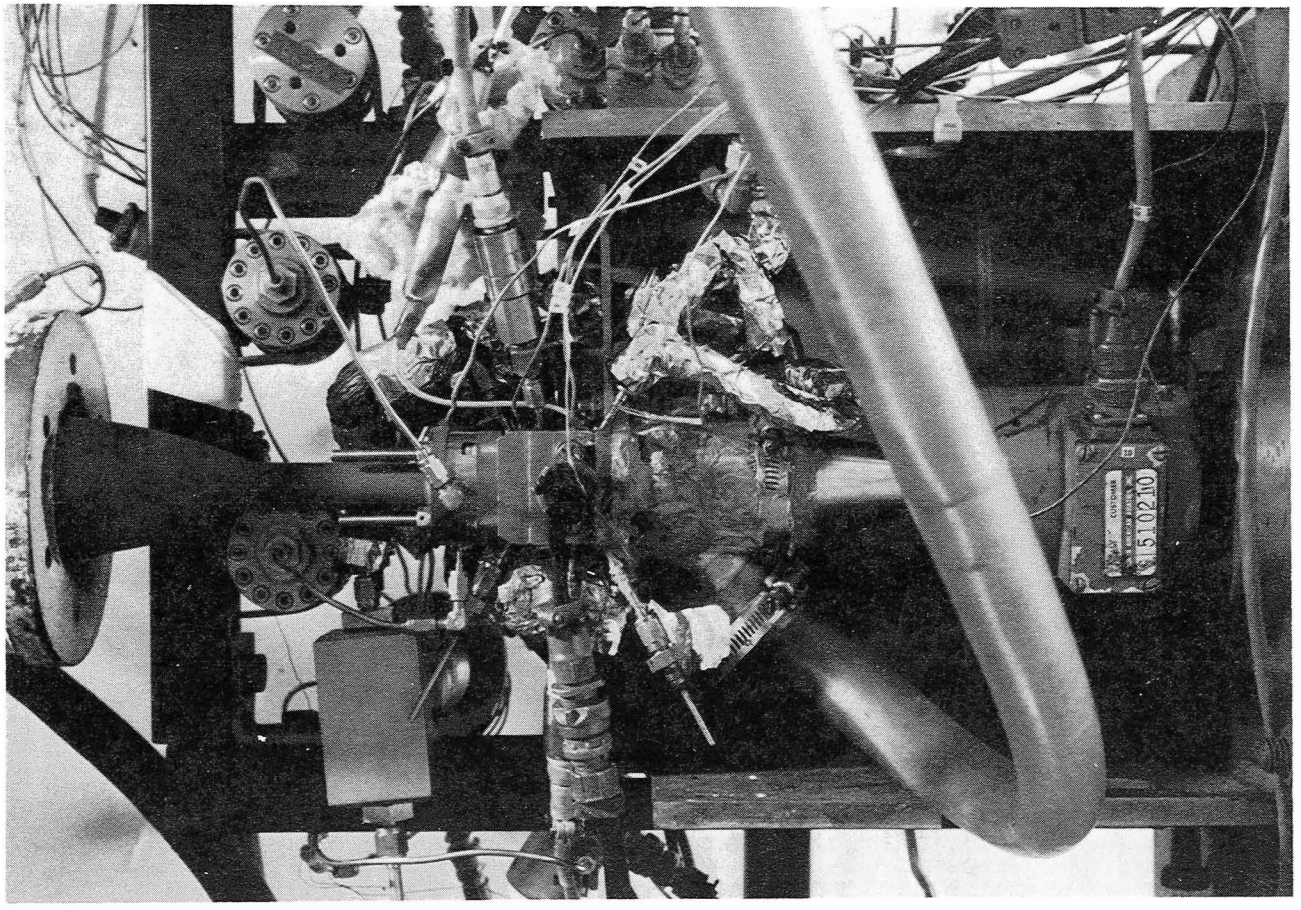

Figure 80. Installation of Durak "B" Coated Molybdenum Thrust Chamber With the BLH Load Cell

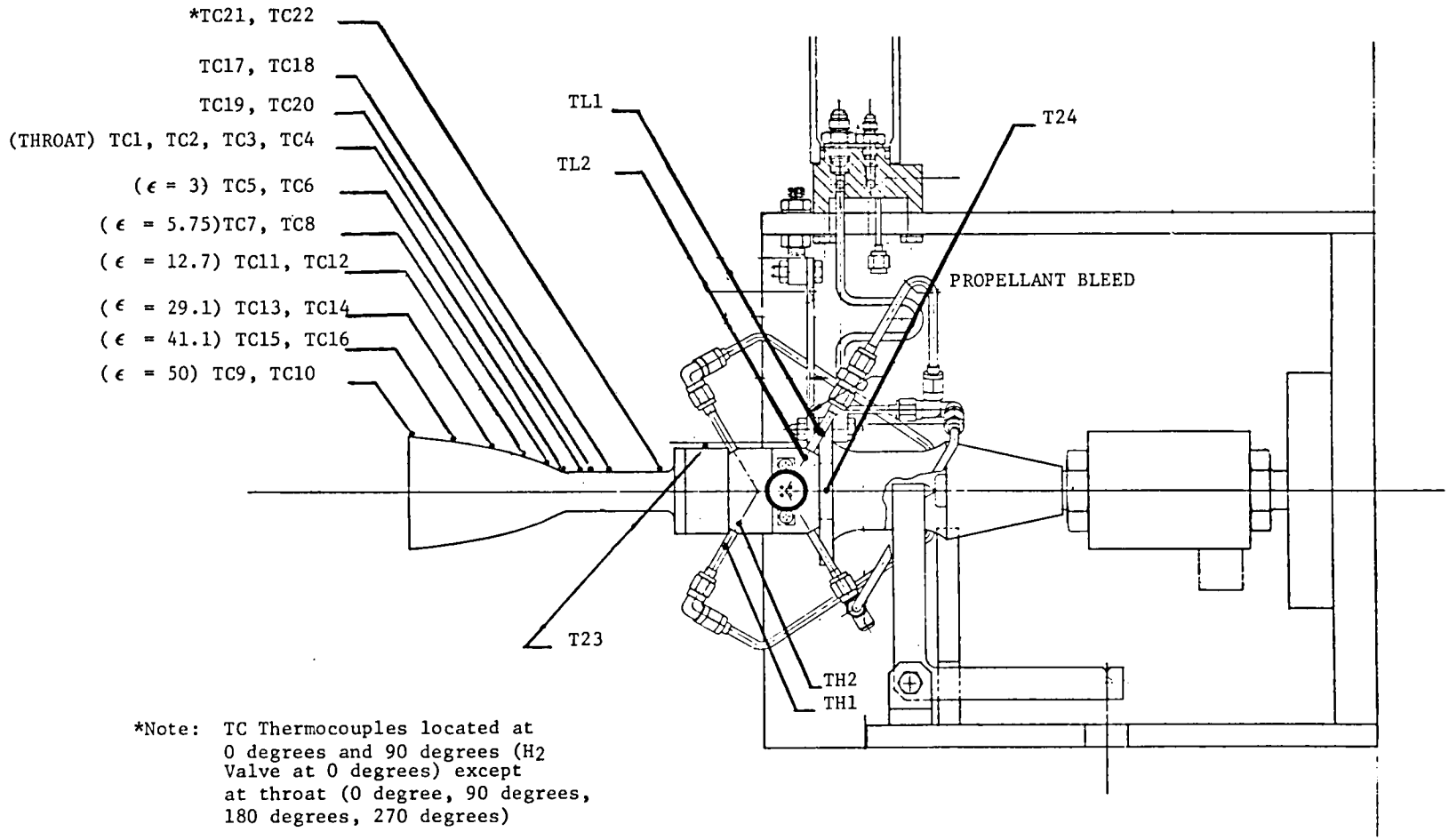

Figure 81. LO_2/LH_2 Thruster Surface Temperature Measurements

The propellant flowrates were measured using Rocketdyne designed subcritical venturi meters. Details of their construction are shown in Fig. 82. A tri-wall stainless-steel construction was used which permitted a continuous flow of LH_2 (in case of the LH_2 venturi) through the inner annular passage, while a vacuum was maintained in the outer annulus. In the case of the LOX venturi meter, an LN_2 flow was maintained in the inner annulus, since subcooled LOX conditions were normally desired. A photograph of a completed venturi meter assembly is shown in Fig. 83.

All transducers were periodically calibrated. Precision pressure gages were used as the reference standards for the pressure transducer calibrations, and the load cell calibrations were performed using weights. These standards were, in turn, kept in calibration by reference to secondary standards maintained by the Los Angeles Division Metrology Laboratory. The Rocketdyne-designed venturi meters were calibrated against turbine flowmeters, and these calibrations were checked by use of a "catch and weigh" procedure.

Recording Systems. The primary data recording system used in all of the tests was a 100-channel Astrodata digital data acquisition system. This recorder produced a digitized data tape which was later reduced to scaled parameters and printed out as numerical data by an IBM 7090 computer.

A selected group of data signals was "Y" patched at the output end of the Astrodata system amplifiers and furnished to graphical recorders. A Honeywell oscillograph recorded pertinent thruster parameters (see Table 6) to provide quick-look data and to monitor thruster transients. This oscillograph normally was operated at a paper speed of 25.4 cm/sec (10 in./sec) and used a self-developing photographic paper.

For continuous monitoring of venturi pressure and temperature measurements, and also of the chamber pressure and thrust parameters, Brush direct-inking strip recorders were used.

In addition to the recorders used, various visible readouts were employed, such as pressure gages and digital readouts.

A remote (black and white) television camera was used to monitor the thruster visually at all times. The firings were recorded on FM tape so that it was possible to replay the firings afterwards.

Test Procedures

Initial operations performed, prior to initiation of system chilldown, involved long purges with gaseous helium. This eliminated the possibility of the presence of condensible gases in any part of the flow systems. Periodically, the line systems were leak checked with pressurized helium and the main propellant valves and system bypass valves were checked for seat and/or stem leakage. In addition, periodic leak checks of the systems also were performed under cryogenic conditions; for these checks, liquid nitrogen was flowed through the systems.

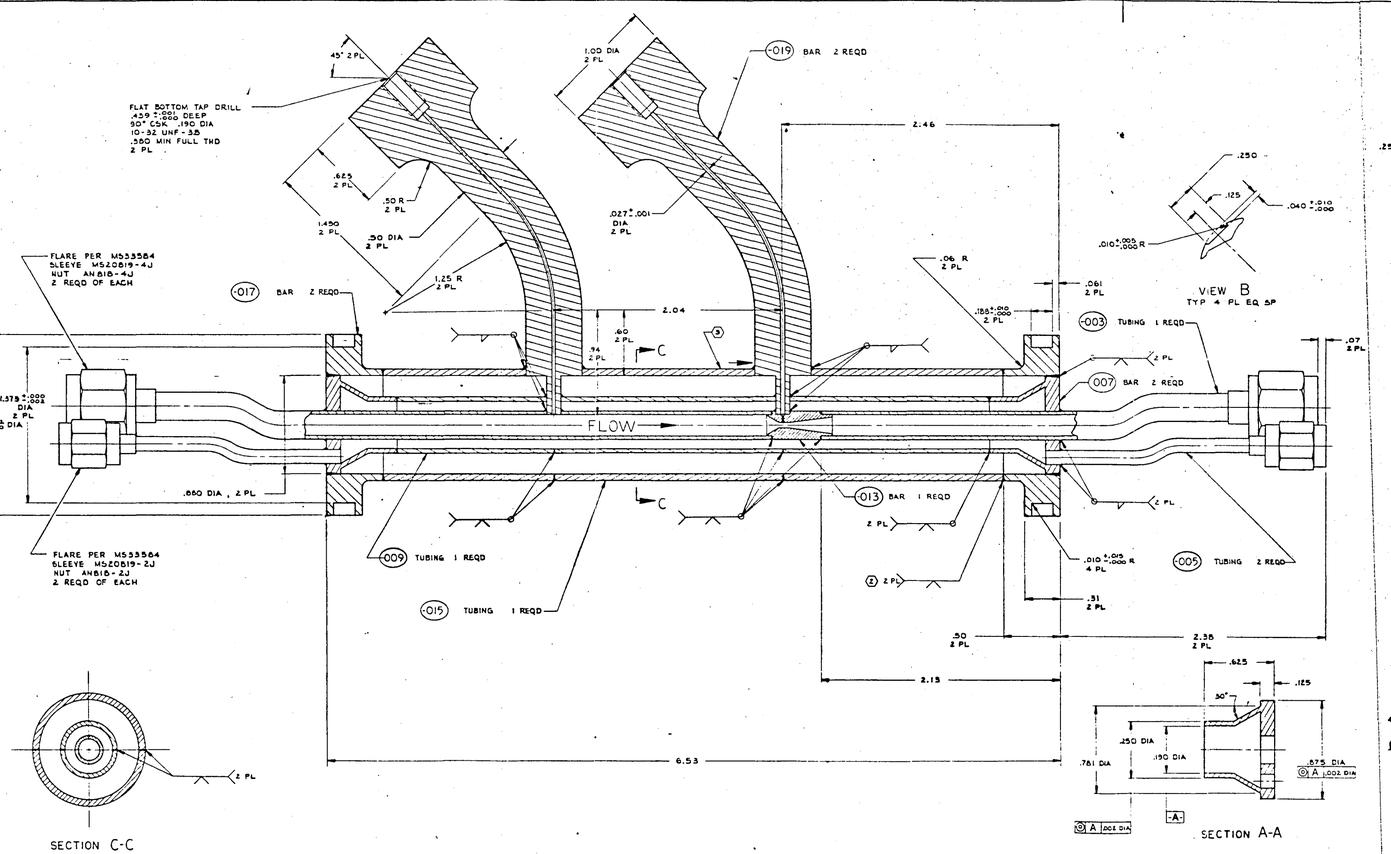

Figure 82. Venturi Assembly

-019	321 CRES BAR	1.00 OD x 4.00 LG	
-017	321 CRES BAR	2.00 OD x .50 LG	
-015	321 CRES TUBING	1.000 OD x .065 W x 6.00 LG	
-013	321 CRES BAR	.50 OD x .75 LG	
-009	321 CRES TUBING	.562 OD x .035 W x 9.50 LG	
-007	321 CRES BAR	1.00 OD x .75 LG	
-005	321 CRES TUBING	.145 OD x .028 W x 3.00 LG	
-003	321 CRES TUBING	.250 OD x .028 W x 1.00 LG	
NO	MATERIAL	SIZE	SPECIFICATION

NEXT ASSY	NONE		Rocketdyne International Corporation Rocketdyne Division Canoga Park, California
FINISH	NONE		YENTURI, ASSY OF, APST
MATL	NOTED		
		SIZE	CODE IDENT NO. 02602
		SCALE 4/1	SHEET 1

DRAWING AP77-076

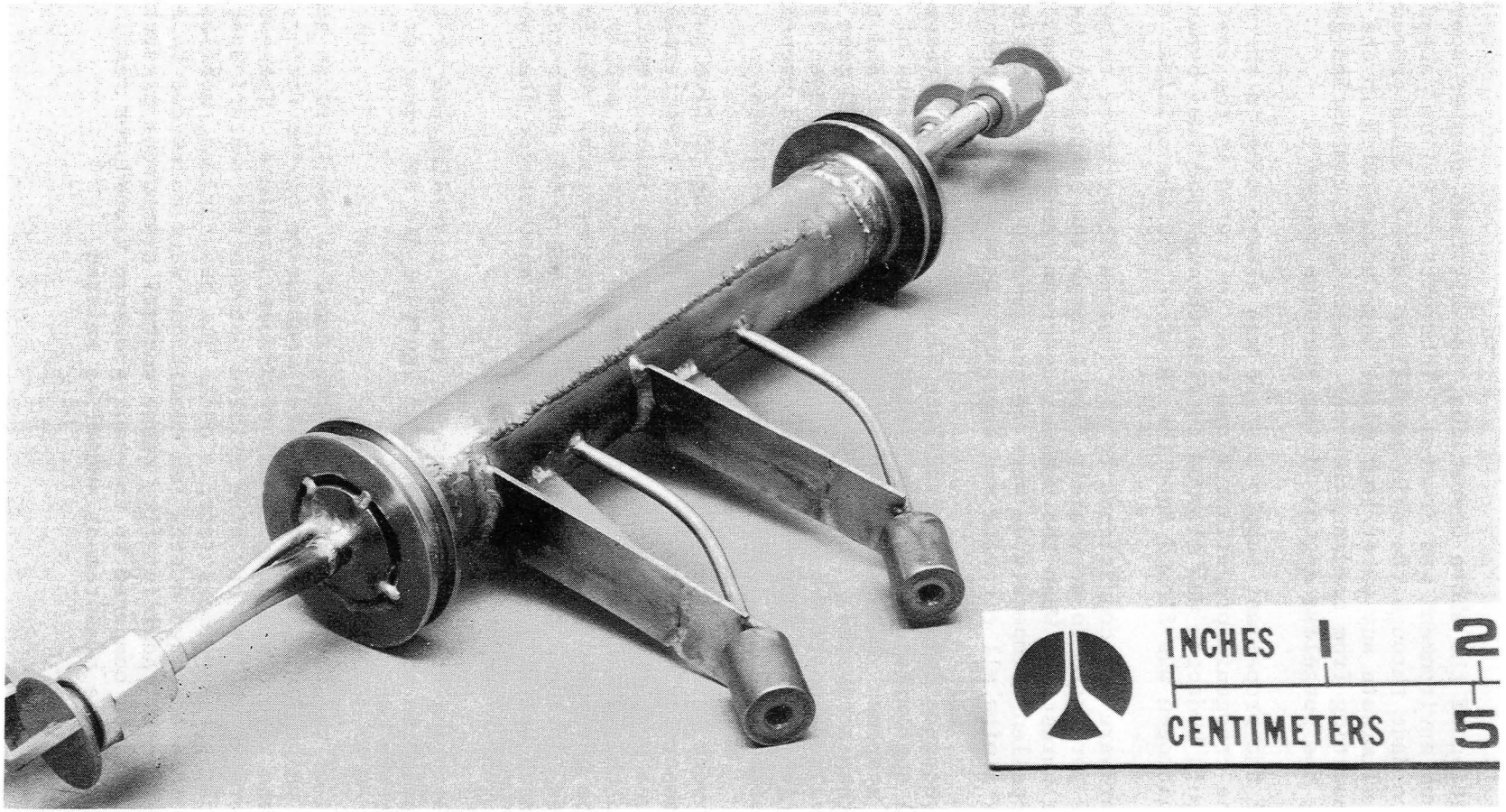

Figure 83. View of Tri-Wall Subcritical Venturi Used for Flowrate Determination

After completion of the above operations, the altitude chamber door was closed and the vacuum environment was created. Intermittent helium purges of the thruster were made through the main propellant valves. This procedure was designed to eliminate any water that might have accumulated in the thruster channels, resulting from condensation and freezing of combustion-generated water during the purgeless engine firing shutdown sequence.

Chilldown of the propellant supply systems was always done in the vacuum environment. The cryogenic propellant flows were initiated in the various line jackets, liquid hydrogen was allowed to flow through the fuel bypass system, and liquid nitrogen was flowed into the thruster via the oxidizer supply line.

After the hardware was conditioned to the desired temperature range, some LH_2 and LO_2 were permitted to separately flow through the propellant main valves and into the thruster. When the venturi upstream temperature sensors indicated that the propellant temperatures were in the desired range, the firings were initiated by arming all circuits and engaging the automatic sequence.

The firing sequence maintained propellant flows through their respective venturi meters until approximately 350 msec before the firing, by means of the propellant bypass systems. These flows were shutoff automatically, and the igniter system was then activated. The spark was initiated about 100 msec before main propellant valve actuation and was maintained for about 100 msec afterwards. The valve drive circuit (see Fig. 84 and 85) opened the main propellant valves with the desired relative leads and lags, as per its settings.

The firings were performed with a continuous monitoring of five parameters, using the comparator circuits to institute an immediate test termination if the redline values were exceeded (see Table 6). The fuel inlet temperature was monitored so that an automatic shutdown occurred if the LH_2 supply depleted. This would be evidenced by a rise in the inlet temperature. The four throat thermocouples (attached to the outer surface of the L-605 chambers) were set to avoid continued operations if temperatures were encountered that would result in possible chamber damage.

Observer monitoring of the brush recorder thrust recording and of the television monitor resulted in manual run aborts if ignition did not occur or if an abnormal heat pattern was noted.

The shutdown of the firing was always programmed to result in an approximate 8 msec fuel valve lag. Immediately after conclusion of the firing, a post-test astrodata record was made of all transducer readings. These data were used to determine whether any bias existed between the venturi upstream and venturi throat pressure measurements under the pressurized, nonflow conditions. The venturi ΔP's computed during run conditions were corrected to eliminate any noted bias effects. Additionally, these venturi transducer pressure measurements also could be compared to the tank pressure transducer reading to discern whether any pressure measurement anomalies existed.

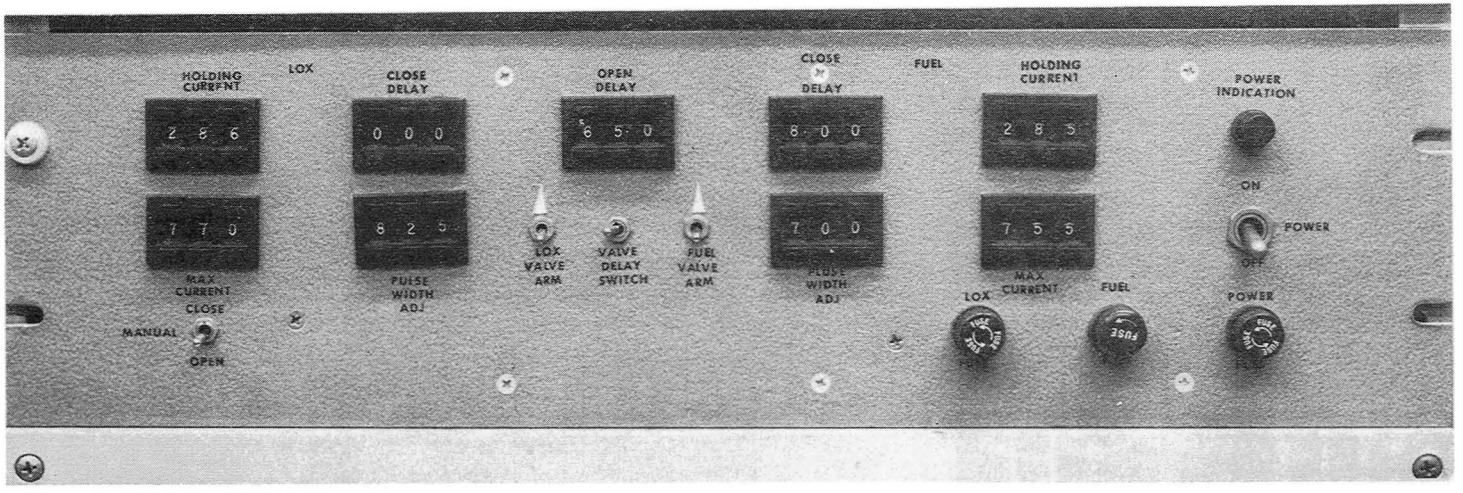

Figure 84. Propellant Valve Driver Circuit Module

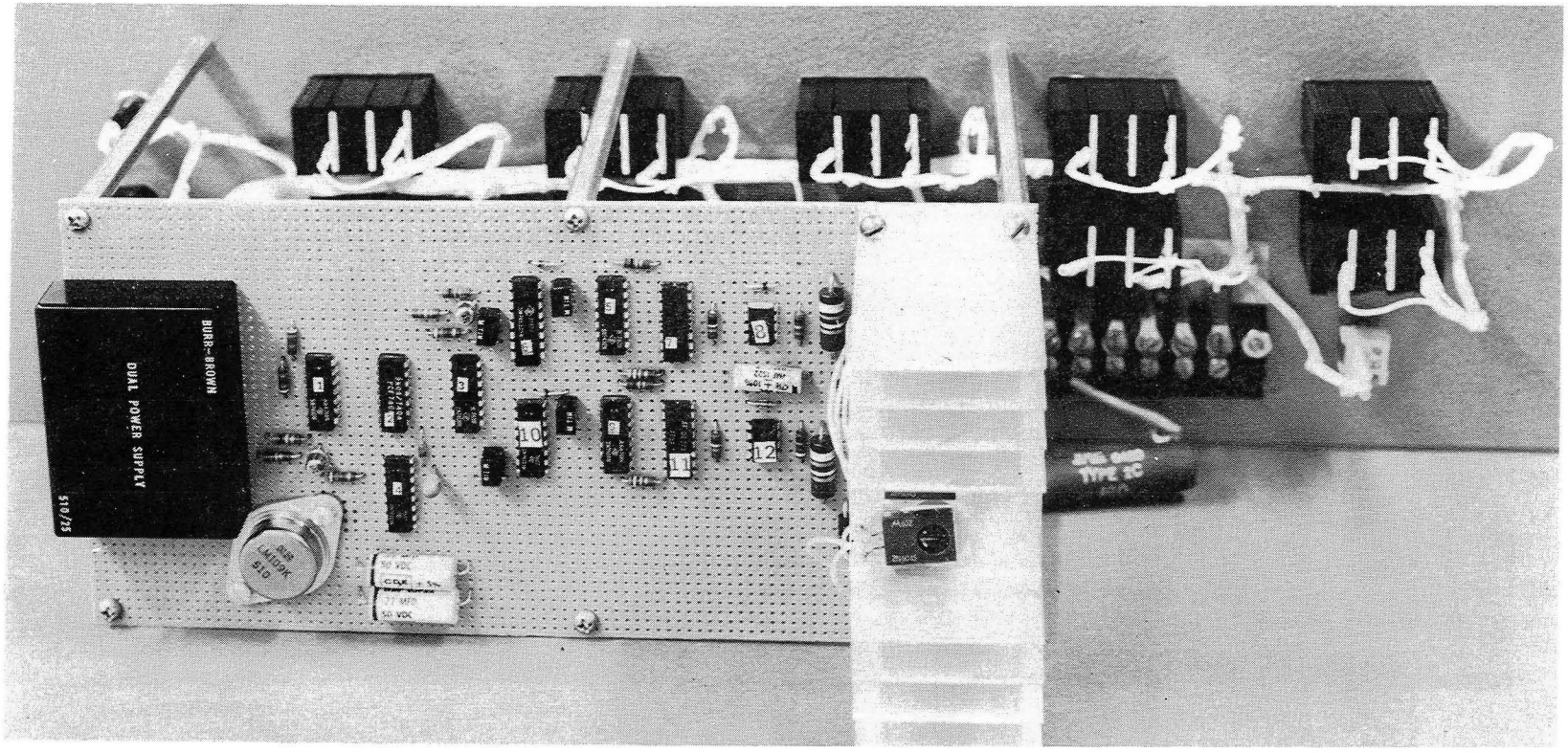

Figure 85. Propellant Valve Driver Circuit Module

DATA AND RESULTS

The hot-firing program was performed over a period of 18 months, and consisted of 100 tests. These tests are summarized in Table 7.

Ignition Tests

The initial area of investigation was the demonstration of reliable ignition of the thruster at various ignition energy levels, with a target objective of achieving ignition at the 10 mJ level. This block of tests included Runs No. 001 through 020 (Table 7). The range of variables encompassed during these tests were:

- LH_2 Temperature — 27 K (49 R) to 31 K (55 R)
- LOX Temperature — 89 K (160 R) to 102 K (184 R)
- Hardware Temperature (TH-2) — 36 K (65 R) to 95 K (171 R)
- Igniter Energy Level — 10 to 100 mJ
- Valve Sequencing — 10 msec lead/lag of MOV

All of these tests used an inductive discharge energy source (Fig. 86) operating at an output frequency of 100 Hz. This was the maximum frequency obtainable with this exciter. This discharge rate presented the possibility of a maximum 10 msec ignition lag penalty if the opening of the lagging propellant valve was out of phase with the peak plasma flow. For this reason, most tests during the entire program used the 100 Hz discharge rate.

Ability to ignite consistently at the 100 mJ level was demonstrated during the Run No. 001 to 020 test series. The Table 7 data show some ignition problems encountered in the course of these tests and sporadically throughout the program. These failures were usually identified to be due to test stand problems which would not be encountered in the actual flight installation. A discussion of these various problems is presented in a following section.

Tests No. 021 through 037 extended the ignition investigation to cover a range of propellant temperatures, preconditioned hardware temperatures, and establishment of optimum propellant entry sequencing to maximize chamber pressure rise rate. The range of variables for these tests were:

- LH_2 Temperature — 27 K (49 R) to 31 K (56 R)
- LOX Temperature — 89 K (161 R) to 103 K (185 R)
- Hardware Temperature (TH-2) — 63 K (113 R) to 263 K (473 R)
- Ignition Energy Level — 10 to 25 mJ
- Propellant Valve Sequencing — Simultaneous openings and 10 msec lead/lag of MOV
- Mixture ratio — 1.9 to 6.9 (4.0 nominal)

TABLE 7. INTEGRATED AUXILIARY PROPULSION SYSTEM 25-POUND LOX/LH_2 THRUSTER TEST HISTORY

TEST No.	TEST DATE	DURATION secs	OBJECTIVE	SPARK SYSTEM			THRUSTER SEQUENCING				PURGE SYSTEM PRESS X 10^{-5} ABS		TANK PRESSURE LOCKUP		TEMPERATURES - K			THRUSTER PERFORMANCE				HYDROGEN FLOWRATE	SPECIFIC IMPULSE	TIME TO 90% P_c	REMARKS
				TYPE	mJ	Hz	TYPE LEAD	LEAD TIME msec	TYPE LAG	LAG TIME msec	LOX N/m^2	LH_2 N/m^2	LOX N/m^2	LH_2 N/m^2	LOX	LH_2	HARDWARE (TH2)	P_c X 10^{-5} N/m^2 abs.	THRUST NEWTON	OVERALL MIXTURE RATIO	OXIDIZER FLOWRATE g/sec	g/sec	secs	(sec)	
87-001	6/23/77	0.5	Ignition checkout	Inductive	50	100	LOX	10	LH_2	8	3.45	3.45	17.24	17.24	99	28	71	2.07	n/m	4.6	44.2	9.66	--	-	Ignition not achieved at vacuum
002	6/23/77	0.5			100	50	LH_2								99	28	69	2.07		4.7	44.0	9.39		-	
003	7/1/77	0.1					LOX								89	29	53	6.83		7.1	35.4	4.99		-	Ignition achieved capsule PR = atmospheric
004	7/1/77	0.5													89	29	*	1.17		3.5	22.0	6.31		-	Ignition not achieved at vacuum
005	7/11/77	1.0				100							16.54	18.82	97	29	37	1.54		4.2	32.2	7.71		-	
006	7/11/77												16.41	18.96	99	31	36	1.19		5.3	28.6	5.44		-	Ignition at shutdown capsule PR = atmospheric
007	7/15/77						LH_2						18.06	18.27	96	29	56	1.05		2.4	20.4	8.62		-	Ignition not achieved at vacuum
008	7/15/77												18.34	18.55	94	28	57	8.41		3.1	23.5	7.62		.107	Ignition achieved capsule PR = atmospheric
009	7/25/77				50								18.00	18.68	89	28	69	0.96		1.8	15.9	8.98		-	Ignition not achieved capsule at vacuum
010	7/25/77												18.13		89	31	91			2.2	17.2	7.80		-	
011	7/28/77		Characterize Ignition										18.06	18.48	96	29	73	7.52		2.9	24.2	8.44		.091	Ignition achieved capsule at vacuum
012	7/29/77				25								18.27	18.68	91	28	71	8.55		3.0	24.3	8.12		.112	
013					10								18.13	17.86	91	28	78	8.48			24.0	7.94		.085	
014													17.93		92	28	95	*		2.8	23.7	8.39		.110	
015													18.06		94	28	65	9.31		3.1	24.7	7.89		.041**	
016														17.79	95	27	82	1.17		3.4	31.2	9.12		-	Ignition not achieved capsule at vacuum
017													18.62	17.65	102	28	84	0.94		2.7	23.8	8.75		-	
018													18.34	17.93	99	29	76	1.11		3.6	30.0	8.26		-	
019					25								18.20		99	28	81	"		"	*	8.80		-	
020	8/3/77				10								18.13	16.89	98	28	70	1.32		*	31.1	*		-	Ignition not achieved - low energy level
021	8/4/77												18.06	18.06	93	28	71	7.24		3.2	25.0	7.80		.120	Ignition achieved
022													18.27	20.13	93	28	68	1.37		3.5	32.2	9.21		-	Ignition not achieved - low energy level
023													17.93	17.17	92	28	66	9.24		3.5	25.7	7.39		.0951	Ignition achieved
024	8/8/77				25								15.65	13.24	91	28	72	7.45		*	16.7	*		.093	Ignition achieved
025													15.58	13.31	89	29	81	7.45		4.2	22.4	5.31		-	Delay ignition; approx. 0.5 sec.
026													18.27	14.62	89	28	72	8.48		3.6	23.7	6.62		.092	Ignition achieved
027													18.55	14.62	90	28	84	8.55		3.6	23.5	6.62		.110	
028													24.68	16.20	89	28	63	9.79		4.1	29.2	7.17		.110	
029	8/11/77												19.44	14.69	97	30	212	9.38		5.4	26.8	4.99		.585	Ignition achieved - unconditioned hardware
030													17.93	14.75	99	29	217	9.51		4.0	22.8	5.72		.470	
031													15.51	18.00	97	27	221	7.10		*	19.7	*		.385	

* Pressure transducer malfunction

** P_c rise initiated before power to lagging value

TABLE 7. (CONTINUED)

TEST No.	TEST DATE	DURATION secs	OBJECTIVE	SPARK SYSTEM TYPE	SPARK SYSTEM mj	SPARK SYSTEM Hz	THRUSTER SEQUENCING TYPE LEAD	THRUSTER SEQUENCING LEAD TIME msec	THRUSTER SEQUENCING TYPE LAG	THRUSTER SEQUENCING LAG TIME msec	PURGE SYSTEM PRESS X 10^{-5} ABS LOX N/m^2	PURGE SYSTEM PRESS X 10^{-5} ABS LH_2 N/m^2	TANK PRESSURES X 10^{-5} ABS LOX N/m^2	TANK PRESSURES X 10^{-5} ABS LH_2 N/m^2	TEMPERATURES - K LOX	TEMPERATURES - K LH_2	TEMPERATURES - K HARDWARE (TH2)	THRUSTER PERFORMANCE P_c X 10^{-5} N/m^2 abs.	THRUSTER PERFORMANCE THRUST NEWTON	THRUSTER PERFORMANCE OVERALL MIXTURE RATIO	THRUSTER PERFORMANCE OXIDIZER FLOWRATE g/sec	HYDROGEN FLOWRATE g/sec	SPECIFIC IMPULSE secs	TIME TO 90% P_c (sec)	REMARKS
032	8/12/77	1.0	Characterize Ignition	Inductive	25	100	LH_2	10	LH_2	8	3.45	0	15.72	18.27	102	31	224	5.65	n/m	1.9	11.4	5.90	--	.418	Ignition achieved - unconditioned hardware
033													19.37	14.75	95	30	263	7.65		6.9	26.2	3.81		.720	
034													15.58	18.41	103	29	88	8.20			19.5	-		.374	
035													22.82	13.44	92	30	113	9.03		6.2	30.0	4.85		-	Delayed Ignition; approx. 0.7 sec.
036							LOX						18.96	15.31	97	28	87	8.96		3.9	25.8	6.62		.047	Ignition achieved
037							0	0					18.89	15.44	94	29	84	0.94		3.9	28.7	7.35		-	Ignition not achieved - unpressurized cable
038	8/16/77	.05 ON 1.00 OFF					LOX	10					19.24	15.03	96	29	187	4.62		~4.0	-	-		-	Eight 50ms pulses
039	9/19/77	5.0	Performance/ Heat Transfer				LOX	10			0		18.82	15.93	90	27	89	4.96		4.6	34.2	7.44		-	No ignition
040							LH_2						18.68	15.93	91	29	99	9.58	114.8	4.7	28.7	6.12	336	.235	Satisfactory Ignition
041		10.0											18.75	15.93	89	28	82	1.45	-	4.8	33.6	7.03	-	-	No ignition
042							LOX						18.82	16.00	89	30	61	10.07	121.4	4.7	29.2	6.26	349	-	Ignition delayed approximately 0.7 sec.
043	9/22/77	0.3											17.79	17.51	91	28	51	6.34	67.6	3.1	29.7	9.66	-	-	Ignition delayed approximately 1.1 sec.
044	11/1/77	1.0											18.27	17.58	93	32	77	1.03	-	5.7	25.4	4.45	-	-	No ignition
045		1.0											18.48	17.58	94	27	109	8.48	95.2	3.2	19.5	6.08	-	.097	Satisfactory ignition
046		5.0											18.75	16.82	98	28	100	8.55	98.8	2.9	20.5	6.99	367	.073	" "
047	11/2/77	11.3											22.06	16.62	96	26	42	1.38	-	3.6	28.8	8.03	-	-	No ignition - Ignitor not armed
048		15.0											22.13	16.69	96	26	111	9.38	113.4	3.5	24.0	6.89	374	.096	Satisfactory ignition
049	11/3/77	3.8											21.72	23.61	91	28	100	-	-	4.1	29.5	7.12	-	-	No ignition
050		15.0			100								21.72	22.55	90	27	120	9.31	105.9	3.4	23.4	6.94	356	.072	Satisfactory ignition
051	11/9/77	3.0											21.58	16.75	102	25	78	-	-	2.4	18.8	7.98	-	-	No ignition-ignition cable not pressurized
052		13.6											21.65	15.17	95	26	86	9.10	113.0	3.9	24.1	6.26	379	.117	Satisfactory ignition
053		2.8											18.41	17.44	98	27	97	-	-	3.4	25.9	7.53	-	-	No ignition
054		29.9											21.24	17.44	94	26	84	9.45	109.4	3.2	23.2	7.30	366	-	Satisfactory ignition
055	12/2/77	4.9											20.62	15.24	92	27	94	8.48	99.2	3.6	22.2	6.17	357	.078	
056	12/3/77	9.5											21.65	16.13	96	27	111	8.55	103.2	3.1	23.0	7.44	346	.126	
057		28.6											23.17	15.31	95	28	96	8.55	97.9	3.8	24.9	6.53	318	.155	
058	12/5/77	28.6											20.82	15.86	88	25	114	8.89	108.5	3.5	22.8	6.53	378	.182	
059		16.2											23.30	14.20	88	25	112	9.10	105.9	4.1	24.9	6.08	348	.117	
060	12/14/77	8.6											23.17	15.44	91	27	104	8.69	-	4.3	25.1	5.90	-	.197	
061		5.6											23.24	15.44	91	28	79	-	-	4.4	25.6	5.81	-	.197	S/N L-605 Chamber - Throat Erosion
062	12/16/77	5.0											21.72	15.86	88	26	42	8.55	106.3	3.6	23.9	6.58	356	.130	S/N 2 L-605 Chamber installed
063		5.0											21.86	15.93	87	26	42	-	103.6	3.9	23.9	6.17	352	-	
064		5.0											21.79	15.86	87	26	43	-	107.2	3.7	23.8	6.35	363	-	
065	1/6/78	5.0											21.58	15.44	98	25	91	7.93	100.5	3.5	23.1	6.53		.086	Trip ring installed
066	1/18/78												20.75	23.17	90	26	91	—	97.9	-	-	7.12	-	-	
067													20.75	23.17	89	27	78	-	97.4	-	-	6.44	-	-	
068													20.55	22.82	89	27	91	-	-	3.8	27.7	7.21	-	-	Non-ignition - Igniter circuit disarmed

TABLE 7. (CONCLUDED)

TEST No.	TEST DATE	DURATION secs	OBJECTIVE	SPARK SYSTEM TYPE	SPARK SYSTEM mJ	SPARK SYSTEM Hz	THRUSTER SEQUENCING TYPE LEAD	THRUSTER SEQUENCING LEAD TIME msec	THRUSTER SEQUENCING TYPE LAG	THRUSTER SEQUENCING LAG TIME msec	PURGE SYSTEM PRESS X 10^{-5} ABS LOX N/m^2	PURGE SYSTEM PRESS X 10^{-5} ABS LH_2 N/m^2	TANK PRESSURES X 10^{-5} ABS LOX N/m^2	TANK PRESSURES X 10^{-5} ABS LH_2 N/m^2	TEMPERATURES - K LOX	TEMPERATURES - K LH_2	TEMPERATURES - K HARDWARE (TH2)	P_c X 10^{-5} N/m^2 abs.	THRUST NEWTON	THRUSTER OVERALL, MIXTURE RATIO	PERFORMANCE OXIDIZER FLOWRATE g/sec	HYDROGEN FLOWRATE g/sec	SPECIFIC IMPULSE secs	TIME TO 90% P_c secs	REMARKS
069	8-16-78	1.0	Performance and Heat Transfer	Inductive	25	100	LOX	10	LH_2	8	0	0	18.34	16.13	~ 93	~ 28	-	~ 9.03	~104.1	~ 3.6	~ 24.9	~ 6.80	-	0.230	No digital acquisition system data
070	8-16-78	1.0											18.34	16.13	94	27	95	9.27	107.8	3.9	26.1	6.67	-	0.126	Suspect LH_2 Leakage
071	8-18-78	5.0											17.10	15.86	95	27	71	9.29	116.7	4.3	29.0	6.71	-	0.228	Chamber and throat erosion occurred (suspect LH_2 leak)
072	9-28-78	1.0			50								16.41	16.75	89	26	85	9.44	~107.6	4.1	26.7	6.58	-	--	Pre-run thrust zero data lost
073	9-29-78	3.6			100								16.69	15.93	94	27	93	-	103.4	3.3	~ 20.7	6.35	-	--	LOX bypass flow on during run
074	9-30-78	5.0											16.89	16.20	92	26	95	9.94	117.5	4.3	25.9	6.03	-	--	Suspect LH_2 Leakage
075	"	5.0											16.20	16.34	91	27	95	9.92	112.8	4.2	25.6	6.17	-	--	Suspect LH_2 Leakage
076	"	5.0											16.55	16.41	91	26	97	9.74	113.9	4.3	25.9	6.03	-	--	Suspect LH_2 Leakage
077	10-16-78	4.2											15.31	16.75	98	27	88	9.42	113.2	3.5	22.5	6.44	391	--	Ave. lock-up pressure correction assumed
078	10-30-78	10.3											16.48	16.69	97	27	-	9.94	116.4	4.0	25.4	6.40	-	--	Suspect LOX bypass valve leakage
079	11-1-78	10.3											17.51	15.93	96	26	86	9.24	107.2	---	-	6.44	-	--	LOX bypass flow on during run
080	11-1-78	9.7											16.27	16.69	96	26	90	9.77	110.3	3.9	25.6	6.58	-	--	Lox bypass flow on during run
081	11-2-78	11.0											18.34	16.06	90	27	85	9.69	111.9	---	-	6.12	-	--	Lox bypass flow on during run
082	11-3-78	12.0											17.72	16.34	89	28	93	9.43	106.3	---	-	6.31	-	--	Lox bypass flow on during run
083	11-7-78	32.5											15.58	16.96	95	26	78	9.48	111.9	3.4	23.3	6.76	380	--	Lox bypass system blanked off during run
084	11-9-78	33.6											16.62	16.82	96	26	68	9.89	117.2	3.9	25.2	6.44	378	--	Lox bypass system blanked off during run
085	11-10-78	33.3											16.82	16.89	96	26	74	-	118.9	4.0	25.5	6.44	379	--	Lox bypass system blanked off during run
086	11-14-78	13.6											15.44	16.75	97	30	111	8.69	97.3	4.8	25.4	5.31	-	--	Suspect hydrogen leakage
087	11-30-78	5.7											16.48	16.82	101	26	122	-	100.0	3.8	25.8	6.80	-	--	Moly chamber, hydrogen leakage
088	12-1-78	10.5											16.48	16.69	93	25	93	10.89	108.9	3.9	24.9	6.40	-	--	Moly chamber, hydrogen leakage
089	1-17-79	5.0											16.34	16.69	100	26	126	-	101.7	3.3	23.1	6.99	-	--	Moly chamber hydrogen leakage
090	1-17-79	5.0											17.03	16.69	100	28	118	-	107.2	3.5	24.0	6.76	-	--	Moly chamber hydrogen leakage
091	1-18-79	33.6											16.89	16.69	92	26	97	-	104.5	3.5	23.9	6.89	-	--	Moly chamber hydrogen leakage
092	2-26-79	1.0	Stand Checkout										16.29	16.10	95	24	124	7.96	90.9	-	-	-	-	0.048	L-605 heavy wall chamber - Checkout firing
093	2-26-79	Pulsed	Pulsing Performance										17.64	17.75	96	26	125	-	-	-	-	-	-	-	18 pulses, 4 ignitions cont. spark
094	3-21-79				50								17.85	17.42	91	25	105	-	-	-	-	-	-	-	21 pulses, 12 ignitions cont. spark
095	3-21-79				100								17.86	17.41	98	25	110	-	-	-	-	-	-	-	7 pulses, 4 ignitions cont. spark
096	3-23-79			Capacitive		250	LH_2						17.79	17.71	89	28	126	-	-	-	-	-	-	-	8 pulses, 2 ignitions pulsed spark
097	3-23-79												17.68	17.51	90	26	126	-	-	-	-	-	-	-	7 pulses, 7 ignitions pulsed spark*
098	3-23-79												17.66	17.53	89	27	124	-	-	-	-	-	-	-	6 pulses, 6 ignitions pulsed spark**
099	3-26-79	29.2											17.91	17.54	88	25	99	10.99	126.2	-	-	-	-	-	6 pulses + 30 sec burn + 1 min soak + 6 pulses**
100	3-26-79	28.6											17.90	17.57	87	24	103	10.94	128.3	-	-	-	-	-	6 pulses + 30 sec burn + 1 min soak + 6 pulses*

0.065 sec ON 1.000 sec OFF pulses

*0.065 sec ON, 3.00 sec OFF

**0.065 sec ON, 2.00 sec OFF

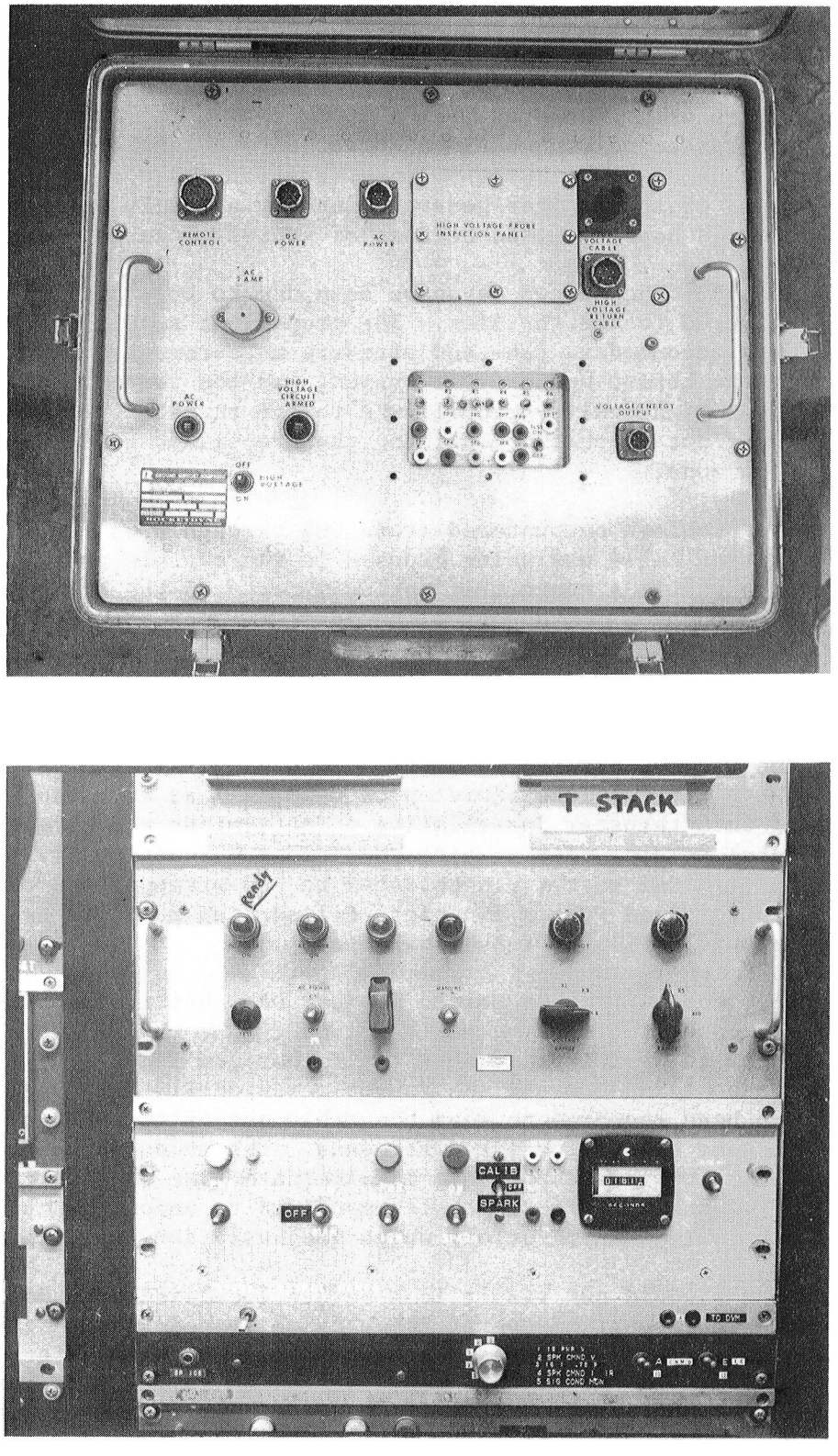

Figure 86. Variable Energy Power Supply and Control Panel

Successful ignition was obtained under most conditions, but some failures and several cases of delayed ignition were noted. The ignition failures were assumed to have possibly been due to a marginal ignition energy level (10 mJ), so subsequent tests were conducted with a 25 mJ energy level. Later experiences with the igniter system (discussed in a following section) tend to indicate the possibility that a deterioration of the ignition cable assembly may have reduced the amount of the exciter-generated energy actually delivered to the igniter. This would have resulted because of increased cable leakages.

The delayed ignition occurrences may have been due to poor quality of the liquid hydrogen as delivered to the thruster. The propellant supply system configurations required to accommodate flow and pressure measurements, and to maximize the accuracy of the thrust measurement system, had the tendency to reduce the ability to deliver high quality propellants to the thruster. In addition, the existing data were not capable of defining the propellant conditions as injected into the ignition zone.

Initial ignition problems encountered (runs 001 through 008, Table 7) resulted because the ignition cable was being exposed to the capsule pressure environment. This low pressure was in a range that seriously reduced the breakdown voltage of the air and encouraged leakage from the igniter input terminal to the igniter steel body. This problem was eliminated by maintaining a pressure slightly above atmospheric for the igniter cable and input end of the igniter (see Fig. 79).

A second area of ignition cable problems encountered was with the igniter terminal end of the cable. Existing high-tension cables, as used in the J-2S engine, were used, but required addition of terminals at both ends to suit the requirements of this thruster installation. The igniter end terminal was (for most of the tests) molded under on-site conditions by casting RTV 511 silicone rubber around a terminal socket pin soldered to the stripped end of the cable. An igniter body, combined with a two-piece cylindrical mold was used to retain the molding compound until the rubber hardened.

The general experience with this molded product was that ignition problems gradually were encountered after a period of use. The physical strength and tear resistance of this silicone rubber are rather low and some ignition cable failures were encountered because the rubber occasionally developed a crack. The fairly sharp bend required to lead the cable out of the thrust mount adapter resulted in some highly localized stresses. The second problem area encountered was that it was not possible to eliminate fine bubbles from being trapped within the rubber. These bubbles appeared to encourage current leakage paths (perhaps by surface conduction) which gradually developed through them.

These leakage paths would not result in a severe localized breakdown, but would gradually reduce the amount of energy actually delivered to the igniter. Typically, a small amount of discoloration would develop on the surface of the molded terminal where an underlying bubble was close to the surface. As a confirmation of this hypothesis, it was noted that ignition problems usually developed only after a series of tests were performed, and that remolding a new terminal usually resulted in the disappearance of these ignition problems.

In an effort to eliminate the problems encountered with the "on-site" molded connectors, a revised configuration was designed and fabricated. This connector is shown in Fig. 87. This terminal was machined from Kel-F stock, to which was then added a molded RTV 511 silicone rubber section that incorporated a preformed right-angle bend. The RTV rubber was molded under partial vacuum conditions to minimize air bubble retention. While the right-angle bend eliminated the bending stresses otherwise encountered in the test installation, it made the central location of the conductor wires within the insulation difficult to assure. This terminal still required an on-site molding of RTV 511 rubber to cover the splice between the prefabricated terminal and the igniter cable.

The Kel-F connector was installed and used for Runs No. 39 through 42. Most of these tests encountered some form of ignition problem. Removal and inspection of the ignition cable shows that a failure of the RTV 511 rubber had occurred. A small black line, approximately 0.15-cm long, with a puncture mark at its center, was found located at the center of the 90-degree bend. The insulation was nominally 0.30-cm thick, but the presence of some small subsurface air bubbles and the possibility that the conductor wire may have shifted in the mold could have reduced the local insulation thickness. No further tests were conducted with this version of the igniter terminal.

Tests No. 043 through 068 were conducted using the previously removed igniter cable assembly. At the 50 mJ energy level, some further ignition failures were noted. The cable was removed again, questionable RTV rubber areas were sliced out of the surface, and additional rubber was cast over the entire surface external to the igniter. At the same time, the ignition energy level was raised to 100 mJ on the assumption that current leakages would have to be expected and that a higher initial input would have a greater tolerance for losses.

A new igniter cable assembly was procedured and used for the remainder of the program, i.e., Runs No. 069 through 100. This cable was considerably thinner, with an approximate 0.41 cm outside diameter, and an insulation* thickness of 0.11 cm. The flexibility of this reduced diameter minimized possibility of surface stresses due to the routing path of the cable. An RTV 511 igniter terminal end was molded on one end of the cable using a partial vacuum to minimize retention of air bubbles. Ignition with this small-diameter cable seemed to require use of the 100 mJ power level. This was interpreted to mean that higher corona losses were being encountered, reducing the effective power actually delivered to the igniter. Since ignition phenomena were no longer being specifically evaluated during this series of runs, this situation was tolerated so that attention could be concentrated on the performance evaluation of the thruster.

*MIL-W-16878 Type FF white silicone rubber

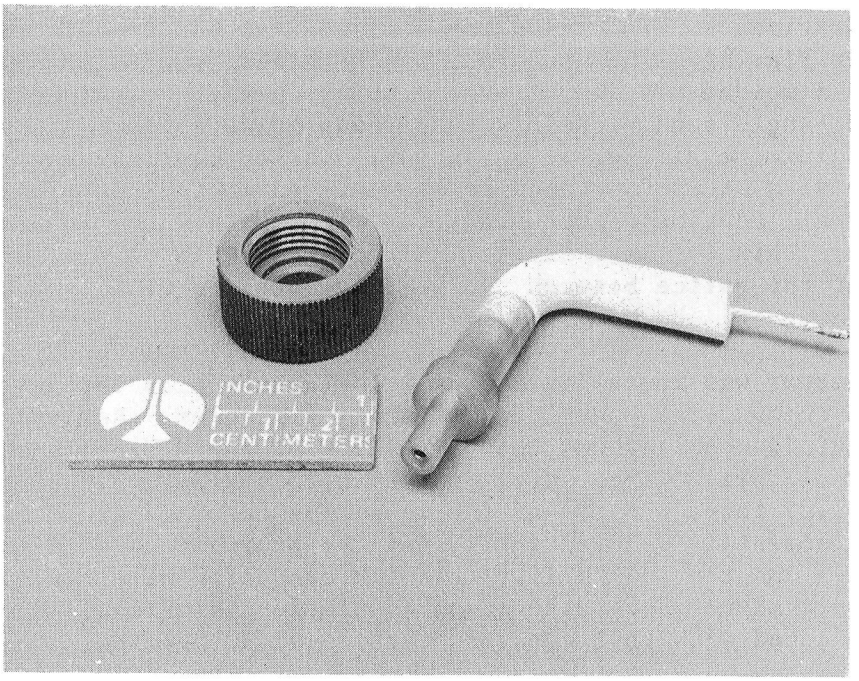

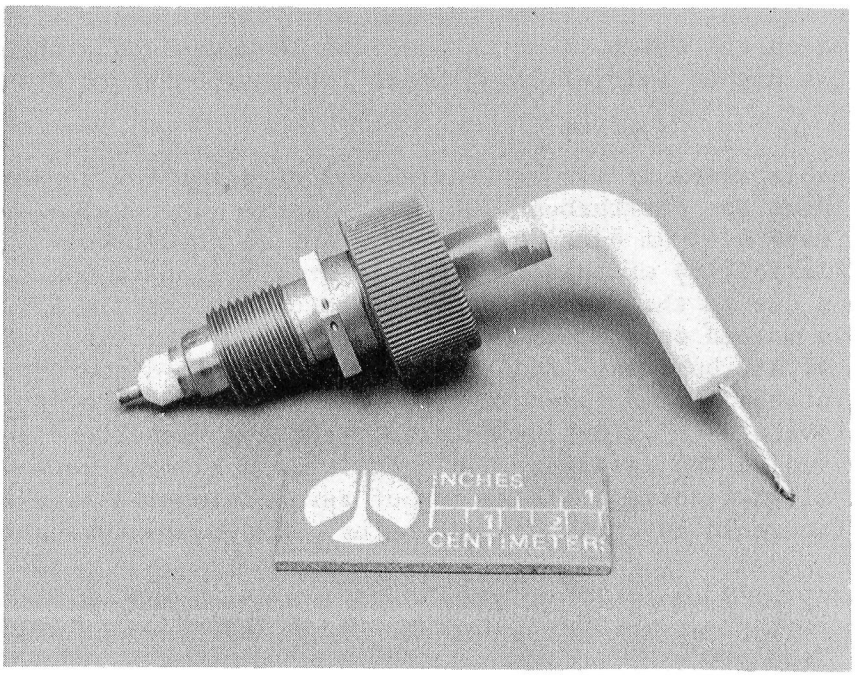

Figure 87. Spark Plug High-Voltage Cable Connector

Performance Tests and Heat Transfer

The evaluation of the thruster performance and investigation of the heat transfer phenomena were the objectives of Runs No. 039 through 091 (Table 7). These tests encompassed variations in the distribution of the relative percentage of the hydrogen flow between the 3 flow circuits, several design modifications of a portion of the thruster, and a systematic variation of the distance upstream of the chamber throat that the boundary layer hydrogen was allowed to exit. The computed specific impulse for these tests ranged from 313 to 391 seconds (390 seconds minimum acceptable, 410 seconds contract goal).

The instances of low apparent performance noted were usually identified to be the results of propellant leakages which constituted part of the measured propellant flows. The engine performance in such cases was necessarily based on a higher flowrate than that which was delivered to the thruster. Tests affected by such problems also tended to show considerable data scatter between similar runs and significant changes in the thruster wall temperature measurements.

As discussed in a later section, it is believed that the thruster did meet the target performance objective, even though many of the tests performed with the final hardware configuration tended to indicate a lower performance level.

Table 8 lists the various changes in the thruster configuration evaluated in the course of the firing program. In summary, the range of variations tested and changes in hardware/stand configuration were:

1. Thruster internal mixture ratios (primary or core flow, with addition of secondary fuel flow, and with addition of boundary layer fuel flow):

   From 50-12-4 to 24-6-4

2. Boundary layer fuel exit plane (distance upstream of thrust chamber throat plane):

   From 1.52 to 3.43 cm (0.6 to 1.35 in.)

3. Overall thruster mixture ratio:

   From 2.4 to 5.7

4. Addition of a boundary layer trip ring to increase mixing of secondary hydrogen flow with the core flow

5. Addition of a mixing ring to inject the secondary hydrogen flow radially into the core flow stream

6. Substitution of a 445 N (100 lb) BLH load cell for the initially used 22240 N (5000 lb) Bytrex load cell

TABLE 8. HYDROGEN FLOW DISTRIBUTIONS INVESTIGATED

RUN NO.	MIXTURE RATIOS			ORIFICE DIA. - mm				*BLC Injection Distance cm
	PRIMARY	SECONDARY	OVERALL	LOX	PRIM. LH_2	SEC. LH_2	BLC LH_2	
1-39	50	12	4	1.00	0.356	0.559	0.838	1.52
39-42	50	7.5	4	1.00	0.356	0.711	0.742	2.16
43	50	7.5	4	1.00	0.356	0.711	0.742•	2.79
44-48	30	7.5	4	1.00	0.406	0.660	0.762	2.79
49-54	30	7.5	4	1.00	0.406	0.660	0.762	3.43
55-57	24	6	4	1.00	0.406	0.660	0.559	3.43
58-64	24	6	4	1.00	0.406	0.660	0.559	2.79
**65-68	24	6	4	1.00	0.406	0.660	0.559	2.79
***69-71	30	7.5	4	1.02	0.417	0.805	0.747	2.79
***72-76	30	7.5	4	1.02	0.417	0.805	0.747	2.16
***77-82	30	7.5	4	1.02	0.417	0.805	0.747	2.79
***83-86	30	7.5	4	1.02	0.417	0.805	0.747	2.16
***87-100	30	7.5	4	1.02	0.417	0.805	0.747	3.05

* Distance upstream of chamber throat that BLC coolant flow was channeled into combustion gas flow.

** Boundary layer trip ring installed

*** Radial injection ring for secondary hydrogen flow installed (8-0.940 mm dia. holes)

The final hardware configuration, which was used from Tests No. 069 through 100, is believed to represent a reasonably optimized configuration. The internal orificing resulted in a nominal mixture ratio of 30 in the core flow, 7.5 with the addition of the secondary fuel flow, and an overall 4.0 ratio. The secondary fuel flow was directed into the core flow stream through eight 0.940 mm (0.037 in.) short tube orifices to promote mixing. A boundary layer fuel injection distance 3.05 cm (1.20 in.) upstream of the throat plan appeared to be optimum.

Figure 88 shows the baseline thruster configuration. In this configuration, both the secondary fuel flow and the boundary layer fuel flow were injected coaxially, and turbulent mixing to arrive at a uniform mixture ratio was assumed to occur. Since the thruster performance could be seriously affected if the length of the available flow path did not result in good mixing of the secondary fuel flow with the core flow, two modifications were tried. The first revision tested was the addition of a boundary layer trip ring immediately downstream of the entry point of the secondary hydrogen. This configuration is shown in Fig. 89 , and details of the trip ring are shown in Fig. 90. Test results did not indicate that this change in the thruster internal geometry had the effect of significantly increasing the performance level; however, the spontaneously induced high level chamber pressure and thrust oscillations encountered with the "trip" ring configuration may have masked any real performance changes. In general, these oscillations did not exhibit a fixed frequency; however, portions of the data appeared to show a characteristic frequency of approximately 30 Hz. The thrust and chamber pressure oscillations were in the range of +15% to -25% of nominal. Because the computed flow variation showed that the oxidizer flow varied by $\pm$5%, while the fuel flow varied from +1% to -23%, it was speculated that the secondary hydrogen flow was responsible for the oscillation phenomena. It is possible that the flow of the secondary combustor hydrogen over the trip ring may have constituted a pseudo-secondary throat that varied in size as the thickness of the hydrogen film over the trip ring fluctuated with hydrogen flowrate.

The final modification tried was retained for the remainder of the program. This consisted of the addition of a machined ring that closed off the end of the sleeve conducting the secondary hydrogen (Fig. 91). This flow was injected through eight short tube orifices inclined 15 degrees from the radial direction in the downstream direction. Details of this mixing ring are shown in Fig. 92. The rationale for the addition of this feature was to attain a significant degree of radial penetration of the core flow stream as shown in Fig. 93. Such penetration would be expected to result in a more rapid and more thorough mixing than could be expected with a coaxial injection.

Heat Transfer Data. A majority of the tests performed during this program were of a relatively short duration to allow a multiplicity of tests before retanking was necessary. Run durations on the order of 30 seconds were periodically conducted to obtain reasonably well-stabilized temperature data. Figure 94 shows a typical plot of the external surface temperatures measured at the throat plan location, for the thick-walled L-605 thrust (run No. 083).

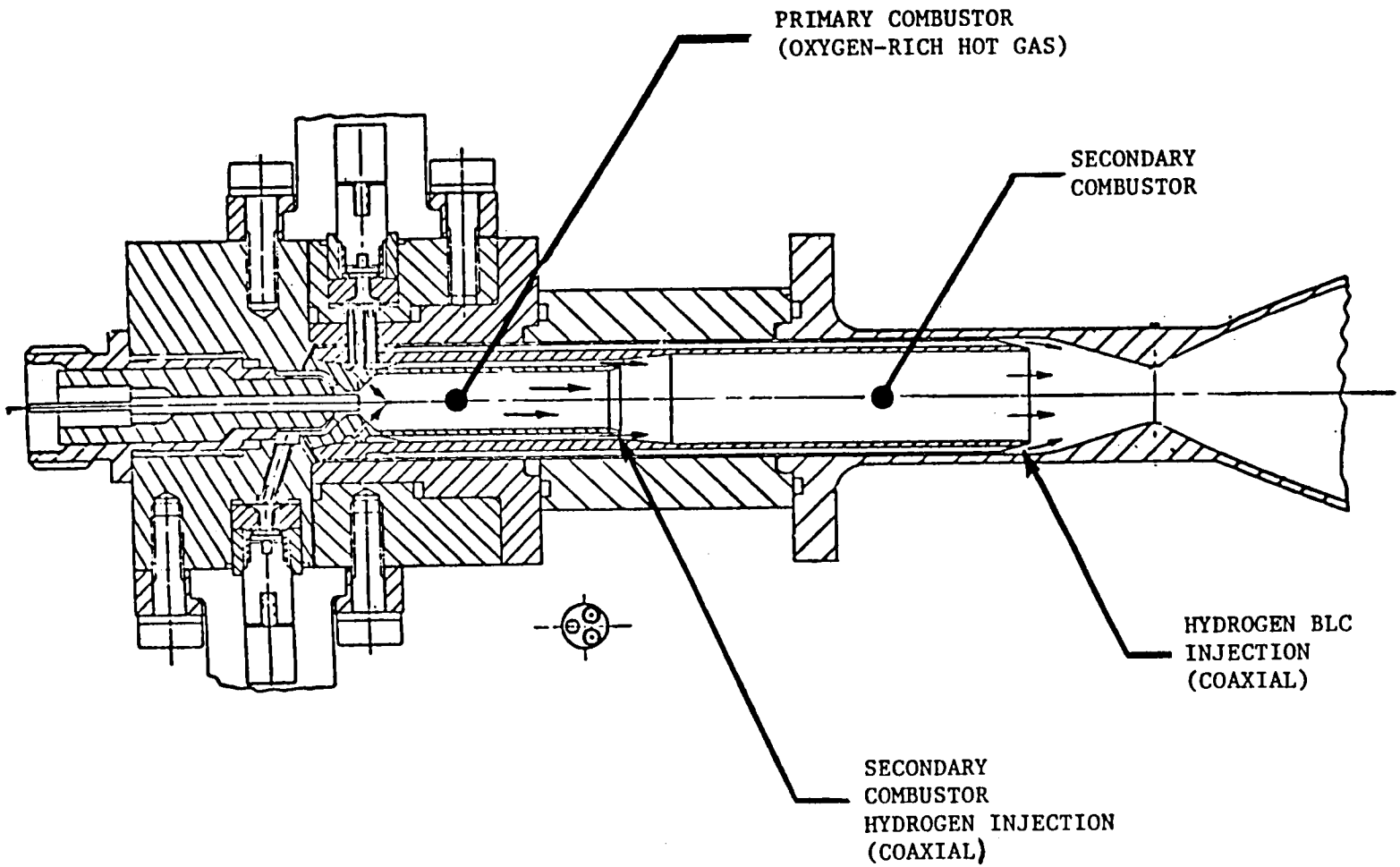

Figure 88. Baseline Thruster Configuration

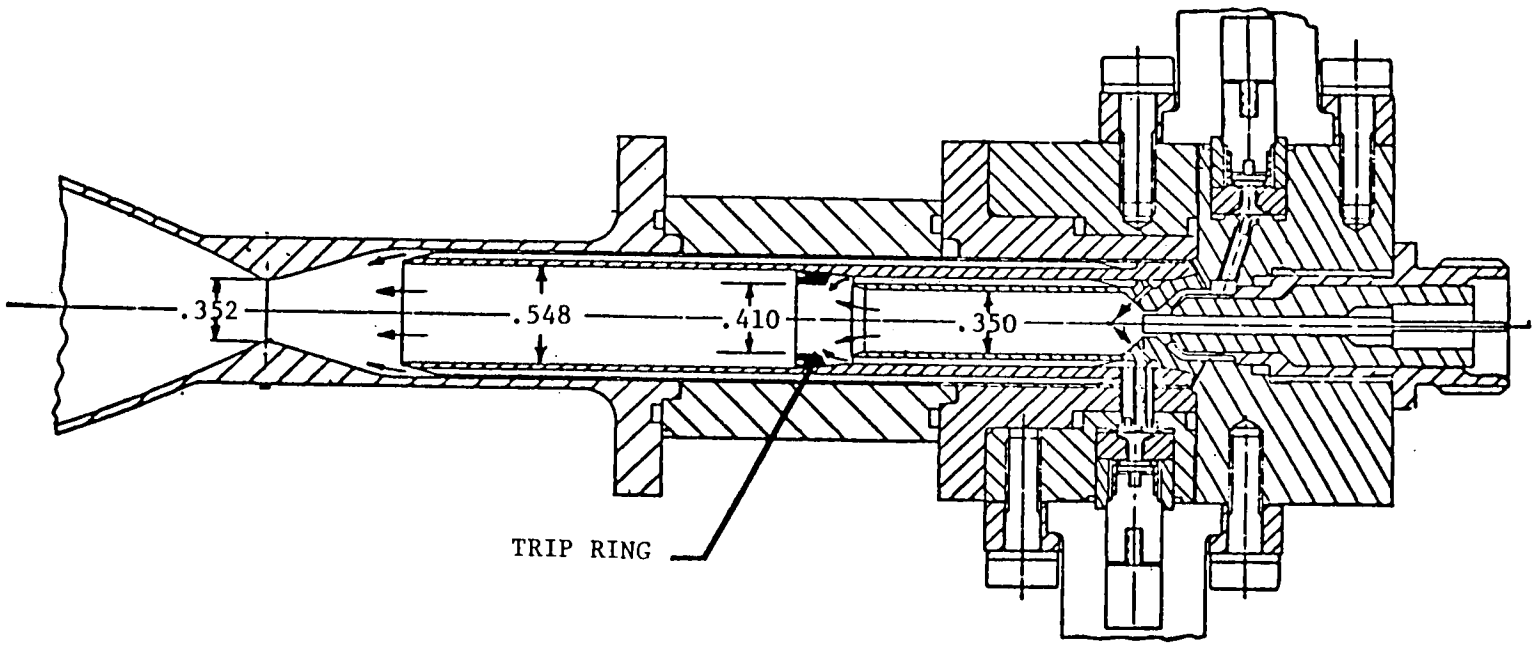

Figure 89. Thruster Configuration With Turbulence "Trip Ring"

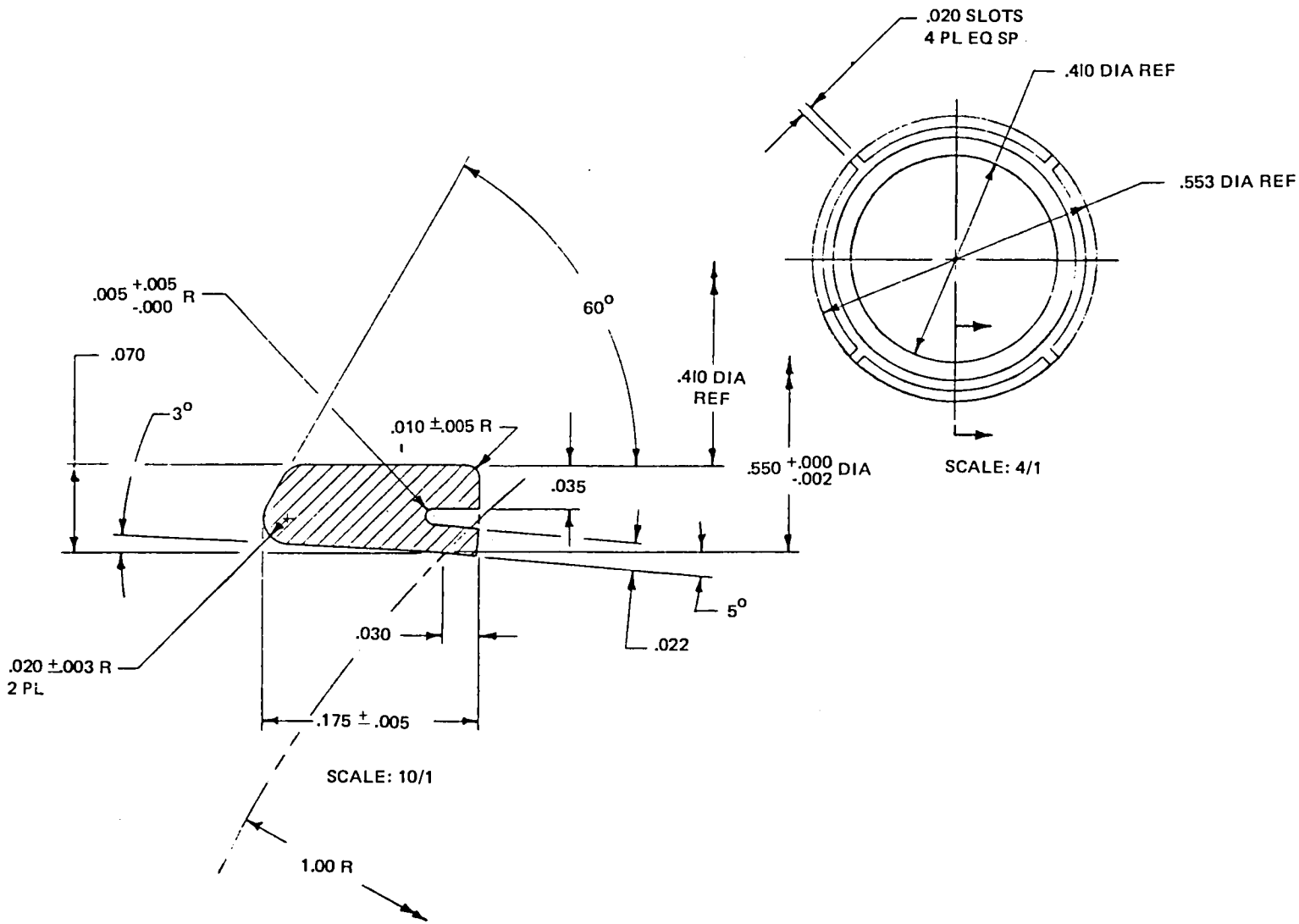

Figure 90. Details of Turbulence "Trip Ring" Configuration

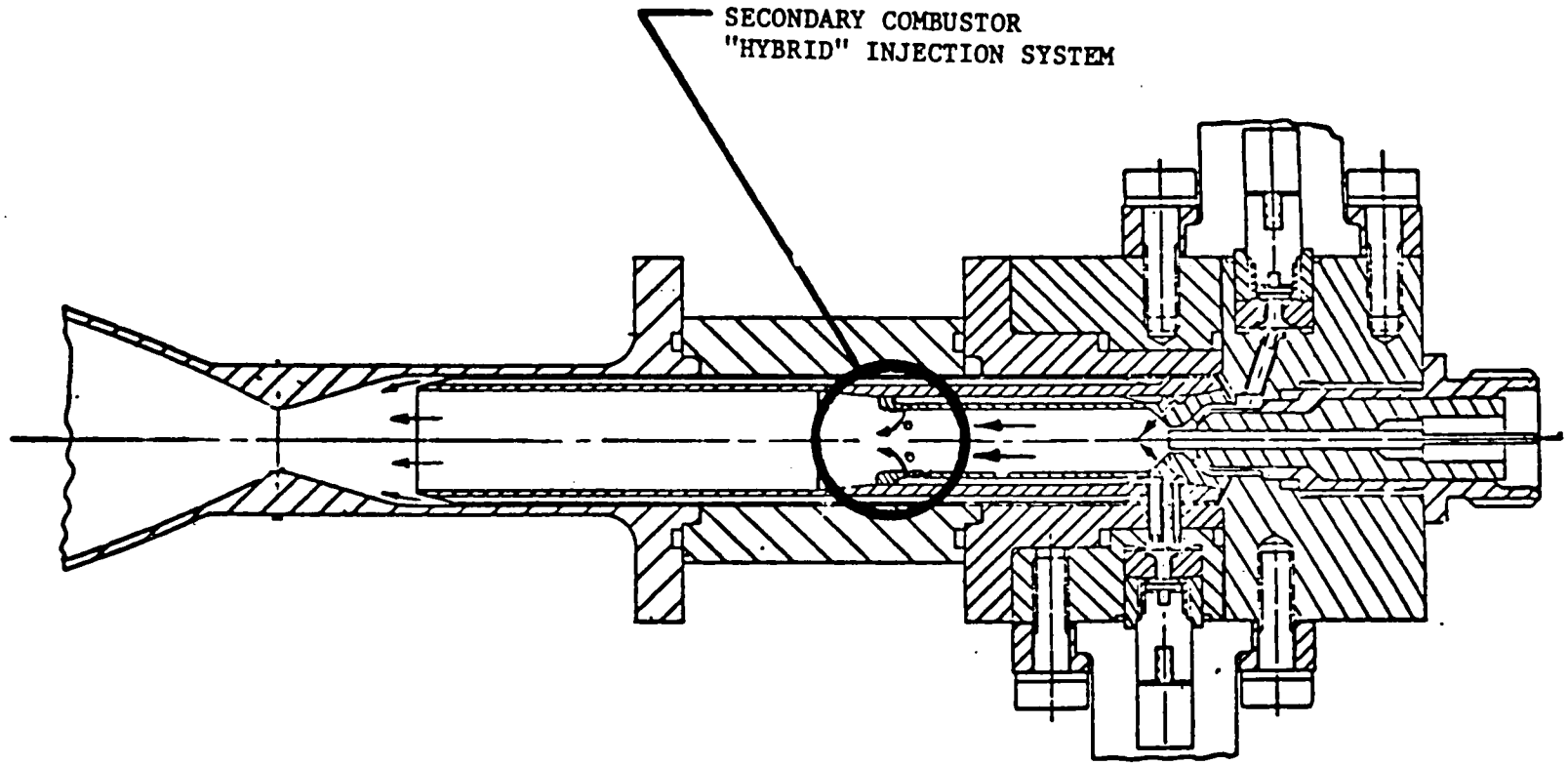

Figure 91. Thruster Configuration With "Hybrid" Injection System

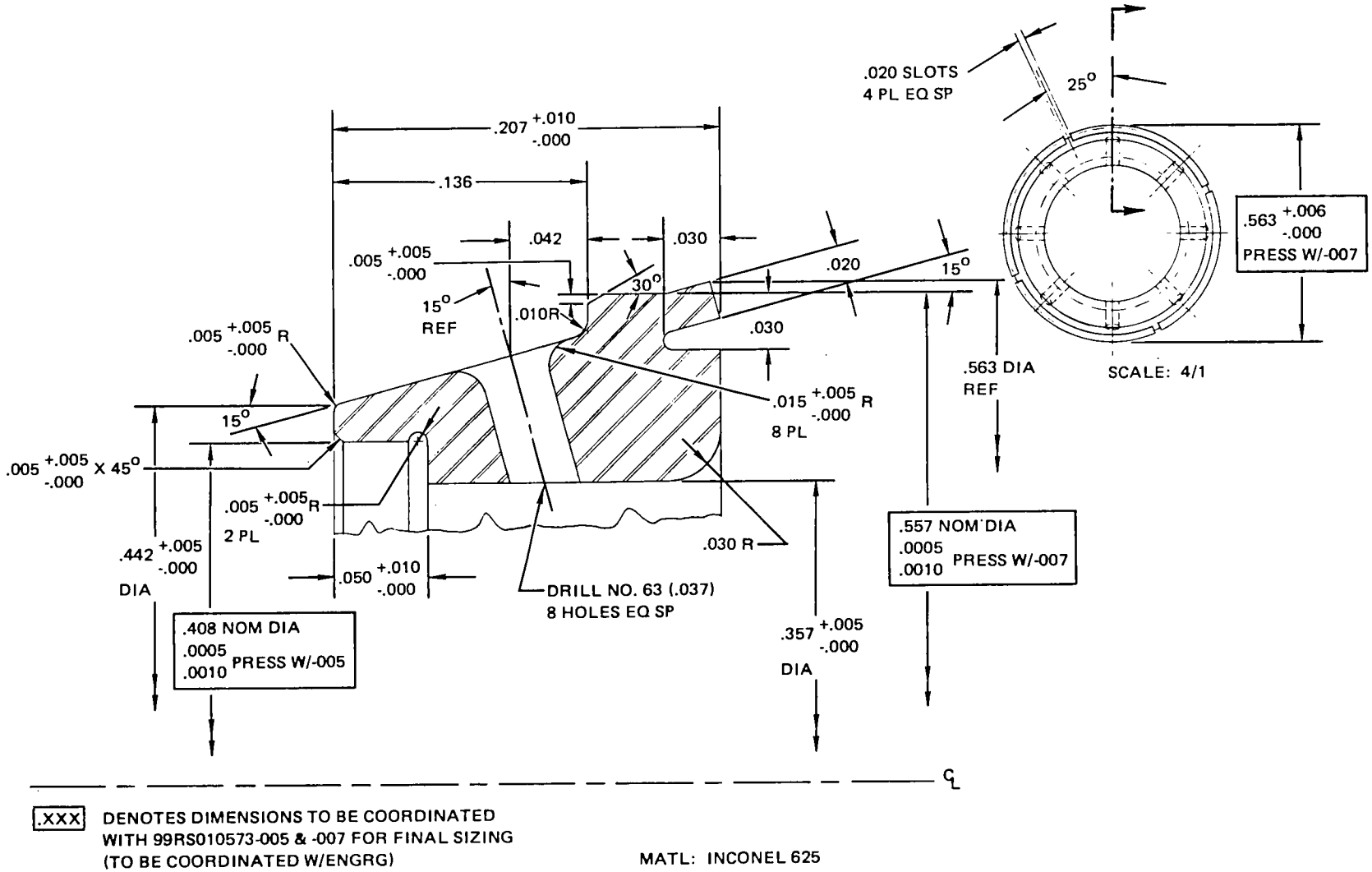

Figure 92. Secondary Combustor Hydrogen Injection Ring Design

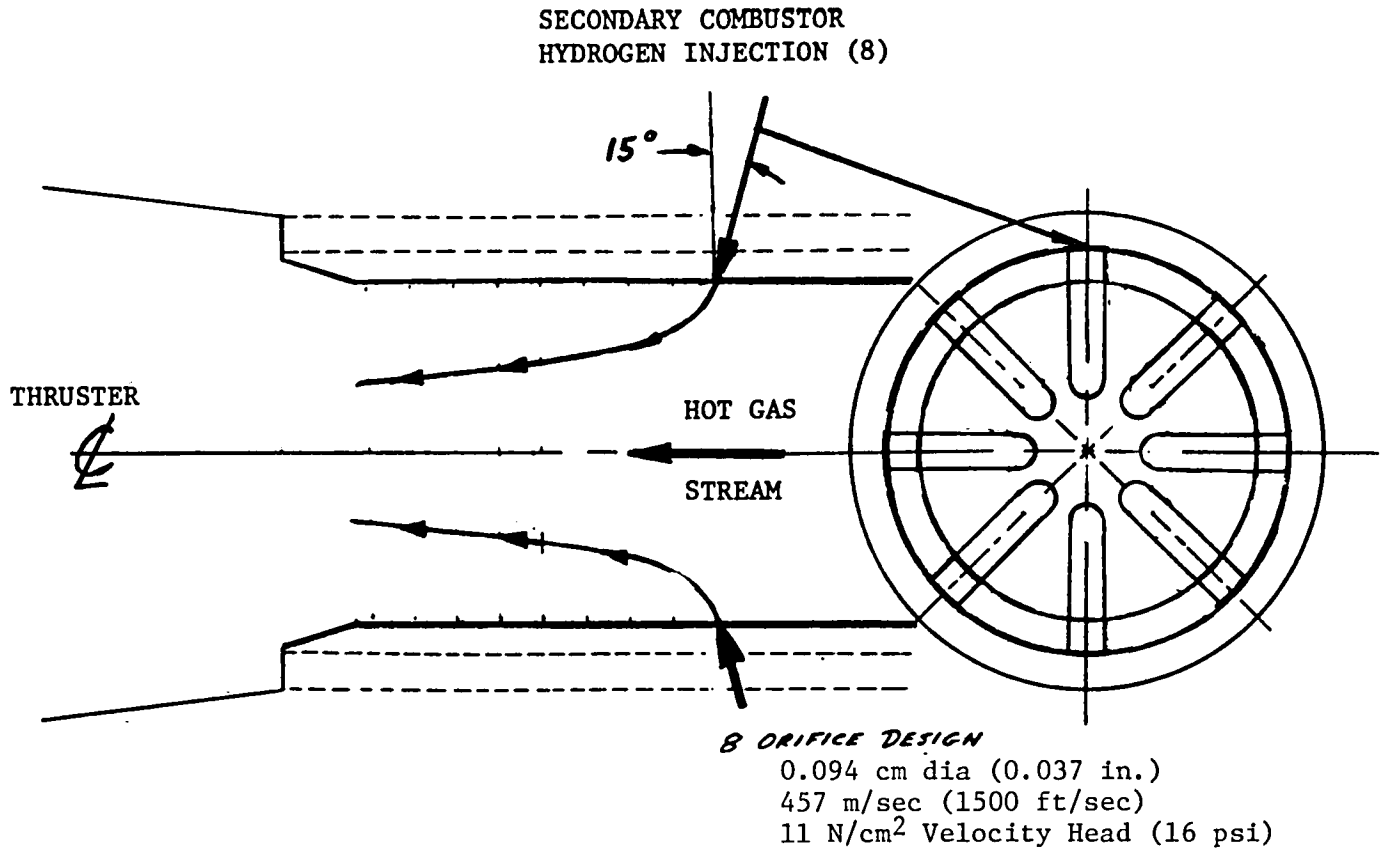

Figure 93. Secondary Combustor Hydrogen/Primary Hot-Gas Predicted Penetration

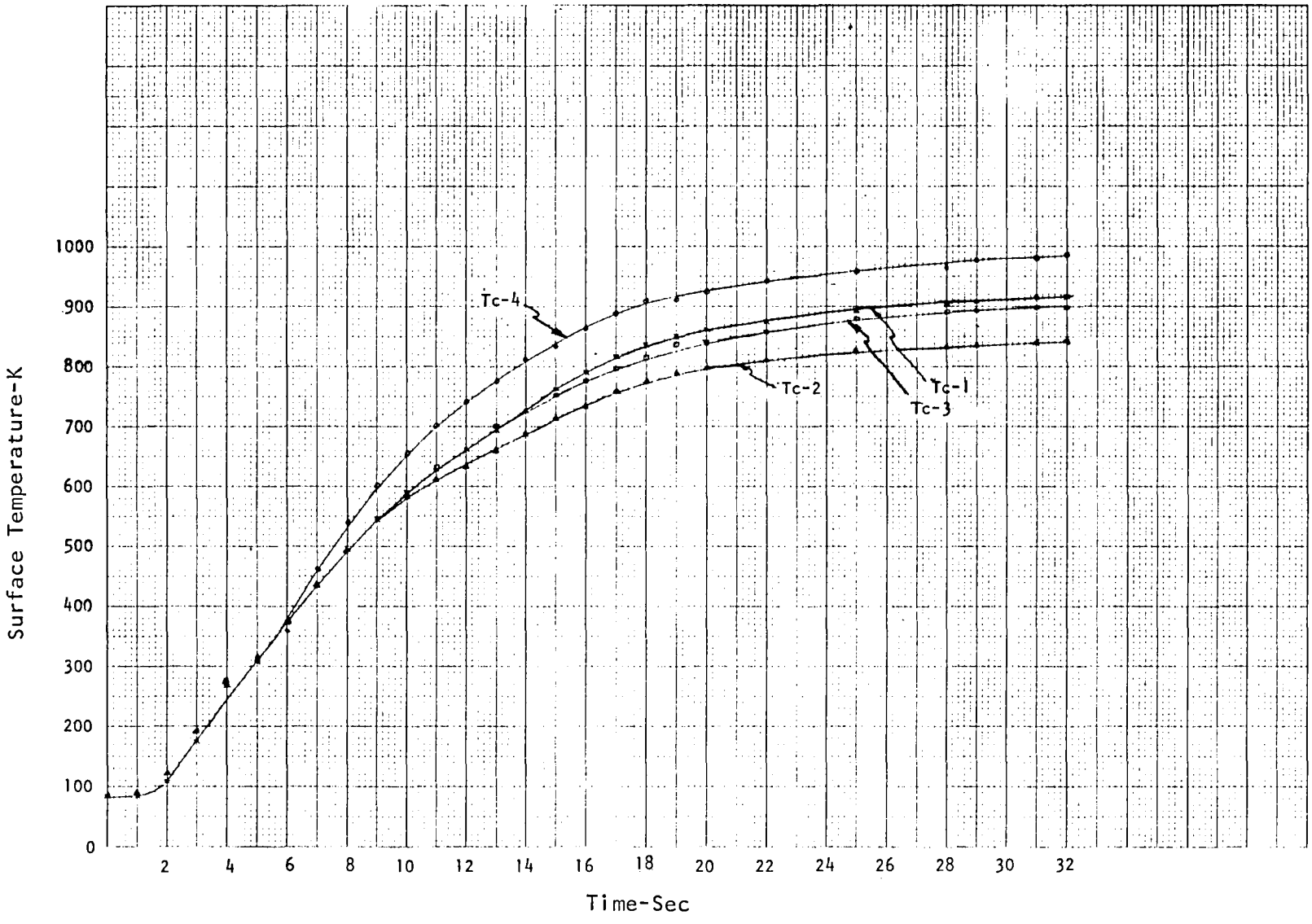

Figure 94. External Surface Temperatures at Throat Plane for L-605 Thruster During Run No. 083

It should be noted that the performance of the thruster during this run (I_s) was 380 seconds. This was a near approach to the actual 390-to-400-second performance level that was believed to actually exist. Under these conditions, the visible heat pattern and the temperature measurements indicate less severe heat transfer conditions than were encountered during some other runs.

The extreme example was run No. 071, which resulted in a considerable degree of melting and erosion of the throat of the thick-wall L-605 chamber. Figure 95 shows the external surface discoloration pattern which is noteworthy in that it indicates high temperatures extending back to the point where the boundary layer hydrogen was released into the stream. Data from runs 084 and 085 show average temperatures of approximately 535 and 558 K (504 and 544 F) at this location. This would be expected since the cool hydrogen gas exiting along the wall at that point would be expected to keep the wall locally cool. Figure 96 shows the damage to the throat region of the thrust chamber resulting from the high temperature operation.

Posttest, it was found that the LH_2 system bypass valve had a serious seat leakage. This would have resulted in an increase in the overall design mixture ratio of 4.0 (with a concomittant increase in combustion gas temperature) and an accompanying decrease in the amount of boundary layer film coolant. This test and others that exhibited abnormal heat zone patterns and abnormally high external surface throat temperatures tend to indicate that apparent losses in indicated performance probably were due to the thruster being credited with the measured hydrogen flowrate, while actually some portion of it was diverted or lost.

Pulse Mode Tests

A number of tests were conducted during this program to characterize pulse mode performance. These consisted of run No. 038 and runs 093 through 100.

Test 038 programmed eight pulses with an 0.050 second ON time and 1.00 second OFF time. Six of the eight pulses ignited. Pulse repeatability appeared to be poor; however, since the propellant supply systems did not realistically reproduce the actual flight system, these results are of minimal interest.

The later series of tests removed the flow instrumentation, extended the jacketed lines much closer to the engine, and maintained a continuous bleed from a point within 5 to 8 cm (2 to 3 in.) of the thruster. The bleed flow was limited by 0.152 cm (0.060 in.) diameter orifices at the bleed line exits.

As shown in Table 7 , some tests did not show ignition for every pulse. The final two firings (runs 099 and 100) simulated a duty cycle consisting of six pulses, a steady 30-second burn, a 1-minute heat soakback period, and then a final series of six pulses. To overcome some of the problems that had arisen, control of these tests was partially automatically sequenced and partially manually sequenced. A 0.075-second ON time was programmed with the OFF time extended to approximately 2 seconds (run 099) and 3 seconds (run 100) to accommodate the manual operations. For these tests, a capacitive discharge exciter

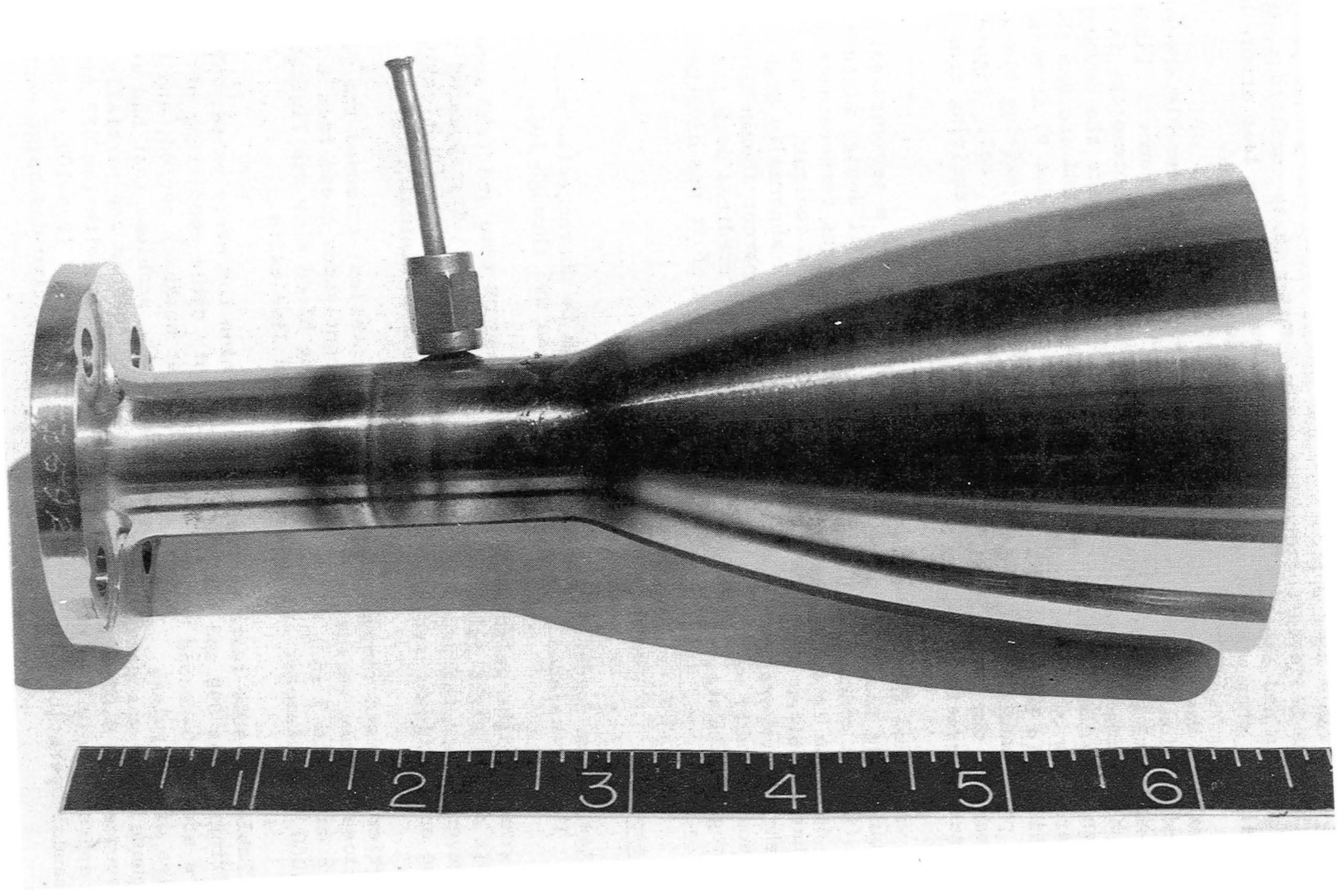

Figure 95. External Surface Heat Discoloration Pattern Shown Posttest 071

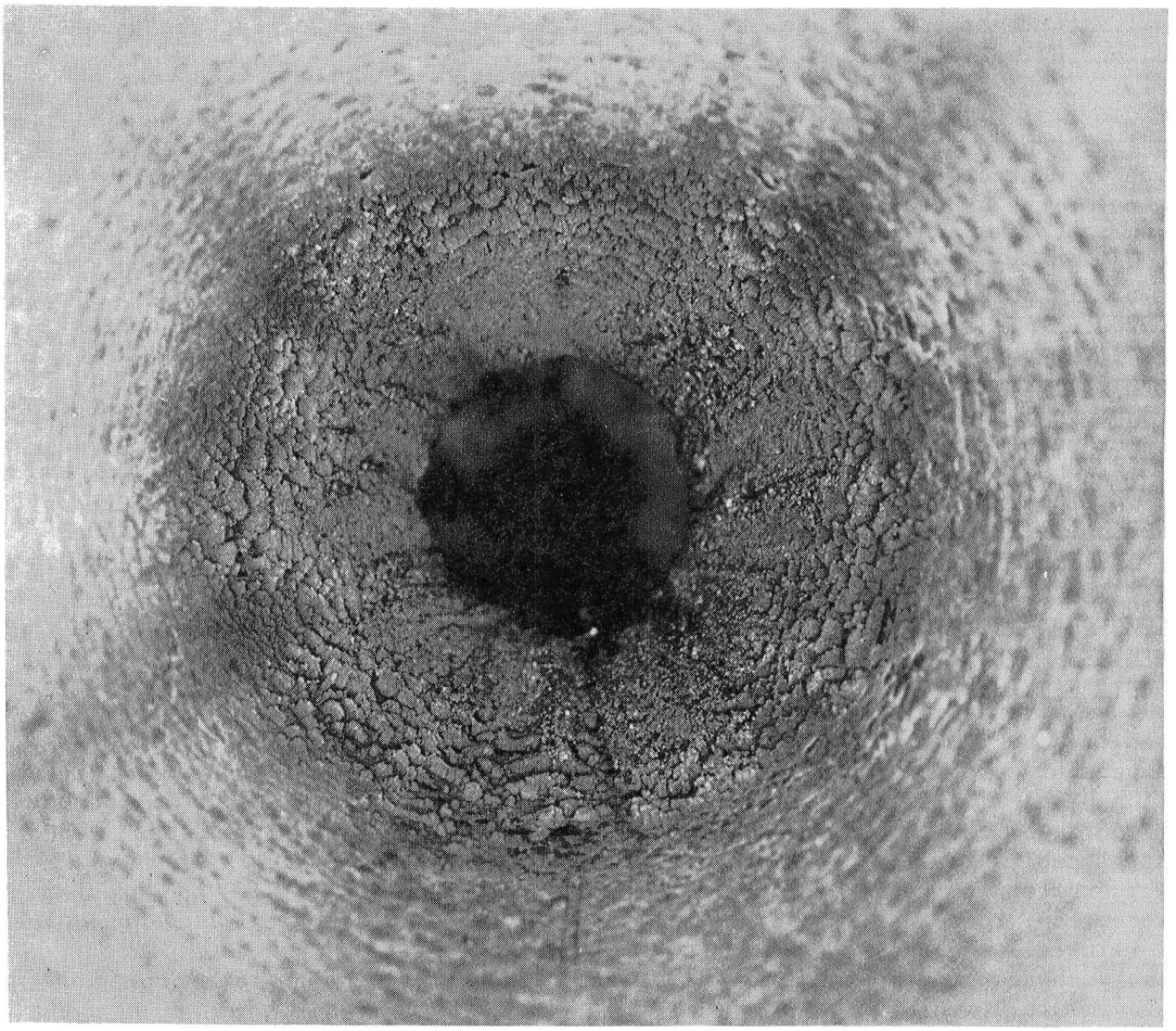

Figure 96. Thrust Chamber Throat Erosion Viewed From Exit End of Nozzle (Posttest 071)

unit was used, operating at a 100 mJ power level and a frequency of 200 Hz. The igniter energy was programmed to start about 10 msec before actuation of the lagging valve opening (LOX valve).

The conversion from an inductive discharge to a capacitive discharge exciter was implemented at this time to evaluate whether a more intense spark discharge, which is characteristic of a capacitive unit, would provide more reliable ionization of the subcooled liquid oxygen.

Run No. 099 ignited three of the initial set of six pulses and two of the final set of six pulses. The initial lead of the spark was advanced slightly for run No. 100. This test ignited all six of the initial pulses, but failed to ignite two of the post-heat soakback set of six pulses. Therefore, evidence of increased difficulty of ignition during pulse mode operation under the supercold propellant delivery conditions created with the use of the revised propellant supply systems continued, as discussed later.

The major operational problems that plagued this series of tests was a serious ignition noise problem that affected the operation of the main fuel valve and the oscillator circuit in the sequencer that normally would have initiated each pulse cycle. The effect of this noise on the fuel valve was that it was subject to unprogrammed openings. This precluded operation with either a continuous spark or with a spark activated well in advance (100 msec) of the start of the pulse. Previous experience indicated that either of these two modes of operation was more desirable than the one actually used by necessity. The ignition noise feedback into the timer oscillator led to erratic changes in timing between pulses. It should be noted that the ignition noise-fuel valve interaction problem would not be expected to exist in an actual flight installation. The source of the problem was pickup of ignition system noise by the unshielded control cables for the propellant valves. This problem did not exist with the lower exciter energy levels used during most of the program. When the problem did develop, there was insufficient time available to procure shielded cables and reinstall the long wiring runs. Various other "fixes" were tried, but usually showed some apparent promise, which later proved to be rather marginal improvements.

The pulse data analyses for Runs No. 099 and 100 are shown in Table 9. The peak pulse pressure and the impulse bit determination were made from the oscillograph recordings of the chamber pressure. The oscillograph was operated at a paper speed of approximately 50.8 cm/sec. The chamber pressure pulses were integrated with a planimeter and the results converted to the scale values shown. No initial chamber pressure records were obtained during run 100 because water from the products of combustion froze and shut off the pressure tap. The ice plug melted out during the course of the following 30-second burn, so that the chamber pressure recordings do exist for the last series of six pulses.

The pulse performance characteristics are discussed in greater detail in a following section of this report.

TABLE 9. PULSE MODE PERFORMANCE CHARACTERISTICS

Run No.	Pulse Series	Pulse No.	Peak Pressure		Impulse		Comments
			$N/m^2 \times 10^{-5}$	Psia	N/m^2-sec	Psia-sec	
099	Initial	1	6.52	94.5	46,990	6.815	Data corrected for post-run spontaneous activations of LH_2 valve.
		2	7.09	102.8	44,620	6.472	
		5	6.83	99.0	46,990	6.815	
	Final	1	11.38	165.0	48,820	7.081	
		2	10.03	145.5	55,390	8.033	
100	Final	1	10.86	157.5	41,730	6.053	Chamber pressure traces had "spiky" characteristic. Data corrected for post-run spontaneous activations of LH_2 valve.
		2	11.69	169.5	45,670	6.624	
		5	9.00	130.5	52,940	6.776	
		6	9.98	144.8	49,080	7.119	

Steady-state chamber pressure noted at end of 10 seconds of operation:

Run 099 - 10.76 $N/m^2 \times 10^5$ (156.1 Psia)

Run 100 - 10.69 $N/m^2 \times 10^5$ (155.0 Psia)

DISCUSSION OF RESULTS

Ignition

The results of the initial block of tests performed during this program showed that reliable ignition could be obtained at a 10 mJ spark energy level. An inductive discharge energy source operating at 100 Hz output frequency was normally used.

The ignition experience during the remainder of the program, indicated, in general, that a wide range of hardware and propellant temperatures could be successfully accommodated. Periodic ignition failures were encountered, but were normally attributable to deterioration of the ignition cable or its pressurization system. Repair of the faulty cable area invariably resulted in the disappearance of the ignition problem.

A final ignition problem area was encountered during pulse mode operation of the thruster. This resulted in the failure to ignite some of the pulses of the pulse trains. The ignition failures did not follow any discernible pattern or trend and were therefore typical of marginal ignition conditions. The available data are not sufficient to definitely prove existence of an ignition problem area or to indicate its cause. The changes in operating conditions or circumstances that could have a bearing on the pulse ignition failures are:

1. The propellants were delivered to the thruster at a lower temperature than during the preceding program phases. This resulted because the propellant supply systems were modified to remove the flow instrumentation sections, extend the cryogenic jacketing much closer to the thruster, and provide for a continuous propellant bypass flow from a point within 6 to 10 cm of the thruster. The propellant temperatures, as measured by the temperature bulbs located well upstream in the system, did not indicate temperatures much lower than previously encountered during various tests. However, it is felt that the supply system revision resulted in significantly lower temperature of the propellants as delivered to the ignition region of the thruster.
2. During pulse tests, the spark was initiated only about 10 msec before the start of propellant flows. Normally, an approximate 100 msec spark lead had been employed. However, since severe ignition system noise feedback was affecting the main fuel valve (resulting in unscheduled openings), such an ignition time lead was not possible. Efforts to eliminate the high-frequency noise disturbances were made but, within the available time constraints, were not effective.
3. The ignition cable used during the pulse mode tests had less insulation than the one used in the majority of the earlier tests. There is a possibility that the energy delivered to the igniter might have been below the 10 mJ level, even though the exciter was operated at a 100 mJ output level.

Ignition Transients. At various times during the course of the program, the chamber pressure rise time was characterized. For these tests, an attempt was made to fill in all extra thruster volumes, such an injection pressure and

injection temperature parts, to minimize propellant fill times. The chamber pressure rise time was computed from the oscillograph records, and was defined as the time from the opening of the lagging propellant valve to the time for attainment of 90% of the full chamber pressure value.

As may be seen in Table 7, attainment of 90% steady-state chamber pressure ranged in time from 0.048 second to some value in excess of 0.5 second. The long time constants were usually related to unconditioned (warm) hardware, where the characterizing temperature (TH-2) was in excess of 200 K. Long rise times characteristically showed gentle chamber pressure ramps, indicating a gradual increase in the propellant mass flowrates. These flowrate changes would result from the higher quality propellants arriving at the injection orifices because of the progressive chilling of the flow passages.

The effect of the other variables investigated for their influence on ignition transients was found to be relatively minor. Propellant leads were investigated over a range of 0 to 10 msec. An oxidizer valve lead of 10 msec was noted to result in a somewhat smaller ignition lag time than either a simultaneous valve opening or fuel valve lead sequence.

Within the 10 to 100 mJ spark energy level investigated, no apparent effect on the ignition transients was noted. Problems were encountered at times with ignition failures attributable to spark plug cable deterioration but, for these cases, the level of the delivered energy to the spark plug was unknown. For example, runs No. 035, 042, and 043 did not ignite until the run had progressed for times ranging from 0.7 to 1.1 seconds. Such occurrences, or the failure to obtain ignition, were usually traced to an ignition cable problem which, when corrected, resulted in a disappearance of the ignition difficulty.

The analytical engine start model designed for this thruster predicted time intervals of 28 or 38 msec, depending on whether an oxidizer lead or fuel lead was used, from the time that the leading valve started to open until the 90% chamber pressure level was attained. A plot of the analytical model results for a 10 msec oxidizer lead is shown in Fig. 97. The start transient chamber pressure histories noted in actual tests took somewhat longer times. A typical start transient with the thruster in its final configuration, and with the propellant supply systems modified to closely approximate the flight system propellant supply conditions, is shown in Fig. 98. The propellant supply system modifications were made to guarantee that the propellants would exit as high-quality liquids to within 5 cm (2 in.) of the thruster at the time thruster flows were initiated. The chamber pressure reached the approximate 90% level in 48 msec.

It is probable that the model did not adequately model heat transfer phenomena, which is the most likely cause of the increased delay times under actual hot-fire conditions. Additionally, since the pressure measurement was made with a Taber transducer, its response rate could effect a P_c rise time longer than the actual time. The response lag would result because the transducer cavity has an appreciable volume of approximately 1.64 cc (0.10 $in.^3$) which has to be filled through a length of 0.31 cm (0.12 in.) tubing. The response delay associated with the flow dynamics depends on the particular gas species involved, but may be on the order of 10 to 15 msec.

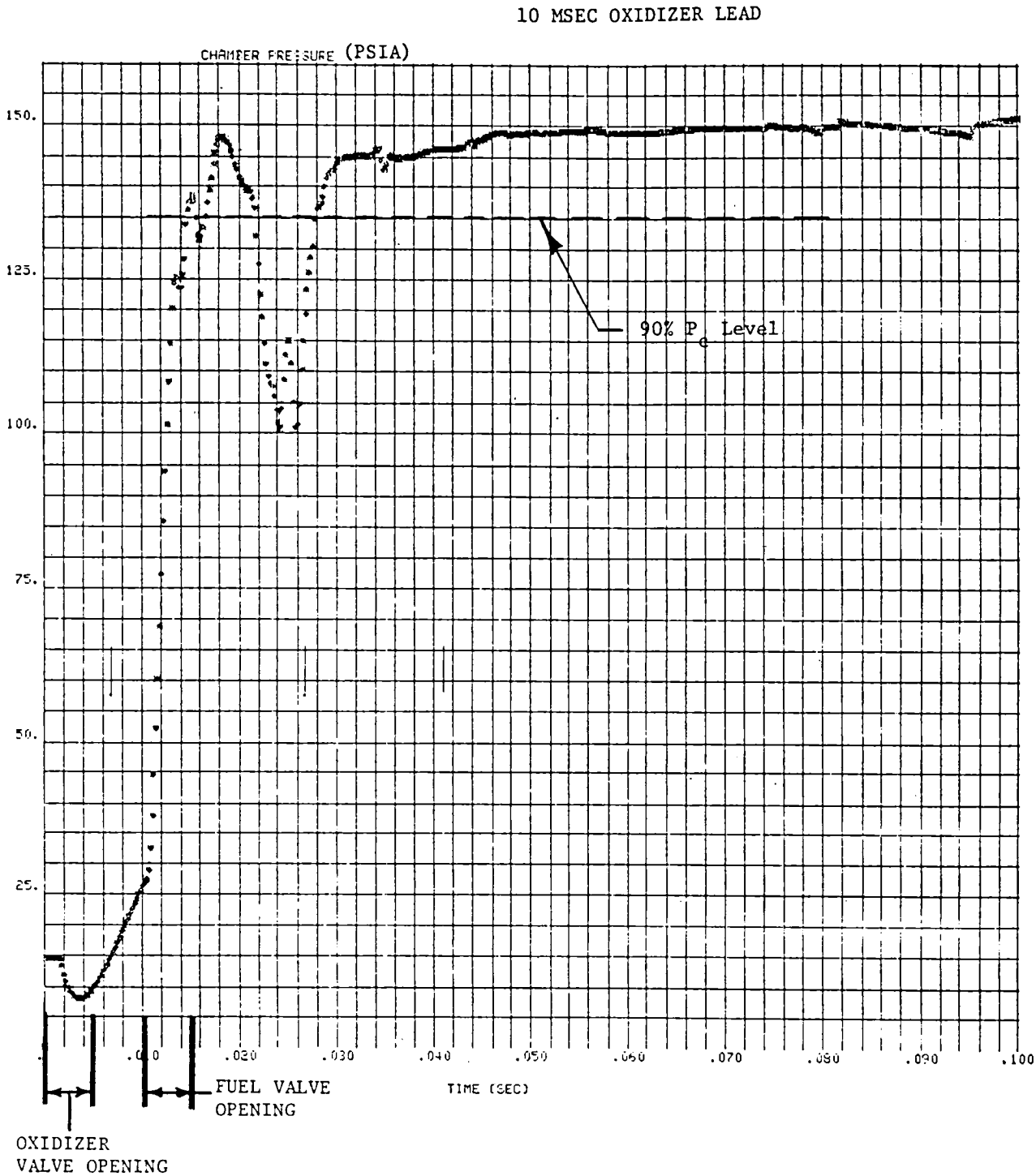

Figure 97. Predicted Chamber Pressure Behavior With Time

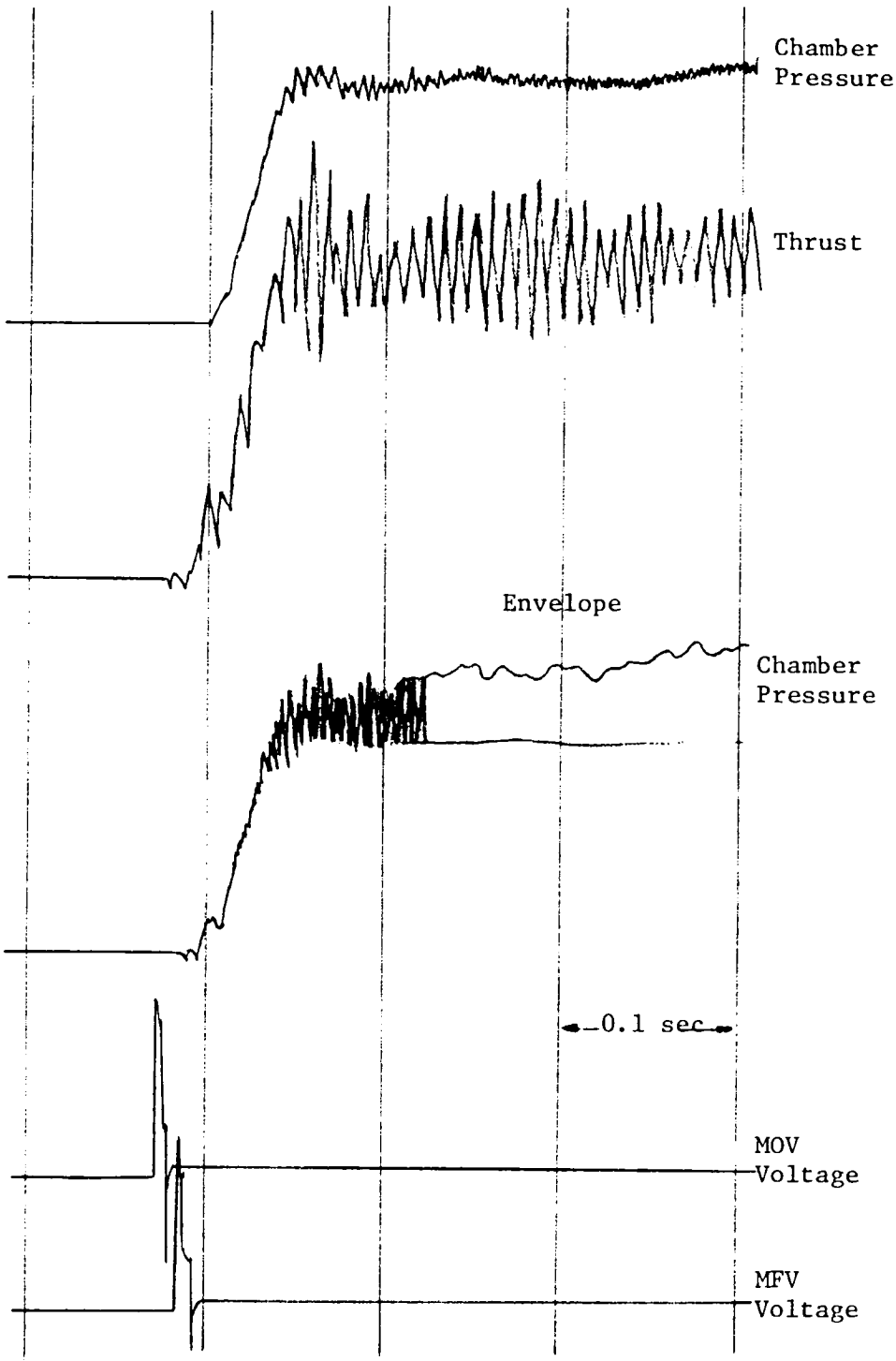

Figure 98. Thruster Start Transients for Run No. 93 (Oscillograph Tracings)

It may be noted that the thrust trace and one of the chamber pressure traces show extensive fluctuations. These are not interpreted as being indications of rough combustion. The thrust cell oscillations (approximately 120 H_z) represent load cell "ringing," which appeared to be easily excited by small disturbances. The oscillations of the chamber pressure record appearing in the middle of Fig. 98 are typical of results obtained with the chamber pressure tap penetrating the chamber wall slightly downstream of the BLC hydrogen exit plane. The high-velocity hydrogen gas blowing across the entrance to the pressure measurement port evidently produced closed-end tube resonance, as in an organ pipe.

Thruster Steady-State Performance. The thruster configuration employed from Runs No. 069 through 100 appeared to be reasonably optimum from a combustion performance standpoint. This resulted in a core mixture ratio of 30, a 7.5 mixture ratio after addition of the secondary hydrogen flow, and an overall mixture ratio of 4 after addition of the boundary layer coolant hydrogen flow. During these tests, the boundary layer coolant flow exit plane varied from 2.16 to 3.05 cm upstream of the throat of the thrust chamber. All of these runs used the "hybrid" thruster configuration (Fig. 91). The secondary hydrogen flow was injected into the core flow by means of eight 0.940-mm diameter, radially directed orifices to secure good mixing.

The computed average specific impulse efficiency for runs with this configuration are shown in Fig. 99, and compared to the results for other thruster configurations. The data used to construct this figure exclude runs where test stand problems were known to exist; these problems are discussed below.

Figure 99 shows that with a boundary layer coolant recess distance of 2.79 cm (1.10 in.), a performance level approximately 1% above the minimum program requirement was demonstrated. The data obtained when the recess distance was decreased to 2.16 cm (0.85 in.) show a performance level approximately 3% below the minimum target level. This trend is in accordance with the results obtained for tests conducted with the baseline thruster configuration (Fig. 88). Because of the nature of the test stand operational problems experienced throughout the program, it is probable that these results are somewhat conservative.

The desirability to operate with a boundary layer coolant recess depth of approximately 2.79 cm (1.10 in.) is indicated to allow reasonable mixing of the boundary layer flow with the total hot-gas stream.

The test stand operational problems alluded to above consisted of: (1) the difficulty in accurately measuring the small propellant flowrates, and (2) the inability to guarantee that the measured flowrates were actually delivered to the thruster.

The most likely appreciable measurement error would be in the liquid hydrogen flowrate. Since this was a 0.635 cm (0.25 in.) system, the propellant temperature had to be monitored approximately 1.5 meters upstream of the venturi meter. The size of the temperature bulb necessitated its location in the larger size upstream plumbing. The sensitivity of the liquid hydrogen density to small temperature changes could result in computations of higher than actual flowrates.

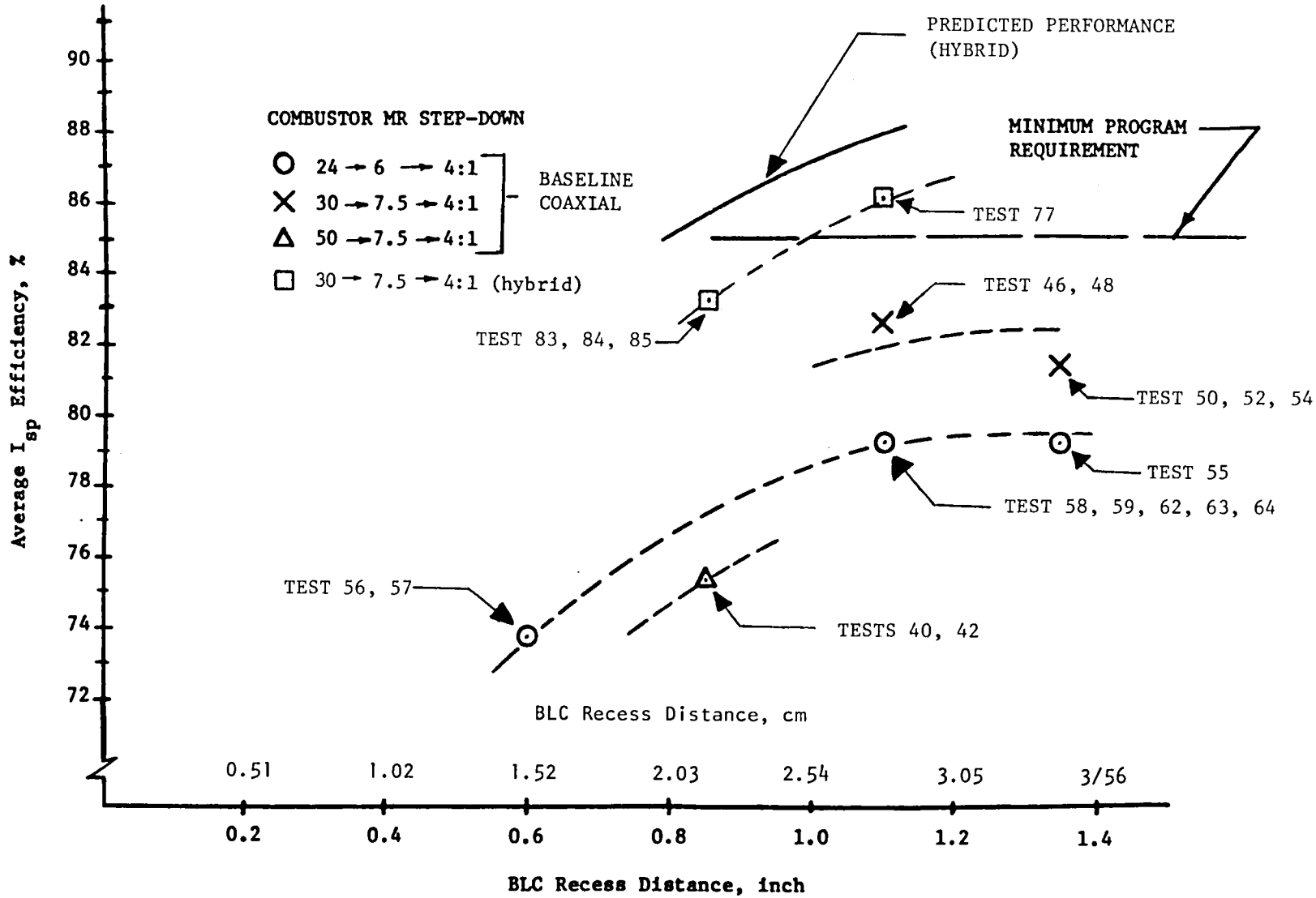

Figure 99. Thruster Specific Impulse Behavior

The second problem was probably more significant and direct evidences of it were noted on several occasions. The propellant bypass systems (Fig. 76) were used to maintain propellant flows through as much of the propellant supply systems as possible until immediately before the firing initiation. This was necessary to ensure the desired propellant temperature conditioning. These bypass systems were automatically shut off just prior to the start of the firing. However, since any flows through these systems were part of the venturi monitored flows, any valve leakages (or other line leaks downstream of the venturi meters) would constitute a flow measurement error insofar as the thruster was concerned.

In the case of the LH_2 system, the bypass valve was a Vacco cryogenic solenoid valve located within the capsule. Potentially, it had both stem and seat leakages possible when it was in the closed condition. In one instance, run 071, extensive throat erosion of the L-605 chamber was noted after a 5-second duration run. The chamber showed the high heat zone extended to the boundary layer coolant injection station, which normally does not exceed temperatures of about 600 K (620 F). Postrun investigations revealed that the hydrogen system bypass valve had developed a sizeable seat leak that did not exist at ambient temperatures, but became readily apparent at liquid nitrogen temperatures. Because of the nature of the valve, stem leakages were difficult to detect, and no direct study was possible with the LH_2 flows because of safety considerations.

Secondary evidence of the probable existence of some LH_2 system leakages downstream of the venturi meter were:

1. A large amount of data scatter, for example, and average I_s* of 379 seconds (for runs 083, 084, and 085), with no appreciable data scatter, followed by the run No. 086 I_s* of 324 seconds. This was a 14% performance decrease.

2. Increases in outer wall temperature measurements and heatup into the cooled boundary layer exit area for the same nominal operating conditions that did not show this phenomenon. A decrease in the actual hydrogen flowrate would reduce the amount of the boundary layer coolant flow, while at the same time resulting in an increase in the mixture ratio. Since the nominal operation mixture ratio was 4.0, a considerable increase in the chamber combustion gas temperatures was possible.

3. Finally, it may be noted that the available procedures for making run-to-run checks for system propellant leakages could not detect the relatively small magnitude leaks that could produce the noted effects on the thruster performance computations. Since venturi meter calculations involve a square root relationship, a leakage of 10% of the design flowrate would produce only 1% of the flow venturi design ΔP. Therefore, prerun monitoring of the venturi ΔPs, to subtract that flow from the measured flowrate during the firing, would require a

*Specific impulse (pound force x seconds/pound mass propellant)

a higher degree of precision in the measurements of the venturi pressures than was possible. The other test performed was to close the propellant tank valves (with all systems pressurized and all other valves closed), and to monitor the decay of the line pressures. Unfortunately, with cryogenic systems, heat leaks into the system could generate pressure rapidly enough to compensate for small leaks.

Thrust Chamber Equilibrium Temperatures. A major portion of the test firings were made using L-605 alloy thrust chambers. In addition, a molybdenum thrust chamber was evaluated in a brief test series (runs 087 through 091).

The long runs performed during this program were on the order of 33 seconds duration. At the end of this time, the throat outer wall temperatures were still changing slightly (see Fig. 94 and 100), but it was computed that stabilization had been obtained on the inner wall. Analytic estimates are that the hot-gas surface temperature, at this time, was approximately 36 K (65 R) degrees hotter than the outer skin temperature. As may be seen in Fig. 94 and 100, some nonuniformity of surface temperature distribution was normally observed. This probably resulted because of a certain amount of nonuniformity in the distribution of the boundary layer hydrogen coolant flow.

Figure 100 presents the throat temperature histories for 33.3-second duration run No. 085, which had a 2.16 cm (0.85 in.) BLC injection distance. The test was conducted at the nominal design conditions: mixture ratio of 4.0 and a thrust level of 118.9 N (26.7 lb). These temperature data agree reasonably well with the analytical predictions shown in Fig. for the noted operating conditions.

Figure 46 predicts a maximum hot-gas wall temperature of 1500 K (2240 F) if a 100% c* efficiency is assumed. If this value is reduced to correspond to a 90% c* efficiency (which is a more realistic value for the tested thruster), then an approximate 1280 K (1844 F) temperature would be predicted.

The actual maximum outside wall temperature noted for run 085 was 1156 K (1621 F). However, this temperature does not appear to be completely stabilized. The extrapolated steady-state temperature would appear to be approximately 1200 K (1700 F) and, if the analytically computed wall ΔT of 36 K (65 F) is applied, a hot-gas-side wall temperature of 1236 K (1765 F) results. This is somewhat lower than the predicted 1280 K (1844 F) value, but is reasonably close.

A comparison of outer wall throat temperature measurements, at a corresponding firing time of 32 seconds (for funs 083, 084, and 085) is tabulated below:

	Run No.		
	083	084	085
Mixture Ratio	3.4	3.9	4.0
Average Throat Temperature, K(F)	911(1179	1044(1420)	1105(1529)
Maximum Δ Between Throat Temperature, K(F)	138(248)	229(412)	97(174)
BLC Injection Distance, cm (in.)	2.16(0.85)	2.16(0.85)	2.16(0.85)

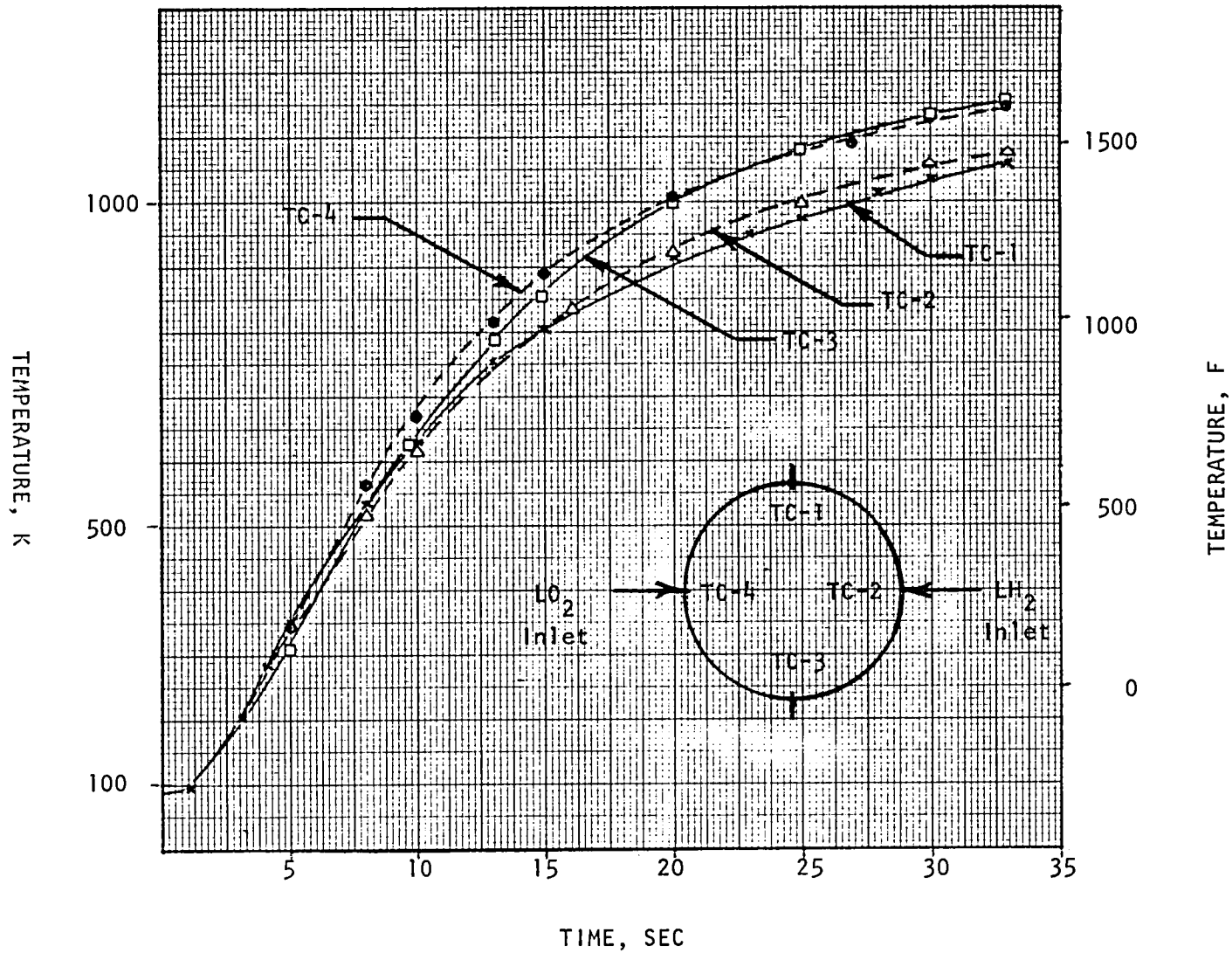

Figure 100. External Surface Temperatures at Throat Plane for L-605 Thruster During Run No. 085

These data show that increased throat temperatures are encountered with increases in the operating mixture ratio. This results from two factors: (1) the increased chamber gas temperature, since the stoichiometric mixture ratio is being approached, and (2) the mass flow of hydrogen (and, therefore, the BLC flowrate) also is being reduced. Extrapolations of these data indicate equilibrium hot-gas surface temperatures of 1756 K (2700 F) at the throat for the 5.6 mixture ratio (abort mode). This temperature exceeds the capabilities of the L-605 alloy; however, the disilicide-coated molybdenum thrust chamber would be satisfactory.

The molybdenum chamber firings were limited to nominal mixture ratio operations (4.0) since problems in making direct surface temperature measurements could not be resolved within the time available. In particular, the lack of such measurements precluded the use of automatic redline cuts used to terminate the test if excessive temperatures were to be encountered because of system malfunctions.

The molybdenum chamber firings were visually monitored by means of a black and white television camera. Color temperatures could not, of course, be perceived, but it was noted that the heatup pattern differed significantly from that of the L-605 chamber. The highly luminous areas included almost the entire chamber, instead of being limited to approximately the BLC injection plane and about the first 50% of the exhaust nozzle exit bell. This heat redistribution from the maximum heat flux region (throat) was experienced because of the approximately 250% higher thermal conductivity of molybdenum. Examination of the thrust chamber after the 33.6-second firing did not indicate any coating degradation.

Control Valves. The fast-acting solenoid valves used for both propellants were demonstrated to be satisfactory. Valve seat leakage were periodically checked by pressurizing the valve with gaseous helium at a pressure of 2.76×10^6 N/m^2 (400 psig) and collecting any flow into the chamber. Noted seat leakage ranged from zero leakage in a 3-minute period to about 5 standard cc in 1 minute.

Pulse Mode Operations. Nine pulse mode tests were made, runs 038 and 093 through 100. The most obvious characteristic of these pulse trains was an intermittent failure to attain ignition with some pulses. The apparent random nature of the igntiion failures tended to favor a marginal ignition energy level hypothesis, due to the low propellant temperatures in the ignition region and/or the inability of the ignition cable to deliver the full level of the generated spark energy. The revised propellant supply systems used for the pulse mode operations were designed to guarantee delivery of liquid propellants to within a few cm of the thruster.

Figure 101 shows the brush chart record of the thrust measurements for a series of six pulses performed with a timing of 0.065 second ON and approximately 2.0 seconds OFF. The length of the OFF period (and the variation therein) resulted because each pulse was initiated manually to overcome spark noise interference with the automatic sequencer timing circuit. Once a pulse was initiated, all spark and valve actuations were performed by the sequencer.

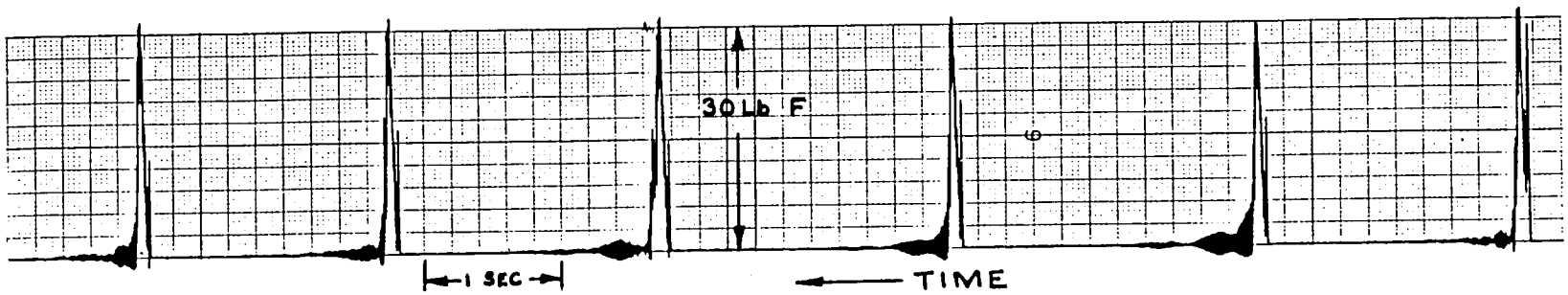

Figure 101. Brush Record of Thrust for Pulse Mode Operation of the 25-Pound Thruster With an 0.065-Second ON Time and 2.00-Second OFF Time (Run 098)

In the traces shown, the initial spike was due to the opening of the lead propellant (fuel) valve. The sensitivity of the load cell resulted in a pronounced "ringing" noticeable with even fairly minor events. It would also be noted that most of the pulses show a secondary "burst" of activity during the tailoff portion of the pulse. This was due to the unprogrammed momentary reopening of the already closed fuel valve. This was induced by high-voltage spark noise signals picked up by the valve control cable.

The corresponding oscillograph record for run 098 was subjected to a computing machine integration program to derive impulse values for each pulse. The oscillograph was operated at approximately 50 cm/sec for these tests, and a photograph enlargement was used for the data analyses.

Two different analyses were performed; (1) the entire pulse cycle was integrated, without attempting to eliminate portions of the wave train that might have resulted because of extraneous fuel valve activities, and (2) integrating only that portion of thepulse wave corresponding to the time that the oxidizer valve was open. The initial computations were of use to characterize the magnitude of the total impulse generated. The second type of calculation was more suitable for repeatability comparisons since the extra valve actuations were excluded. These calculations showed:

Pulse No.	Computed Impulse	
	N/sec	lb/sec
1	5.38	1.21
2	4.24	0.95
3	5.05	1.13
4	4.58	1.03
5	4.56	1.03
6	4.69	1.06

The average value and range for these impulses are 4.75 $^{+13\%}_{-11\%}$ N/sec (1.07 $^{+13\%}_{-11\%}$ lb/sec).

A complete integration of the pulse No. 5 thrust record was performed to include the impulse-bit contribution of the initial fuel lead and final tailoff portions of the pulse cycle. This was possible because no unprogrammed reopenings of either propellant valve occurred during this pulse. The integration, therefore, produced a total impulse-bit value, as compared to the restricted integration interval performed, to produce the comparative repeatability values shown in the table above. A total impulse-bit of 7.39 N/sec (1.66 lb/sec) was computed for pulse No. 5. This is approximately 62% greater than the 4.56 N/sec (1.03 lb/sec) value derived for pulse No. 5 when integrated only over the time interval where the oxidizer main valve was open.

Figure 102 shows the shape of the pulse No. 5 thrust trace as reconstructed from the oscillograph record to remove the load cell "ringing." A least-squares routine was used to generate points which were then curve-fitted by means of a

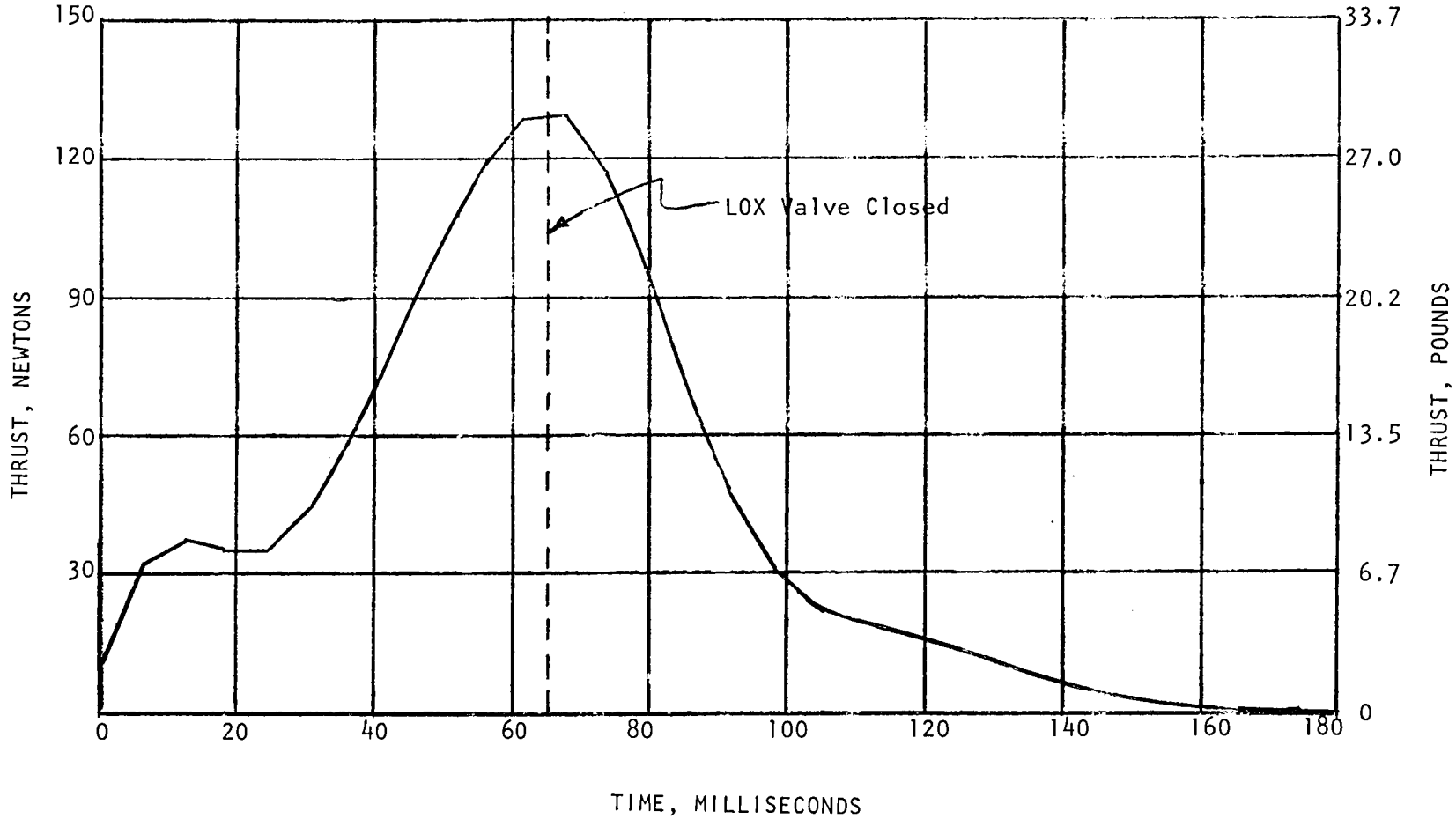

Figure 102. Computer Reconstruction of the Thrust Curve for Pulse No. 5 of Run No. 098

third-order equation. As can be seen, a considerable impulse-bit contribution exists after the time the oxidizer main valve closes.

It was not possible to characterize the pulse performance during the pulse test series, since the propellant flowrates were not measured. The propellant supply plumbing systems were modified to ensure that good quality propellants would be available at the thruster. The system revisions included the removal of the flow measurement components (venturis). However, it is possible to calculate an approximate performance level from consideration of the Fig. pulse profile.

A steady-state thrust level of 124 N (27.85 lb) was assumed to act for the 65 msec pulse duration. This was the indicated thrust at the end of 10 seconds of the run 098 30-second burn. This results in a nominal 8.05 N/sec (1.81 lb/sec) impulse-bit that would be expected under steady-state conditions. The planimeter integration of the area under the Fig. 102 curve resulted in an indicated 6.83 N/sec (1.75 lb/sec) impulse-bit. This impulse-bit has to be reduced by 6% to account for the additional propellant flow during the 10 msec interval before and after the actual pulse because of thepropellant lead/lag shutdown sequence employed. With this correction, the indicated pulse efficiency (relative to steady-state operation) is 7.63 N/sec/8.05 N/sec x 100% = 91%. Now, if the thruster specific performance efficiency during steady-state operation is assumed to be on the order of 85%, the resultant pulse efficiency would be approximately of 0.91 x 85 = 77%.

A study of the chamber pressure oscillograph records for runs No. 099 and 100 shows no discernible time lag between the opening of the lagging valve, and the start of a sharp chamber pressure rise. The 65 msec pulse duration was not sufficiently long, in general, to attain the steady-state (10 seconds) chamber pressure level. Table shows a significant difference in the peak chamber pressure levels obtained in pulses performed before the 30-second burn and the pulses that followed the long burn. The pulse series designated "final" followed the long burn, and tended to approach or exceed the steady-state chamber pressure value. By contrast, the "initial" pulses preceding the long burn peaked out below the referenced steady-state values. These results are undoubtedly due to different thruster internal hardware temperature conditions existing because of the long burn.

CONCLUSIONS AND RECOMMENDATIONS

The Liquid Oxygen/Liquid Hydrogen Auxiliary Propulsion System Thruster Investigation Program was conducted both to develop design criteria for, and provide a feasibility demonstration of, a small cryogenic thruster. The following conclusions and recommendations are made based on the results of this design, fabrication, and test effort:

1. The feasibility of a small cryogenic thruster in the size range of 111 to 444 N (25 to 100 lb) was demonstrated. However, the 111 N (25 lb) level would appear to be near the lower flowrate limit based on propellant thermal management and propellant flowrate measurement considerations.

2. Steady-state specific impulse values in excess of 390 seconds are possible with a film/radiation-cooled thrust chamber concept.

3. Rapid thrust buildup is possible with a small cryogenic thruster when proper attention is given to propellant thermal management within the thruster body. Buildup rates from 0 to 90% were demonstrated in 48 msec.

4. The use of a disilicide-coated molybdenum thruster chamber with a liquid oxygen/liquid hydrogen propulsion system was successfully demonstrated.

5. Facility problems were encountered in maintaining the very low temperatures in the propellant supply systems; however, these were primarily associated with, and accentuated by, special instrumentation requirements. When these provisions were removed during pulse mode demonstration testing, the supply of good quality propellants to the thruster was no problem. This latter configuration would be more typical of the end-item space application.

6. Due to development flexibility features on both the test hardware and facility, the susceptibility for leakage of unknown magnitude was present at several seal joints. Because the thruster propellant flowrates were extremely small, any leakage had a pronounced effect on the measured performance. Therefore, it is recommended that on any future small cryogenic thruster development programs, the use of welded rather than flanged seal joints be employed at the expense of less development flexibility.

7. During the pulse demonstration test phase, when extremely cold propellants were delivered to the thruster, random nonignitions were encountered. These results tend to indicate a marginal condition relative to spark energy, even at a 100 mJ level, where earlier testing during the performance characterization phase resulted in ignition down to energy levels of 10 mJ. The primary operational difference in these test phases was propellant inlet temperature. Cold propellants did exist during the performance test phase,but they did not approach a subcooled condition as during the pulse mode test phase. It appears that ionization of the "cold" liquid oxygen requires a larger amount of energy than was necessary during earlier development

programs that utilized a similar plasma ignition concept. While these programs utilized cold propellants in the supply system to the igniter, the lack of internal thermal insulative devices within the manifolding system precluded liquid oxygen at the spark gap.

Based on these observations, it is recommended that additional igniter characterization teting, specifically designed to explore the effect of liquid oxygen at the spark plug during ignition, be conducted during future plasma igniter technology programs.

8. The overall design criteria and an injection/combustion system have now been sufficiently defined and demonstrated to warrant incorporation of this thruster concept into a breadboard propulsion system. Therefore, it is recommended that when the other major system components reach a similar level of development, a breadboard system demonstration program be initiated.

REFERENCES

1. Williams, F. A., Combustion Theory, Chapter 3, "Diffusion Flames and Drop Burning," Addison-Wesley Publishing Co., Reading, MA, 1965.

2. Chandler, W. T. and R. J. Walter, "Hydrogen Effects in Refractory Metals," Refractory Metal Alloys: Metallurgy and Technology, Plenum Press, New York, 1968, pp 197-249.

DISTRIBUTION LIST (NAS3-20373)

Addresses	Copies
National Aeronautics & Space Administration Lewis Research Center 21000 Brookpark Road Cleveland, Ohio 44135	
Attn: Contracting Officer, MS 500-306	1
E. A. Bourke, MS 501-5	5
Technical Utilization Office, MS	1
Technical Report Control Office, MS 5-5	1
AFSC Liaison Office, MS 501-3	2
Library, MS 60-3	2
Office of Reliability & Quality Assurance, MS 500-211	1
J. P. Wanhainen, MS 501-7	15
Patent Counsel, MS 500-318	1
National Aeronautics & Space Administration Headquarters Washington, D.C. 20546	8
Attn: Office of Aeronautics & Space Technology	
Director, Study, Analysis & Planning/RX	
Director, Space Propulsion & Power/RP	
Director, Materials & Structures/RW	
F.W. Stephenson/RP	
P. N. Herr/MHE-7	
Attn: Office of Space Flight	
Director, Advanced Programs/MT	
Director, Advanced Studies/MTE	
Attn: Office of Industry Affairs & Technology Utilization	
Director, Technology Utilization/KT	
National Aeronautics & Space Administration Ames Research Center Moffett Field, California 94035	1
Attn: Library	
National Aeronautics & Space Administration Flight Research Center P.O. Box 273 Edwards, California 93523	1
National Aeronautics & Space Administration George C. Marshall Space Flight Center Huntsville, Alabama 35812	4
Attn: Library	
J. L. Sanders/PD13	
J. P. McCarty/EA01	
J. A. Lombardo/EP21	
R. J. Richmond/EP24	

Addresses	Copies
National Aeronautics & Space Administration Goddard Space Flight Center Greenbelt, Maryland 20771 Attn: Library	1
National Aeronautics & Space Administration John F. Kennedy Space Center Cocoa Beach, Florida 32931 Attn: Library	1
National Aeronautics & Space Administration Lyndon B. Johnson Space Center Houston, Texas 77001 Attn: Library J.G. Thibadaux/EP C. W. Yodzis/EP2 H.P. Davis/ER	4
National Aeronautics & Space Administration Langley Research Center Langley Station Hampton, Virginia 23365 Attn: Library B. Z. Henry, MS 365 I. O. MacConoehie, MS 365	3
NASA Scientific & Technical Information Facility P.O. Box 8785 Baltimore-Washington International Airport Baltimore, Maryland 21240 Attn: Accessioning Department	10
Office of the Director of Defense Research & Engineering Washington, D.C. 20301 Attn: Office of Ass't Director (Chemical Technology)	1
U.S. Army Research Office (Durham) Box CM, Duke Station Durham, North Carolina 27706 Attn: Library	1
U. S. Army Missile Command Redstone Scientific Information Center Redstone Arsenal, Alabama 35808 Attn: Document Section	1
U.S. Naval Missile Center Point Mugu, California 93041 Attn: Technical Library	1
U.S. Naval Weapons Center China Lake, California 93557 Attn: Library	1

Addresses	Copies
Aerojet General Corp. 9100 E. Flair Dr. El Monte, California 91734 Attn: Library	1
Aerojet Liquid Rocket Co. P.O. Box 13222 Sacramento, California 95813 Attn: Library L. Bassham J. Mellish	4
Aerospace Corporation 2350 E. El Segundo Blvd. Los Angeles, California 90045 Attn: Library R. L. Doebler I. Madison	3
AiResearch Mfg. Co. of California A Division of the Garret Corp. 2525 W. 190th St. Torrence, California 90509 Attn: Library	1
U. S. Air Force, Office of Information Office of Secretary of Air Force The Pentagon Washington, D. C. 20330	1
Air Force Aero Propulsion Laboratory Research & Technology Division Air Force Systems Command U. S. Air Force Wright-Patterson AFB, Ohio 45433 Attn: Library	1
Arnold Engineering Development Center Air Force Systems Command Tullahoma, Tennessee Attn: Library	1
Space & Missile Systems Organization Worldway Postal Center P. O. Box 92960 Los Angeles, California 90009 Attn: Library (Technical Data Center) Lt. Col. J. Graetch	2
Bureau of Naval Weapons Department of the Navy Washington, D.C. Attn: Library	1

Addresses	Copies
Naval Research Branch Office 1030 E. Green Street Pasadena, California 91101 Attn: Library	1
Picatinny Arsenal Dover, New Jersey 07801 Attn: Library	1
U. S. Naval Research Laboratory Washington, D. C. 20390 Attn: Library	1
AiResearch Mfg. Co. of Arizona A Division of the Garrett Corp. 402 South 36th St. Phoenix, Arizona 85034 Attn: Library	1
Atlantic Research Corp. 5390 Cherokee Ave. Alexandria, Va. 22314 Attn: Library	1
Battelle Memorial Institute 505 King Avenue Columbus, Ohio 43201 Attn: Library	1
Bell Aerospace Company Box 1 Buffalo, New York 14240 Attn: Library	
Boeing Company Space Division P.O. Box 868 Seattle, Washington 98124 Attn: Library	1
Chemical Propulsion Information Agency Applied Physics Laboratory John Hopkins Rd., Laurel, Maryland 20810	1
Chrysler Corp. Defense-Space Group P.O. Box 757 Detroit, Michigan 48231 Attn: Library	

Addresses	Copies
Curtiss-Wright Corporation One Rotary Drive Woodrige, New Jersey 07075 Attn: Library	1
Fairchild Republic Co. Fairchild Industries Farmingdale, L.I., N.Y. 11735 Attn: Library	
General Dynamics/Convair P.O. Box 1128 San Diego, California 92112 Attn: Library	1
General Electric Co. Valley Forge Space Technology Center P.O. Box 8555 Philadelphia, Pennsylvania 19101 Attn: Library	1
Grumman Aerospace Corporation Bethpage, L.I., N.Y. 11714 Attn: Library	1
Hamilton Standard Corporation Windsor Locks, Conn. 06096 Attn: Library	1
Honeywell, Inc. Aerospace & Defense Group Honeywell Plaza Minneapolis, Minnesota 55408 Attn: Library	1
Honeywell, Inc. 13350 U.S. Highway 19 St. Petersburg, Florida 33733 Attn: G. Gessler	1
Hughes Aircraft Co. Space and Communications Group P.O. Box 92919 Los Angeles, California 90009 Attn: Library	1
ITT Research Institute Technology Center Chicago, Illinois 60616 Attn: Library	1

Addresses	Copies
Walter Kidde & Co. Belleville Division 675 Main St. Belleville, New Jersey 07109 Attn: Library	1
Lockheed Missiles & Space Company P.O. Box 504 Sunnyvale, California 94087 Attn: Library	1
Marquardt Corporation 16555 Saticoy Street Box 2013 South Annex Van Nuys, California 91409 Attn: Library T. Hudson	2
Martin-Marietta Corporation P.O. Box 179 Denver, Colorado 80201 Attn: Library	1
McDonnell Douglas Astronautics 5301 Bosa Avenue Huntington Beach, California 92647 Attn: Library	1
Northrop Corp. 1800 Century Park East Century City, California 90067 Attn: Library	1
Pratt & Whitney Aircraft Group United Technologies Corp. 400 Main St. East Hartford, Conn. 06108 Attn: Library	1
Pratt & Whitney Aircraft Group Government Products Division P.O. Box 2691 West Palm Beach, Florida 33402 Attn: Library R. R. Atherton J. R. Brown	3

Addresses	Copies
Rocketdyne A Division of Rockwell International 6633 Canoga Avenue Canoga Park, California 91304 Attn: Library	1
Space Division A Division of Rockwell International 12214 Lakewood Blvd. Downey, California 90241 Attn: Library	1
Rocket Research Corporation Willow Road at 116th Street Redmond, Washington 98052 Attn: Library	1
Sundstrand Aviation Mechanical 2421 Eleventh Street Rockford, Illinois 61101 Attn: Library	1
Thiokol Corp. P.O. Box 1000 Newton, Pa 18940 Attn: Library	
TRW Systems Group 1 Space Park Redondo Beach, California 90278 Attn: Library	1
TRW 23555 Euclid Avenue Cleveland, Ohio 44117 Attn: Library	1
Vought Corporation P.O. Box 5907 Dallas, Texas 75222 Attn: Library	1
Jet Propulsion Laboratory 4800 Oak Grove Drive Pasadena, California 91103 Attn: Library D. Dipprey	2

Addresses	Copies
Defense Documentation Center Cameron Station Building 5 5010 Duke Street Alexandria, Virginia 22314 Attn: TISIA	1
Defense Advanced Research Projects Agency 1400 Wilson Blvd. Arlington, Virginia 22209 Attn: Library	1
Aeronautical Systems Division Air Force Systems Command Wright-Patterson Air Force Base Dayton, Ohio Attn: Library	1
Air Force Missile Test Center Patrick Air Force Base Florida Attn: Library	1
Air Force Systems Command Andrews Air Force Base Washington, D. C. 20332 Attn: Library	1
Air Force Rocket Propulsion Laboratory Edwards, California 93523 Attn: Library D. A. Hart	2
Air Force Office of Scientific Research 1400 Wilson Blvd. Arlington, Virginia 22209 Attn: Library	1